Coherent terabit/s communications using chip-scale optical frequency comb sources

Zur Erlangung des akademischen Grades eines

DOKTOR-INGENIEURS

von der KIT-Fakultät für Elektrotechnik und Informationstechnik
des Karlsruher Instituts für Technologie (KIT)

genehmigte

DISSERTATION

von

Juned Nassir Kemal, M. Sc.

geboren in

Addis Abeba, Äthiopien

Tag der mündlichen Prüfung:	03.07.2020
Hauptreferent:	Prof. Dr. Christian Koos
Korreferenten:	Prof. Dr.-Ing. Dr. h.c. Wolfgang Freude
	Prof. em. Dr. Abderrahim Ramdane

Table of Contents

Abstract (German)

Der Visual Networking Index (VNI) der Firma Cisco weist für den weltweiten Internetverkehr eine durchschnittlichen jährlichen Wachstumsrate von 26% aus und prognostiziert 2022 einen jährliche Datenverkehr von 4,8 Zettabyte [1]. Um diesem Anstieg des Netzwerkverkehrs zu begegnen, ist die kohärente Datenübertragung in Kombination mit sogenanntem Wellenlängenmultiplex (engl. *wavelength-division multiplexing*, WDM) in Langstrecken-Glasfasernetzwerken zum Standard geworden. Mit der verstärkten Nutzung von Cloud-basierten Diensten, dem wachsenden Trend, Inhalte in die Nähe der Endbenutzer zu bringen, und der steigenden Anzahl angeschlossener Geräte in sog. Internet-of-Things-(IoT-)Szenarien, wird der Datenverkehr auf allen Netzebenen voraussichtlich weiter drastisch ansteigen. Daher wird erwartet, dass die WDM-Übertragung mittelfristig auch kürzere Verbindungen verwendet werden wird, die in viel größeren Stückzahlen eingesetzt werden als Langstreckenverbindungen und bei denen die Größe und die Kosten der Transceiver-Baugruppen daher wesentlich wichtiger sind. In diesem Zusammenhang werden optische Frequenzkammgeneratoren als kompakte und robuste Mehrwellenlängen-Lichtquellen eine wichtige Rolle spielen. Sie können sowohl auf der Sender- als auch auf der Empfängerseite einer kohärenten WDM-Verbindung eine große Anzahl wohldefinierter optischer Träger oder Lokaloszillator-Signale liefern. Ein besonders wichtiger Vorteil der Frequenzkämme ist die Tatsache, dass die Spektrallinien von Natur aus äquidistant sind und durch nur zwei Parameter − die Mittenfrequenz und den freien Spektralbereich − definiert werden. Dadurch kann eine auf eine individuelle Frequenzüberwachung der einzelnen Träger verzichtet werden, und etwaige spektrale Schutzbänder zwischen benachbarten Kanälen können stark reduziert werden oder komplett wegfallen. Darüber hinaus erleichtert die inhärente Phasenbeziehung zwischen den Trägern eines Frequenzkamms die gemeinsame digitale Signalverarbeitung der WDM-Kanäle, was die

Empfängerkomplexität reduzieren und darüber hinaus auch die Kompensation nichtlinearer Kanalstörungen ermöglichen kann.

Unter den verschiedenen Kammgeneratoren sind Bauteile im Chip-Format der Schlüssel für künftige WDM-Transceiver, die eine kompakte Bauform aufweisen und sich kosteneffizient in großen Stückzahlen herstellen lassen sollen. Gegenstand dieser Arbeit ist daher die Untersuchung von neuartigen Frequenzkammgeneratoren im Chip-Format im Hinblick auf deren Eignung für die massiv parallele WDM-Übertragung. Diese Bauteile lassen sich nicht nur als Mehrwellenlängen-Lichtquellen auf der Senderseite einsetzen, sondern bieten sich auch als Mehrwellenlängen-Lokaloszillatoren (LO) für den parallelen kohärenten Empfang mehrerer WDM-Kanäle an. Bei den untersuchten Bauteilen handelt es sich um gütegeschaltete Laserdioden (engl. Gain-Switched Laser Diodes), modengekoppelte Laserdioden auf Basis von Quantenstrich-Strukturen (Quantum-Dash Mode-Locked Laser Diodes, QD-MLLD) und sog. Kerr-Kamm-Generatoren, die optische Nichtlinearitäten dritter Ordnung in Ringresonatoren hoher Güte ausnutzen. Der Schwerpunkt liegt dabei auf Datenübertragungsexperimenten, die die Eignung der verschiedenen Kammquellen untersuchen und die in den internationalen Fachzeitschriften *Nature* und *Optics Express* veröffentlicht wurden [J1]-[J4].

Kapitel 1 gibt eine allgemeine Einführung in das Thema der optischen Datenübertragung und der zugehörigen WDM-Verfahren. In diesem Zusammenhang werden die Vorteile optischer Frequenzkämme als Lichtquellen für die WDM-Datenübertragung und den WDM-Empfang erläutert. Die einige Inhalte dieses Kapitels sind dem Buchkapitel [B1] entnommen, wobei Änderungen zur Anpassung an die Struktur und Notation der vorliegenden Arbeit vorgenommen wurden.

In *Kapitel 2* wird eine grundlegende Einführung in optische Kommunikations-systeme mit Schwerpunkt auf Hochleistungsverbindungen gegeben, die auf WDM und kohärenten Übertragungsverfahren beruhen. Außerdem wird die integrierte Optik als wichtiges technologisches Element zum Bau kostengünstiger und kompakter WDM-Transceiver vorgestellt. Das Kapitel gibt ferner einen Überblick über verschiedene optische Frequenzkammgeneratoren

im Chip-Format, die sich als Mehrwellenlängen-Lichtquellen für solche Transceiver anbieten, und es werden grundlegende Anforderungen an optische Frequenzkammgeneratoren formuliert, die für WDM-Anwendungen relevant sind. Das Kapitel endet mit einer vergleichenden Diskussion der verschiedenen Kammgeneratoren sowie einer Zusammenfassung ausgewählter WDM-Datenübertragungsexperimente, die mit diesen Kammgeneratoren demonstriert wurden.

In *Kapitel 3* wird die kohärente WDM-Sendetechnik und der kohärente WDM-Empfang mit einer gütegeschalteten Laserdiode (GSLD) diskutiert. Im Mittelpunkt der Arbeit steht ein Versuchsaufbau, in dem der empfängerseitige Kammgenerator aktiv mit dem senderseitigen Generator synchronisiert wurde. Das Experiment stellt die weltweit erste Demonstration einer kohärenten WDM-Übertragung mit Datenraten von über 1 Tbit/s dar, bei dem synchronisierte Frequenzkämme als Mehrwellenlängen-Lichtquelle am Sender und als Mehrwellenlängen-LO am Empfänger verwendet werden.

Kapitel 4 untersucht das Potenzial von QD-MLLD als Mehrwellenlängen-Lichtquellen für die WDM-Datenübertragung. Diese Kammgeneratoren sind aufgrund ihrer kompakten Größe und des einfachen Betriebs besonders attraktiv. Die erzeugten Kammlinien weisen jedoch ein hohes Phasenrauschen auf, das die Modulationsformate in früheren Übertragungsexperimenten auf 16QAM begrenzte. In diesem Kapitel wird gezeigt, dass QD-MLLD die WDM-Übertragung mit Modulationsformaten jenseits von 16QAM unterstützen kann, wenn eine optische Rückkopplung durch einen externen Resonator zur Reduzierung des Phasenrauschens der Kammlinien verwendet wird. In den Experimenten wird eine Reduzierung der intrinsischen Linienbreite um etwa zwei Größenordnungen demonstriert, was eine 32QAM-WDM-Übertragung ermöglicht. Die Demonstration der Datenübertragung mit einer Rate von 12 Tbit/s über eine 75 km lange Faser mit einer spektralen Netto-Effizienz von 7,5 Bit/s/Hz stellt dabei die höchste für diese Bauteile gezeigte spektrale Effizienz dar.

Gegenstand von *Kapitel 5* ist die WDM-Übertragung und der kohärente Empfang mit QD-MLLD vor. Die Vorteile der Skalierbarkeit von QD-MLLD

für massiv parallele WDM-Verbindungen werden also nicht nur am Sender, wie in Kapitel 4 beschrieben, sondern auch am Empfänger ausgenutzt. So konnte ein Datenstrom mit einer Rohdatenrate von 4,1 Tbit/s über eine Distanz von 75 km übertragen werden, indem ein Paar von QD-MLLD mit ähnlichen freien Spektralbereichen verwendet wurde – ein Bauteil zur Erzeugung der optischen Träger am WDM-Sender und ein weiteres Bauteil zur Bereitstellung der erforderlichen LO-Töne für den kohärenten WDM-Empfang.

Kapitel 6 beschreibt WDM-Datenübertragungsexperimente mit Hilfe von Kerr-Kamm-Generatoren. Dazu werden sog. dissipative Kerr-Solitonen (engl. dissipative Kerr solitons, DKS) in integriert-optischen Mikroresonatoren genutzt, die wegen zur Erzeugung einer streng periodischen Folge ultra-kurzer optischer Impulsen im Zeitbereich und damit zu einem breitbandigen, für WDM-Systeme sehr gut geeigneten Frequenzkamm führen. Mit diesen DKS-Kämmen wird ein Datenstrom mit einer Rohdatenrate von 55,0 Tbit/s über eine 75 km lange Faser übertragen. Zum Zeitpunkt der Veröffentlichung war dies die höchste Datenrate, welche mit einer chip-basierten Frequenzkammquelle erreicht wurde. Das Ergebnis zeigt das Potenzial der Kammquellen für WDM-Übertragung. Darüber hinaus wird der kohärente Empfang von 93 WDM-Kanälen mit einer Datenrate von 37,2 Tbit/s unter Verwendung eines DKS-Kamms als Multiwellenlängen-LO demonstriert; die Übertragung erfolgt über eine 75 km lange Faser. Diese Arbeiten wurde in der international renommierten wissenschaftlichen Zeitschrift *Nature* publiziert.

Kapitel 7 fasst die Arbeit zusammen und gibt einen Ausblick auf die Anwendung der diskutierten Kammgeneratoren in zukünftigen WDM-Systemen.

Preface

According to Cisco's Visual Networking Index (VNI), global internet traffic is growing at a compound annual growth rate of 26% and it is expected to reach 4.8 zettabytes per year by 2022 [1]. For addressing this surge in network traffic, coherent transmission along with wavelength-division multiplexing (WDM) has become the standard in long-haul optical fiber networks. However, with the increased adoption of cloud-based services, the growing trend of moving content close to end users, and the rising number of connected devices in Internet-of-Things-(IoT-)scenarios, data traffic is expected to grow drastically across all network levels. As a consequence, WDM transmission is expected to also dominate shorter links, which are deployed in much larger quantities and which are much more sensitive to size and cost of the transceiver assemblies than their long-haul counterparts. In this context, optical frequency comb generators will play a key role as compact and robust multi-wavelength light sources that can provide large numbers of well-defined optical tones both at the transmitter and at the receiver side of a WDM link. A particularly important advantage of frequency combs is the fact that the comb lines are inherently equidistant in frequency and that they can be controlled by just two parameters – the center frequency and the free spectral range (FSR). This avoids frequency control of individual tones and the need for guard bands between neighboring WDM channels. In addition, the inherent phase relationship between the tones of a frequency comb facilitates joint digital signal processing of the received WDM signals, which may reduce receiver complexity and even enable compensation of nonlinear channel impairments.

Among the various comb generators, chip-scale devices are key for future WDM transceivers, which require compact footprint and that are amenable to cost-efficient mass production. These devices can be exploited not only as multi-wavelength light sources at the WDM transmitter side, but also as multi-wavelength local oscillators (LO) for parallel coherent reception of WDM signals. This thesis hence investigates three concepts for chip-scale frequency comb generators with a special emphasis on the performance of the devices in

massively parallel WDM. These device concepts comprise gain-switched laser diodes (GSLD), quantum-dash mode-locked laser diodes (QD-MLLD), and microresonator-based Kerr-comb generators. The focus is on data transmission experiments, which investigate the suitability of different comb sources and which have been published in the international journals *Nature* and *Optics Express* [J1]-[J4].

Chapter 1 gives a general introduction to the topic of optical communications and wavelength-division multiplexing (WDM). In this context, we explain the advantage of using of optical frequency combs as light sources for WDM data transmission and reception. Some content in this chapter is adapted from a book chapter [B1] with the appropriate changes to fit the structure and notation of this thesis.

In Chapter 2, a basic introduction to optical communication systems with emphasis on high-capacity links that rely on WDM and coherent modulation formats is given. We also introduce photonic integration as a key element for building compact and low-cost WDM transceivers. The chapter gives an overview of different chip-scale optical frequency comb generators that lend themselves as multi-wavelength light sources for such transceivers. The chapter further formulates basic requirements on optical frequency comb generators for WDM application. A comparative discussion of the different chip-scale comb generators along with a summary of selected WDM data transmissions demonstrated with the devices concludes the chapter.

Chapter 3 discusses coherent WDM transmission and reception using a GSLD. The comb generation technique and the experimental setup are introduced. The receiver comb was actively synchronized to the transmitter comb using a closed-loop control. The work represents the first demonstration of terabit/s coherent WDM transmission using a pair of synchronized frequency combs – one as a multi-wavelength source at the transmitter and the other as a multi-wavelength LO at the receiver.

Chapter 4 explores the potential of QD-MLLD as multi-wavelength light sources for WDM data transmission. These comb generators are particularly

attractive due to their compact size and simple operation. However, the generated comb lines exhibit high phase noise, which limited earlier WDM transmission demonstrations with these devices to 16QAM. The experiments described in this chapter show that QD-MLLD can support WDM transmission with modulation formats beyond 16QAM if external-cavity optical feedback is used to reduce the phase noise of the comb lines. In the experiments, a reduction of the intrinsic linewidth by approximately two orders of magnitude is demonstrated, thus enabling 32QAM WDM transmission. This allows to transmit a 12 Tbit/s data stream over a 75 km-long fiber at a net spectral efficiency of 7.5 bit/s/Hz, which is the highest spectral efficiency reported for QD-MLLD.

Chapter 5 presents coherent WDM transmission and reception using QD-MLLD. The scalability advantages of QD-MLLD for massively parallel WDM links is exploited not only at the transmitter as in Chapter 4, but also at the receiver. A data stream with a line rate of 4.1 Tbit/s could be transmitted over a distance of 75 km using a pair of QD-MLLD with similar free spectral ranges (FSR) – one device to generate the optical carriers for the WDM transmitter, and the other device to provide the required LO tones for coherent WDM reception.

Chapter 6 describes WDM data transmission and reception experiments using microresonator-based Kerr-comb generators. The demonstration relies on so-called dissipative Kerr solitons (DKS) that are generated in integrated optical microresonators and that lead to a strictly periodic sequence of short optical pulses in the time domain, corresponding to a broadband frequency comb that is well suited for WDM transmission. Using DKS combs, a data stream with a line rate of 55.0 Tbit/s is transmitted over a 75 km-long fiber. At the time of publication, this represented the highest data rate achieved with any chip-scale frequency comb source. The result shows the potential of the comb sources for WDM transmission. In addition, coherent reception of 93 WDM channels using a DKS comb as a multi-wavelength LO is demonstrated with a data rate of 37.2 Tbit/s transmitted across a 75 km-long fiber.

Chapter 7 summarizes the work and gives an outlook on the application of the investigated comb generators in future WDM systems.

Achievements of the present work

This thesis aims at investigating and comparing the viability and performance of different chip-scale optical frequency comb generators for massively parallel optical communications using wavelength-division multiplexing (WDM). The devices are used either as multi-wavelength light sources for massively parallel data transmission or as multi-wavelength local oscillator (LO) for coherent reception. In the following, the main achievements of this work are highlighted.

Real-time synchronization of center frequency and free spectral range of two optical frequency combs using closed-loop control based on digital signal processing (DSP): A DSP algorithm is implemented on a field programmable gate array (FPGA) for estimating the offset in center frequency and the offset in free spectral range (FSR) between the transmitter comb and the LO comb. Control signals generated by the FPGA are used to maintain the two combs actively synchronized [J1].

First demonstration of a coherent Tbit/s WDM link that relies on synchronized frequency combs as light sources both at the transmitter and the receiver: WDM data transmission at line rates of more than 1 Tbit/s is demonstrated using a pair of GSLD – one device as a multi-wavelength source at the transmitter and the other device as a multi-wavelength LO at the receiver [J1]. Using the developed comb synchronization algorithm, the tones of the two GSLD are maintained in frequency aligent, keeping the intradyne frequencies for all WDM channels below 15 MHz. To the best of our knowledge, this is the first demonstration of coherent WDM transmission using synchronized frequency combs as light source at the transmitter and as multi-wavelength LO at the receiver.

First demonstration of 32-state quadrature amplitude modulation (32QAM) WDM transmission using QD-MLLD: Exploiting coherent feedback from an external cavity to drastically reduce the phase noise of QD-MLLD tones, we experimentally demonstrate the first 32QAM WDM

transmission using QD-MLLD. The experiment relies on 60 carriers derived from a QD-MLLD, leading to an aggregate line rate of 12 Tbit/s [J2].

First demonstration of a coherent WDM link that relies on QD-MLLD both at the transmitter and the receiver: For the first time, coherent data transmission and reception is shown using a pair of QD-MLLD with similar free spectral ranges (FSR). A data stream with a line rate of 4.1 Tbit/s is transmitted over a 75 km-long fiber span [J3].

First demonstration of massively parallel data transmission using dissipative Kerr soliton (DKS) comb sources: In a joint experiment [J4] we demonstrate the first massively parallel WDM transmission using DKS combs. We use the devices both as a multi-wavelength light source at the transmitter and as a multi-wavelength LO at the receiver. The WDM signals that span across the telecommunication C and L bands, leading to a line rate of up to 55 Tbit/s. At the time of publication, this represented the highest line rate achieved with any chip-scale frequency comb source.

1 Introduction

From the use of smoke signals by ancient Chinese soldiers to Alexander G. Bell's photophone demonstrations in 1880 [2], humans have been communicating optically for a long time. The development of the laser in the 1960s and the work of Charles Kao on optical fibers [3] led to the introduction of commercial optical fiber links in the late 1970s. These links, however, required electrical regeneration to bridge long distances. With the introduction of erbium-doped fiber amplifiers (EDFA), communication links spanning thousands of kilometers relying solely on direct optical amplification became possible. The advent of EDFA also spurred the utilization of wavelength-division multiplexing (WDM) for long-haul optical fiber links increasing the capacity in existing fiber infrastructure tremendously to cope with the increasing network traffic. For such links, the cost of transceiver components is comparatively low as compared to the fiber infrastructure. However, with the increased adoption of cloud-based services, the growing trend of moving content close to end users, and the growing number of connected devices in Internet-of-Things-(IoT-)scenarios, global data traffic is expected to grow drastically across all network levels. As a consequence, WDM is also expected to dominate shorter links, which are deployed in much larger quantities and which are much more sensitive to cost and size of the transceiver assemblies. This evolution is, e.g., witnessed by a strong market growth in the field of so-called data-center interconnects, which link two or more datacenters or parts thereof across a metropolitan-area with typical distances of less than 100 km [4]. In the future, even shorter WDM links are expected to emerge, e.g., in the context of high-throughput campus-area networks, which connect datacenter buildings over distances of up to a few kilometers. At present, these networks still rely on parallel transmission using spatially separated channels in thousands of single-mode fibers, each of which is operated with a comparatively low data rate of at most a few hundred Gbit/s. However, it is foreseeable that the concept of spatial parallelization will soon reach its scalability limits, and that it must be complemented by spectral parallelization of data streams in each

fiber to sustain further increases in data rates. This unlocks an entirely new application space for WDM techniques, in which utmost scalability of channel counts and data rates is of the highest importance.

In this context, optical frequency comb generators may play a key role as multi-wavelength light sources that can provide large numbers of well-defined optical carriers. A particularly important advantage of frequency combs is the fact that the comb lines are inherently equidistant in frequency, hence relaxing the requirements for inter-channel guard bands [5] and avoiding frequency control of individual lines as needed in conventional schemes that combine arrays of independent distributed-feedback (DFB) lasers. Note that these advantages do not apply only to the WDM transmitter, but also to the receiver, where an array of discrete local oscillators (LO) may be replaced by a single comb source [J1], [J4], [6]. Using an LO comb further facilitates joint digital signal processing of the WDM channels, which may reduce receiver complexity and increase phase-noise tolerance [7]. Moreover, parallel coherent reception using an LO comb with frequency-locked tones might even allow to reconstruct the time-domain waveform of the overall WDM signal and thus permit compensation of impairments caused by optical nonlinearities of the transmission fiber [8].

Besides these conceptual advantages of comb-based transmission, compact footprint and cost-efficient mass production is key for future WDM transceivers. Among the various comb generators, chip-scale devices are therefore of particular interest [J1]–[J4], [9]–[18]. When combined with highly scalable photonic integrated circuits for modulation, multiplexing, routing, and reception of data signals, such devices may become the key to compact and energy-efficient WDM transceivers that can be fabricated in large quantities at low cost while offering transmission capacities of tens of Tbit/s per fiber.

This thesis investigates coherent optical transmission systems that rely on chip-scale frequency comb generators for high throughput coherent WDM systems. These devices can be used both as multi-wavelength light sources at the WDM transmitter and as multi-wavelength local oscillators (LO) for parallel coherent detection at the receiver.

The basic setup of a WDM transmitter with an optical frequency comb generator (FCG) as a multi-wavelength source is depicted in Figure 1.1a. The comb lines are first separated in a demultiplexer (DEMUX) and then fed to electro-optic modulators (EOM). For best spectral efficiency, advanced quadrature amplitude modulation (QAM) formats are usually employed [19], [20]. After recombining the data channels in a multiplexer (MUX), the WDM signal is transmitted through a single-mode fiber (SMF). Figure **1.1**b shows the corresponding WDM receiver, exploiting LO tones from a second FCG for multi-wavelength coherent detection. The channels of the incoming WDM signal are separated by a demultiplexer and then fed to an array of coherent receivers (Coh. Rx). The demultiplexed tones of the LO comb serve as phase reference for each coherent receiver.

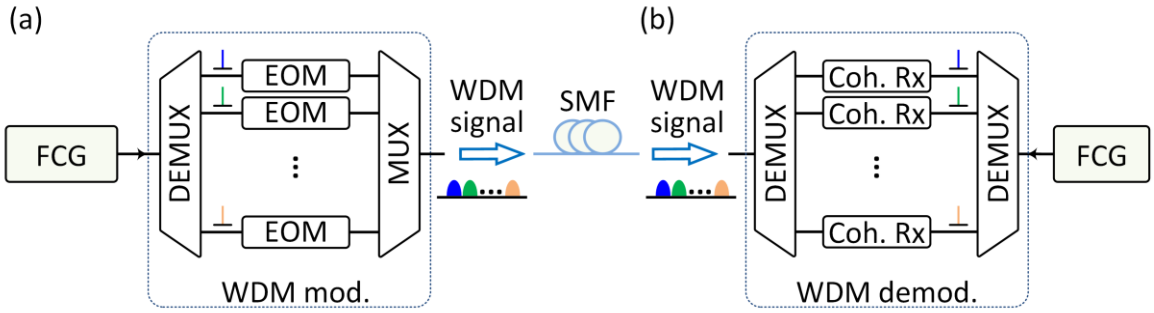

Figure 1.1: Concept of comb-based WDM transmission and coherent reception. **(a)** WDM transmitter using a multitude of carriers from a first frequency comb generator (FCG). Information is encoded onto the various carriers via electro-optic modulators (EOM) using advanced quadrature amplitude modulation (QAM) formats. DEMUX: demultiplexer, MUX: multiplexer. **(b)** Coherent WDM receiver using a multitude of local oscillator (LO) tones that are derived from a second FCG.

Three different comb generators have been investigated in the framework of this thesis: Gain-switched laser diodes (GSLD), quantum-dashed mode-locked laser diodes (QD-MLLD), and dissipative Kerr soliton (DKS) comb sources.

GSLD [21] were provided by the start-up company Pilot Photonics[1] in the framework of the European FP7 project BigPipes[2]. The potential of GSLD as

[1] https://www.pilotphotonics.com
[2] http://www.bigpipes.rwth-aachen.de/

multi-wavelength light sources and as multi-wavelength local oscillators for WDM is shown in Chapter 3 [J1]. QD-MLLD [22] were fabricated by the Centre National de la Recherche Scientifique (CNRS)[3] in collaboration with III-V Lab[4], who were also members of the BigPipes consortium. Chapter 4 and Chapter 5 discuss the WDM experiments carried out with the devices [J2], [J3]. Chapter 6 shows the first WDM transmission and reception experiments performed using DKS comb sources that rely on a CW-driven silicon nitride microresonator [J4]. The microresonators were designed and fabricated at École Polytechnique Fédérale de Lausanne[5] in Switzerland. In all these demonstrations, we achieved important insights and ground-breaking results, which are summarized on page xiii at the beginning of this work.

[3] http://www.cnrs.fr
[4] http://www.3-5lab.fr
[5] https://www.epfl.ch/labs/k-lab/

2 Background

In this chapter, we summarize the background necessary for better understanding of the experimental investigations presented in this thesis. Section 2.1 gives a basic introduction to optical communication systems with emphasis on high-capacity optical links that rely on quadrature amplitude modulation (QAM). In this context, we introduce the fundamental concepts of coherent optical communications and wavelength-division multiplexing (WDM), which have become ubiquitous with high-capacity links. We also introduce photonic integration as a key technological element of compact low-cost optical transceivers. Section 2.2 introduces optical frequency combs as promising multi-wavelength light sources for these low-cost and compact transceivers. The section is taken from a book chapter [B1] that was published with equal contribution from me and Pablo Marin-Palomo. It is modified to fit modified to fit the structure and notations of this thesis. Expanded work on this topic is also published by Pablo Marin-Palomo [23].

2.1 Optical communication systems

A basic optical communication system linking an information source and an information sink is depicted in Figure **2.1**. The optical transmitter is responsible for bringing the source information from the electrical domain into the optical domain. This electrical-to-optical (EO) conversion is accomplished by modulating the information signal onto an optical carrier. The channel corresponds to an optical fiber link through which the optical signal from the transmitter is sent to the receiver. Optical fibers utilize total internal reflection to guide a light signal through them with low loss and high bandwidth while being highly resilient to environmental conditions. As fiber optic transmission offers a tremendous amount of bandwidth that cannot be used by a single transmitter, wavelength-division multiplexing (WDM) is widely employed. This involves using multiple optical carriers at different wavelengths to carry

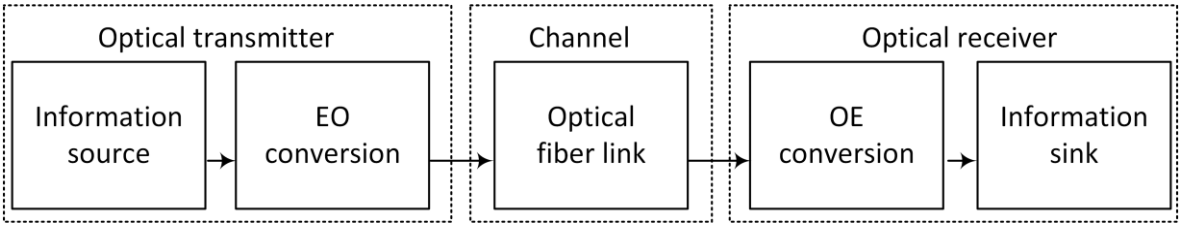

Figure 2.1: Block diagram of an optical communication system. At the optical transmitter, the electrical signal from the information source is upconverted to optical carrier frequencies (electrical-to-optical (EO) conversion). The optical fiber link transports the optical signal from the transmitter to the receiver. The optical receiver downconverts the signal into the electrical domain (optical-to-electrical (OE) conversion) to recover the transmitted information.

data signals across the fiber, see Section 2.1.2 for more details. The optical receiver converts the incoming optical signal to the electrical domain (optical-to-electrical (OE) conversion) for use by the sink.

Depending on the modulation and detection technique employed, optical communication schemes are categorized as non-coherent or coherent. Non-coherent optical communications mostly rely on the modulated intensity of an optical carrier to transmit information across a channel. The corresponding receiver demodulates the detected intensity levels of the received signal and recovers the transmitted information. This intensity modulation and direct detection (IM/DD) scheme has been used since the advent of fiber-optic communications and it is still widely employed for links with a reach of up to 10 km [24]. Coherent communication uses the amplitude and the phase of an optical carrier to convey information whereby coherent detection is used to demodulate the incoming signal with an optical local oscillator (LO) laser serving as a phase reference. The use two independent attributes of the optical field instead of only its intensity leads to a two-fold spectral efficiency improvement from IM/DD. Coherent communication scheme is employed in this thesis and it is discussed in more detail in Section 2.1.1.

2.1.1 Coherent optical communications

The electric field of an optical carrier wave with real amplitude $E_{\mathrm{c}}(t)$, angular frequency ω_{c}, and phase $\phi_{\mathrm{c}}(t)$ can be described as an analytic signal

$$\underline{E}(t) = E_{\mathrm{c}}(t)\mathrm{e}^{\mathrm{j}\phi_{\mathrm{c}}(t)}\mathrm{e}^{\mathrm{j}\omega_{\mathrm{c}}t} \tag{2.1}$$

In addition, the field will also have a specific polarization. Data can be encoded on to this carrier wave by modulating its amplitude, phase, frequency and polarization. In this thesis, amplitude and phase modulation are utilized to encode data whereas frequency and polarization are used merely for obtaining higher data rates by multiplexing.

2.1.1.1 Quadrature-amplitude modulation (QAM)

Consider a baseband complex signal $\underline{A}(t)$ with real amplitude $A_{\mathrm{s}}(t)$ and phase $\varphi_{\mathrm{s}}(t)$ that is given as

$$\underline{A}(t) = A_{\mathrm{s}}(t)\mathrm{e}^{\mathrm{j}\varphi_{\mathrm{s}}(t)} \tag{2.2}$$

Taking an ideal carrier with no amplitude and phase noise, i.e., assuming $E_{\mathrm{c}}(t) = 1$ and $\phi_{\mathrm{c}}(t) = 0$, an amplitude- and phase-modulated optical signal can mathematically be given as an analytic signal in terms of the complex signal $\underline{A}(t)$ as

$$\underline{E}_{\mathrm{s}}(t) = \underline{A}(t)\mathrm{e}^{\mathrm{j}\omega_{\mathrm{c}}t} = A_{\mathrm{s}}(t)\mathrm{e}^{\mathrm{j}\varphi_{\mathrm{s}}(t)}\mathrm{e}^{\mathrm{j}\omega_{\mathrm{c}}t} \tag{2.3}$$

A physical channel can transmit only a physically measureable real valued signal. The fact that an amplitude- and phase-modulated real signal can be represented as the real part of an analytic signal with complex amplitude, however, leads to a recipe that can be used as a basis for transmitting complex signals. Taking the real part of Eq. (2.3), we have

$$E_{\mathrm{s}}(t) = A_{\mathrm{s}}(t)\cos\left(\omega_{\mathrm{c}}t + \varphi_{\mathrm{s}}(t)\right) . \tag{2.4}$$

Now a simple trigonometric manipulation of Eq. (2.4) leads to

$$\begin{aligned} E_{\mathrm{s}}(t) &= A_{\mathrm{s}}(t)\cos\left(\varphi_{\mathrm{s}}(t)\right)\cos\left(\omega_{\mathrm{c}}t\right) - A_{\mathrm{s}}(t)\sin\left(\varphi_{\mathrm{s}}(t)\right)\sin\left(\omega_{\mathrm{c}}t\right) \\ &= \mathrm{Re}\{\underline{A}(t)\}\cos\left(\omega_{\mathrm{c}}t\right) - \mathrm{Im}\{\underline{A}(t)\}\sin\left(\omega_{\mathrm{c}}t\right) \\ &= I(t)\cos\left(\omega_{\mathrm{c}}t\right) - Q(t)\sin\left(\omega_{\mathrm{c}}t\right) \end{aligned} . \tag{2.5}$$

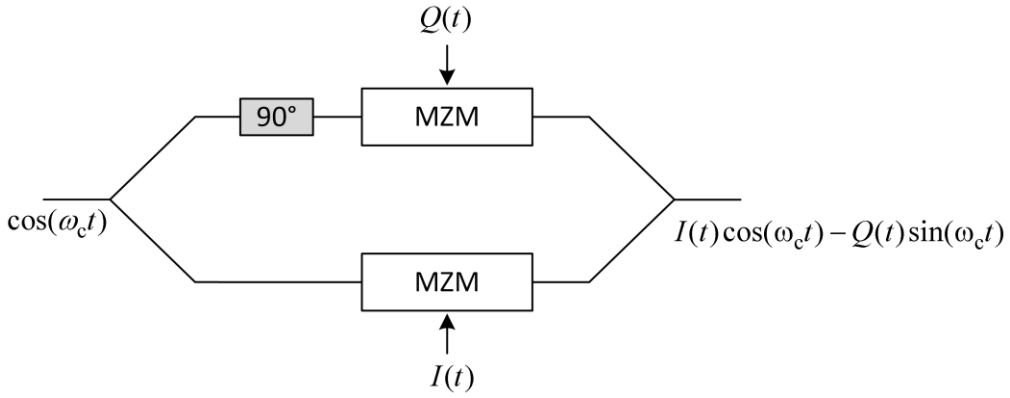

Figure 2.2: Schematic of an in-phase/quadrature (IQ) modulator. It consists of two nested Mach-Zehnder modulators (MZM) with an additional 90° phase shift in one arm. The 90° phase shifter leads to quadrature carrier signals $\cos(\omega_c t)$ and $-\sin(\omega_c t)$. The carrier $\cos(\omega_c t)$ is modulated with the in-phase signal $I(t)$ using the MZM in the lower arm. The MZM on the upper arm encodes $Q(t)$ on the carrier $-\sin(\omega_c t)$. The output of the IQ modulator corresponds to modulated signal given in Eq. (2.5).

In Eq. (2.5), the signals $I(t)$ and $Q(t)$ denote the real and the imaginary parts of the complex signal $\underline{A}(t)$, respectively. The actually transmitted signal $E_s(t)$ is, however, a real-valued signal and can be measured at the receiver. The signal $I(t)$ is referred to as the in-phase component since the real part of $\underline{A}(t)$ is in-phase with the carrier $\cos(\omega_c t)$. $Q(t)$ is called the quadrature component as the imaginary part of $\underline{A}(t)$ is in-phase with $-\sin(\omega_c t)$, which is at a relative phase shift of 90°(or 'in quadrature') with $\cos(\omega_c t)$, i.e., $-\sin(\omega_c t) = \cos(\omega_c t - \pi/2)$. Therefore, it can be seen from Eq. (2.5) that one can transmit complex data signals by using the mixing of the real part with a carrier $\cos(\omega_c t)$ and the mixing of the imaginary part with the carrier $-\sin(\omega_c t)$. This is the basic principle of quadrature-amplitude modulation. Equation (2.5) shows how the so-called in-phase/quadrature (IQ) modulator works. An optical IQ modulator consists of two nested Mach-Zehnder modulators (MZM) with a 90° phase shift in one arm, see Figure 2.2. One MZM modulates $I(t)$ on the carrier $\cos(\omega_c t)$ whereas the second MZM modulates $Q(t)$ on the carrier $-\sin(\omega_c t)$, which is obtained by advancing $\cos(\omega_c t)$ with a 90° phase shift.

In modern communication systems, the modulating signal $\underline{A}(t)$ is a digital signal consisting a discrete set of complex numbers corresponding to signal

states that are associated with certain symbols. Each symbol represents a set of binary numbers. The complete set of symbols is called a symbol alphabet. This symbol alphabet can be conveniently depicted in a so-called constellation diagram showing the phaser $\underline{A}(t)$ on the complex plane. The I and Q components of $\underline{A}(t)$ represent the real and imaginary axis of the complex plane, respectively. Different modulation formats can be defined based on the arrangement of the symbol alphabet on the constellation diagram. Each symbol on the constellation diagram represents a set of binary numbers. In general, a modulation format having an alphabet with M symbols can encode $\log_2 M$ bits per symbol.

The constellation diagrams for the modulation formats used in this thesis are depicted in Figure 2.3. The constellation diagram for quadrature phase shift keying (QPSK), which can be generated by a pure phase modulation, is depicted in Figure **2.3**a. The corresponding symbol alphabet can be given as {1+j, -1+j, -1-j, 1-j}. Two bits can be mapped to a symbol in QPSK. As an example, the binary numbers corresponding to Gray coded symbols are indicated in the figure. The square-shaped constellation diagram in Figure **2.3**b depicts a 16-state quadrature amplitude modulation (16QAM), which encodes four bits of information per symbol. Figure 2.3c depicts the cross-shaped constellations of 32-state quadrature amplitude modulation (32QAM) that encodes five bits per symbol.

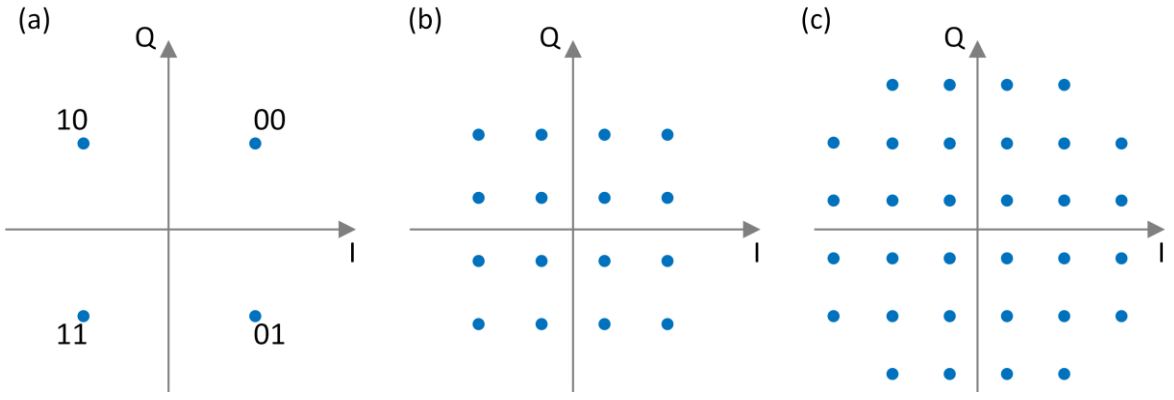

Figure 2.3: Constellation diagrams of the modulation formats utilized in subsequent chapters. **(a)** Quadrature phase shift keying (QPSK). **(b)** 16-state quadrature amplitude modulation (16QAM). **(c)** 32-state quadrature amplitude modulation (32QAM)

2.1.1.2 Coherent receiver

To recover the transmitted information, the receiver needs to convert the incoming data signal from the optical domain to the electrical domain. A phase-sensitive coherent receiver is employed to recover the complex modulation signal described in the previous section.

The receiver architecture is depicted in Figure **2.4**. It consists of a 90° optical hybrid and a pair of balanced photodetectors. The received signal field E_s is superimposed with an LO field E_{LO} and detected by the balanced photodetector BPD 1. The signal field E_s is superimposed also with a 90°-phase-shifted version of the LO field E_{LO} and detected by a second balanced photodetector BPD2. Neglecting power splitting factors of the couplers, assuming the signal field is given as $E_s(t) = A_s(t)\cos\left(\omega_c t + \phi_c(t) + \varphi_s(t)\right)$, and the LO field is given as $E_{LO}(t) = \cos\left(\omega_{LO} t + \phi_{LO}(t)\right)$, the generated photocurrents i_I and i_Q can be expressed as

$$\begin{aligned} i_I(t) &\propto \left|A_s(t)\right|\cos\left(\omega_{IF} t + \varphi_s(t) + \Delta\phi(t)\right) \\ i_Q(t) &\propto \left|A_s(t)\right|\sin\left(\omega_{IF} t + \varphi_s(t) + \Delta\phi(t)\right) \end{aligned} \tag{2.6}$$

where $\omega_{IF} = \omega_c - \omega_{LO}$ is the intermediate frequency (IF) at which the photocurrents oscillate and $\Delta\phi(t) = \phi_c(t) - \phi_{LO}(t)$ is the phase difference between the signal carrier and the LO. In Eq. (2.6), we neglected amplitude noise of the carrier and the LO.

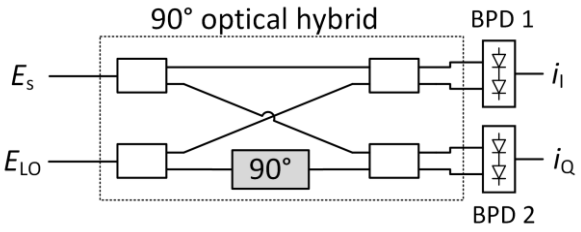

Figure 2.4: A coherent receiver based on a 90° optical hybrid. The signal field E_s is mixed with the local oscillator (LO) field E_{LO} on a balanced photodetector BPD 1 resulting in the photocurrent i_I. The signal field E_s is mixed also with a 90°-phase-shifted version of the LO field E_{LO} on a second balanced photodetector BPD 2 resulting in the photocurrent i_Q.

Different coherent reception schemes exist based on the frequency and phase relationship between the signal carrier and the LO. If the LO laser is phase locked to the signal carrier such that $\omega_{\mathrm{IF}} = 0$ and $\Delta\phi(t) = 0$, Eq. (2.6) reduces to the I and Q components of $\underline{A}(t)$ defined in Eq. (2.5). This is referred to as homodyne reception. When free running signal and LO lasers are used such that ω_{IF} is more than three times the signal bandwidth B, i.e., $|\omega_{\mathrm{c}} - \omega_{\mathrm{LO}}| > 3B$, heterodyne reception can be employed using analog electronics. Intradyne reception employs an LO at an angular frequency ω_{LO} that is separated from the signal carrier by a frequency offset which is smaller than the signal bandwidth, i.e., $|\omega_{\mathrm{c}} - \omega_{\mathrm{LO}}| < B$. This is the scheme used in this thesis.

In intradyne reception, the photocurrents i_{I} and i_{Q} are sampled using fast analog-to-digital converters (ADC) and digital signal processing (DSP) is used to retrieve the transmitted [28] information [25]. The DSP involves numerical removal of the frequency offset ω_{IF} and continuous estimation of $\Delta\phi(t)$, which is fluctuating with time as a result of phase noise both from the carrier and the LO. The I and the Q-components of the modulating complex data can then be recovered from photocurrents i_{I} and i_{Q} using Eq. (2.6). Note that, in real systems, i_{I} and i_{Q} will also include the impact of optical and electrical noise.

2.1.2 Wavelength-division multiplexing

Wavelength-division multiplexing (WDM) exploits different carrier wavelengths to send several data signals through the same fiber. WDM offers a simpler alternative for increasing the data rate transmitted through a standard single-mode fiber (SSMF) and hence better utilizes the fiber bandwidth. The principle of a WDM based optical link is depicted in Figure **2.5**. For simplicity, a simple point-to-point WDM link with no amplification and dispersion compensation is considered. At the transmitter side of the WDM link, a total of N optical carriers at wavelengths $\lambda_1, \lambda_2, ..., \lambda_N$ are independently modulated, combined using an optical multiplexer (MUX), and sent through the fiber. The modulated carriers, which are referred to as a WDM channel, are then separated at the receiver using an optical demultiplexer (DEMUX) and received with N

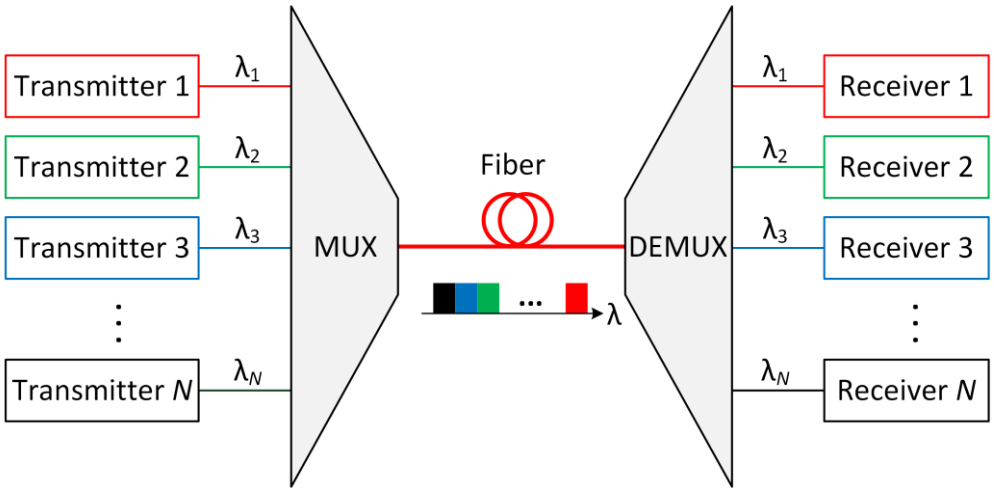

Figure 2.5: Wavelength division multiplexing (WDM). The modulated signals from *N* transmitters having different carrier wavelengths $\lambda_1, \lambda_2, \ldots, \lambda_N$ are combined using an optical multiplexer (MUX) and sent through a single fiber. At the receiver site, the different channels are demultiplexed (DEMUX) and received independently.

independent coherent receivers. Setting aside nonlinear interaction of the WDM channels in the fiber, each transmitter-receiver pair can be considered as being operated independently within a single fiber link.

There are, in general, two flavors of WDM: coarse WDM (CWDM) and dense WDM (DWDM). In commercial WDM systems, International Telecommunication Union (ITU) standards are used to select the carrier wavelengths and the spacing between carriers. In CWDM, ITU recommendation G.694.2 specifies 18 carrier wavelengths spanning >300 nm across multiple transmission windows of an optical fiber with a 20 nm spacing between the carriers [26]. In the case of DWDM, the operating window is located around 1550 nm to benefit from the low loss of SSMF in this region. Most commonly, the conventional (C) and long (L) wavelength bands are used since they also benefit from the availability of erbium-doped fiber amplifiers (EDFA). Carrier spacing grids ranging from 12.5 GHz (0.1 nm) to 100 GHz (0.8 nm) and integer multiples thereof are specified by ITU recommendation G.694.1 for DWDM [27]. As modulation symbol rate defines the bandwidth of a WDM channel and hence the lowest carrier spacing needed, having multiple grids enables a spectrally efficient optical transmission.

In this thesis, we investigate chip-scale comb generators operating in the C and L bands with comb line spacings of up to 100 GHz. This makes the comb generators highly compatible with DWDM. Hence, DWDM is the targeted application whenever we are discussing WDM systems throughout this thesis.

2.1.3 Photonic integration

The growing adoption of data-rate intensive technologies across the globe is putting stringent cost, size, and energy-consumption requirements on future optical transceiver modules. Photonic integration is a technology which is used to address these requirements as it enables cost-efficient mass production of compact devices with more functionality. Photonic integration draws its parallel from electrical integrated circuits, where multiple electrical circuits are shrunk in size and integrated on a single semiconductor substrate. From the perspective of optical transceivers, photonic integration requires the development of key devices such as light sources, modulators, multiplexers, and detectors, which can be integrated on semiconductor substrates. Therefore, research on the development of these devices has attracted much attention in recent years.

Unlike electrical integration, where silicon is the technological platform of choice, photonic integration still relies on the coexistence of different material platforms, each with individual strengths and weaknesses. The indium phosphide (InP) platform [28], based on a direct bandgap III-V semiconductor, is ideal for building light sources and semiconductor optical amplifiers. In addition, efficient optical modulators, photodetectors, and passive elements have been demonstrated on the InP platform. Silicon photonics (SiP) has also emerged as a promising integration platform offering high integration density, high yield, and low cost by leveraging mature fabrication processes from complementary metal-oxide semiconductor (CMOS) microelectronics. However, silicon photonics currently does not offer light sources and efficient electro-optic (EO) modulators as InP does, because silicon is an indirect bandgap semiconductor without $\chi^{(2)}$-nonlinearity. Nonetheless, new heterogeneous [29] and hybrid integration techniques [30]–[33] have enabled

the use of III-V semiconductors together with silicon, and thus make silicon photonics an ideal candidate for building photonic integrated circuits (PIC).

Conventional WDM systems rely on arrays of discrete light sources which all need to be individually frequency-controlled. To this end, chip-scale optical frequency comb generators offer a particular advantage − instead of using independent light sources, tones of a single frequency comb can be used as carriers for the various WDM channels. Therefore, optical frequency combs can potentially offer a size and cost advantage. In addition, since the tones of frequency combs can be controlled by just two parameters − by the center frequency and by the free spectral range (FSR), combs offer a control advantage over an array of discrete light sources. Frequency combs have been also shown to be more power efficient at higher channel counts in comparison to an array of independent lasers [J4]. In the following sections, we will give an overview on different chip-scale frequency comb sources and discuss WDM demonstrations carried out with such devices.

2.2 Optical frequency combs

In this section, we give an overview on different chip-scale frequency comb generators and discuss the viability of these devices for massively parallel WDM with respect to important performance metrics for optical frequency combs in optical communications. These metrics will help to select the most suitable comb generator for a specific communication application and will build the base of a comparative discussion of different comb generator concepts in Section 2.2.3. Selected works showing high-capacity WDM transmission using optical frequency combs are presented.

The schematic of a frequency-comb spectrum is shown in Figure **2.6**. The comb consists of a set of narrowband spectral lines numbered by an integer index m, evenly spaced in frequency around a central line with frequency f_c. The comb line frequencies $f_m = f_c + m f_r$ are hence fully determined by the center frequency f_c and by the so-called free spectral range (FSR) f_r, which is equivalent to the repetition frequency of the time domain optical pulses emitted

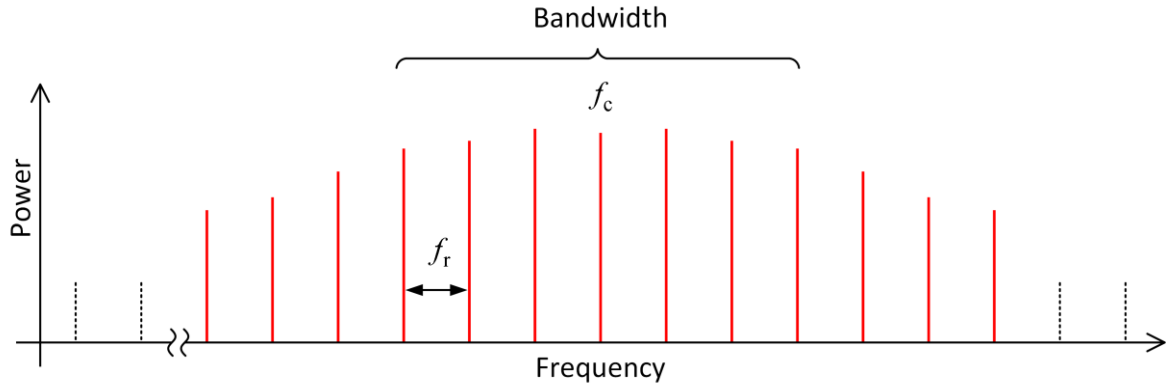

Figure 2.6: Schematic illustration of an optical frequency comb spectrum. The comb consists of a set of narrow-band tones that are evenly spaced by the repetition frequency f_r of the time domain optical pulses. The quantity f_c denotes the center frequency of the comb.

by the frequency comb source. The center frequency is usually defined as the frequency of the comb line near the middle of the used spectral bandwidth of the comb, see Figure 2.6.

2.2.1 Properties of optical frequency combs

2.2.1.1 Center frequency, line spacing, and line count of frequency combs

The choice of the center frequency depends essentially on the link length and on the data rate. If chromatic dispersion of standard single-mode fibers is an issue, light sources operating close to the zero-dispersion wavelength 1.3 µm are desirable. However, if minimum fiber attenuation and the availability of widely used telecommunication devices like erbium-doped fiber amplifiers are important, a center wavelength near 1.55 µm is preferable.

The frequency spacing of the comb lines should be tens of gigahertz and adhere to the ITU standard for WDM transmission specifying line spacings of 12.5 GHz, 25 GHz, 50 GHz, or 100 GHz and integer multiples thereof. For isolated point-to-point links, e.g., in proprietary data-center networks, the line spacing could also deviate from the ITU standards. In general, comb generators with tunable line spacing provide highest flexibility.

Finally, the number of lines is a crucial parameter, dictating the number of WDM channels that can be transmitted or detected in parallel. Note that there is no generally accepted metric for quantifying the line count of a frequency comb – publications may refer to the number of lines within the 3 dB-bandwidth [34], [35] or the 10 dB-bandwidth [36] of the comb or to the number of lines that were usable for data transmission [5], [18]. As the total comb power is generally limited, the individual lines will have lower power as the number of lines increases. For large line counts, optical amplifiers are needed to boost the optical power prior to modulation, and this will have direct impact on the achievable optical signal-to-noise power ratio (OSNR) of the WDM transmitter, see the Subsection 2.2.1.3 below. The optical amplifier bandwidth may additionally limit the number of usable tones if the comb is amplified as a whole.

2.2.1.2 Optical linewidth and relative intensity noise

The performance of comb-based WDM systems does not only depend on the number and the spacing of the carriers, but also on their power as well as on the phase and the amplitude noise. In optical communication systems that rely on advanced modulation formats, the phase of the optical carrier is also used to transmit information, and phase noise may have detrimental effects on the signal quality. Phase noise is usually quantified by the linewidth Δf of the carrier as an easy-to-handle figure of merit. Note that this parameter does not reveal the complete statistical characteristics of the phase noise that can, e.g., be obtained from the so-called FM noise spectrum [37]. Strictly speaking, the linewidth Δf represents the spectral width of a Lorentzian spectral line that is associated with a white, i.e., frequency-independent FM noise spectrum. It does not account for an increase of the FM noise spectrum towards lower frequencies.

The impact of phase noise on the data transmission performance depends on the random change of the carrier phase during one optical symbol. Phase noise hence becomes less problematic at shorter symbol durations T_s, i.e., higher symbol rates. For a given modulation format and a chosen symbol rate, the linewidth requirements can therefore be expressed by the product of the carrier linewidth Δf and the symbol duration T_s. To quantify these requirements, the

Table 2.1: Maximum product $\Delta f T_s$ of linewidth Δf and symbol duration T_s for different modulation formats, leading to a 1dB OSNR penalty at a reference bit error ratio (BER) of 10^{-3} [38]. QPSK: Quadrature phase-shift keying, 16QAM: 16-state quadrature amplitude modulation, 64QAM: 64-state quadrature amplitude modulation.

Modulation format	$\Delta f T_s$
QPSK	4.1×10^{-4}
16QAM	1.4×10^{-4}
64QAM	4.0×10^{-5}

linewidth-induced penalty of the optical signal-to-noise power ratio (OSNR) for a reference bit error ratio (BER) of 10^{-3} is considered [38]. In general, the OSNR penalty is specified by the ratio of the OSNR that is actually required to achieve a certain reference BER in a real transmission setup and the OSNR that would theoretically be required in an ideal transmission setup without phase noise. Table 2.1 specifies the products of linewidth and symbol duration $\Delta f T_s$ corresponding to a 1dB OSNR penalty [38]. As expected, higher-order modulation formats are less tolerant to phase noise as more discrete phases need to be discriminated for correct detection of a symbol.

Besides phase noise, relative intensity noise (RIN) of the comb tones may additionally reduce the transmission performance. For WDM systems, the RIN of the individual comb lines is more important than the RIN of the comb as a whole. As an example, mode partition noise in quantum-dash mode-locked laser diodes results in spectral lines having a large RIN whereas the total comb power shows a much smaller RIN [39], [40]. This can be attributed to the fact that all lines are fed by the same gain medium and that the line powers are hence correlated such that a power increase in one line is compensated by a power decrease of other lines.

2.2.1.3 Comb-line power and OCNR

Besides phase noise and RIN of an individual comb line, additive noise arising from spontaneous emission in the comb source or in the amplifiers along the transmission link may impair the performance of a WDM system. The level of the additive noise background is generally quantified by the optical signal-to-

noise power ratio (OSNR), which is defined as the power ratio of the data signal to the noise power within a certain reference bandwidth B_{ref}. In the following, the OSNR is specified with respect to a constant reference bandwidth of $B_{\mathrm{ref}} = 12.5\,\mathrm{GHz}$, corresponding to a reference wavelength span of 0.1 nm at a center wavelength of $1.55\mu\mathrm{m}$, see Appendix A.2 for a more detailed explanation. The OSNR within the reference bandwidth can be translated into the signal-to-noise power ratio $\mathrm{OSNR}_{\mathrm{sig}}$ that refers to the actual bandwidth B of a specific data signal by means of Eq. (A.8) in Appendix A.2.

The performance of a WDM system is eventually quantified by the optical signal-to-noise ratio at the receiver, which is denoted as $\mathrm{OSNR}_{\mathrm{Rx}}$ and which depends both on the comb line power P_ℓ and on the optical carrier-to-noise power ratio (OCNR) of the comb line OCNR_ℓ. In analogy to the OSNR, the OCNR_ℓ relates the comb line power to the power of the background noise, measured again within a reference bandwidth B_{ref} centered at the comb line frequency. Comb line power, OCNR and additional noise added by optical amplifiers along the link determine the $\mathrm{OSNR}_{\mathrm{Rx}}$ of a WDM channel and thus limit the link reach, restrict the choice of the modulation format, and set the maximum symbol rate. For a quantitative analysis, consider the WDM link depicted in Figure 2.7a consisting of a WDM transmitter, a link with $\nu_{\max}$ fiber spans, and a WDM receiver. Note that the comb line powers P_ℓ of most chip-scale comb generators are usually much weaker than the power levels emitted by state-of-the-art continuous-wave laser diodes as used in conventional WDM systems. It is therefore necessary to amplify the comb tones prior to modulation by sending them through a dedicated comb amplifier with gain G_0. Data is encoded onto the various carriers by a WDM modulator unit (WDM mod.), comprising a WDM demultiplexer, an array of dual-polarization in-phase/quadrature modulators (IQ modulators), and a WDM multiplexer, see Figure **1.1**a. The power transmission factor of the WDM modulator unit is denoted as g_0 and accounts for the insertion losses of the multiplexer and the demultiplexer as well as for the insertion and modulation losses of the IQ modulators. The WDM signal is then boosted by a post-amplifier with gain G_1 and transmitted through a fiber link of at least one span, where each of the

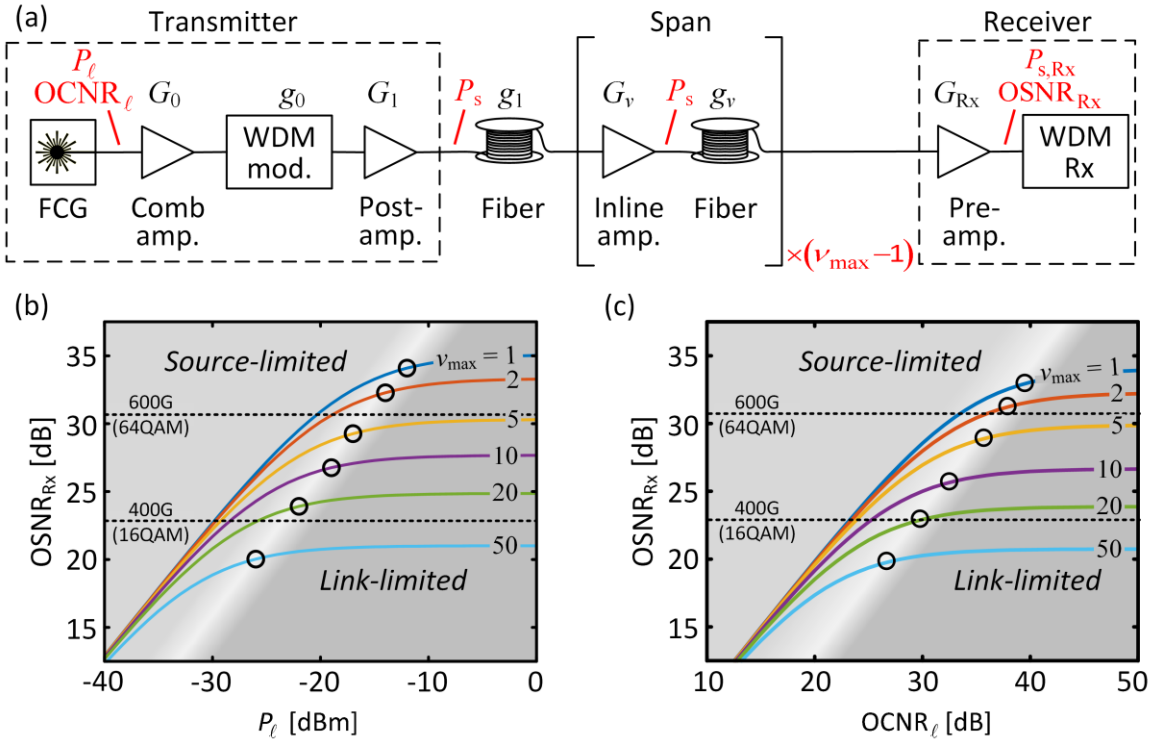

Figure 2.7: Influence of the comb line power P_ℓ and of the carrier-to-noise power ratio OCNR$_\ell$ on the achievable optical signal-to-noise power ratio OSNR$_{Rx}$ at the receiver for different numbers ν_{max} of spans. **(a)** Schematic of a WDM transmission and reception system. The comb lines are first amplified by a comb amplifier ('Comb amp.') before data is encoded on each line in the WDM modulation unit ('WDM mod.'). The WDM signal is then boosted by a post-amplifier ('Post-amp.') and transmitted through the fiber link consisting of at least one span. Each of the $\nu_{max}-1$ additional spans contains an in-line amplifier ('Inline amp.') which compensates the loss of the corresponding fiber section. The data from each WDM channel are recovered at the WDM receiver ('WDM-Rx'), which contains an optical pre-amplifier ('Pre-amp'). **(b)** OSNR$_{Rx}$ as a function of P_ℓ in the limit of high OCNR$_\ell$. The plot reveals two regimes: For source-limited transmission at low line powers, the OSNR$_{Rx}$ is dominated by the contribution of the comb amplifier, whereas the contributions of the various amplifiers along the link dominates for link-limited transmission at high line powers. The transition between both regimes is indicated by black circles, which mark the points where the OSNR$_{Rx}$ has decreased by 1 dB in comparison to its limit at high comb line powers P_ℓ. The dashed horizontal lines indicate the minimum OSNR$_{Rx}$ required for transmission of a net data rate of 400 Gbit/s using 16QAM and of 600 Gbit/s using 64QAM as a modulation format. **(c)** OSNR$_{Rx}$ as a function of OCNR$_\ell$ for comb line powers P_ℓ that correspond to the transition points marked by circles in Subfigure (b). For low OCNR$_\ell$, OSNR$_{Rx}$ is dominated by the noise of the comb source, and the link performance is source-limited. For high OCNR$_\ell$, the OSNR$_{Rx}$ is independent of the OCNR$_\ell$, and the transmission performance is link-limited.

($\nu_{\max}-1$) additional spans contains an in-line amplifier and a fiber section. Each of the fiber sections attenuates the signal power by a factor $g_\nu<1$, which is compensated by the gain $G_\nu=1/g_\nu$ of the post-amplifier or the corresponding inline amplifier, $\nu=1...\nu_{\max}$. For simplicity, the signal power P_s of a single WDM channel is assumed to be 0 dBm at the beginning of each fiber span, offering a good compromise between nonlinear impairments of the data channels and OSNR [41], [42]. All spans are assumed to be identical, $G_\nu=G$, $g_\nu=g$, $Gg=1$, and all amplifiers have the same noise figure $F_\nu=F$. At the receiver, a pre-amplifier with gain G_{Rx} and noise figure F_{Rx}, amplifies the received signal. A WDM receiver, comprising a WDM demodulator unit (WDM demod.) and a FCG is used to recover the transmitted data, see Figure **1.1**b. For simplicity, the gain and the noise figure of the receiver pre-amplifier is assumed to be identical to that of the in-line amplifiers, leading to a signal power of 0 dBm per wavelength channel at the input of the receiver DEMUX. Note that for a high number of spans, the noise of the receiver pre-amplifier does not play a role any more, since the noise background is dominated by the contributions from the various amplifiers along the link. Note also that the additive noise background of the LO comb tones can be neglected with respect to that of the received signal. The amplitude noise of the LO comb is hence not considered further in the subsequent analysis.

To obtain the $\mathrm{OSNR}_{\mathrm{Rx}}$ for a single WDM channel at the receiver, the ratio of the received signal power and the noise power in the reference bandwidth B_{ref} needs to be calculated, see Appendix A.1 for a detailed mathematical description. For a given line power P_ℓ and OCNR_ℓ, the $\mathrm{OSNR}_{\mathrm{Rx}}$ can be expressed as

$$\mathrm{OSNR}_{\mathrm{Rx}}=\frac{g_0G_0P_\ell}{\underbrace{\frac{g_0G_0P_\ell}{\mathrm{OCNR}_\ell}}_{\text{ampl. FCG noise}}+\underbrace{hfB\left(g_0(G_0-1)F_0+g\nu_{\max}(G-1)F+\frac{(G_{\mathrm{Rx}}-1)}{G_{\mathrm{Rx}}}F_{\mathrm{Rx}}\right)}_{\text{amplifier noise}}}. \quad (2.7)$$

In this relation, the quantity hf is the photon energy of the comb line under consideration. Equation (2.7) is the foundation of Figure 2.7b, which shows the $\mathrm{OSNR}_{\mathrm{Rx}}$ as a function of the line power P_ℓ and the number $\nu_{\max}$ of fiber spans

for a realistic comb-based WDM system. For this plot, the OCNR_{ℓ} of the comb lines is assumed to be infinite, i.e., the FCG itself does not introduce any practically relevant additive noise background. This can, e.g., be accomplished by Kerr comb generators. The various parameters used for this study are specified in Table 2.2. For the WDM modulator unit, an overall insertion loss of 25 dB is assumed, comprising 3.5 dB of insertion loss each for the WDM demultiplexer and the multiplexer [43], 13 dB of loss for the dual-polarization IQ modulators [44], and an additional 5 dB of modulation loss, which are assumed to be independent of the modulation format for simplicity. Note that the results shown in Figure 2.7b do not change significantly when varying these losses by a few dB. The fiber spans are assumed to feature a power loss of 15 dB each, corresponding to 75 km of single-mode fiber with a propagation loss of 0.2 dB/km. The power loss of each span is exactly compensated by the 15 dB gain of the corresponding post-amplifier or in-line amplifier. The gain G_0 of the comb amplifier is adjusted such that this launch power is reached after the post-amplifier.

Table 2.2: Model parameters used for generating Figure 2.7b, c from Eq. (2.7). The fiber attenuation g_ν, amplifier gain G_ν, and noise figures F_ν are assumed to be the same for all $\nu_{\max}$ fiber links ($\nu = 1...\nu_{\max}$).

Variable	Description	Value	
B_{ref}	Reference bandwidth for OSNR and OCNR calculation	12.5 GHz	
P_{s}	Signal power in a single WDM channel at the input of each fiber span	1 mW	(0 dBm)
g_0	Power transmission factor of WDM modulator unit	3.2×10^{-3}	(−25 dB)
G_0	Power gain factor of comb amplifier	$P_{\mathrm{s}}/(P_{\ell} g_0 G)$	
F_0	Noise figure of comb amplifier	3.2	(5 dB)
$g_\nu = g$	Power transmission factor of fiber section	3.2×10^{-2}	(−15 dB)
$G_\nu = G = g^{-1}$	Power gain factor of post- and inline-amplifier	32	(15 dB)
$F_\nu = F$	Noise figure of post- and inline-amplifiers	3.2	(5 dB)
G_{Rx}	Power gain factor of pre-amplifier	32	(15 dB)
F_{Rx}	Noise figure of pre-amplifier	3.2	(5 dB)

For low line powers P_ℓ, Figure 2.7b shows that the noise level at the receiver is dominated by the contribution of the comb amplifier. As a consequence, the $\mathrm{OSNR}_{\mathrm{Rx}}$ increases in proportion to P_ℓ and is essentially independent of the span count $\nu_{\max}$. In this regime, transmission performance is limited by the comb source and its associated amplifier ("source-limited"). For high comb line powers P_ℓ, in contrast, the noise level at the receiver is dominated by the contributions of the various amplifiers along the link ("link-limited"). In this regime, the $\mathrm{OSNR}_{\mathrm{Rx}}$ is essentially independent of P_ℓ and decreases with each additional span. The transition between both regimes is indicated by black circles in Figure 2.7b, indicating the points where the $\mathrm{OSNR}_{\mathrm{Rx}}$ has decreased by 1 dB in comparison to its limit at high line power P_ℓ. When using frequency combs in WDM systems, operation in the link-limited regime is preferred. Depending on the number of spans, this requires a minimum comb line power between $-25\,\mathrm{dBm}$ and $-15\,\mathrm{dBm}$. Note that, in principle, the gain G_1 of the post-amplifier could be decreased by increasing the gain G_0 of the comb amplifier. For source-limited transmission, the overall impact would be small since the $\mathrm{OSNR}_{\mathrm{Rx}}$ is mainly dictated by the comparatively low line power P_ℓ that enters the comb amplifier. For link-limited transmission over a small number of spans, the $\mathrm{OSNR}_{\mathrm{Rx}}$ can be slightly improved by approximately 2 dB by decreasing the gain G_1 and increasing the gain G_0 while maintaining realistic power levels at the output of the comb amplifier.

Figure 2.7b can be used as a guide for estimating the performance requirements for comb sources in WDM applications. As a reference, the plot indicates the minimum $\mathrm{OSNR}_{\mathrm{Rx}}$ required for transmission of a net data rate of 400 Gbit/s and 600 Gbit/s per WDM channel, using 16QAM and 64QAM as a modulation format, respectively. In both cases, advanced forward-error correction schemes with 11 % overhead and BER thresholds of 1.2×10^{-2} [45] are assumed, requiring a symbol rate of 56 GBd to provide the specified net data rates.

For many practically relevant comb sources, their finite OCNR_ℓ will further decrease the transmission performance. Figure 2.7c shows the $\mathrm{OSNR}_{\mathrm{Rx}}$ as a function of OCNR_ℓ for various span counts $\nu_{\max}$. In this plot, the comb line power P_ℓ was assumed to correspond to the minimum value required for link-

limited transmission, as indicated by the corresponding transition points in Figure 2.7. For low OCNR_ℓ, the noise level at the receiver is dominated by the noise background of the comb source, and the OCNR_ℓ and $\mathrm{OSNR}_{\mathrm{Rx}}$ are essentially identical. In this case, the link performance is again source-limited. For high OCNR_ℓ, the $\mathrm{OSNR}_{\mathrm{Rx}}$ is independent of the OCNR_ℓ, and the transmission performance is link-limited. Depending on the number of spans, the minimum OCNR_ℓ values needed for link-limited transmission range between 25 dB and 40 dB. The transition between both regimes is again marked by black circles in Figure 2.7c, indicating the points where the $\mathrm{OSNR}_{\mathrm{Rx}}$ has decreased by 1 dB in comparison to its respective limit at high OCNR_ℓ.

2.2.2 Chip-scale optical frequency comb generators

Besides the performance parameters discussed in the previous section, comb generators have to provide compact footprint and be amenable to cost-efficient mass production to qualify as light sources in highly scalable WDM transceivers. In this context, chip-scale devices or assemblies are of particular interest. This section provides an overview and a comparative discussion of different concepts for chip-scale comb generators.

2.2.2.1 Mode-locked laser diodes

The phenomenon of mode-locking was first observed [46]–[48] and theoretically explained [49]–[51] in the 1960s and subsequently became the foundation of pulsed femtosecond solid-state lasers [52]–[54]. A mode-locked laser emits a regular train of pulses that are spaced by the repetition period T_r in the time domain, corresponding to a broad frequency comb with free spectral range $f_r = T_r^{-1}$ in the frequency domain. In general, mode-locking requires an active medium with an inhomogeneously broadened gain spectrum that allows different longitudinal modes to oscillate simultaneously in the laser cavity, in combination with an additional mechanism that establishes a fixed phase relationship between these modes. The line spacing of the comb is then dictated by the free spectral range of the cavity, which is the inverse of the cavity round-trip time. For line spacings of tens of GHz as used in WDM applications, so-called passive mode-locking techniques are particularly important [55], offering

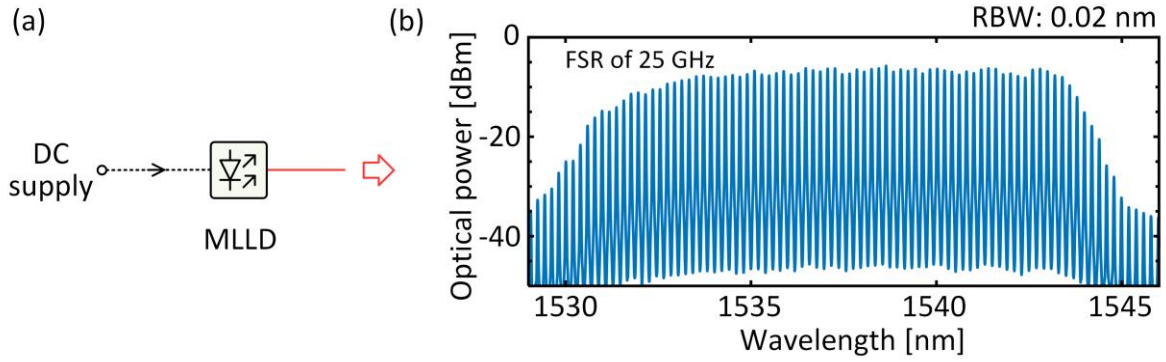

Figure 2.8: Concept of frequency comb generation in mode-locked laser diodes that rely on InAs/InGaAsP quantum dashes as an active material. **(a)** Quantum-dash mode-locked laser diodes (QD-MLLD) stand out due to easy operation – a frequency comb can simply be generated by driving the device with a DC pump current. **(b)** QD-MLLD can generate combs with broad and smooth spectral envelopes, featuring 3 dB-bandwidths well in excess of 1 THz, which corresponds to a wavelength span of approximately 10 nm at a center wavelength of 1.55 µm. The line power amounts to approximately −10 dBm

stable device operation at manageable technical complexity. In general, passive mode-locking requires a nonlinear optical element that allows the various optical modes to interact.

Regarding mode-locked lasers as multi-wavelength light sources for WDM transmission, experimental demonstrations were mainly based on devices that exploit low-dimensional structures of III-V semiconductors such as quantum dashes and quantum dots as active media. Quantum-dash mode-locked laser diodes (QD-MLLD) rely on four-wave mixing, or cross-gain modulation as passive mode-locking mechanisms [22], [56]. The devices can be operated by a simple DC current, Figure **2.8**a, and provide a relatively flat comb spectrum that may span 3 dB-bandwidths in excess of 1 THz, see Figure **2.8**b. QD-MLLD have been realized with repetition rates from 10 GHz [57], [58] to more than 300 GHz [59], dictated by the cavity length of the respective device. The simple operation and the compact footprint of QD-MLLD in combination with the comparatively broad and smooth spectral envelope of the associated combs make these devices promising candidates for particularly compact WDM transceivers. In communication experiments, QD-MLLD have been shown to allow for WDM transmission of more than 50 channels and data rata rates in

excess of 10 Tbit/s [J2]. These experiments also revealed strong low-frequency phase noise of the QD-MLLD as one of the main limitations of transmission performance, see Section 2.2.3 for more details. If this problem can be overcome, e.g., by advanced digital phase-tracking techniques [10] or external optical feedback, see Chapter 4 [J2], comb line powers of the order of −10 dBm [60], [61], Figure **2.8**b, and OCNR values in excess of 40 dB would allow for link-limited transmission using QD-MLLD in realistic WDM systems, see Figure 2.7b,c.

2.2.2.2 Electro-optic modulators for comb generation

Frequency combs may also be generated by periodic modulation of a continuous-wave (CW) laser tone, using high-speed electro-optic modulators, see Figure **2.9**a for an illustration of the concept. The output of a CW laser is fed into a single EOM or a series thereof. The EOM are usually driven with a sinusoidal electrical signal from a radio frequency (RF) oscillator. This leads to modulation sidebands at the output of the EOM, which are spaced by the fundamental frequency of the RF drive signal. Over the last years, various approaches have been explored to improve the spectral bandwidth and flatness of EOM-based combs [62], which are generally limited by the modulation depth that can be achieved in the various EOM. These approaches have relied on asymmetrically driven Mach-Zehnder modulators [63] or cascades of intensity and phase modulators [64], [65]. Figure **2.9**b gives an example of a comb spectrum generated in such a cascade, featuring approximately 30 lines within a 3 dB bandwidth of approximately 900 GHz, corresponding to a wavelength span of 8 nm [64]. Note, however, that these demonstrations were still obtained with conventional lithium niobate ($LiNbO_3$) modulators in benchtop-type laboratory setups. While the concept is clearly amenable to chip-scale integration, the performance of integrated modulator-based comb generators is still inferior to that of the discrete counterparts. Integrated modulator-based comb generators have been demonstrated on the indium phosphide (InP) [66]–[68] and the silicon photonic [12], [18], [69] platform. Using an integrated silicon-organic hybrid (SOH) modulator, combs with up to 7 lines in a 3 dB

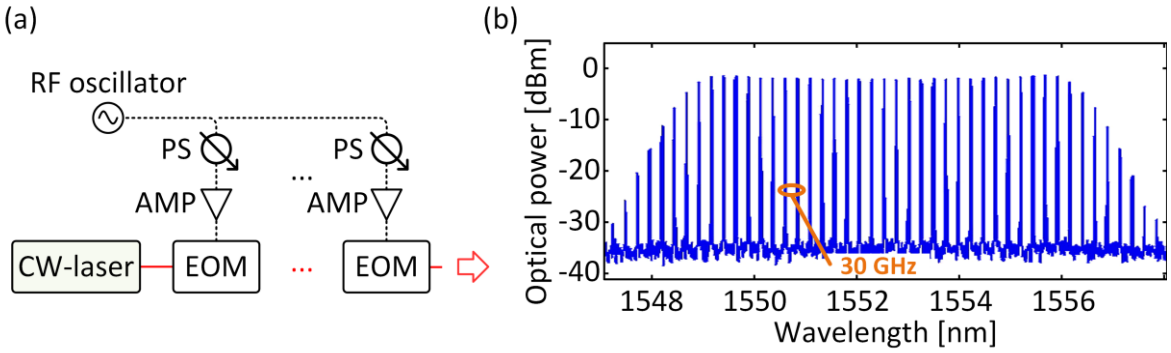

Figure 2.9: Optical frequency comb generation using single or cascaded electro-optic modulators (EOM). **(a)** Schematic of the comb generator. The output of a continuous-wave (CW) laser is sent through a single EOM or through a cascade of EOM. The EOM are driven by sinusoidal signals that are derived from a common RF oscillator and that are carefully adjusted in amplitude and phase. This allows for generation of comparatively broadband combs with flat spectral envelopes; AMP: RF amplifier; PS: RF phase shifter. **(b)** Example spectrum of a frequency comb generated by cascading a lithium-niobate ($LiNbO_3$) phase and intensity modulator in a benchtop type setup [64]. EOM-based com generators are amenable to chip-scale integration [12], [18], [66], [68], [69]. (Adapted from [64]. © 2014 Elsevier.)

bandwidth of 280 GHz and WDM data rates of up to 1 Tbit/s were demonstrated [18]. Assuming that the performance of integrated modulator-based comb generators may be improved to match that of their discrete-element counterparts in the future, line powers in excess of -10 dBm, Figure **2.9**b [64], might make link-limited transmission a realistic scenario provided that the corresponding OCNR requirements according to Figure 2.7c can be met.

Modulator-based comb generators stand out due to their flexibility: The center frequency can be adjusted by simply tuning the emission wavelength of the CW laser, and the FSR can be set via the RF modulation frequency. However, they suffer from the limited number of lines as well as from the comparatively high complexity that is associated with driving a multitude of modulators with RF signals of precisely defined amplitude and phase. Modulator-based comb generators might therefore be a viable option for transmission of WDM superchannels with a limited number of lines and flexible line spacing.

2.2.2.3 Gain-switched laser diodes

Another technique for generating frequency combs with tunable line spacing relies on gain switching of a semiconductor laser diode that is injection-locked by a CW master laser. Figure **2.10**a shows the concept of comb generation in a gain-switched laser diode (GSLD). A semiconductor slave laser is biased close to its threshold and driven by a sinusoidal signal from an RF oscillator. This periodically brings the carrier concentration in the active zone of the slave laser from below to above the lasing threshold, thus generating a train of strongly chirped optical pulses with a repetition rate corresponding to the RF modulation frequency. External injection of CW light emitted from a master laser is used to establish phase coherence between the generated pulses, thus leading to a frequency comb with discrete narrowband lines [21], see Figure **2.10**b. The bandwidth of the comb is dictated by the intrinsic relaxation dynamics of photons and electrons in the slave laser. The injection also increases the relaxation frequency of the semiconductor lasers, enabling the generation of frequency combs with a larger FSR as compared to the case without external

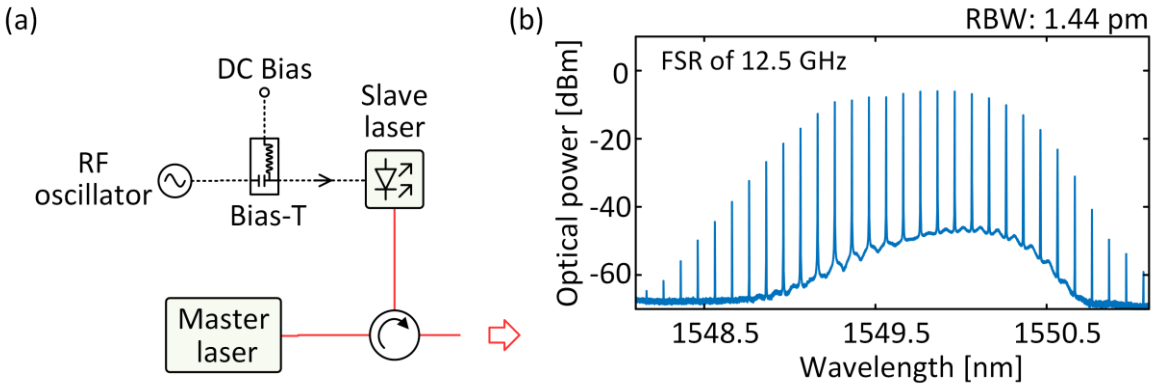

Figure 2.10: Optical frequency comb generation by gain-switched laser diodes (GSLD). **(a)** Schematic setup. A semiconductor laser, biased close to threshold, is driven by a sinusoidal signal from an RF oscillator. This leads to a train of chirped output pulses with a repetition rate determined by the frequency of the RF drive signal. External injection of CW light from a master laser establishes phase coherence between the pulses and hence allows for frequency comb formation. **(b)** Spectrum of the frequency comb from a gain-switched DFB slave laser. Taking into account the 1.44 pm resolution bandwidth of the optical spectrum analyzer (OSA), an OCNR of approximately 30 dB can be estimated from the spectrum – a typical value for GSLD-based combs.

injection [70]. In this scheme, the linewidth and RIN characteristics of the master laser are transferred to each of the comb lines [71]. This allows for generation of low-noise frequency combs by using a master laser with low linewidth and small RIN.

For frequency combs from GSLD, both the center frequency and the FSR can be adjusted by tuning the emission wavelength of the master laser and by adjusting the RF modulation frequency [72]. GSLD-based frequency combs typically cover 3 dB-bandwidths of approximately 200 GHz and provide line spacings of up to 20 GHz along with typical line powers of the order of −10 dBm [16], [21]. Using GSLD-based combs, WDM transmission on 24 channels with data rates of up to 2 Tbit/s was reported [16]. Note that these demonstrations were still performed with benchtop-type GSLD setups built from discrete devices. Integration of the slave and the master laser on a common InP chip has been demonstrated [73], but the performance is currently still inferior to that of a discrete-element setup. Note also that the overall transmission performance of GSLD-based combs in WDM is not only limited by the line spacing and the number of lines, but also by the OCNR values that typically amount to approximately 30 dB [J1], [16]. According to Figure 2.7c, the transmission performance might then be limited by the source rather than by the transmission link itself.

2.2.2.4 Kerr-nonlinear waveguides for spectral broadening

One of the most stringent limitations of the comb sources discussed in the previous sections is the limited number of carriers. A potential solution to this problem is spectral broadening of narrowband seed combs using waveguides with strong third-order nonlinearities such as self-phase modulation (SPM), cross phase modulation (XPM), and four-wave mixing (FWM). This concept has been exploited for WDM communications using benchtop-type comb generators in combination with highly nonlinear fibers (HNLF) for spectral broadening [74], [75]. However, for generating flat comb spectra, these schemes often rely on delicate schemes for dispersion management [74] or spectral stitching [75], that usually require intermediate fiber amplifiers and that are

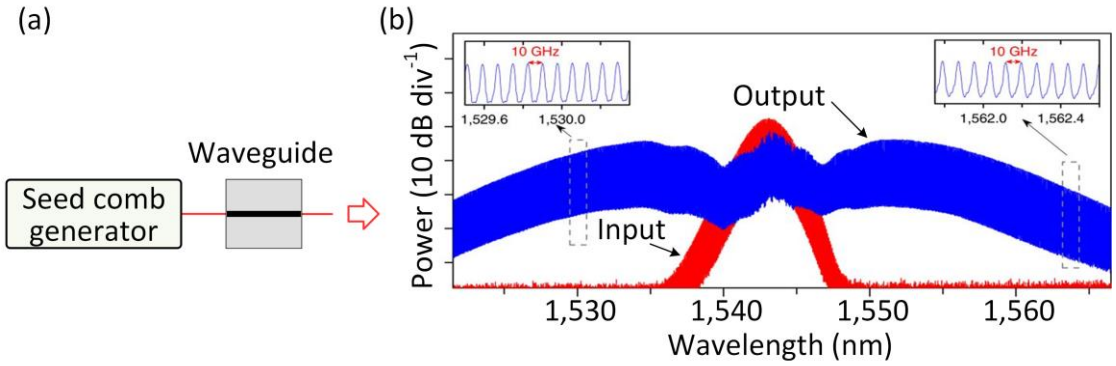

Figure 2.11: Integrated Kerr-nonlinear waveguides for spectral broadening of narrowband seed combs. **(a)** Schematic setup. A narrowband seed comb is coupled to an integrated optical waveguide with high Kerr nonlinearity. Self-phase modulation (SPM) and cascaded four-wave mixing (FWM) leads to a broadband comb. **(b)** Spectra of seed frequency comb at the input and of the broadened comb at the output of an aluminum-gallium-arsenide-on-insulator (AlGaAsOI) waveguide, pumped by a solid-state mode-locked laser [13]. (Adapted from [13]. © 2018 Springer.)

hence not amenable to chip-scale integration. This can be overcome by using Kerr-nonlinear integrated optical waveguides for spectral broadening instead of HNLF [13], [76], [77]. The viability of integrated Kerr-nonlinear waveguides (KNWG) for spectral broadening has been demonstrated by using low-loss aluminum-gallium-arsenide-on-insulator (AlGaAsOI) waveguides that feature high nonlinearity parameters of up to 660 $(Wm)^{-1}$. These devices allow for generation of more than 300 densely spaced carriers within the telecommunication C-band (1530 nm … 1565 nm), offering a WDM transmission capacity of 22 Tbit/s [13]. The underlying comb generation scheme is summarized in Figure **2.11**a, and the corresponding spectra are shown in Figure **2.11**b. Line powers of more than –15 dBm make this approach promising for link-limited transmission, see Figure 2.7b. Since spectral broadening of combs in Kerr-nonlinear waveguides works independently of the seed-comb line spacing and – within limitations – independently of the center wavelength, the approach could be particularly interesting for broadband comb generation with tunable FSR and center frequency. Note that in the experiments published so far [13], the seed comb was still generated by a solid-state mode-locked laser with a repetition rate of 10 GHz followed by an erbium-doped fiber

amplifier to achieve sufficient launch power into the integrated waveguide. Moreover, spectral stitching was used to achieve a flat and high-quality frequency comb for the data transmission demonstration. Transferring this concept to a chip-scale assembly would require co-integration of all these elements.

2.2.2.5 Microresonator-based Kerr-comb generators

A particularly promising option to generate frequency combs in chip-scale devices relies on resonantly enhancing Kerr-nonlinear interaction in integrated optical waveguides. This leads to the concept of Kerr comb generation in micro-ring resonators [78], [79], which is illustrated in Figure **2.12**a. A high-*Q* resonator is resonantly pumped by a CW laser, thus producing a strong intra-cavity power. Under appropriate conditions, degenerate and non-degenerate four-wave mixing leads to formation of new spectral lines by converting pairs of pump photons into pairs of photons that are up-shifted and down-shifted in frequency. The broadband nature of parametric gain can be used to convert the CW pump into octave-spanning combs, without the need for any additional spectral broadening [80]. Over the previous years, comb generation has been demonstrated in a variety of different Kerr-nonlinear microresonators, comprising silica toroidal cavities [78], crystalline whispering-gallery mode microresonators [81], as well as silicon nitride (Si_3N_4) ring resonators [79], [82], which are particularly well suited for wafer-level mass production [79].

Of particular interest for WDM applications are so-called single dissipative Kerr soliton (DKS) states, which consist of only one ultra-short pulse circulating around the microresonator. This leads to broadband combs with particularly smooth spectral envelopes [83], [84]. An example of a DKS comb spectrum is shown in Figure **2.12**b. The comb offers more than 100 carriers spaced by approximately 100 GHz within the telecommunication C and L-band (1530 nm … 1610 nm) [J4]. In the center of the comb, the line powers reach –11 dBm, and the OCNR amounts to approximately 48 dB [J4]. This would safely permit link-limited transmission in realistic WDM systems. Towards the edges of the C and L-band, the line powers still drop to slightly lower levels, requiring further device improvements.

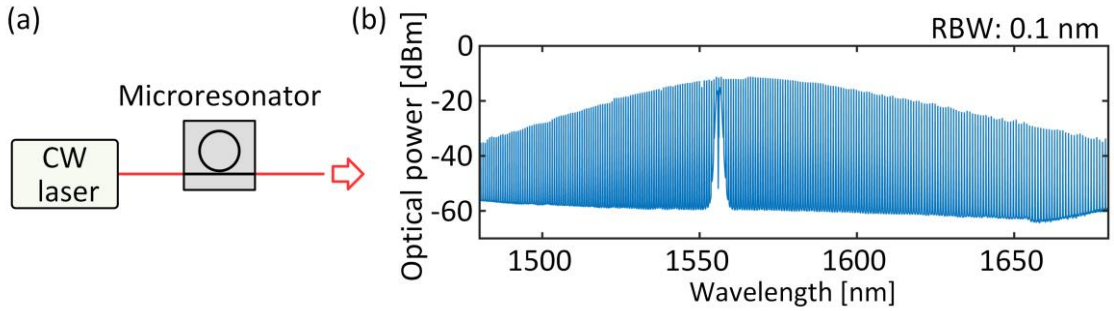

Figure 2.12: Kerr comb generation in high-*Q* microresonators. **(a)** Principle of Kerr comb generation. A high-*Q* microring resonator is pumped by a continuous-wave (CW) laser. Under appropriate conditions, degenerate and non-degenerate four-wave mixing leads to formation of new spectral lines. Of particular interest for optical communications are so-called single dissipative Kerr soliton (DKS) states, for which the superposition of the phase-locked optical tones forms an ultra-short soliton pulse circulating in the cavity. This leads to a comb spectrum with a broadband smooth envelope. **(b)** Spectrum of a DKS frequency comb generated in a Si_3N_4 microresonator [J4]. The comb offers more than 100 carriers in the telecommunication C and L-band (1530 nm … 1610 nm), spaced by approximately 100 GHz. In the center of the spectrum, the comb line power amounts to −11 dBm, and the OCNR is approximately 48 dB. (Adapted from [J4].)

For the WDM transmission experiments demonstrated so far, DKS comb generation has still relied on benchtop-type setups with high-power EDFA that provide CW pump powers of more than 30 dBm at the input of the microresonator chip [J4]. For chip-scale integration of WDM transceiver modules, these power levels must be reduced. In this context, improvement of microresonator fabrication is key, allowing to increase the quality-factors (Q-factors) of the cavities and thus to enable single-soliton comb formation at pump powers down to a few milliwatts [85]–[87], which can be provided by a co-integrated light source [87], [88]. Even though the output power levels of these comb generators is still below the threshold of link-limited transmission, the experiments show the great potential of reducing the pump-power requirements of Kerr comb sources by improved design and fabrication techniques.

2.2.3 Comparative discussion

Chip-scale comb sources have been used in a variety of WDM transmission experiments, relying on different comb generation approaches and covering a wide range of data rates, channel counts, and line spacings. Table 2.3 gives an overview on selected examples of such demonstrations, specifying the type of comb source along with the number of lines, the maximum and minimum power of the native comb lines, as well as the spacing f_r, and the intrinsic optical linewidth Δf of the comb lines used for transmission, see Column 1 … 5 of Table 2.3. Note that not all techniques of measuring the optical linewidth actually allow to directly extract the intrinsic linewidth that is associated with the spectrally white background of the FM noise spectrum [37]. Some of the values provided in Column 5 of Table 2.3 and in the associated references have therefore to be understood as an upper limit of the corresponding intrinsic linewidth. Columns 6 … 9 of Table 2.3 finally give the symbol rate, the modulation format, the aggregate net data rate, and the net spectral efficiency (SE) for dual-polarization WDM transmission. In this context, the net data rate refers to the usable rate for transmission of payload data after subtracting the overhead associated with the respective forward-error correction scheme. Note that the line powers in Column 3 refer to the native comb lines prior to any spectral flattening that is usually applied to achieve a more uniform spectrum of carriers. For link-limited transmission over a single-span WDM connection with realistic technical parameters, linepowers should not be less than approximately –12 dBm, see Figure 2.7. In some of the experiments [J1], [J4], chip-scale comb generators were used both as multi-wavelength light source at the transmitter and as multi-wavelength LO at the receiver – the corresponding data rates are marked with a star in the second column. Note that all experiments listed in Table 2.3 were performed at center wavelengths around 1550 nm, relying on the telecommunication C and L bands that are most commonly used for WDM transmission. However, the concepts may be also transferred to other wavelength ranges, e.g., around 1300 nm.

Table 2.3: Selected experimental demonstrations of wavelength-division multiplexing (WDM) transmission using different chip-scale frequency comb generators as multi-wavelength light sources. The third column specifies the maximum and the minimum power of the native comb lines, prior to any spectral flattening. The net data rate refers to the aggregate rate that is usable for transmission of payload data after subtracting the forward-error correction (FEC) overhead.
QD-MLLD – quantum-dash mode-locked laser diode, Section 2.2.2.1; EOM − electro-optic modulator, Section 2.2.2.2; GSLD − gain switched laser diode, Section 2.2.2.3; KNWG – Kerr-nonlinear waveguides for spectral broadening of narrowband seed comb, Section 2.2.2.4; Kerr comb – Comb generation in Kerr-nonlinear microresonators, Section 2.2.2.5; N.A. − values are not available.

Comb source	# lines	P_ℓ max/min	f_r [GHz]	Δf [MHz]	Sym. rate [GBd]	Mod. format	Net data rate [Tbit/s]	SE [bit/s/Hz]	Ref.
QD-MLLD	36	N.A.	34.5	< 4	12.5	QPSK	1.89	1.5	[9]
QD-MLLD	52	−5/−20	42.0	< 2	40.0	QPSK	7.74	3.5	[60]
QD-MLLD	60	−10/−20	25.0	< 0.1	20.0	32QAM	11.22	7.5	[J2]
EOM	5	5/−5	20.0	< 0.1	16.0	16QAM	0.75	7.5	[12]
EOM	9	−17/−27	40.0	< 0.1	28.0	QPSK	0.94	2.6	[18]
GSLD	6	−4/−7	12.5	0.3	12.0	QPSK	0.24	3.2	[17]
GSLD	13	−5/−20	12.5	< 0.1	12.0	16QAM/ QPSK	1.03*	5.2	[J1]
GSLD	24	−10/−30	12.5	< 0.1	12.0	16QAM/ QPSK	1.87	6.2	[16]
KNWG	320	−10/−30	10.0	< 0.1	40.0	16QAM	22.03[a]	6.9	[13]
Kerr comb	6	10/−10	690	< 0.1	20.0	16QAM	0.90	0.22	[14]
Kerr comb	20	0/−20	25.0	N.A.	18.0	QPSK	1.35	2.7	[11]
Kerr comb	20	10/−20	230	< 0.1	20.0	64QAM	4.04	0.88	[15]
Kerr comb	94	−10/−20	95.8	< 0.1	40.0	16QAM	28.0	3.1	[J4]
Kerr comb	179	−18/−28	95.8	< 0.1	40.0	16QAM/ QPSK	50.2[b]	5.2	[J4]
Kerr comb	93	−10/−20	95.8	< 0.1	50.0	16QAM	34.6*	3.9	[J4]

* These experiments rely on frequency combs both as multi-wavelength light source at the transmitter and as multi-wavelength LO at the receiver.
[a] The indicated data rate refers to the WDM capacity of a single-mode fiber core. In the experiment, WDM was combined with space-division multiplexing on 80 parallel fiber cores, leading to an overall data of 661 Tbit/s [13],
[b] The transmission experiment relies on interleaved frequency combs that were obtained from a pair of separate Kerr comb generators.

Among the various comb generation concepts, EOM-based approaches, GSLD and spectral broadening in KNWG allow for frequency comb generation with tunable line spacing. The same is true for spectral broadening in KNWG, provided that the tunability is supported by the seed comb generator. For these devices, the line spacings are typically below 50 GHz. In contrast to that, the line spacing of combs generated in QD-MLLD or Kerr-nonlinear microresonators is determined by the cavity length and can hence not be tuned over a significant range. However, these devices also allow to access large line spacings, which may range up to hundreds of gigahertz for very small cavities [89].

Comparing the demonstrated WDM transmission performances, EOM and GSLD are useful for aggregate WDM data rates up to a few Tbit/s at high spectral efficiency. The transmission capacity is mainly limited by the available number of lines and by the line spacing, which restricts the usable symbol rate. The number of lines can be increased by using QD-MLLD as light sources, leading to aggregate WDM data rates in excess of 10 Tbit/s [J2]. These light sources, however, may still suffer from comparatively strong phase noise, both in terms of intrinsic linewidth and with respect to a strong increase of the FM noise power towards small frequencies [60], [90], [91]. The strong phase noise has initially limited transmission demonstrations with QD-MLLD to rather simple modulation formats such as QPSK. Later experiments showed that these limitations may be overcome by dedicated phase-noise reduction schemes, relying, e.g., on feed-forward phase-noise compensation of the carrier prior to modulation at the transmitter [92], advanced digital phase tracking [10], or self-injection locking, which allows to reduce the optical linewidths from a few MHz to less than 100 kHz, see Chapter 4 [J2]. Note that the viability of these schemes has been demonstrated using benchtop-type experimental setups, and that chip-scale integration has not yet been addressed. Note also that frequency combs from QD-MLLD exhibit RIN due to mode partition noise [39], [40], but the impact on the performance of coherent transmission schemes is usually small, unless the comb is used as a multi-wavelength LO, see Chapter 5 [J3].

Regarding scalability to large WDM channel counts, Kerr combs and spectral broadening in KNWG appear as the most promising concepts. Both approaches were shown to permit generation of combs that span more than an octave of frequencies [77], [93], which would in principle allow to cover all optical telecommunication bands in the near infrared by a single device. Note, however, that spectral broadening in KNWG usually results in a comb with an irregular spectral envelope and may require spectral slicing techniques for high-performance WDM transmission [13]. In contrast to that, single DKS states lead to combs with smooth spectral envelopes that can be readily used for WDM transmission. Using a combination of two interleaved Kerr comb generators, WDM transmission with aggregate net data rates of more than 50 Tbit/s could be demonstrated, see Section 6.3 and [J4] for a more detailed description.

Another important aspect of the various comb sources is the power consumption and the wall-plug efficiency, i.e., the ratio of the optical output power of the comb and the associated electrical input power. In this respect, quantitative considerations are only available for few exemplary cases [J4], [16], [94] such that a broad comparison of different comb generation schemes is not possible. Qualitatively, QD-MLLD seem attractive not only due to their simple operation scheme, but also in terms of energy efficiency, converting a DC laser pump current directly into a frequency comb at the output of the device. In comparison to GSLD or EOM-based schemes, this avoids additional RF sources and amplifiers, that may easily feature power consumptions of a few Watts which come on top of the power consumption of the laser source [16], [68]. Moreover, QD-MLLD do not feature any lossy optical coupling interfaces that would decrease the overall efficiency. Regarding KNWG, a very good optical power conversion efficiency of 66% from the seed comb to the broadened comb at the device output is reported [13]. Note, however, that this does not account for generation of the seed comb and that the overall efficiency of KNWG-based comb generators is always worse than that of the underlying seed comb source , see Section C.6 [J4]. For Kerr combs, the main hurdle towards power-efficient operation is the optical conversion efficiency from the CW pump to the comb tones. Reported conversion efficiencies range from less than 1% up to 30% for bright and dark soliton combs, respectively [J4], [95]. Also here, this figure does

not account for the wall-plug efficiency of the CW pump laser, which might need to be complemented by an optical amplifier. Nevertheless, despite the rather low efficiency of the nonlinear conversion process, Kerr comb generators or devices based on spectral broadening in KNWG can reduce the overall power consumption of a WDM transceiver by eliminating the need for individual frequency control of a multitude of CW lasers, see Chapter 6 [J4].

3 Gain-switched laser diodes for terabit/s transmission and reception

This chapter explores gain-switched laser diode (GSLD) as multi-wavelength light sources both at the transmitter and receiver sides of a WDM link. It is taken from paper [J1], which was published in *Optics Express*. The material from the publication is reproduced here with the appropriate changes to fit the structure and notation of this thesis.

[*Beginning of paper [J1]*]

Copyright © 2016 Optical Society of America

Multi-wavelength coherent transmission using an optical frequency comb as a local oscillator

Optics Express, Volume 24, Issue 22, pp. 25432-22445, 2016
DOI: 10.1364/OE.24.025432

J. N. Kemal,[1] J. Pfeifle,[1] P. Marin-Palomo,[1] M. D. G. Pascual,[3] S. Wolf, [1] F. Smyth,[3] W. Freude,[1,2] and C. Koos[1,2]

[1] Institute of Photonics and Quantum Electronics (IPQ), Karlsruhe Institute of Technology (KIT), Germany
[2] Institute of Microstructure Technology (IMT), Karlsruhe Institute of Technology (KIT), Germany
[3] Pilot Photonics Ltd., Ireland

Steadily increasing data rates of optical interfaces require spectrally efficient coherent transmission using higher-order modulation formats in combination with scalable wavelength-division multiplexing (WDM) schemes. At the transmitter, optical frequency combs (OFC) lend themselves to particularly precise multi-wavelength sources for WDM transmission. In this work we demonstrate that these advantages can also be leveraged at the receiver by using an OFC as a highly scalable multi-wavelength local oscillator (LO) for coherent detection. In our experiments, we use a pair of OFC that rely on gain switching

of injection-locked semiconductor lasers both for WDM transmission and intradyne reception. We synchronize the center frequency and the free spectral range of the receiver comb to the transmitter, keeping the intradyne frequencies for all data channels below 15 MHz. Using 13 WDM channels, we transmit an aggregate line rate (net data rate) of 1.104 Tbit/s (1.032 Tbit/s) over a 10 km long standard single mode fiber at a spectral efficiency of 5.16 bit/s/Hz. To the best of our knowledge, this is the first demonstration of coherent WDM transmission using synchronized frequency combs as light source at the transmitter and as multi-wavelength LO at the receiver.

3.1 Introduction

Driven by increasing pressure on data-center and telecom operators to handle escalating traffic, optical interfaces with data rates of 400 Gbit/s are currently being standardized, and Tbit/s interfaces are already under discussion [96]–[98]. To keep symbol rates compliant with the electrical bandwidth of energy-efficient CMOS driver circuitry, a technical implementation of such interfaces requires higher-order modulation formats along with parallel transmission on a multitude of wavelength channels [99], [100]. In this context, optical frequency combs (OFC) lend themselves to particularly attractive sources to generate a number of well-defined wavelength-division multiplexing (WDM) carriers in a single chip-scale device. Unlike the carriers derived from a bank of individual lasers, the tones of a comb are intrinsically equidistant in frequency and can be controlled by just two parameters – by the center frequency and by the free spectral range (FSR). This enables transmission of orthogonal frequency division multiplexing (OFDM) [101] or of Nyquist-WDM [75] signals at highest spectral efficiency. In addition, stochastic frequency variations of the various comb lines are strongly correlated, which considerably facilitates compensation of impairments caused by nonlinearities of the transmission fiber in WDM links [8]. OFC with tunable center frequency and tunable FSR are of particular interest, enabling dynamic adaption of the symbol rate and the carrier spacing to the bandwidth demand and the required reach [102], [103]. Such

devices might be key to next-generation flex-grid networks as recommended by the International Telecommunication Union (ITU), ITU-T G.694.1.

OFC have previously been used as optical sources for WDM transmission, and a variety of experiments demonstrate Tbit/s line rates, both with integrated chip-scale devices [11], [16], [18], [104] and with systems that rely on conventional setups of discrete components [74], [75], [101]. However, most of these experiments still employ a high-quality single-wavelength external-cavity laser (ECL) as a local oscillator (LO) for channel-by-channel demodulation of the coherent signals. Simultaneous reception of all data channels in a practical transmission system would require an array of stabilized LO lasers corresponding to the number of transmitted carriers. The associated technical effort is considerable, in particular when it comes to large channel numbers. For massively parallel WDM systems, it might hence be highly attractive to leverage the scalability advantages of optical frequency combs also at the receiver side. In this context, different schemes have been discussed, using either phase-locked [105] or free-running [6], [106] LO combs. To achieve phase locking, dual-mode injection locking of a semiconductor laser was used [105]. However, this scheme does not allow for significant tuning of the FSR and is only applicable to comb sources which can be injection locked. Moreover, the associated experimental demonstrations were so far limited to data transmission over a single WDM channel at a comparatively low data rate of 316.5 Mbit/s using simple on-off-keying (OOK) as a modulation format. Regarding free-running LO combs, spectrally sliced signal processing was demonstrated to be a viable scheme for wideband coherent detection [107]. This scheme was used for reception of orthogonal frequency division multiplexing (OFDM) signals. In a first experiment [106], the OFDM signal was generated by modulating identical data on 32 comb lines spaced by approximately 10 GHz. A subset of spectral slices carrying approximately 100 Gbit/s of data was then successfully detected using an LO that consists of only two lines, spaced by approximately 40 GHz. In another work [6], spectrally sliced detection was used to receive a high-speed 214 GBd single-carrier dual-polarization quadrature phase shift keying (QPSK) signal within a bandwidth of 228 GHz, leading to a data rate of 856 Gbit/s and a spectral efficiency of

3.51 bit/s/Hz. In this scheme, the data signal was generated by advanced temporal interleaving using high-speed $LiNbO_3$ modulators, hence exploiting the scalability advantages of OFC only at the receiver side. In general, OFC-supported spectrally sliced detection represents a very powerful approach that allows a full reconstruction of arbitrary optical waveforms at bandwidths beyond those accessible by electronic signal processing. However, the scheme requires arrays of parallelized high-speed digitizers that are precisely synchronized, thereby limiting scalability with respect to larger channel counts. Moreover, the digital signal processing (DSP) required for waveform reconstruction goes significantly beyond that of conventional coherent receivers. This leads to considerable technical complexity that still appears prohibitive for implementation in current receiver systems.

In this work we demonstrate that OFC can be used as multi-tone LO for simultaneous coherent reception of WDM signals using arrays of independent digitizers and conventional DSP. In our experiment, we use a pair of OFC that rely on switching the gain of injection-locked semiconductor lasers for both WDM transmission and intradyne reception. We synchronize the center frequency and the free spectral range of the receiver comb to the transmitter, keeping the intradyne frequencies for all data channels below 15 MHz. In extension of our previous results [108], we use 13 WDM carriers to transmit an aggregate line rate (net data rate) of 1.104 Tbit/s (1.032 Tbit/s) over a 10 km long standard single mode fiber. Using two polarizations and a combination of QPSK and 16-state quadrature amplitude modulation (16QAM) to encode the data, we achieve a net spectral efficiency of 5.16 bit/s/Hz. We analyze the results based on measured phase-noise characteristics of both the transmitter and the receiver combs and show that the signal quality in our experiment is currently limited by the presence of high-frequency FM noise. Our experiment represents, to the best of our knowledge, the first demonstration of coherent WDM transmission using a pair of synchronized frequency combs as a multi-wavelength source at the transmitter and as a multi-wavelength LO at the receiver.

3.2 Comb-based coherent WDM transmission and reception

The basic setup for a WDM transmission link with optical frequency combs used both as a multi-wavelength source for the transmitter (Tx) and as a multi-wavelength local oscillator (LO) is shown in Figure 3.1. Free-running optical frequency comb sources (Tx comb, LO comb) with center frequencies $f_{\mathrm{Tx},0}$, $f_{\mathrm{LO},0}$ and free spectral ranges (FSR) $f_{\mathrm{r,Tx}}$, $f_{\mathrm{r,LO}}$ supply optical carriers to the WDM transmitter and to the LO. The LO comb must be synchronized in center frequency $f_{\mathrm{LO},0}$ and FSR $f_{\mathrm{r,LO}}$ to its Tx counterpart. The frequencies of the Tx comb lines Figure 3.1 (Inset (1)) and of the LO comb lines Figure **3.1** (Inset (2)) are denoted by

$$f_{\mathrm{Tx},m} = f_{\mathrm{Tx},0} + m f_{\mathrm{r,Tx}}, \qquad f_{\mathrm{LO},m} = f_{\mathrm{LO},0} + m f_{\mathrm{r,LO}},$$
$$m = -|M_{\mathrm{low}}|, -(|M_{\mathrm{low}}|-1), \ldots, -2, -1, 0, +1, +2, \ldots, +(M_{\mathrm{high}}-1), +M_{\mathrm{high}}. \tag{3.1}$$

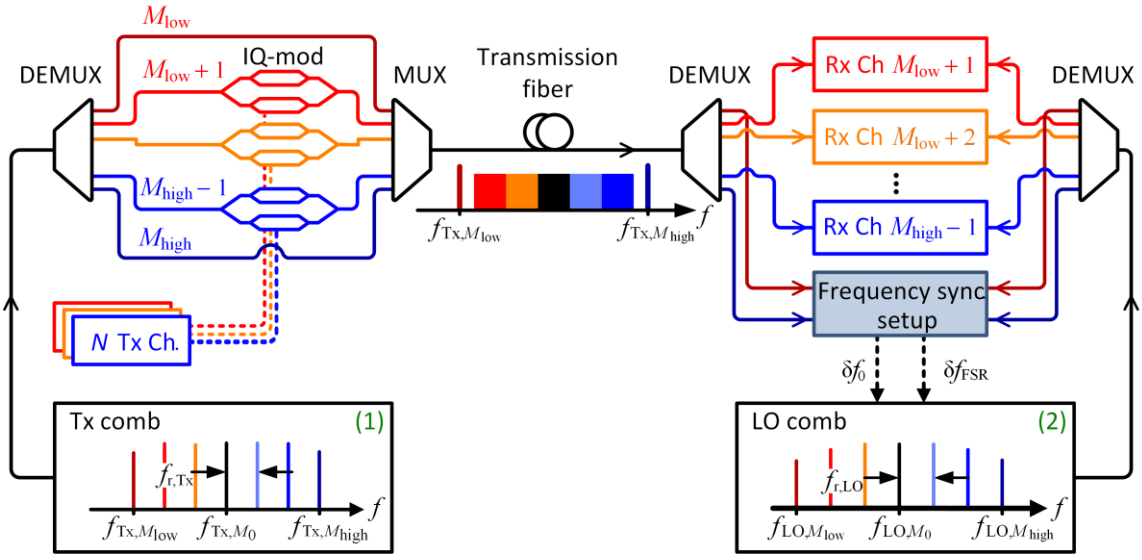

Figure 3.1: Basic WDM transmission link using multi-wavelength intradyne reception. Inset (1) shows a schematic of the transmitter comb having a center frequency $f_{\mathrm{Tx},0}$ and an FSR $f_{\mathrm{r,Tx}}$. The frequencies $f_{\mathrm{Tx},m}$ of the Tx comb lines are denoted by $f_{\mathrm{Tx},m} = f_{\mathrm{Tx},0} + m f_{\mathrm{r,Tx}}$ where $m = -|M_{\mathrm{low}}|, -(|M_{\mathrm{low}}|-1), \ldots -2, -1, 0, +1, +2, \ldots, +(M_{\mathrm{high}}-1), +M_{\mathrm{high}}$ is a signed integer ($M_{\mathrm{low}} < 0$, $M_{\mathrm{high}} > 0$). The same convention is used for the LO lines, see Inset (2). The "inner" carriers numbered $m = -(|M_{\mathrm{low}}|-1), \ldots, 0, \ldots, +(M_{\mathrm{high}}-1)$ are used for coherent data transmission, whereas the "outmost" comb lines $m = -|M_{\mathrm{low}}|$ and $m = +M_{\mathrm{high}}$ serve for synchronizing the LO comb frequencies to the Tx comb.

The quantity m is a signed integer ranging from $M_{\mathrm{low}} < 0$ to $M_{\mathrm{high}} > 0$. The "inner" carriers numbered $m = -\left(\left|M_{\mathrm{low}}\right| - 1\right), \ldots, 0, \ldots, +\left(M_{\mathrm{high}} - 1\right)$ are used for coherent data transmission, whereas the "outermost" two comb lines $m = -\left|M_{\mathrm{low}}\right|$ and $m = +M_{\mathrm{high}}$ serve for synchronizing the LO comb frequencies to the Tx comb by minimizing the frequency offset $\delta f_0 = f_{\mathrm{Tx},0} - f_{\mathrm{LO},0}$ measured at line $m = 0$ and the FSR offset $\delta f_{\mathrm{FSR}} = f_{\mathrm{r,Tx}} - f_{\mathrm{r,LO}}$. This synchronization ensures that all WDM channels are received within a frequency offset that is compatible with real-time intradyne reception, and that most of the receiver and digital-to-analog converter bandwidth is devoted to data reception. To this end, the beat frequencies between the "outermost" Tx comb lines M_{low}, M_{high} and their respective LO counterparts are continuously measured in a dedicated frequency synchronization setup,

$$\begin{aligned} f_{\mathrm{Tx},M_{\mathrm{high}}} - f_{\mathrm{LO},M_{\mathrm{high}}} &= \delta f_0 + M_{\mathrm{high}} \delta f_{\mathrm{FSR}}, \\ f_{\mathrm{Tx},M_{\mathrm{low}}} - f_{\mathrm{LO},M_{\mathrm{low}}} &= \delta f_0 + M_{\mathrm{low}} \delta f_{\mathrm{FSR}}, \\ \delta f_0 = f_{\mathrm{Tx},0} - f_{\mathrm{LO},0}, &\quad \delta f_{\mathrm{FSR}} = f_{\mathrm{r,Tx}} - f_{\mathrm{r,LO}}. \end{aligned} \tag{3.2}$$

From these difference-frequency data, the FSR offset and the center frequency offset can be calculated,

$$\begin{aligned} \delta f_{\mathrm{FSR}} &= \frac{\left(f_{\mathrm{Tx},M_{\mathrm{high}}} - f_{\mathrm{LO},M_{\mathrm{high}}}\right) - \left(f_{\mathrm{Tx},M_{\mathrm{low}}} - f_{\mathrm{LO},M_{\mathrm{low}}}\right)}{M_{\mathrm{high}} + \left|M_{\mathrm{low}}\right|}, \\ \delta f_0 &= \left(f_{\mathrm{Tx},M_{\mathrm{high}}} - f_{\mathrm{LO},M_{\mathrm{high}}}\right) - M_{\mathrm{high}} \delta f_{\mathrm{FSR}}. \end{aligned} \tag{3.3}$$

A controller circuit then adjusts the LO comb parameters $f_{\mathrm{LO},0}$ and Δf_{LO} for minimum offsets δf_{FSR} and δf_0, respectively. The results obtained for this system architecture are discussed in subsequent sections.

As an alternative approach, frequency offset estimation carried out during demodulation of any two data channels can be used to estimate the center frequency and the FSR offset between the two combs instead of using the beat signals between two unmodulated carriers. This alternative method is beneficial

as it will increase the spectral efficiency of the transmission link since no unmodulated Tx comb lines need to be reserved. The receiver complexity becomes slightly larger, since at least two data channels have to be simultaneously received in real time.

Another approach would be to synchronize the Tx and LO comb's center wavelength and FSR with absolute wavelength and absolute frequency references, respectively. This approach can help maintain the combs within a given frequency grid. As such frequency references were not available to us, we decided to use the simpler approach based on unmodulated carriers.

3.3 Frequency comb generation

To generate the Tx and the LO comb we switch the gain of an injection-locked distributed feedback (DFB) slave laser [21]. A schematic of such a gain-switched laser diode (GSLD) is depicted in Figure 3.2. The DFB slave laser is gain switched by a large sinusoidal drive signal, which is generated by a voltage-controlled oscillator (VCO). The sinusoidal is superimposed on a DC bias current set at five times the threshold current of the slave laser. This leads to a pulsed output from the slave laser. A master laser injects continuous-wave light into the slave via a polarization maintaining circulator thereby establishing coherence between subsequent pulses. This leads to formation of an OFC output from the slave. The master laser also fixes the center frequency f_0 of the slave, and transfers its low optical linewidth (100 kHz) to the individual comb lines of the slave [21], [72]. In addition, injection of the master laser light into the slave reduces the RIN of the comb lines [109]. The center frequency of the resulting comb can be adjusted with a micro-controller (µC) in a predetermined fashion through temperature-tuning with thermo-electric coolers (TEC) of both the master and the slave using a control voltage $V_{\delta f_0}$. The FSR is altered (control voltage $V_{\delta f_{\mathrm{FSR}}}$) by varying the VCO frequency [110]. Gain-switched laser diodes (GSLD) can be built using monolithically integrated semiconductor lasers [111], which enables the fabrication of broadband chip-scale OFC.

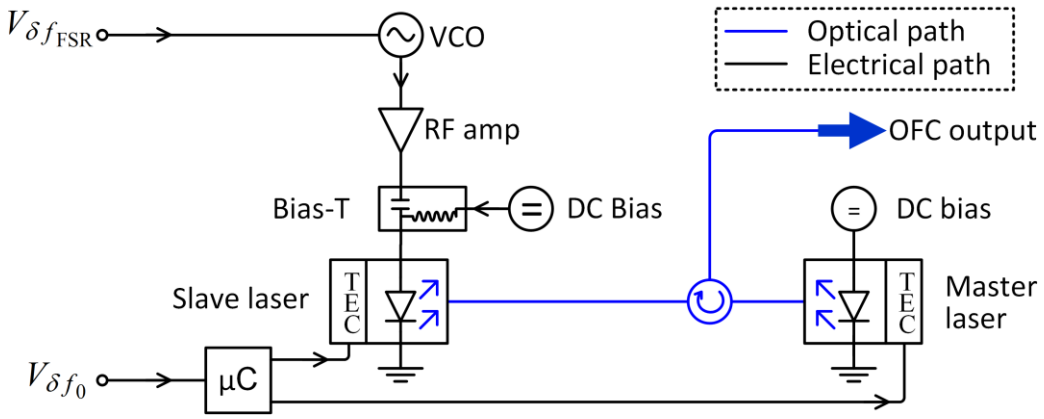

Figure 3.2: Setup schematic of a tunable gain switched laser diode (GSLD). A distributed feedback (DFB) slave laser is gain-switched by a large sinusoidal drive signal from a voltage-controlled oscillator that is superimposed on a DC bias current set at five times the threshold current. A master laser injects continuous-wave light into the slave via a polarization maintaining circulator thereby improving the coherence between subsequent optical pulses. This results in an optical frequency comb with low optical linewidth (100 kHz), dictated by the linewidth of the master laser. In addition, injection locking reduces the RIN of the generated comb lines. The center frequency of the resulting comb can be adjusted by temperature-tuning both master and slave with control voltage $V_{\delta f_0}$. The FSR is altered by varying the VCO frequency with control voltage $V_{\delta f_{FSR}}$.

Figure 3.3a,b show the measured power spectra of the Tx comb and of the LO comb used in our experiment. The resolution bandwidth (RBW) of the optical spectrum analyzer used to record the two spectra is 20 MHz. The line numbering according to Eq. (3.1) is displayed on the upper horizontal axis. The right vertical axis shows the optical carrier-to-noise spectral power density ratio (OCN_0R), which is marked by red filled circles at the combs lines used as data carriers and as local oscillators. The OCN_0R is defined by the ratio of the power of the unmodulated carrier to the underlying noise power in a spectral bandwidth of 1 Hz. It is possible to trade OCN_0R for spectral flatness of the combs [112].

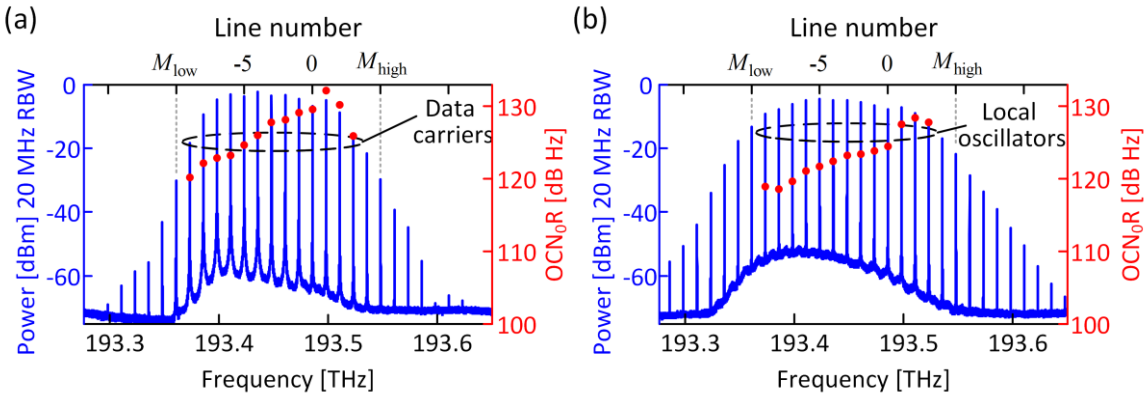

Figure 3.3: Power spectra of the frequency locked combs. **(a)** Tx comb and **(b)** LO comb from the gain-switched laser diode (GSLD) recorded using a resolution bandwidth of 20 MHz. The line numbering according to Eq. (3.1) is shown on the upper horizontal axis. The right vertical axis gives the optical carrier-to-noise power density ratio (OCN_0R), which is marked as red filled circles for the comb lines used as data carriers and as local oscillators. It is possible to trade OCN_0R for spectral flatness of the combs [112].

3.4 Frequency synchronization of two combs

In this section we first discuss the implementation of the synchronization of Tx and LO combs, and then report the associated experimental results.

3.4.1 Implementation using DSP

The setup used for synchronizing the LO comb with the Tx comb is depicted in Figure **3.4**a. Note that this setup was realized using a standard off-the-shelf polarization-diverse 90° optical hybrid (PDOH) and could be simplified considerably by using dedicated hardware components. The setup consists of fiber-optic components such as erbium-doped fiber amplifiers (EDFA1, EDFA2), a polarization beam combiner (PBC), polarization controllers (PC), the PDOH, as well as electronic components such as a field-programmable gate array (FPGA) with analog-to-digital and digital-to-analog converters (ADC, DAC) and a PID controller for adjusting the FSR and the center frequency of the LO comb. Blue lines in Figure **3.4** denote polarization-maintaining (PM) optical connections, red lines denote standard single-mode fibers (SSMF),

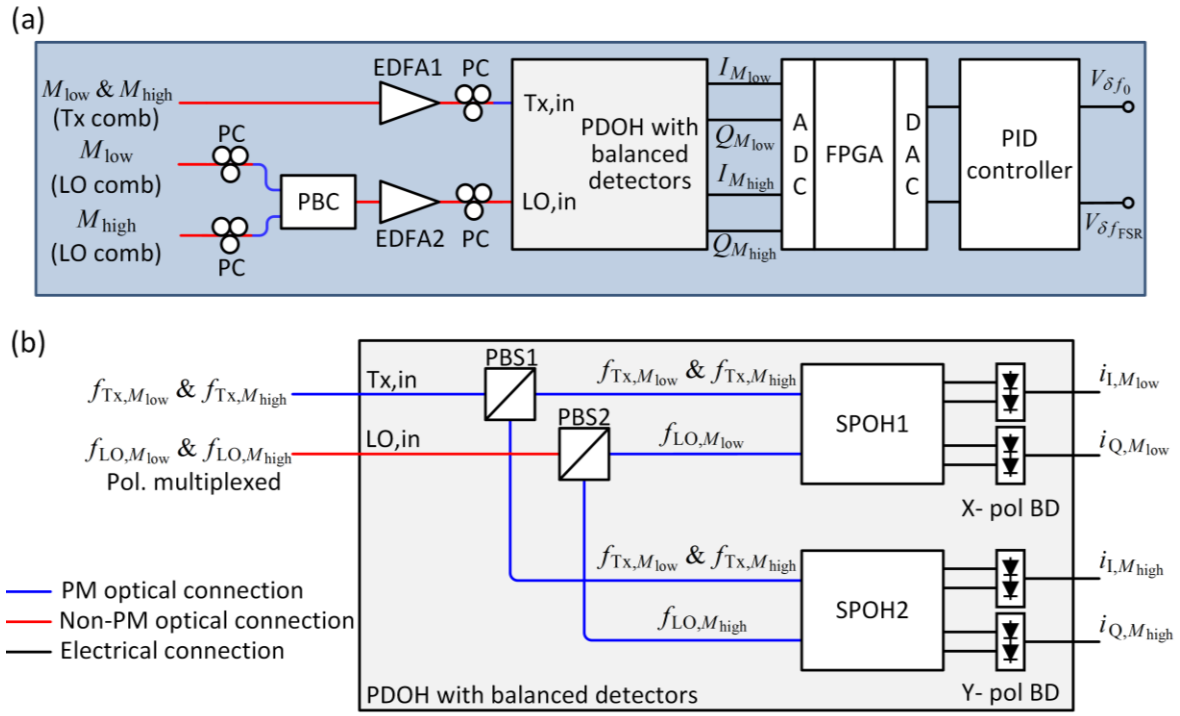

Figure 3.4: Setup for frequency synchronization of two combs. **(a)** Overall setup: Blue lines denote polarization-maintaining (PM) optical connections, red lines denote standard single-mode fibers (SSMF), and black lines denote electrical lines. The Tx comb lines arrive with an arbitrary state of polarization (SOP) in a standard single-mode fiber (SSMF) and are first amplified to compensate for losses in the setup. Using a polarization controller (PC), the lines are then adjusted to one principal axis of the polarization-maintaining (PM) fiber port "Tx,in" of a polarization-diverse 90° optical hybrid (PDOH), which is depicted in more detail in Subfigure (b). The LO comb lines arrive on two separate SSMF, also with arbitrary SOP, and are adjusted to the main axes of the polarization beam combiner (PBC) to superimpose them on orthogonal polarizations states. **(b)** Simplified diagram of the PDOH structure: The principal axis of the PM fiber at the "Tx,in" port is aligned at an angle of 45° with respect to the main axis of a polarization beam splitter (PBS1) such that roughly equal shares of Tx comb lines are coupled to the single-polarization 90° optical hybrids SPOH1 and SPOH2. Regarding the LO signals, the polarization at the SSMF "LO,in" port is adjusted such that the LO lines at frequencies $f_{\mathrm{LO},M_{\mathrm{low}}}$ and $f_{\mathrm{LO},M_{\mathrm{high}}}$ are separated by PBS2 and fed to SPOH1 and SPOH2, respectively. The in-phase and the quadrature components ($i_{\mathrm{I},M_{\mathrm{low}}}$, $i_{\mathrm{Q},M_{\mathrm{low}}}$, $i_{\mathrm{I},M_{\mathrm{high}}}$, $i_{\mathrm{Q},M_{\mathrm{high}}}$) of the beat notes between the LO and Tx comb lines at frequencies $f_{\mathrm{Tx},M_{\mathrm{low}}}$, $f_{\mathrm{LO},M_{\mathrm{low}}}$ and $f_{\mathrm{Tx},M_{\mathrm{low}}}$, $f_{\mathrm{LO},M_{\mathrm{low}}}$ are detected by two sets of balanced photodiodes (BD1, BD2) and sampled by a 4-channel analog-to-digital converter (ADC, FMC126 from 4DSP, 1.25 GSa/s per channel). These samples are passed on to a Xilinx VC707 field-programmable gate array (FPGA) to extract the frequency differences and to control LO the comb via a PID controller.

and black lines denote electrical lines. The PDOH is depicted in more detail in Figure 3.4b. It consists of two polarization beam splitters (PBS1, PBS2), followed by a pair of single-polarization 90° optical hybrids (SPOH1, SPOH2) and two sets of balanced photodiodes (BD1, BD2) to extract the in-phase and the quadrature component of the beat signals of each polarization. Note that PBS1 is connected to the input port "Tx,in" of the PDOH by a polarization maintain fiber (blue), whereas PBS2 is connected to the "LO,in"-port by a standard single-mode fiber (red).

The frequency synchronization setup is fed by two comb lines at frequencies $f_{\mathrm{Tx},M_{\mathrm{low}}}$ and $f_{\mathrm{Tx},M_{\mathrm{high}}}$ as received from the transmitter (Tx comb lines), and by the corresponding LO comb lines at frequencies $f_{\mathrm{LO},M_{\mathrm{low}}}$ and $f_{\mathrm{LO},M_{\mathrm{high}}}$ extracted from the receiver (LO comb lines). The Tx comb lines arrive with an arbitrary state of polarization (SOP) in a common SSMF. These lines, after amplification by EDFA1, are adjusted in polarization to one principal axis of the PM fiber port "Tx,in" of the PDOH. This axis is aligned at an angle of 45° with respect to the main axes of PBS1, such that roughly equal-powered shares of Tx comb lines are coupled to SPOH1 and SPOH2. The LO comb lines M_{low} and M_{high} arrive on two separate SSMF in an arbitrary SOP, and are adjusted to the main axis of the PBC to superimpose them on orthogonal polarizations states at the output of the PBC. The M_{low} and M_{high} LO tones need not be phase coherent as we are using intradyne reception, where phase offset is compensated digitally. Note that the time delay between the M_{low} and M_{high} LO comb tones is much shorter than the respective coherence time between the tones such that we can always reliably estimate the FSR offset and the center frequency offset to synchronize the Tx and LO combs. The SSMF output of the PBC is then amplified and fed to the LO,in port of the PDOH, while adjusting the polarization such that the LO lines at frequencies $f_{\mathrm{LO},M_{\mathrm{low}}}$ and $f_{\mathrm{LO},M_{\mathrm{high}}}$ are separated by PBS2 and fed to SPOH1 and SPOH2, respectively. As a consequence, the in-phase and the quadrature component ($i_{\mathrm{I},M_{\mathrm{low}}}$, $i_{\mathrm{Q},M_{\mathrm{low}}}$) of the beat note between the LO and Tx comb lines at frequencies $f_{\mathrm{Tx},M_{\mathrm{low}}}$ and $f_{\mathrm{LO},M_{\mathrm{low}}}$ can be detected at the first set of balanced photodiodes BD1, whereas the corresponding components $i_{\mathrm{I},M_{\mathrm{high}}}$ and $i_{\mathrm{Q},M_{\mathrm{high}}}$ of the beat note at frequencies $f_{\mathrm{Tx},M_{\mathrm{high}}}$ and $f_{\mathrm{LO},M_{\mathrm{high}}}$ can be detected at the second set (BD2). Note that the

beat notes of lines at $f_{\mathrm{LO},M_{\mathrm{low}}}$ and $f_{\mathrm{Tx},M_{\mathrm{high}}}$ and of lines at $f_{\mathrm{LO},M_{\mathrm{high}}}$ and $f_{\mathrm{Tx},M_{\mathrm{low}}}$ are not visible in the photocurrents due to the limited bandwidth of the photodetectors. The electrical outputs of the balanced photodiodes are sampled by a 4-channel analog-to-digital converter (ADC, FMC126 from 4DSP) having a sampling rate of 1.25 GSa/s per channel. These samples are passed on to a Xilinx VC707 FPGA board. A digital delay-line frequency discriminator (DLFD) [113] extracts the frequency differences $f_{\mathrm{LO},M_{\mathrm{low}}} - f_{\mathrm{Tx},M_{\mathrm{low}}}$ and $f_{\mathrm{LO},M_{\mathrm{high}}} - f_{\mathrm{Tx},M_{\mathrm{high}}}$ including the sign. The FSR offset δf_{FSR} and the center frequency offset δf_0 are then calculated by using Eq. (3.3). A digital-to-analog converter (DAC) on the FPGA board converts the calculated frequencies to analog voltages. These voltages serve as error signals for two PID controllers that continuously compensate the relative drifts of the LO comb via the voltages $V_{\delta f_{\mathrm{FSR}}}$ and $V_{\delta f_0}$ which tune the FSR and the center frequency of the LO comb, see Figure **3.2**.

3.4.2 Frequency synchronization performance

To verify the synchronization of the Tx comb and the LO comb, the system response for a step-like perturbation and the system's long-term frequency stability were investigated. Figure **3.5**a and Figure **3.5**b show the responses of the center frequency offset and the FSR offset for a closed-loop system in reaction to a step-shaped error signal. It can be seen that the LO comb tracks the center frequency offset and the FSR offset of the Tx comb. The step responses show that the center frequency tuning of the LO comb is relatively slow compared to the FSR tuning. This is expected since the center frequency is tuned by temperature, while the FSR is set by the faster reacting VCO frequency, see Figure **3.2**.

Long-term measurements of the center frequency offset and the FSR offset between the the LO comb and the Tx comb are shown in Figure **3.5**c and Figure **3.5**d, respectively. As can be seen in Figure **3.5**c, the synchronization setup maintains the long-term center frequency offset within the range of ± 10 MHz with a standard deviation of 2 MHz. Figure 3.5d shows that the FSR offset between the two combs is kept within a ± 2 MHz range having a standard

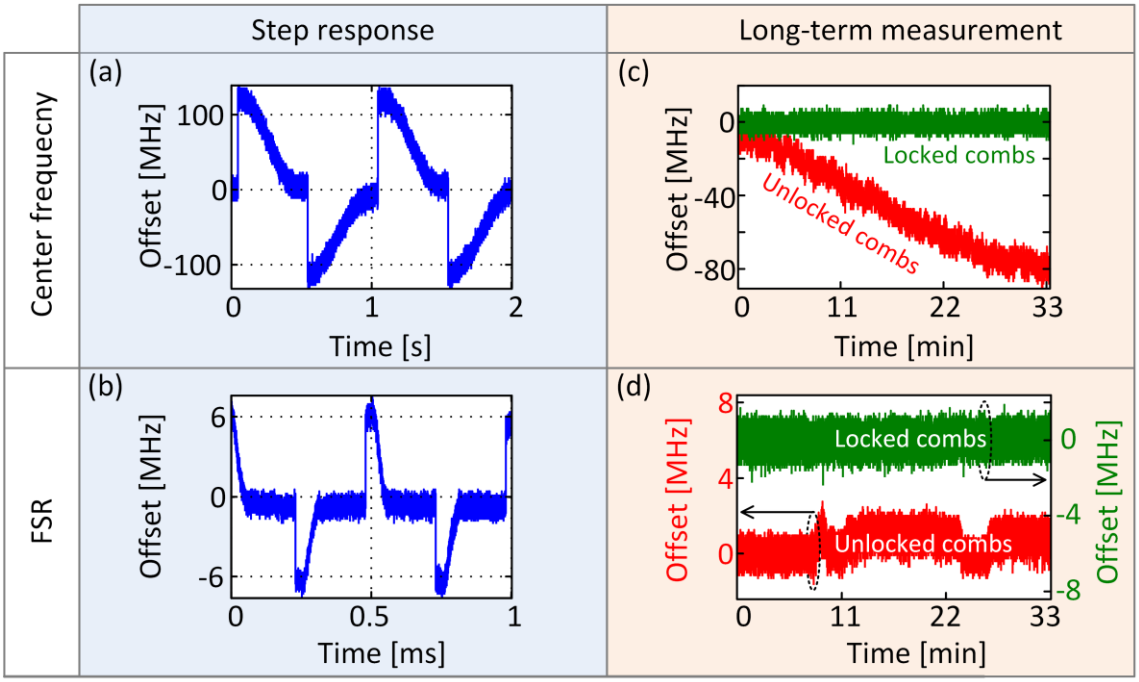

Figure 3.5: Center frequency and FSR synchronization of Tx and LO combs. **(a)**, **(b)** Closed-loop system response for a step like perturbation. For the case of a center frequency offset perturbation shown in (a), a 1 Hz square signal was used since the center frequency tuning speed of the LO comb is within the range of a few Hertz due to the large time constants associated with thermal tuning. For the case of an FSR offset perturbation depicted in (b), a 2 kHz square signal was used. In both cases, the frequency synchronization manages to compensate the perturbations. **(c)** Long-term plots of center frequency offset sampled at 50 Hz both for synchronized ("locked") combs that are controlled by the frequency synchronization setup, and for free-running ("unlocked") combs. **(d)** Long-term plots of FSR offset sampled at 50 Hz, again for locked and for unlocked combs. Two separate vertical axes are used to show the random drift in FSR of the unsynchronized combs. Plots (c) and (d) show that the control of the LO comb maintains low offsets in both center frequency and FSR

deviation of less than 1 MHz. Without synchronization we observe random FSR offsets. The standard deviation of the comb offsets could be further improved if a larger averaging time is used to determine the frequency offsets for the control loop. However, this would result in a delayed response to fast frequency perturbations.

3.5 Tbit/s data transmission experiment

3.5.1 Experimental setup

The experimental setup used to characterize WDM data transmission with two synchronized GSLD is depicted in Figure 3.6. In this experiment, a FSR of 12.5 GHz is used for the Tx comb. The Tx comb is first passed through a programmable filter WS1 (Finisar wavelength-selective switch) to separate the Tx comb lines into two sets. The first set consists of comb lines that are to be used as carriers for the WDM data stream. These are output through Port 1 of WS1 and further dis-interleaved into even and odd carriers. The dis-interleaver (Dis-int.) together with two separate IQ modulators emulates WDM transmission by modulating each group of carriers with an independent pseudo-random binary data sequence of length $2^{11} - 1$.

We use either a 16QAM or a QPSK modulation format, depending on the signal quality achievable with the employed carriers. The symbol rate is 12 GBd, and the pulses are shaped according to a raised-cosine spectrum with a roll-off factor of 0.04. With an FSR of 12.5 GHz, this results in a guard band of 20 MHz between neighboring WDM channels. The frequency offset between the Tx carrier and the corresponding LO comb line needs to be maintained below this guard band value to avoid deterioration of the received signal quality. After modulation, the odd and even channels are combined by a polarization-maintaining 3 dB coupler. Polarization-division multiplexing (PDM) is then emulated by splitting the data stream into two paths and re-combining them on orthogonal polarizations with a decorrelating delay in one path and an attenuator in the other one for maintaining the same power levels. The second set of Tx comb lines at $f_{\mathrm{Tx,M_{low}}}$ and $f_{\mathrm{Tx},M_{\mathrm{high}}}$ consists of two outermost spectral lines at the edges of the Tx comb, and are output at port 4 of WS1. These lines are used for synchronization of the Tx comb's center frequency and the FSR to the corresponding quantities of the LO comb. The two outermost lines are combined with the modulated carriers by a 3 dB coupler, and all are transmitted through a 10 km long standard single mode fiber (SSMF).

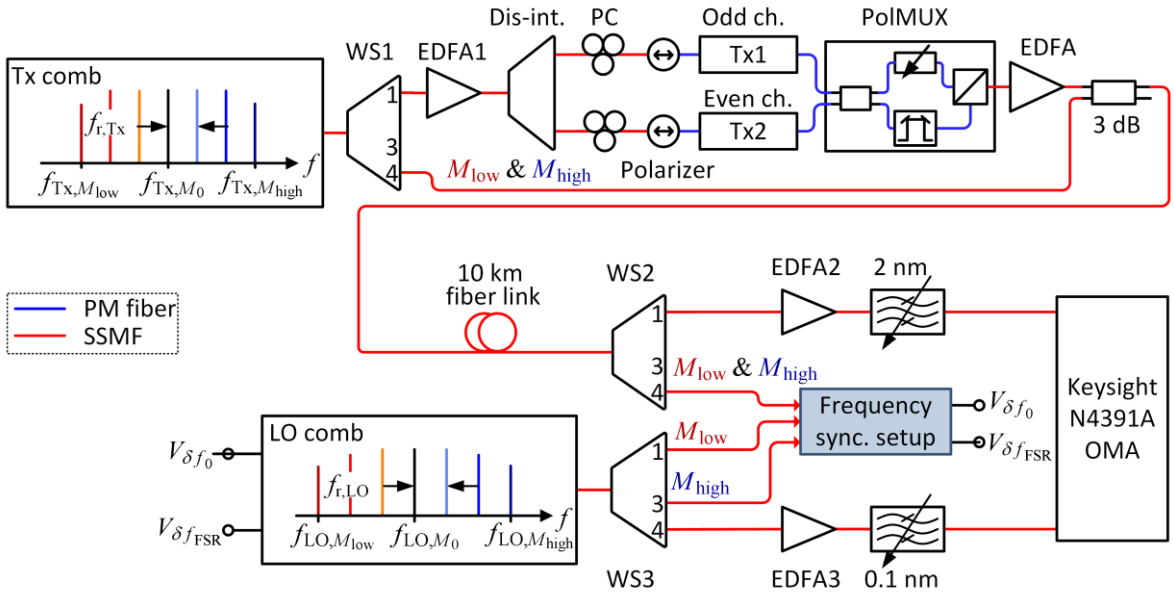

Figure 3.6: Experimental setup for emulation of Tbit/s WDM transmitter and coherent receiver with multi-wavelength intradyne reception. The WDM data signal is generated by separating and independently modulating even and odd carriers. Polarization multiplexing (PolMUX) is emulated by merging decorrelated copies of the data stream onto two orthogonal polarizations. The outermost Tx comb lines M_{low} & M_{high} are selected using a programmable filter WS1 and then combined with the modulated carriers. The resulting signal is transmitted through a 10 km long fiber link to the receiver section of our setup. A programmable filter WS2 selects individual WDM channels (port 1) for detection at the receiver. In addition, it selects the M_{low} & M_{high} Tx comb lines (port 4) for use in the frequency synchronization setup. WS3 selects an LO comb line (port 4) that matches the carrier frequency of the selected WDM channel for coherent detection of the transmitted signal. WS3 is also used to select the M_{low} & M_{high} comb lines of the LO comb and routes them separately to port 1 and port 3 for use in the frequency synchronization setup. This frequency synchronization unit, see Figure 3.4, synchronizes the LO comb with the Tx comb. PC: polarization controller. Tx1, Tx2: Data sources and IQ modulators

At the receiver, a second programmable filter WS2 selects individual WDM channels (port 1) for detection by an optical modulation analyzer (OMA, Keysight N4391A). The two unmodulated Tx comb lines are selected and sent to port 4 of WS2 for use in the frequency synchronization setup, see Figure **3.4**. A third programmable filter WS3 selects an LO comb line (port 4) that matches the carrier frequency of the selected WDM channel for coherent detection of the transmitted signal. This LO comb line is amplified and filtered with a narrow-bandwidth bandpass filter (BPF), which suppresses neighboring comb lines and

out-of-band amplified spontaneous emission (ASE) noise. WS3 also selects two spectral lines of the LO comb at frequencies $f_{\mathrm{LO},M_{\mathrm{low}}}$ and $f_{\mathrm{LO},M_{\mathrm{high}}}$ (port 1 and port 3) for use in the frequency synchronization setup.

3.5.2 Data transmission performance

For demonstrating the viability of a GSLD as an LO for intradyne data reception, we extract 13 carriers from the Tx comb, modulate and transmit them, and evaluate the signal quality with the OMA. Figure **3.7**(a) shows the spectrum of the transmitted signal captured with a resolution bandwidth (RBW) of 0.01 nm at the output of the 3 dB coupler in Figure **3.6**. The subscripts M_{low} and M_{high} denote the spectral lines of the Tx comb that are used for frequency synchronization. The WDM channels carry PDM-16QAM signals and are labelled according to the comb line numbering in Figure **3.3**. Channels -9, -8 and $+3$ could not be used with the same modulation format because carrier power and OCN_0R were too low. However, these carriers were still sufficient for transmitting PDM-QPSK signals. Channel $+4$ was underperforming even with QPSK modulation. It could have been used as comb line M_{high}, but due to the limited steepness of the WS2 filter slope the performance of Channel $+3$ would degrade. Channel -9, however, was not degraded, what we attribute to a better alignment of line M_{low} to the spectral pixel location of the liquid crystal-on-silicon (LCOS) matrix used in the programmable filter.

After transmission and coherent detection, a digital brick wall filter is used to limit the spectrum to our reference bandwidth 12.5 GHz. The OMA performs an adaptive equalization before determining the bit error ratio (BER) for each channel. We evaluate 500,000 bits for each WDM channel to accurately estimate the BER. Figure **3.7**b shows the BER values for all 13 channels for 16QAM transmission (triangles) and for QPSK (circles). Example constellation diagrams of Channels -1 and $+3$ are shown in Figure **3.7**c. BER values for two of the QPSK channels (open circles) are set at 2×10^{-6} because we did not find

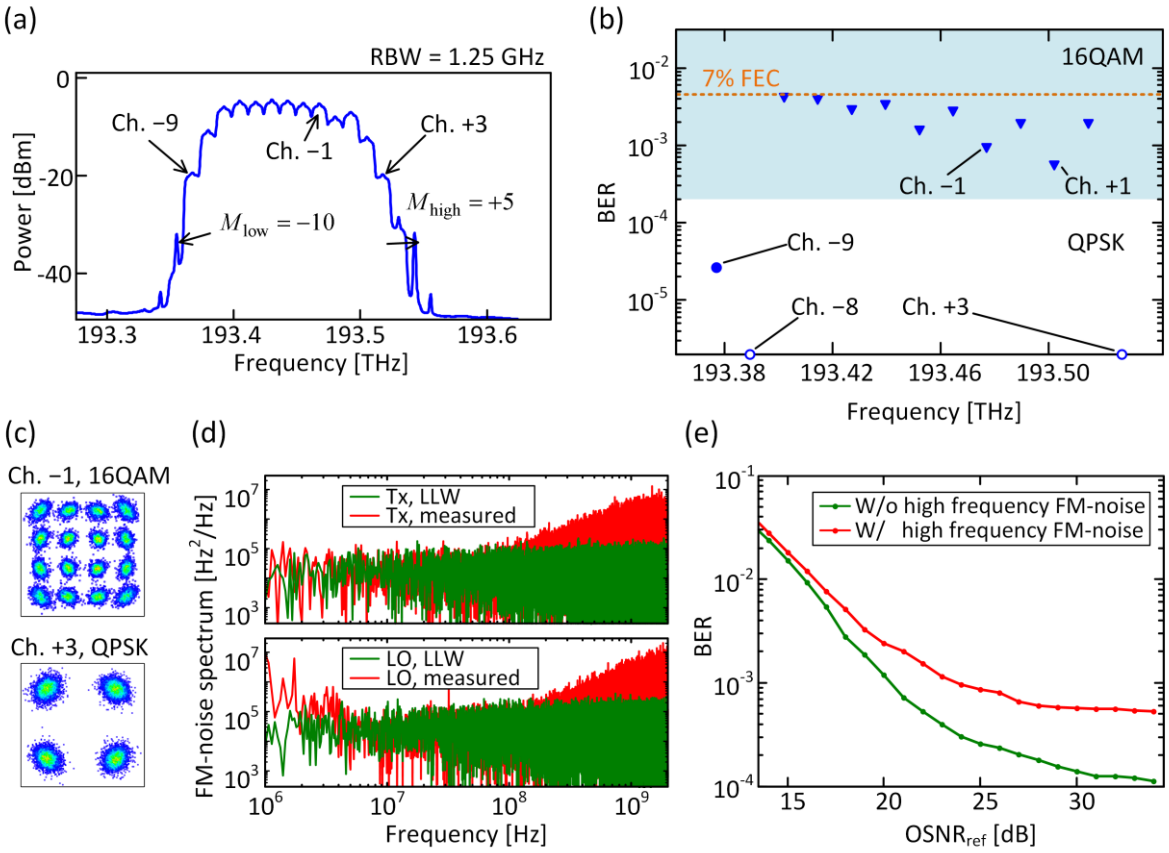

Figure 3.7: Data transmission results using an LO frequency comb. **(a)** Tx comb spectrum measured at the output of the 3 dB coupler in Figure 3.6. Lines M_{low} and M_{high} denote the Tx comb lines used for frequency synchronization. **(b)** Bit error ratio (BER) for all WDM channels transmitting 16QAM (▼) or QPSK (●, ○). All 13 channels exhibit a BER below the threshold for forward-error correction (FEC) with 7 % overhead. Open symbols (○) indicate that no error could be found in a record length of 500,000 bit. The slight oscillations of the BER are attributed to power differences between comb lines, and to slightly different transmitter performances when encoding data on the carriers of the even and odd channels. **(c)** Example constellation diagrams of Channels −1 and +3. **(d)** Measured frequency noise spectra of Tx and LO comb lines of Channel −1 (red traces in the top and bottom subplots, respectively) featuring strong high-frequency FM noise, along with plots of simulated frequency noise spectra of idealized lasers that feature the same Lorentzian line widths (LLW) but do not exhibit high-frequency FM-noise (green). The LLW of Channel −1 Tx and LO comb lines amount to 70 kHz and 120 kHz, respectively. **(e)** Simulated BER vs. $OSNR_{ref}$ in a reference bandwidth of 12.5 GHz (0.1 nm) with (red) and without (green) high-frequency FM-noise. The results indicate that high-frequency FM-noise in the GSLD limits the received signal quality for high values of $OSNR_{ref}$. This limitation can be overcome by adjusting the injection locking parameters and by balancing spectral flatness and FM-noise level of the GSLD, thereby reducing high-frequency FM-noise [26].

any error in our maximum record length of 500,000 bit. The horizontal line indicates the BER limit for forward-error correction (FEC) with an overhead of 7 % [114]. We find all 13 channels to have a BER below this threshold. Hence, taking into account the 7 % overhead, a line rate of 1.104 Tbit/s corresponding to a net data rate of 1.032 Tbit/s is achieved. Since 16 comb lines are utilized from the Tx and LO combs for this transmission experiment including the frequency synchronization comb lines and one idle comb line next to Channel $+3$, a net spectral efficiency (SE) of 5.16 bit/s/Hz is obtained. The SE could be improved up to 6.3 bit/s/Hz if the estimation of the frequency offsets is done from a real-time evaluation of two data channels as stated in Section 3.2. In the course of this experiment, the frequency synchronization setup kept the LO comb in close synchronism with the Tx comb, resulting in intradyne frequencies of less than 15 MHz for all of the evaluated data channels.

It is evident from the shape of the constellation diagrams in Figure **3.7**c that there is more angular spread of the constellation points than radial spread. This suggests a dominant phase noise contribution degrading the signal quality. It was reported in [112] that GSLD exhibit high-frequency FM-noise which may lead to such a reduction of the received signal quality. To further illustrate the effect of high-frequency FM-noise in the Tx and LO GSLD, we investigate its impact on the signal quality by two series of data transmission simulations using the commercial tool OptSim [115] with a 12 GBd 16QAM modulation. In these simulations, we do not include fiber transmission and assume an ideal receiver without any electrical noise. The simulation results should hence give a lower boundary for the measured BER.

Tx and LO comb lines of Channel -1 are used to investigate the transmission performance in the presence of high-frequency FM-noise. The measured FM-noise spectra $S_F(f)$ of the Tx and LO comb lines of Channel -1 are depicted in Figure **3.7**d as red traces in the top and bottom subplots, respectively. $S_F(f)$ is a crucial function for evaluating the phase noise characteristics of a laser [37]. For calculating $S_F(f)$ of a comb line, we first measure the phase fluctuations $\phi_{\mathrm{comb}}(t)$ of the comb line. To this end, the comb line and a 10 kHz line from a highly stable tunable reference laser (Keysight, N4391A) with reference phase

$\phi_{\text{ref}}(t)$ are mixed, and their phase difference $\Delta\phi(t) = \phi_{\text{comb}}(t) - \phi_{\text{ref}}(t)$ is evaluated as a function of time from the intermediate frequency (IF) signal. Assuming that $\phi_{\text{ref}}(t)$ does not vary much in comparison to $\phi_{\text{comb}}(t)$, the phase difference $\Delta\phi(t)$ is then used as an approximation of $\phi_{\text{comb}}(t)$. After obtaining $\phi_{\text{comb}}(t)$, the time increments $\Delta\phi_\tau(t) = \phi_{\text{comb}}(t+\tau) - \phi_{\text{comb}}(t)$ of $\phi_{\text{comb}}(t)$ for various delay times τ are estimated, and the instantaneous frequency fluctuations $f_i(t) = \Delta\phi_\tau(t) / 2\pi\tau$ are extracted for $\tau \to 0$. The FM-noise spectrum which is defined as the power-spectral-density (PSD) function of the instantaneous frequency fluctuation $f_i(t)$ is then calculated as $S_F(f) = \left|\text{FFT}\{ f_i(t)\Delta t\}\right|^2 / T$, where FFT represents the fast Fourier transform. The quantity Δt is the sampling interval, and T is the total sample duration.

In the first series of simulations, OptSim laser models were made to have similar FM-noise characteristics as the actually measured Tx and LO comb lines of Channel −1. We did so by phase modulating the light emitted from the ideal OptSim laser models with the measured phase fluctuations $\phi_{\text{comb}}(t)$ of the Tx and LO comb lines of the channel under consideration. The resulting signals from the laser models emulate the actual comb lines, and are then used as the signal and LO tones for a transmission experiment simulation. The obtained dependence of BER for a 16QAM signaling on the optical signal-to-noise ratio (OSNR_{ref}) is shown by the red trace in Figure **3.7**e. Here, the OSNR_{ref} is defined as the ratio of total signal power and noise power measured in a reference bandwidth of 12.5 GHz (0.1 nm).

In the second series of simulations, Lorentzian lineshape laser models without high-frequency FM-noise were used as provided by OptSim. For a realistic connection to the measured data, the Lorentzian linewidths (LLW) of the Tx and the LO comb lines in the simulation are chosen as $\text{LLW} = 2\pi \cdot S_F^{\text{white}}(f)$, where $S_F^{\text{white}}(f)$ is the flat FM-noise component in the low-frequency region of the measured FM-noise spectra $S_F(f)$ of Channel −1 [37]. Using this procedure, the linewidth in the simulation is set to be 70 kHz (120 kHz) for the Tx (LO) laser. The FM-noise spectra of the OptSim Lorentzian lineshape laser models are also depicted as green traces in Figure **3.7**d. As expected, the BER is better for the simulated Lorentzian lineshapes as compared to the sources

which feature additional high-frequency FM-noise, see green trace in Figure **3.7**e. The difference becomes more pronounced as the $OSNR_{ref}$ level increases.

In our experiment, a direct measurement of the $OSNR_{ref}$ was not possible due the densely packed channel spectra that made it impossible to measure the noise background of the data signal. Hence, a direct comparison of the simulation results to the measured BER is difficult. However, in the presence of high-frequency FM noise, the simulated BER of approximately 4×10^{-4} in the limit of high $OSNR_{ref}$ compares well to the best experimentally obtained BER of 6×10^{-4} observed for Channel +1, see Figure **3.7**b. This indicates that high-frequency FM-noise in GSLD limits the received signal quality, indeed. The limitations could be overcome by adjusting the injection locking parameters and balancing spectral flatness and FM-noise level of the GSLD which leads to a reduction of high-frequency FM-noise [112].

3.5.3 Scalability and power consumption

As it is not possible to generate a significantly larger number of lines from our GSLD, we will need to use multiple transmitter/receiver groups to further increase the overall transmission capacity. This can be done by integrating multiple GSLD on one chip [111].

In general, frequency combs have the advantage of a greatly simplified wavelength stability of the individual carriers as the control of center frequency and FSR is sufficient to stabilize and synchronize all Tx and Rx comb lines. This advantage becomes particularly important for large channel counts. Of course, nothing comes for free, and the power per line decreases as the number of lines increases, which in our experiment requires an additional EDFA before the modulator (EDFA1 in Figure 3.6). Taking this amplifier into account, we obtain between 10 dBm and 14 dBm of optical power per tone, which compares well to the optical output power of common integrated tunable laser assemblies (ITLA) [116]. At the same time, the electrical power consumption of an integrated GSLD is estimated to be about 2 W per line, taking into account a power consumption of 10 W for the GSLD [16] and an additional 8 W for the EDFA [117]. This total power consumption is already slightly below that of a

commercial ITLA [116]. The advantages of using frequency combs become even more pronounced when moving to higher channel counts. We have recently shown WDM transmission using approximately 100 carriers derived from a so-called Kerr soliton comb [104], [118]. For this device, we estimate an overall power consumption of less than 1 W per line, including all EDFA required to boost the comb to optical power levels of about 10 dBm per line. We hence are convinced that the concept of using frequency combs is an attractive option to realize highly scalable optical multi-wavelength sources for WDM transmission.

3.6 Summary

We demonstrate that a GSLD is suitable to serve as a multi-wavelength local oscillator (LO) for intradyne reception of WDM signals. Center frequency and FSR of the LO comb are synchronized to the transmitter frequency comb. We demonstrate the viability of the concept in a proof-of-principle experiment by transmitting a net aggregate data rate of 1.032 Tbit/s through a 10 km long SSMF with a net spectral efficiency of 5.16 bit/s/Hz. Using simulations based on measured phase-noise characteristics, we show that the performance is limited by the presence of high-frequency FM-noise which, however, can be decreased by a proper parameter optimization of the comb sources.

[*end of paper [J1]*]

4 Quantum-dash mode-locked laser diodes for multi-terabit/s transmission

This chapter explores quantum-dash mode-locked laser diodes (QD-MLLD) as multi-wavelength light sources at the transmitter side of a high-capacity WDM link, operating at a line rate of 12 Tbit/s. It is taken from paper [J2], which is accepted to *Optics Express*. The material from the publication is reproduced here with the appropriate changes to fit the structure and notation of this thesis.

[*Beginning of paper [J2]*]

Copyright © 2020 Optical Society of America

32QAM WDM transmission at 12 Tbit/s using a quantum-dash mode-locked laser diode (QD-MLLD) with external-cavity feedback

Optics Express, Volume 28, Issue 16, pp. 23594-23608, 2020
DOI: 10.1364/OE.392007

Juned N. Kemal,[1] Pablo Marin-Palomo,[1] Kamel Merghem,[2,3] Guy Aubin,[2] François Lelarge,[4] Abderrahim Ramdane,[2] Sebastian Randel,[1] Wolfgang Freude,[1] and Christian Koos[1,5]

[1] Institute of Photonics and Quantum Electronics (IPQ), Karlsruhe Institute of Technology (KIT), Germany
[2] Centre de Nanosciences et de Nanotechnologies (CNRS), Univ. Paris-Sud, C2N - Université Paris-Saclay, France
[3] Now at Institut Mines-Télécom - Télécom SudParis, EVRY, France
[4] Now with Almae Technologies, Marcoussis, France
[5] Institute of Microstructure Technology (IMT), Karlsruhe Institute of Technology (KIT), Germany

Chip-scale frequency comb generators lend themselves as multi-wavelength light sources in highly scalable wavelength-division multiplexing (WDM)

transmitters and coherent receivers. Among different options, quantum-dash (QD) mode-locked laser diodes (MLLD) stand out due to their compactness and simple operation along with the ability to provide a flat and broadband comb spectrum with dozens of equally spaced optical tones. However, the devices suffer from strong phase noise, which impairs transmission performance of coherent links, in particular when higher-order modulation formats are to be used. Here, we exploit coherent feedback from an external cavity to drastically reduce the phase noise of QD-MLLD tones, thereby greatly improving the transmission performance. In our experiments, we demonstrate 32QAM WDM transmission on 60 carriers derived from a single QD-MLLD, leading to an aggregate line rate (net data rate) of 12 Tbit/s (11.215 Tbit/s) at a net spectral efficiency (SE) of 7.5 bit/s/Hz. To the best of our knowledge, this is the first time that a QD-MLLD optical frequency comb has been used to transmit an optical 32QAM signal. Based on our experimental findings, we perform simulations that show that feedback-stabilized QD-MLLD should also support 64QAM transmission with a performance close to the theoretical optimum across a wide range of technically relevant symbol rates.

4.1 Introduction

With escalating data traffic on all levels of optical communication networks [119], wavelength-division multiplexing (WDM) is becoming a necessity not only for long-haul links, but also for shorter transmission distances of a few tens of kilometers as typically found in data-center interconnects and in metropolitan or campus-area networks. To provide utmost scalability, these links should rely on compact WDM transceivers that can be efficiently produced in large quantities and that offer multi-terabit/s connectivity. In this context, chip-scale frequency comb generators have emerged as promising building blocks of WDM transceivers [23], [120], acting either as multi-wavelength light source for massively parallel data transmission [J4], [9], [12], [13], [16], [18], [121] or as multi-wavelength local oscillator (LO) for coherent reception [J1], [J4], [105], [107], [122]. Among different comb generator concepts that have been used for WDM transmission at Tbit/s data rates and that

relied, e.g., on electro-optic modulators [12], [18], gain-switched laser diodes [J1], [16], Kerr-nonlinear waveguides [13] or micro-resonators [J4], [121], quantum-dash mode-locked lasers (QD-MLLD) [9], [10], [92] are a particularly attractive option due to their compact size and operational simplicity. Driven by a DC current, a QD-MLLD can emit a broadband comb containing tens of evenly spaced tones with a flat spectral envelope [22], [56]. However, while the power and the optical carrier-to-noise ratio (OCNR) of QD-MLLD would permit high-speed communication using advanced modulation formats [10], [23], [123], the devices suffer from large optical linewidths of the individual tones, which strongly impairs transmission of signals that rely on advanced modulation formats. As a consequence, previous demonstrations of WDM transmission with native QD-MLLD had to rely on intensity modulation of the optical carriers [124], [125], were limited to rather simple modulation formats such as quadrature phase-shift keying (QPSK) [J3], [9], or required advanced phase tracking schemes to permit 16-state quadrature amplitude modulation (16QAM) transmission [10].

In this paper, we show that QD-MLLD can support WDM transmission with modulation formats beyond 16QAM if external-cavity optical feedback is used to reduce the phase noise [J2]. In our experiments, we demonstrate a reduction of the intrinsic linewidth by approximately two orders of magnitude, and we use the devices to demonstrate 32QAM WDM transmission at a symbol rate of 20 GBd, limited by the free spectral range (FSR) of the comb generator. We transmit 60 channels derived from a single comb source over a 75 km-long standard single mode fiber (SSMF). Using two polarizations, we achieve an aggregate line rate (net data rate) of 12 Tbit/s (11.215 Tbit/s) at a net spectral efficiency (SE) of 7.5 bit/s/Hz. To the best of our knowledge, this is the first time that a QD-MLLD optical frequency comb has been used with 32QAM signaling, leading to the highest spectral efficiency reported for such a device. Our experiments complement recent WDM demonstrations that exploit feedback-stabilized quantum-dot MLLD for 16QAM signaling at comparable data rates [J3]. Combining our results with recently demonstrated integrated optical feedback circuits based on ring resonators [126] opens a route towards chip-scale WDM transceivers supporting line rates of tens of Tbit/s.

4.2 QD-MLLD comb sources and external feedback

The basic structure of the QD-MLLD used in this work is depicted in Figure **4.1**a. The devices comprise an active region made from three separate layers of InAs quantum dashes (QD) grown by molecular beam epitaxy on an InP substrate. The InAs QD layers are separated by 40 nm-thick InGaAsP barriers using a dash-in-a-barrier design [22]. The dash-barrier stack is terminated at the top and the bottom by 80 nm-thick InGaAsP separate confinement heterostructure (SCH) layers. The optical mode is guided by a buried-ridge waveguide, having a width of 1.0 µm and a length of 1.71 mm, which is formed by the dash-barrier stack. Cleaved chip facets form a Fabry-Perot laser cavity having a free spectral range of approximately 25 GHz. Light is emitted from both facets. The active region of the QD-MLLD is electrically pumped via p-doped and the n-doped InP layers using top and bottom contact pads. Proton (H+) implantation ensures lateral confinement of the pump current [22]. Shape and size variations of the QD result in an inhomogeneous broadening of the gain spectrum, which leads to multiple longitudinal modes oscillating simultaneously with nearly the same strength [127]. Nonlinear interaction of these longitudinal modes results in mode-locking, characterized by equidistant optical tones with strongly correlated phase noise [128].

It has been shown both theoretically and experimentally that coupling a properly adjusted external resonator to a passively mode-locked semiconductor laser leads to a reduction of the optical linewidth [129]–[133], and this concept was also transferred to QD-MLLD [134], [135]. In this work, we rely on a free-space optical feedback, see Figure 4.1b for a sketch of the experimental setup. The output light of the laser diode enters an external cavity formed by the cleaved facet and a highly reflecting plane metallic mirror, placed 30 cm away from the chip facet. A plano-convex lens collimates the beam emitted from the laser, and a variable attenuator is used to adjust the quality factor of the cavity, thereby adapting the level of optical feedback to avoid unstable operation [132]–[134]. The mirror position is manually adjusted such that the cavity length is close to

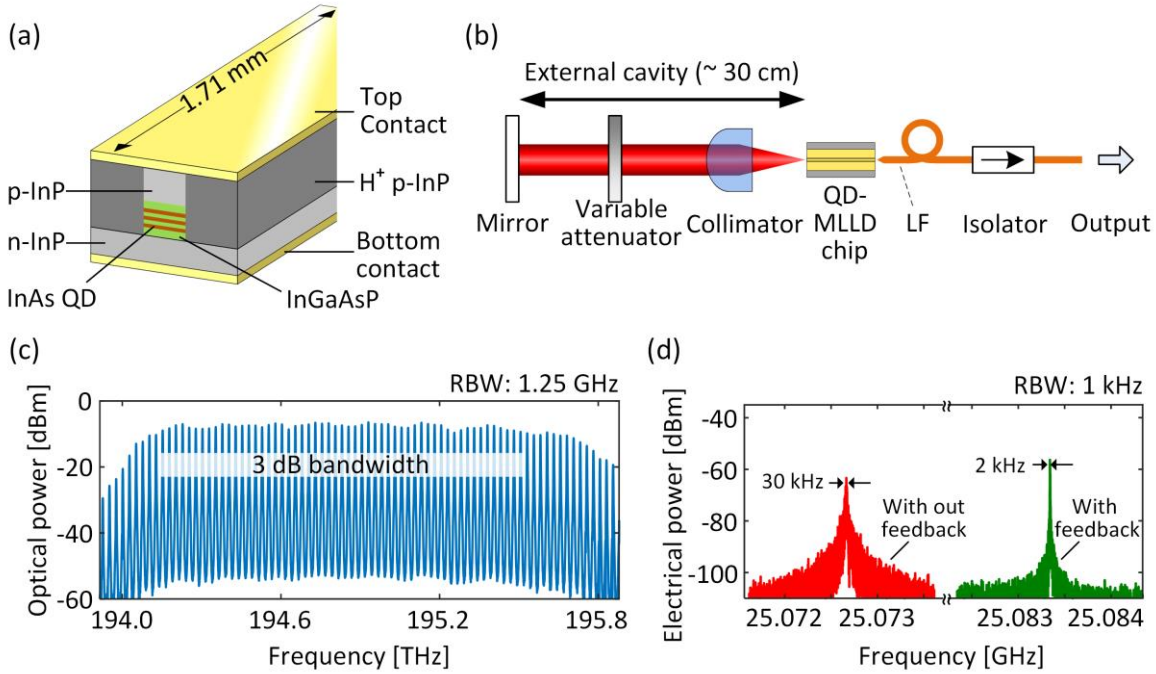

Figure 4.1: Quantum-dash mode-locked laser diode (QD-MLLD) with optical feedback from an external cavity. **(a)** Schematic of a QD-MLLD: The device consists of stacked layers of InAs quantum dashes (QD, red) that are separated by InGaAsP barriers (green). Separate confinement heterostructure (SCH) InGaAsP layers terminate the dash-barrier stack at the top and the bottom. The optical mode is guided by a dash-barrier stack acting as a buried ridge waveguide of 1.0 µm width. Cleaved chip facets form a Fabry-Perot laser cavity having a length of 1.71 mm, thus leading to a free spectral range (FSR) of 25 GHz. The active region of the QD-MLLD is electrically pumped via p-doped and n-doped InP layers using top and bottom contact pads. **(b)** Optical setup for external feedback: An anti-reflection-coated collimating lens directs the output light of the laser diode to a highly reflecting external mirror. The mirror position can be mechanically adjusted to match the FSR of the QD-MLLD and the external Fabry-Perot cavity, which is formed by the mirror and the cleaved laser facet. A variable attenuator in the external cavity allows to adjust the level of the optical feedback into the laser. The attenuator is necessary to avoid excessive feedback, which could lead to unstable operation of the QD-MLLD [132]–[134]. **(c)** Optical comb spectrum of the QD-MLLD with optical feedback. **(d)** Measured RF spectrum of the photo-mixed comb lines without (red) and with (green) optical feedback.

an integer multiple of the effective optical length of the Fabry-Perot laser cavity. In our case, the chip FSR equals 50 times the external-cavity FSR. The adjustment of the cavity mirror is reasonably stable and only needs some minor tuning from time to time to compensate for temperature drift of our

experimental setup. During our data transmission experiments, which took many hours, we typically needed to re-adjust the cavity mirror position every 2-3 hours. The variable attenuator was left untouched in all cases. In real-world systems based on integrated optical feedback circuits [126], such adjustments might either be unnecessary or can be accomplished using a simple control loop. The light emitted from the second facet of the QD-MLLD enters a lensed fiber and a subsequent isolator. Figure 4.1c depicts the frequency comb spectrum obtained at the isolator output for a drive current of 312 mA. The comb is centered at 1545 nm and exhibits a 3 dB bandwidth of more than 1 THz. The comb lines exhibit optical carrier-to-noise power ratios (OCNR) in the range of 36…38 dB, specified with respect to a reference noise bandwidth of 0.1 nm. Unlike single-line or dual-line injection locking [136], [137], which lead to pronounced spectral variations of the comb tone powers, a simultaneous feedback for all lines qualitatively preserves the flat and broadband spectral envelope of the native comb [135], [138]. However, as discussed in [138], [139], a slight reduction of the overall comb bandwidth could occur, depending on the feedback conditions. In addition, a small spectral red shift of the whole comb spectrum is observed, which we attribute to a decrease in threshold carrier density due to a slight reduction of the laser cavity mirror losses with coherent feedback [140]**.** As a quickly accessible experimental indicator for adjusting the external-cavity feedback, we use the electric radio-frequency (RF) spectrum of the photocurrent obtained by detecting the comb on a high-speed photodiode. We consider the linewidth of the first harmonic of the photocurrent, occurring at the FSR frequency of approximately 25 GHz, see Figure 4.1d. This so-called RF linewidth of the comb [141] reduced from 30 kHz for a free-running QD-MLLD to approximately 2 kHz once the external-cavity feedback level is properly adjusted. A reduced RF linewidth indicates an improved overall coherence of the comb tones and hence a better mode-locking [142], [143]. At the same time, a slight spectral shift of the RF beat note can be observed once the comb is locked to the external cavity, which amounts to approximately 10 MHz in the example shown in Figure 4.1d. We attribute this shift to the fact that the FSR of the native comb is not an integer multiple of the external-cavity FSR [129].

Note that the RF linewidth only represents the relative phase noise of neighboring comb lines. It is not an indicator of the optical linewidth of the individual optical tones and that is relevant for the transmission performance. To characterize the phase noise of the individual optical carriers, we use the setup shown in Figure 4.2a and we follow the technique described in references [10], [37], [144] to extract the frequency-noise spectrum $S_{f_\mathrm{i}}(f)$ of different comb tones without and with external-cavity feedback. A tunable band-pass filter (TBF) is used to select a tone from the frequency comb. This tone is sent through a polarization controller (PC) and then superimposed with a local oscillator (LO) laser in a 90° optical hybrid. The LO is a high quality external-cavity laser (ECL, Keysight N7714) with intrinsic optical linewidth smaller than 10 kHz. At the output of the optical hybrid, balanced photodetectors (BPD) followed by an 80 GSa/s real-time oscilloscope (RTO) are used to capture the in-phase (I) and the quadrature (Q) component of the beat signal. The duration of the recorded signal window was 200 µs. The beat signal is centered on an intermediate frequency (IF) of 2 GHz defined by the detuning of the LO and the comb tone of interest. We then extract the time-dependent phase of the complex beat signal and remove the intermediate frequency by fitting a linear function to the unwrapped measured phases and by subtracting the fitted function to remove the slope. This leads to the time-dependent phase fluctuations $\phi(t)$, from which the instantaneous optical frequency $f_\mathrm{i}(t)$ is calculated by means of a differentiation,

$$f_\mathrm{i}(t) = \frac{1}{2\pi}\frac{\mathrm{d}\phi(t)}{\mathrm{d}t} \approx \frac{1}{2\pi}\frac{\phi(t+\tau)-\phi(t)}{\tau} \tag{4.1}$$

In this relation, the time step τ corresponds to the sampling period of the RTO. The spectrum $S_{f_\mathrm{i}}(f)$ is then calculated by taking the Fourier transform of the autocorrelation function of f_i.

Generally, the frequency noise spectrum $S_{f_\mathrm{i}}(f)$ of a laser is composed of flicker frequency noise ($\propto f^{-1}$), random-walk frequency noise ($\propto f^{-2}$), and a spectrally constant “white” frequency noise. If, as in our setup, the measured phase of the laser is additionally impacted by additive white Gaussian noise (AWGN) caused by, e.g., the ASE of an optical amplifier in the measurement

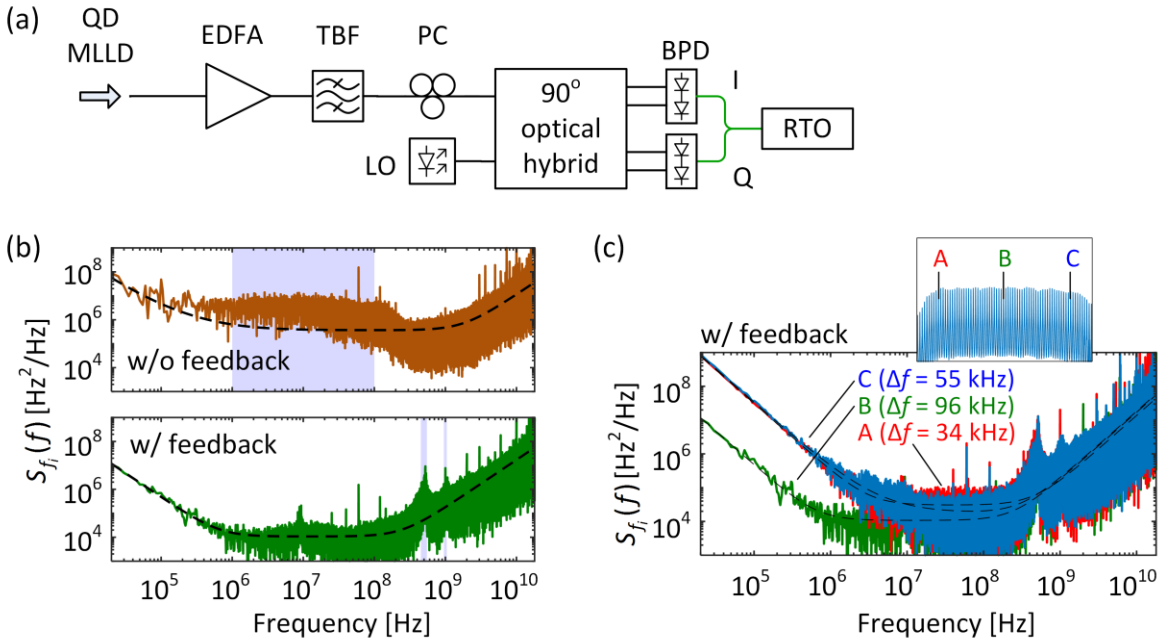

Figure 4.2: Phase-noise characterization of QD-MLLD with and without optical feedback. **(a)** Experimental setup. A tunable narrow band-pass filter (TBF) is used to select distinct tones from the comb. A polarization controller (PC) at the input of a 90° optical hybrid is used to match the polarization of the selected tone to that of the narrowband local-oscillator (LO) tone at the input of the hybrid. Balanced photodetectors (BPD) are used to extract the in-phase (I) and the quadrature (Q) component of the beat note. The electrical signals are sampled by a real-time oscilloscope (RTO) for offline processing. **(b)** Measured FM-noise spectra of a QD-MLLD tone (designated as B in Figure 4.2c) without (upper plot) and with external-cavity feedback (lower plot). The dashed lines indicate the model fit to the measured frequency noise spectrum according to Eq. (4.2). In these fits, the measurement data within the grey shaded areas was ignored since it is not represented by the rather simple model of Eq. (4.2). The fits reveal intrinsic linewidths of 1.1 MHz for the free-running QD-MLLD without feedback, and of 34 kHz for the device with optical feedback. **(c)** Measured FM-noise spectra of three tones of a QD-MLLD with feedback and without (brown thin line). The inset indicates the relative location of the respective comb tones inside the comb spectrum. The intrinsic linewidths amount to $\Delta f_A = 96\,\mathrm{kHz}$, $\Delta f_B = 34\,\mathrm{kHz}$, and $\Delta f_C = 55\,\mathrm{kHz}$, respectively. Hence, despite the typical increase of the intrinsic linewidths of the tones towards the edge of the comb [142], [143], the external-cavity feedback can greatly reduce the frequency noise throughout the comb spectrum when compared to the FM noise without external feedback.

setup, the frequency noise spectrum will also have a component with an f^2 - dependence, which becomes dominant at higher frequencies. The measured frequency noise spectrum can thus be modeled as [144], [145]

$$S_{f_i}(f) = S_0 f^0 + S_1 f^{-1} + S_2 f^{-2} + S_3 f^2. \quad (4.2)$$

The coefficients $S_0 \ldots S_3$ quantify the different frequency noise contributions. The intrinsic (short-term) Lorentzian linewidth Δf of a laser can be estimated from the white frequency-noise level as $\Delta f = \pi S_0$.

Figure **4.2**b, upper plot depicts the frequency-noise spectrum of a QD-MLLD comb tone without external-cavity feedback. The dashed line indicates the model fit to the measured frequency noise spectrum according to Eq. (4.2). The measured noise spectrum in the range 1…100 MHz (shaded in grey) is not considered when performing the fit – the enhanced frequency noise in this region is attributed to relaxation oscillations of the carrier density in the QD gain section, which are not contained in the rather simple model according to Eq. (4.2) [144], [146], [147]. Including this effect would introduce at least three additional free parameters related to the damping and the resonance frequency of the relaxation oscillation as well as to the linewidth enhancement factor (α-factor) of the laser to properly describe the Schawlow-Townes-Henry frequency noise [148]. Fitting Eq. (4.2) to the remaining regions of the measured frequency noise spectrum leads to $S_0 = 3.6 \times 10^5$ Hz, $S_1 = 2.5 \times 10^{11}$ Hz^2, $S_2 = 1.7 \times 10^{16}$ Hz^3, and $S_3 = 1.1 \times 10^{-13}$ Hz^{-1}. The estimated white frequency-noise level corresponds to an intrinsic linewidth of about $\Delta f = \pi S_0 = (1.1 \pm 0.2)$ MHz for this comb tone, where the specified uncertainty refers to the 95 % confidence interval. Note that the omission of the frequency range 1…100 MHz in the fit should still lead to a reliable prediction of the data transmission performance: Frequency-noise components below 100 MHz are usually anyway compensated by phase tracking, whereas spectral components above 100 MHz can lead to degradation of the signal quality [10]. The lower plot in Figure **4.2**b depicts the frequency-noise spectrum of the same QD-MLLD comb tone under the influence of external-cavity feedback. The dashed line indicates again the model fit of the measured frequency noise spectrum according to Eq. (4.2). Also here, the relatively broadband noise peaks in the ranges 450…550 MHz and 0.95…1.05 GHz. These ranges are not considered when performing the fit – we attribute the peaks to side modes of the comb tone induced by the external-cavity feedback which are not contained

in the model leading to Eq. (4.2). Note these noise peaks may be avoided by using dual-cavity resonant feedback [138]. The fit leads to $S_0 = 1.1\times10^4$ Hz, $S_2 = 4.7\times10^{14}$ Hz^3, $S_3 = 1.7\times10^{-13}$ Hz^{-1}, and a negligible S_1. The estimated white frequency-noise level corresponds to an intrinsic linewidth of $\Delta f = (34\pm10)$ kHz, corresponding to a reduction of approximately two orders of magnitude as compared to the case without external-cavity feedback. This is in good agreement with other reported results [131], [135].

To investigate the effect of optical feedback on the optical properties of different comb lines, we evaluated the frequency noise spectra of three widely separated tones of the comb, see Figure **4.2**c. The dashed lines indicate again the model fits to the measured spectra according to Eq. (4.2). The relative locations of the comb tones within the comb spectrum are indicated in the inset. The results presented in Figure **4.2**b correspond to comb line B with an intrinsic linewidth of $\Delta f_\mathrm{B} = 34$ kHz. For the comb lines A and C, we find intrinsic linewidths of $\Delta f_\mathrm{A} = 96$ kHz and $\Delta f_\mathrm{C} = 55$ kHz, respectively. Hence, despite the typical increase of the intrinsic linewidths of the tones towards the edge of the comb [142], [143], the external-cavity feedback can greatly reduce the frequency noise throughout the comb spectrum when compared to the frequency noise without external feedback. Note that, due to the presence of flicker ($\propto f^{-1}$) and random-walk ($\propto f^{-2}$) frequency noise, the intrinsic optical linewidths of the various tones are not any more directly connected to the RF linewidth [149], since the underlying relations derived in [143] are only valid under the assumption that all linewidths are dominated by the spectrally white (f^0) component.

4.3 WDM transmission over 75 km at a net data rate of 11.215 Tbit/s using 32QAM

To demonstrate that feedback-stabilized QD-MLLD are well suited as multi-wavelength light sources for high-speed communications with higher-order modulation formats, we perform a WDM experiment using 32-state quadrature amplitude modulation (32QAM). The experimental setup is shown in Figure

4.3a. An erbium-doped fiber amplifier (EDFA1) is used to boost the total power of the QD-MLLD comb from approximately 8 dBm to approximately 17 dBm. A total number of 60 carriers out of the full QD-MLLD comb are then selected, 55 of which lie within the 3 dB bandwidth of the comb while an additional 5 carriers are within the 4 dB bandwidth. The comb is spectrally flattened by a programmable filter (PF). WDM is emulated by encoding different data in neighboring "odd" and "even" channels. To this end, we de-interleave the frequency comb lines (FSR = 25 GHz) into odd and even tones using the programmable filter (PF). Since at this FSR, the PF has a rather low extinction of approximately 20 dB, we use a 25 GHz-to-50 GHz de-interleaver (De-int.) as a second filtering element. This leads to an extinction of the unwanted tones by more than 45 dB, see power spectrum P1 in Figure **4.3**b that shows the odd and even carriers combined in one graph. The odd and the even carriers are separately amplified by EDFA2 and EDFA3 and independently modulated with data of pseudo-random binary sequences (PRBS), which are mapped to 32QAM symbols at a rate of 20 GBd. We chose a PRBS length of $2^{11}-1$, dictated by limitations of the memory size and the memory granularity of the arbitrary-waveform generator (AWG) that was used to generate the data signals. In previous experiments [J3], that relied on the same equipment but were performed at slightly different ratios of symbol rate and sample rate, we have verified that the performance of our system does not change if we use longer PRBS length such as $2^{15}-1$. We use pulses having raised-cosine power spectra with a 20 % roll-off. After modulation, odd and even channels are combined, and polarization division multiplexing (PDM) is emulated by a split-delay-combine method [75]. The data stream is amplified and transmitted over 75 km of standard single-mode fiber (SSMF), see lower power spectrum P2 in Figure **4.3**b. For avoiding nonlinearities, we limit the total power entering the fiber to 10 dBm.

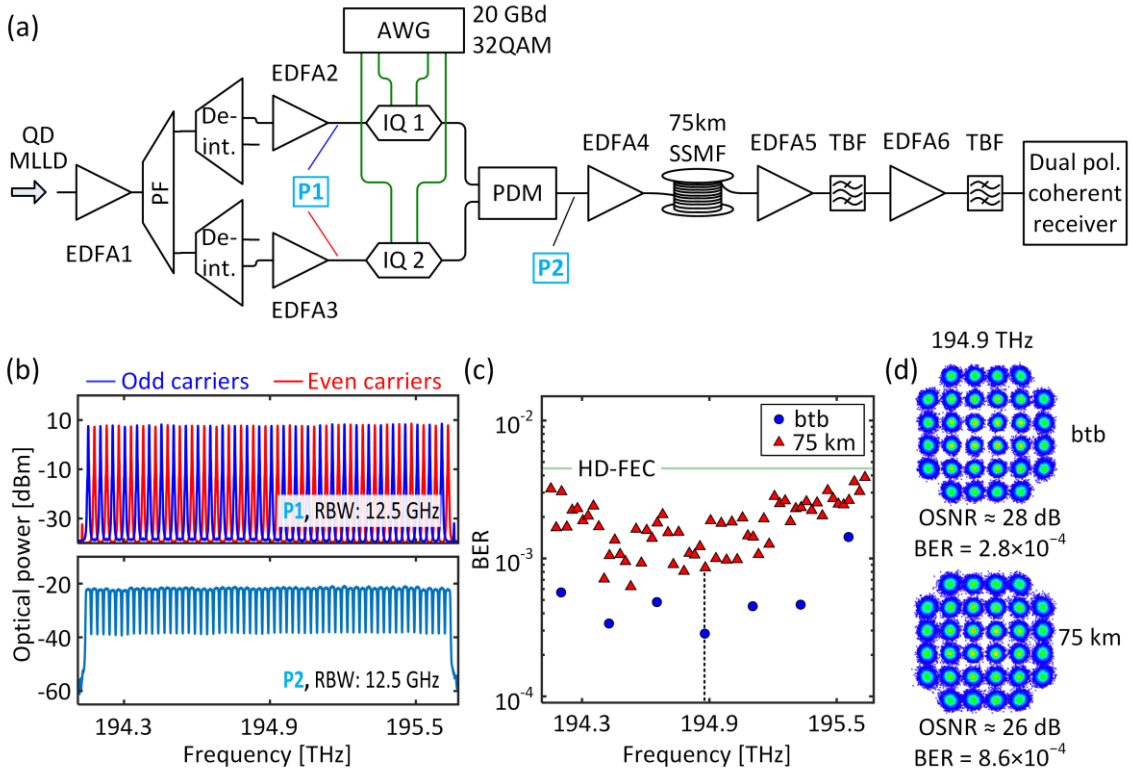

Figure 4.3: WDM transmission experiment using a feedback-stabilized QD-MLLD comb according to Figure 4.1b. **(a)** Setup for the WDM experiment. An erbium-doped fiber amplifier (EDFA1) boosts the total power of the QD-MLLD comb to approximately 17 dBm and a total of 60 carriers are then selected and spectrally flattened by a programmable filter (PF). The PF is also used to de-interleave the frequency comb lines (FSR = 25 GHz) into odd and even tones for emulating WDM transmission by encoding different data in neighboring channels. In addition, we use a 25 GHz-to-50 GHz de-interleaver (De-int.) as a second filter element to further increase the extinction of the unwanted tones. Both the odd and the even carriers are amplified by subsequent EDFA2 and EDFA3 and independently modulated with 32QAM symbols at a rate of 20 GBd. We use pulses having raised-cosine power spectra with a 20 % roll-off. After modulation, odd and even channels are combined, and polarization division multiplexing (PDM) is emulated by a split-delay-combine method. The data stream is amplified and transmitted over 75 km of standard single-mode fiber (SSMF). **(b)** Combined spectra of both odd and even carriers taken at position P1, i.e., before modulation (top) and spectrum of 60 modulated channels measured at position P2 (bottom). **(c)** BER of the transmitted channels for both back-to-back (btb) and 75 km fiber transmission. **(d)** Example constellation diagrams of the channel at 194.9 THz (indicated by the vertical dashed line) for btb and 75 km fiber transmission. TBF: tunable band pass filter.

At the receiver we employ a two-stage amplification scheme using a first fiber amplifier (EDFA5) for boosting the WDM signal as a whole, then selecting the channel of interest with a tunable bandpass filter (TBF) for amplification with a second amplifier (EDFA6), followed by another tunable band pass filter (passband 1.5 nm) to suppress out-of-band amplified spontaneous emission (ASE). At the input of EDFA6, the power of the selected WDM channels varies between −19 dBm and −16 dBm, depending on the spectral position of the channel. Given the flat spectrum of the transmitted WDM signal, Figure **4.3**b, we attribute these variations to the slightly wavelength-dependent gain of EDFA4 and EDFA5. Note, however, that EDAF6 is operated in constant-output-power mode, such that the power levels at the input of the coherent receiver do not vary significantly from channel to channel. The selected channel is then received with an optical modulation analyzer (OMA, Keysight N4391A), and processed using Keysight's vector signal analyzer (VSA) software. The VSA processing comprises spectral filtering, blind Stokes-space polarization demultiplexing [150], chromatic dispersion compensation, and a 55-tap adaptive blind equalizer based on the decision-directed least-mean-squares (LMS) algorithm. Carrier phase estimation in done through a block-wise Viterbi & Viterbi algorithm with a block length of 1024 symbols [151]. We also measured the optical signal-to-noise power ratio (OSNR) of our WDM channels at the receiver. To this end, we had to rely on the received electrical signal, since the channel separation was too small for a reliable measurement with an optical spectrum analyzer. We found OSNR values in the range of 23…26 dB, defined with respect to the usual reference noise bandwidth of 0.1 nm.

Figure 4.3c depicts the extracted bit error ratios (BER) for fiber transmission of all channels along with the back-to-back (btb) BER for seven randomly selected channels. When transmitting over a 75 km-long SSMF, all BER values are below 4.0×10^{-3} with a 95% confidence level [152] and are hence compatible with the threshold of 4.45×10^{-3} for forward error correction (FEC) with 7 % overhead [114]. This leads to a line rate (net data rate) of 12 Tbit/s (11.215 Tbit/s) with a net spectral efficiency (SE) of 7.5 bit/s/Hz after deduction of FEC overhead. Note that this SE is significantly below the 10 bit/s/Hz that could be theoretically achieved by dual-polarization 32QAM signaling. The

reduced SE is a direct consequence of the rather high roll-off of 20 % that was chosen deliberately to avoid problems with the clock recovery in the VSA software. Using a more robust clock-recovery technique would allow to reduce the roll-off and thus to increase the SE. Example constellation diagrams of the comb line at carrier frequency 194.9 THz for both back-to-back and 75 km fiber transmission are shown in Figure 4.3d along with the corresponding OSNR and BER values. The back-to-back experiment exhibits higher OSNR than the transmission experiment and performs better in terms of BER. We thus believe that the signal quality in our transmission experiments is limited by OSNR and that phase noise of the optical carrier does not play a role once stabilization by external-cavity feedback is used. This is in line with the fact that the constellation points in Figure 4.3d have an approximately symmetric circular spread. A closer observation of the back-to-back constellation diagram may also reveal the impact of relative intensity noise (RIN), which leads to a scattering of the constellation points that is most pronounced for the outer symbols. Therefore, the relatively high RIN of QD-MLLD could still be a limitation at high OSNR values, even if external-cavity feedback is employed, see Appendix B for a RIN characterization of the QD-MLLD with and without external-cavity feedback. We also tried 20GBd 32QAM-transmission without external-cavity feedback but could not recover the signal at the receiver because of excessive phase noise. To the best of our knowledge, these experiments represent the first demonstration of 32QAM transmission using a QD-MLLD as a multi-wavelength light source, leading to the highest spectral efficiency reported for such a device. The line rate of 12 Tbit/s and the transmission distance of 75 km is on par with the 11.55 Tbit/s and the 75 km achieved by using native QD-MLLD with advanced phase tracking [10] and compares well with the 12.032 Tbit/s that were demonstrated for 16QAM back-to-back signaling with feedback-stabilized quantum-dot MLLD for 16QAM [153].

4.4 Extension to higher symbol rates

In our experiments, we used rather low symbol rates of 20 GBd because we had access to QD-MLLD chips only with an FSR of approximately 25 GHz. In

addition, this choice allows us to better isolate the impact of phase noise, exploiting the fact that signals with lower symbol are more prone to phase noise and less sensitive to ASE noise. Clearly, the reduced phase noise should also improve the transmission performance at higher symbol rates beyond 50 GBd that are expected to become the standard in coherent transmission [154], [155]. Note that, with OCNR values in excess of 37 dB and comb line powers in excess of -10 dBm as indicated in Figure 4.1c, QD-MLLD should support link-limited transmission of up to 56 GBd 64QAM (600 Gbit/s) per line over more than 10 fiber spans of 75 km each, i.e., for a reach of > 700 km [23]. To investigate the transmission performance of QD-MLLD in such scenarios, we performed Matlab simulations using the measured phase-noise characteristics of our QD-MLLD along with different levels of AWGN, quantified by the OSNR. To this end, we first extract time series of random phase fluctuations from the phase-noise measurements presented in Figure 4.2b. Note that the measured phase-noise time series is also impacted by the ASE of the EDFA in the measurement setup, see Figure 4.2a. This leads to an f^2- component in the corresponding frequency-noise spectrum, Figure 4.2b, which we suppress by applying a first-order low-pass filter with amplitude transfer function $1/(1+\mathrm{j}(f/f_{3\mathrm{dB}}))$ to the measured frequency-noise time series, where the cut-off $f_{3\mathrm{dB}}=\sqrt{S_0/S_3}$ is defined by the frequency for which the f^2- component starts to dominate the power spectral density of the frequency noise. Figure 4.4a shows the measured frequency-noise spectrum of a tone (tone B in Figure **4.2**c) extracted from a free-running QD-MLLD (black) and the corresponding model fit according to Eq. (4.2) (black/white dotted) along with the filtered power spectrum (blue) and the model fit without the f^2- component (blue/white dotted). Figure **4.4**b shows the corresponding quantities for the same tone extracted from the feedback-stabilized device. The corresponding time series $\phi_\mathrm{c}(t)$ of the carrier phase fluctuations is obtained by integrating the time series of the frequency-noise over time.

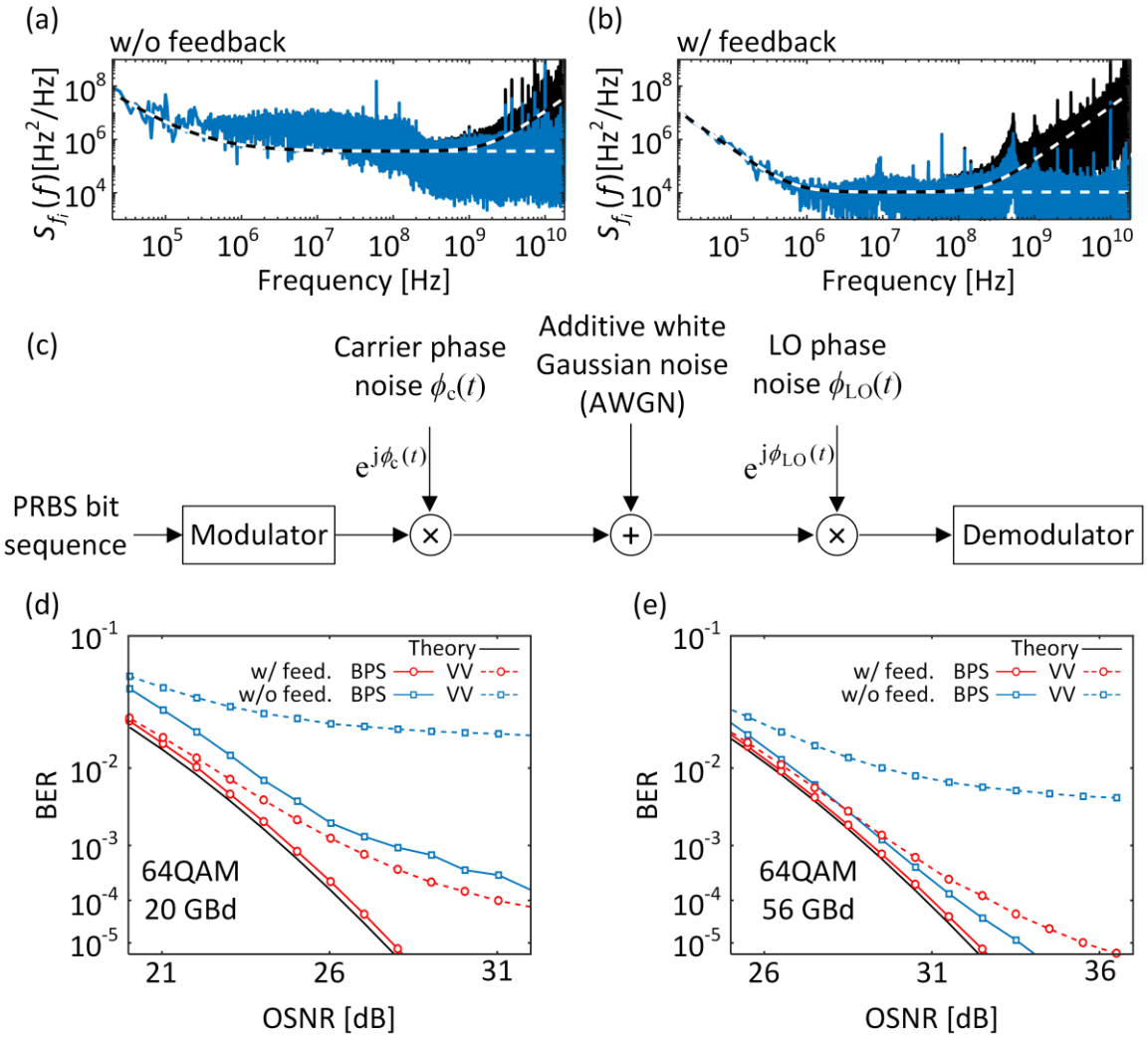

Figure 4.4: Simulation of 64QAM transmission performance of feedback-stabilized and free-running QD-MLLD. **(a, b)** Measured frequency-noise spectra (black) for QD-MLLD without (w/o) and with (w/) external-cavity feedback, respectively, along with filtered counterparts (blue) that are used to emulate the phase noise of the carrier and the LO tone in the transmission simulation. The filtering is used to suppress the unwanted impact of ASE noise ($\propto f^2$) in the phase-noise measurement. The dashed lines correspond to the respective model fits according to Eq. (4.2), see also Figure 4.2b. **(c)** Simulation setup. A PRBS bit sequence is mapped to a 64QAM symbol pattern with one sample per symbol in the modulator. Measured phase data is added to the phase of the modulated symbols using phasor multiplication to emulate the carrier phase noise $\phi_c(t)$ and the LO-tone phase noise $\phi_{LO}(t)$. AWGN is added to the resulting modulated signal to emulate different optical signal-to-noise power ratios (OSNR) at the receiver. The received signal is then demodulated by employing the blind phase search (BPS) algorithm for carrier recovery. **(d, e)** Simulated bit error ratios (BER) as a function of OSNR for 64QAM signaling at symbol rates of 20 GBd and 56 GBd, respectively. (Caption continued on next page)

Figure 4.4 continued: We use highly effective symbol-wise blind phase search (BPS) with 45 test angles and numerically much simpler Viterbi-Viterbi (VV) processing with fourth-power phase estimation. For BPS, the BER obtained for the feedback-stabilized QD-MLLD ('w/ feedback', red) is close to the theoretical values ('Theory', blue) that are estimated only based on the OSNR, without any phase noise at all. In contrast to that, the free-running QD-MLLD ('w/o feedback', blue) performs worse. A clear performance advantage is found even for the higher symbol rate of 56 GBd, which should be much less prone to phase noise than the 20 GBd transmission. For the numerically less complex VV algorithm, the benefit of phase-noise reduction by external-cavity feedback becomes even more prominent, indicating that feedback stabilization of QD-MLLD may also allow to simplify digital phase estimation.

The time series $\phi_c(t)$ of the carrier phase fluctuations is then used in the Matlab simulation, which is schematically illustrated in Figure 4.4c. In a first step, a PRBS is mapped to a 64QAM symbol pattern with one sample per symbol in the modulator. The carrier phase noise is then emulated by resampling the time series $\phi_c(t)$ at the symbol rate and by adding the fluctuations to the phase of the modulated symbols using phasor multiplication. AWGN is added to the resulting modulated signal to emulate different OSNR levels at the receiver. The OSNR is specified with respect to the usual reference bandwidth of 0.1 nm (12.5 GHz). In our transmission scenario, we assume that the LO tone at the coherent receiver is also derived from a QD-MLLD that is nominally identical to the device at the transmitter. This is emulated by adding a time series of LO phase fluctuations $\phi_{LO}(t)$ to the phases of the data signal prior to reception. For simplicity, we derive the time series $\phi_{LO}(t)$ from a previously unused section of the measured carrier phase fluctuations $\phi_c(t)$, i.e., $\phi_{LO}(t) = \phi_c(t - \tau_d)$, where the delay τ_d is chosen much larger than the inverse of the intrinsic linewidth to ensure statistically independent phase-noise processes. The received signals are then demodulated by employing two different phase-estimation techniques: Symbol-wise blind phase search (BPS) with 45 test angles [10], [38] and numerically much simpler Viterbi-Viterbi (VV) processing with fourth-power phase estimation [156], [157]. Other processing steps that are usually employed in conventional coherent receivers, e.g., for polarization demultiplexing or equalization, are not relevant here as these effects are not included in the rather simple AWGN channel model.

Figure 4.4d,e show the BER obtained by BPS and VV at symbol rates of 20 GBd and 56 GBd at different OSNR levels with and without phase-noise suppression by external-cavity feedback. For BPS, we use an averaging block length between 8 and 64 symbols, which is optimized individually for each OSNR value. For both 20 GBd and 56 GBd, the BER obtained for the feedback-stabilized QD-MLLD ('w/ feedback', red) is close to the theoretical values ('Theory', blue) that are estimated only based on the OSNR, without considering phase noise at all. We hence conclude that, for feedback-stabilized QD-MLLD and practically relevant OSNR levels at the receiver, the transmission performance obtained with BPS is limited by OSNR rather than by phase noise, and that the peaks that occur in the frequency-noise spectra of Figure **4.2**b and Figure **4.4**b do not represent a relevant limitation. In contrast to that, the free-running QD-MLLD ('w/o feedback', blue) performs worse. As expected, the positive impact of phase-noise reduction is more pronounced at the lower symbol rate of 20 GBd than at 56 GBd. The benefit of phase-noise reduction by external-cavity feedback becomes even more prominent when using simpler phase estimation techniques such as VV. Also, here we adapt the block individually for each OSNR value. Within the considered range of OSNR, the BER achieved with VV and a free-running QD-MLLD exceeds the threshold of 4.45×10^{-3} for FEC with 7 % overhead [114], even for a symbol rate of 56 GBd, but improves drastically once feedback stabilization is used. We hence conclude that feedback stabilization of QD-MLLD offers a clear performance advantage for a wide range of technically relevant OSNR levels and may even allow to reduce the complexity of the phase estimation algorithm.

4.5 Summary

We demonstrate that QD-MLLD with coherent external feedback can be used for spectrally efficient high-speed data transmission using advanced modulation formats beyond 16QAM. In our experiment, we use 32QAM signaling on 60 carriers to transmit at a line rate of 12 Tbit/s (net data rate 11.215 Tbit/s) over a 75 km-long standard single mode fiber link at a spectral efficiency of 7.5 bit/s/Hz. To the best of our knowledge, this is the first time that an optical

frequency comb from a QD-MLLD has been used for data transmission with 32QAM as a modulation format. We also show by simulations that external-cavity feedback should give clear performance advantages for 64QAM signaling and symbol rates of, e.g., 56 GBd. For real-world systems, the free-space external cavity may be replaced by integrated optical feedback circuits that rely, e.g., on ring resonators [126]. The requirements with respect to the quality of these resonators are relatively low – significant linewidth reductions may already be achieved with external-cavity round-trip losses of more than 20 dB [134]. Established ring-resonator technologies [158], [159] should allow to easily fulfill these requirements, thereby opening a route towards chip-scale WDM transceivers that exploit feedback-stabilized QD-MLLD to support line rates of tens of Tbit/s.

[*end of paper [J2]*]

5 Quantum-dash mode-locked laser diodes for multi-terabit/s transmission and reception

This chapter investigates quantum-dash mode-locked laser diodes (QD-MLLD) as multi-wavelength light sources both at the transmitter and receiver sides of a WDM link. It is taken from paper [J3], which was published in *Optics Express*. The material from the publication is reproduced here with the appropriate changes to fit the structure and notation of this thesis.

[*Beginning of paper [J3]*]

Copyright © 2019 Optical Society of America

Multi-wavelength coherent transmission using an optical frequency comb as a local oscillator

Optics Express, Volume 27, Issue 22, pp. 31164-31175, 2019
DOI: 10.1364/OE.27.031164

Juned N. Kemal,[1] Pablo Marin-Palomo,[1] Vivek Panapakkam,[2] Philipp Trocha,[1] Stefan Wolf,[1] Kamel Merghem,[3] François Lelarge,[4] Abderrahim Ramdane,[2] Sebastian Randel,[1] Wolfgang Freude,[1] and Christian Koos[1,5]

[1] Institute of Photonics and Quantum Electronics (IPQ), Karlsruhe Institute of Technology (KIT), Germany
[2] Centre de Nanosciences et de Nanotechnologies (CNRS), Univ. Paris-Sud, C2N - Université Paris-Saclay, France
[3] Now at Institut Mines-Télécom - Télécom SudParis, EVRY, France
[4] Now with Almae Technologies, Marcoussis, France
[5] Institute of Microstructure Technology (IMT), Karlsruhe Institute of Technology (KIT), Germany

Quantum-dash (QD) mode-locked laser diodes (MLLD) lend themselves as chip-scale frequency comb generators for highly scalable wavelength-division multiplexing (WDM) links in future data-center, campus-area, or metropolitan networks. Driven by a simple DC current, the devices generate flat broadband frequency combs, containing tens of equidistant optical tones with line spacings of tens of GHz. Here we show that QD-MLLDs can not only be used as multi-wavelength light sources at a WDM transmitter, but also as multi-wavelength local oscillators (LO) for parallel coherent reception. In our experiments, we demonstrate transmission of an aggregate net data rate of 3.9 Tbit/s (23 × 45 GBd PDM-QPSK, 7 % FEC overhead) over 75 km standard single-mode fiber (SSMF). To the best of our knowledge, this represents the first demonstration of a coherent WDM link that relies on QD-MLLD both at the transmitter and the receiver.

5.1 Introduction

Driven by the explosive growth of data traffic on all levels of optical communication networks [119], wavelength-division multiplexing (WDM) has become a necessity not only for long-haul transmission, but also for shorter links that connect, e.g., data centers across metropolitan or campus-area networks. These links crucially rely on compact WDM transceivers that offer multi-terabit/s aggregate data rates and that can be deployed in large quantities at low cost. In this context, optical frequency combs have emerged as a promising approach towards compact and efficient light sources that provide a multitude of tones for parallel WDM transmission [J1], [J2], [J3], [J4], [5], [11], [13], [16], [18], [21], [74], [75], [121], [160], [161]. Unlike the carriers derived from a bank of individual lasers, the tones of a comb are intrinsically equidistant in frequency and are defined by just two parameters – the center frequency and the free spectral range (FSR).

Over the last years, various high-speed WDM transmission experiments have been carried out using a wide variety of different chip-scale comb generators that rely, e.g., on highly nonlinear GaAlAs waveguides for spectral broadening

of narrowband seed combs [13], on Kerr-nonlinear high-Q silicon-nitride microresonators [J4], [11], [121], on gain switching of semiconductor lasers [J1], [16], [21], or on electro-optic modulators [5], [18], [160], [161]. Among the different frequency comb sources, quantum-dash mode-locked laser diodes (QD-MLLD) [22], [162] are particularly interesting due to their technical simplicity: Driven by a direct current, these devices emit broadband frequency combs consisting of tens of optical carriers, spaced by free spectral ranges of, e.g., 25 GHz or 50 GHz, as determined by the cavity length. In previous experiments [J2], [J3], the potential of QD-MLLD has been demonstrated by using the devices as multi-wavelength optical sources for parallel transmission in tens of WDM channels, achieving aggregate lines rates of more than 10 Tbit/s. In these experiments, symbol-wise blind phase-search (BPS) algorithm [38] or self-injection locking [J2], [163] was used to overcome the limitations imposed by the rather high intrinsic linewidth of the QD-MLLD tones. However, while these demonstrations show the great potential of QD-MLLDs as multi-wavelength light sources at the WDM transmitter site, demodulation of the coherent signals still relies on a single-wavelength external-cavity laser (ECL), which acts as a local oscillator (LO) and needs to be tuned to the respective channel of interest. The scalability advantages of QD-MLLD for massively parallel WDM transmission have hence only been exploited at the transmitter, but not at the receiver site.

In this work, we demonstrate that QD-MLLD can also act as multi-wavelength local oscillators for intradyne reception of a multitude of optical channels [61]. In our experiments, we use a pair of QD-MLLDs with similar free spectral ranges (FSR) – one device to generate the optical carriers for the WDM transmitter, and the other device to provide the required LO tones for parallel coherent reception. We use 23 carriers separated by 50 GHz to transmit data at a symbol rate of 45 GBd using QPSK signaling, thereby obtaining data streams with an aggregate line rate of 4.14 Tbit/s and an aggregate net data rate of 3.87 Tbit/s which are transmitted over 75 km of standard single mode fiber (SSMF). To the best of our knowledge, this is the first demonstration of a QD-MLLD acting as a multi-wavelength LO in coherent transmission. When combined with highly integrated coherent transceiver circuits [164]–[167] and

advanced digital signal processing (DSP) schemes implemented, e.g., in 7 nm CMOS technology [168], [169], our approach could open a path towards coherent WDM transceivers with unprecedented compactness and scalability.

5.2 Optical frequency combs for WDM transmission and reception

The basic concept of a point-to-point WDM link using optical frequency combs is shown in Figure **5.1**. The tones from the transmitter comb (Tx comb) are demultiplexed (DEMUX), and data is encoded onto the individual carriers by in-phase/quadrature modulators (IQ mod.). The optical channels are combined using a frequency multiplexer (MUX), amplified if needed, and transmitted through the transport fiber. At the WDM receiver, the channels are demultiplexed and sent to an array of independent coherent receivers (Coh. Rx). The demultiplexed spectral lines of a second frequency comb (LO comb) serve as local oscillator tones for the various coherent receivers.

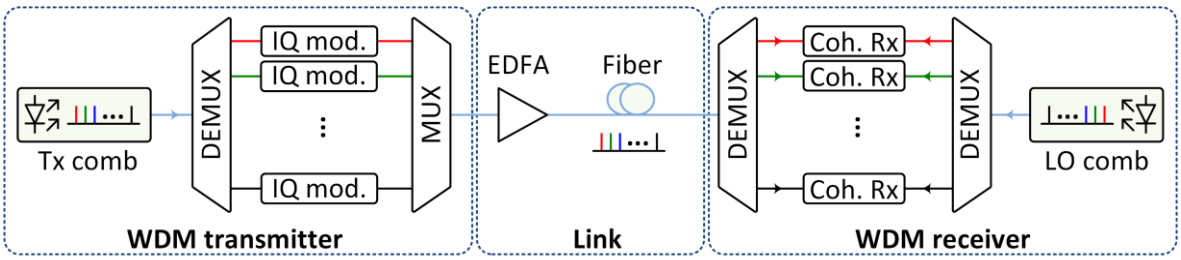

Figure 5.1: Setup of a coherent WDM transmission link using optical frequency combs as light sources both at the transmitter and the receiver. WDM transmitter: Carriers from a transmitter comb (Tx comb) are demultiplexed (DEMUX) and modulated separately using in-phase/quadrature modulators (IQ mod.). The channels are then multiplexed (MUX) to form the WDM signal. Link: The WDM signal is amplified and transmitted. WDM receiver: The channels are demultiplexed and sent to an array of independent coherent receivers (Coh. Rx). The demultiplexed spectral lines of a local oscillator comb (LO comb) serve as LO tones for the various coherent receivers. EDFA: Erbium-doped fiber amplifier.

For our data transmission experiment, we use two QD-MLLDs – one as the Tx comb and the second as the LO comb. Figure **5.2**a shows the basic structure of

a QD-MLLD with an active region that consists of three stacked layers of InAs quantum dashes separated by InGaAsP barriers. Each QD layer is 2 nm thick and the barriers have a thickness of 40 nm. Two 80 nm-thick separate confinement heterostructure (SCH) layers of InGaAsP terminate the dash-barrier stack towards the top and bottom InP layers [22], [128]. The optical mode is guided by a buried ridge waveguide of 1.0 µm width. Cleaved chip facets form a Fabry-Perot laser cavity with a length of 1.71 mm, leading to an FSR of 25 GHz. Top and bottom gold layers provide electrical contacts to the active region of the MLLD via p-doped and n-doped InP layers, respectively. Lateral confinement of carriers is obtained by proton implantation [22]. Multiple longitudinal modes can coexist in the laser cavity due to the inhomogeneously broadened gain of the active region originating from the shape distribution of the QDs. Mode locking due to mutual sideband injection [128] produces an optical frequency comb output centered at 1545 nm with a line spacing of 25 GHz.

In coherent reception, it is desired to maintain a low frequency offset between the carrier of each channel and the corresponding LO tone at the receiver. This requires a Tx comb and an LO comb with similar center frequencies and free spectral ranges. To this end, we used two QD-MLLDs that are taken from the same wafer and are carefully cleaved to have very similar cavity lengths, thus resulting in overlapping spectra for appropriately set operating currents and temperatures. The cleaved chips were mounted with indium solder on a copper submount. The submount, in addition to serving as a heatsink, allows easier handling of the devices as compared to the bare chips. To select the operating conditions of the two QD-MLLDs, we characterized the devices using the setup in Figure **5.2**b. The emitted light is coupled to a lensed fiber, which is equipped with anti-reflection (AR) coating for 1550 nm and connected to an optical isolator to reduce optical back-reflection into the laser cavity. Different instruments, denoted by C, D, and E, are connected to the output of the isolator for measuring the data of Figure **5.2**c-e.

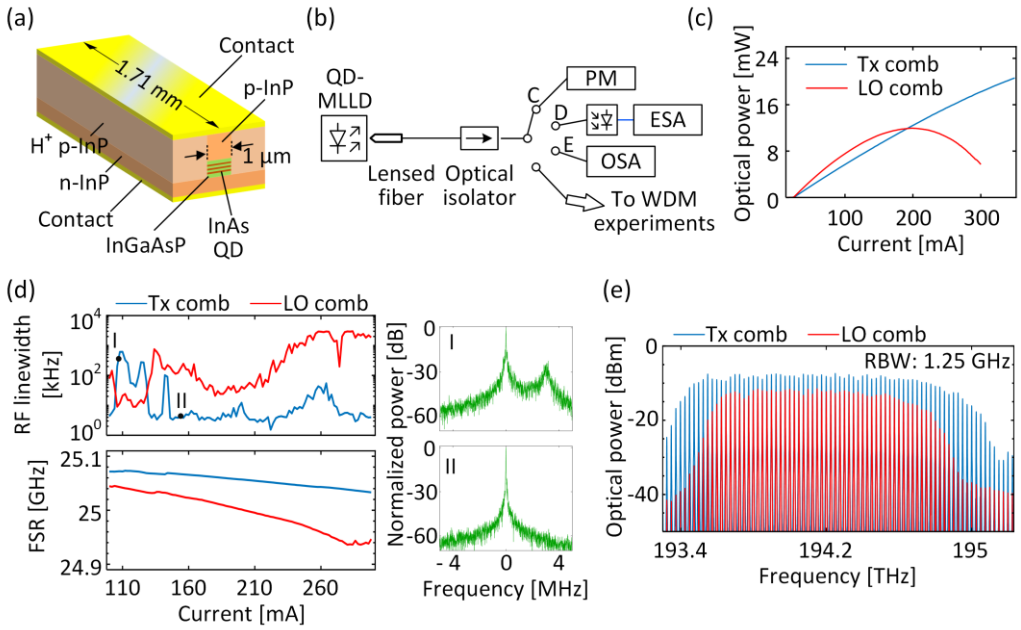

Figure 5.2: Concept and characterization of quantum-dash mode-locked laser diodes (QD-MLLD). **(a)** Three-dimensional schematic of a QD-MLLD. The active region consists of three stacked layers of InAs QD, which are separated by InGaAsP barriers. The buried ridge waveguide has a width of 1.0 µm. Cleaved chip facets form a Fabry-Perot laser cavity with a length of 1.71 mm, leading to an FSR of 25 GHz. Top and bottom gold layers provide electrical contacts to the active region of the QD-MLLD via p-doped and n-doped InP layers. **(b)** Basic optical setup for using the QD-MLLD comb source. The device is driven by a constant injection current (not shown). The emitted light is collected by a lensed fiber, and an optical isolator is used to reduce back-reflections into the QD-MLLD. Setups C, D, and E are used for measuring the data of Subfigures (c), (d), and (e), respectively. PM: Power meter; ESA: Electrical spectrum analyzer; OSA: Optical spectrum analyzer. **(c)** Measured total comb power versus injection current of the Tx and the LO combs. **(d)** Full-width half maximum (FWHM) of the radio-frequency (RF) beat note (upper plot) as a function of the drive current for the Tx comb (blue) and for the LO comb (red), and free spectral range (FSR, lower plot) as a function of the drive current for the Tx comb (blue), and for the LO comb (red). For some drive currents, we observe distinctively higher RF linewidths, see, e.g., Point I. In these cases, we often observe more than one beat note in the RF spectrum, Inset I, which we attribute to the coexistence of two sub-combs with slightly different FSR [33]. For such operating states, the depicted large RF linewidth values are to be understood as an indication of unstable operation by the MLLD. Inset II shows the measured RF beat note corresponding to a stable single sub-comb operation of the QD-MLLD. In the insets, the spectral power is normalized to the dominant peak, and the frequency axis is defined with respect to the spectral position of this peak. **(e)** Optical power spectra of the Tx comb (blue) and the LO comb (red). RBW: Resolution bandwidth of the OSA.

Figure 5.2c shows the total output optical power of the Tx comb and the LO comb as a function of the injection current. Insertion losses of coupling interface to the lensed fiber (2 dB) and the isolator (1 dB) are taken into account. At a pump current of 300 mA, the output power radiated from the facet of the Tx comb exceeds 18 mW (12.5 dBm). The LO comb power peaks at 12 mW (10.8 dBm) for an injection current of 200 mA. We attribute the smaller output power of the LO comb to imperfect mounting and thermal coupling of the associated chip in our experiment. This is also confirmed by carrying out a thermal resistance measurement of both the Tx and LO combs according to [170]. The Tx comb exhibits a thermal resistance of 24 K/W which is as expected for our devices whereas the LO comb has a very high thermal resistance of 152 K/W. This high thermal resistance leads to high operating temperatures for the LO comb and, therefore, poor lasing performance as is expected for semiconductor lasers [171], [172].

Figure 5.2d, upper plot shows the measured FWHM of the RF beat note, commonly referred to as the RF linewidth, as a function of the injection current both for the Tx comb and the LO comb. The RF beat note results from mixing neighboring tones of a comb in a photodiode and is measured by connecting the photodiode to an electrical spectrum analyzer (ESA), see Figure **5.2**b, Setup D. A narrow RF linewidth indicates a reduced optical phase noise of the individual comb lines [143], which is advantageous for coherent optical communication. For certain drive currents, we observe comparatively large RF linewidths, see, e.g., Point I in Figure **5.2**d. In these cases, we often observe more than one beat note in the RF spectrum, Inset I in Figure **5.2**d, which we attribute to the coexistence of two sub-combs with slightly different FSR in the QD-MLLD cavity [173]. For such operating states, the large RF linewidth values refer to the dominant spectral peak and should only be taken as indicators for unstable operation by the QD-MLLD. Figure **5.2**d, Inset II shows the measured RF beat note corresponding to a stable operation state of the QD-MLLD with a single sub-comb. The lower plot in Figure **5.2**d shows the measured FSR of the Tx comb and the LO comb as a function of the injection current. During the above current sweeps, the submounts of the Tx and LO MLLD chips are temperature-stabilized at 23.6 °C and 18.9 °C, respectively. These temperatures were chosen

such that the tones of the two combs roughly coincide in center frequency. As can be seen in Figure **5.2**d, the Tx comb has a small RF linewidth for a wide range of injection currents above 130 mA, whereas the LO comb exhibits a small RF linewidth only for injection currents between 90 mA and 130 mA. We attribute this to the higher operating temperature of the LO comb chip as a result of its high thermal resistance. Thermal variations, just like injection current, affect the mode locking stability (RF linewidth, repetition rate) through the competition of different mode locking regimes [173], [174]. For the subsequent WDM experiments with the two combs, we used injection currents of 278 mA and 125 mA for the Tx comb and the LO comb, respectively. This resulted in a small FSR difference (ΔFSR) of about 4 MHz between the two combs while maintaining RF linewidths of less than 20 kHz. The low RF linewidth of 20 kHz results from the fact that, in a stable mode-locked state, neighboring comb lines of a QD-MLLD are phase correlated as a result of nonlinear processes in the gain medium [173], [175], [176]. The optical spectra of the combs operated at the selected injection currents are shown in Figure **5.2**e. The LO comb has a lower 3 dB bandwidth than the Tx comb, thereby limiting the total number of WDM channels that can be received.

The modulation formats and the symbol rates employed in a coherent communication link depend on the combined short-term linewidth of the transmitter carrier and the receiver LO [38]. This can be determined from the linewidth of the beat note generated by mixing a carrier and an LO tone. Figure **5.3**a shows the experimental setup used for estimating the combined linewidth of the QD-MLLD Tx and LO comb tones. Tunable band-pass filters (TBF) select single comb tones with comparable optical frequencies from the Tx comb and the LO comb. The selected tones are coupled to a 90° optical hybrid with a polarization controller in the Tx comb path to align the polarizations of the tones. The in-phase and quadrature outputs of the optical hybrid are detected with balanced photodetectors (BPD), and the electrical signals are sampled with two-channels of a real-time oscilloscope (RTO). Figure **5.3**b, green trace, shows the power spectrum of the beat note between a carrier tone of the Tx comb and the corresponding tone of the LO comb. The plot is obtained by a Fourier transform of the sampled time-domain data, which was recorded over a duration

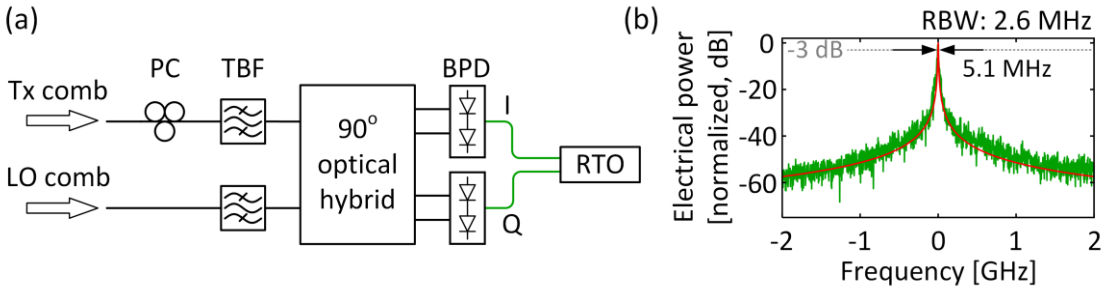

Figure 5.3: Phase-noise characterization of QD-MLLD. **(a)** Experimental setup. Narrow-band tunable band-pass filters (TBF) are used to select distinct lines with comparable frequencies from the Tx comb and the LO comb. A polarization controller (PC) is used to match the polarizations of the selected tones at the input of a 90° optical hybrid. Balanced photodetectors (BPD) deliver the electrical in-phase (I) and quadrature (Q) signals, which are sampled with a real-time oscilloscope (RTO) for offline processing. **(b)** Power spectrum of the beat note between the two tones selected from the Tx comb and the LO comb as a function of the offset from the beat note frequency (green trace). The duration of the corresponding time-domain signals is 0.4 µs. We use the IQ data to independently extract a short-term Lorentzian linewidth of 5.1 MHz. The associated line shape (red trace) coincides well with the measured spectrum.

of 0.4 µs. The horizontal axis refers to the frequency offset from the center of the beat note.

For further analysis of the phase-noise characteristics, we extract the phases $\phi(t)$ of the recorded I/Q signal and use it for determining the combined short-term (Lorentzian) linewidth of the tones from the Tx and LO combs. To this end, the differences of the phases $\Delta\phi_\tau(t)=\phi(t+\tau)-\phi(t)=2\pi f_i(t)\tau$ are calculated for various delay times $\tau>0$ and the variance $\sigma^2_{\Delta\phi}(\tau)$ is computed. From this, the short-term Lorentzian linewidth Δf is extracted from the slope of the variance $\sigma^2_{\Delta\phi}(\tau)$ at small time delays [37],

$$\Delta f=\lim_{\tau\to 0}\frac{\sigma^2_{\Delta\phi}(\tau)}{2\pi\tau}. \tag{5.1}$$

This technique leads to a 5.1 MHz Lorentzian linewidth for the beat note. The same result is obtained by analyzing the FM noise spectrum and extracting the spectrally constant white-noise component [144]. This linewidth of the beat note between a tone of the Tx comb and a tone of the LO comb is significantly

larger than the RF linewidth of the Tx and LO combs separately, because the tones of two independent QD-MLLDs have no phase correlation. The Lorentzian lineshape corresponding to the estimated 5.1 MHz linewidth is plotted in Figure **5.3**b, red trace, and shows good agreement with the directly measured lineshape, green trace. This indicates that, for the chosen observation time of 0.4 µs, the lineshape is dominated by high-frequency phase noise rather than by low-frequency drift. Since the estimated linewidth of the QD-MLLD tones is relatively high compared to that obtained from benchtop-type continuous-wave (CW) ECL, we use QPSK signaling at high symbol rates and employ symbol-wise BPS for carrier recovery as in [10] for the transmission experiments discussed in Section 5.3. Signaling with 16QAM and higher order modulation formats was not possible with a QD-MLLD as an LO, and it would require more robust carrier recovery schemes, for instance, using pilot symbols [177] or hardware-based phase noise reduction schemes [J2], [163].

5.3 Coherent optical communications using QD-MLLD

5.3.1 Experimental setup

For an experimental demonstration of coherent WDM transmission with QD-MLLDs as light sources both at the transmitter (Tx) and receiver (Rx), we use the setup depicted in Figure **5.4**a. The total Tx comb output power of 9 dBm is boosted by an erbium-doped fiber amplifier (EDFA-1). The spacing between the amplified comb lines is increased to 50 GHz by selecting every second line with a programmable filter (PF-1, Finisar) such that a symbol rate of 45 GBd can be used, see spectrum in Figure **5.4**b which was taken at point P1 of the experimental setup. The programmable filter PF-1 is additionally used to flatten the comb spectrum. We emulate WDM traffic by encoding independent data streams on neighboring carriers. This is done by de-interleaving 23 spectral lines from the Tx comb into even and odd carriers using PF-1. The

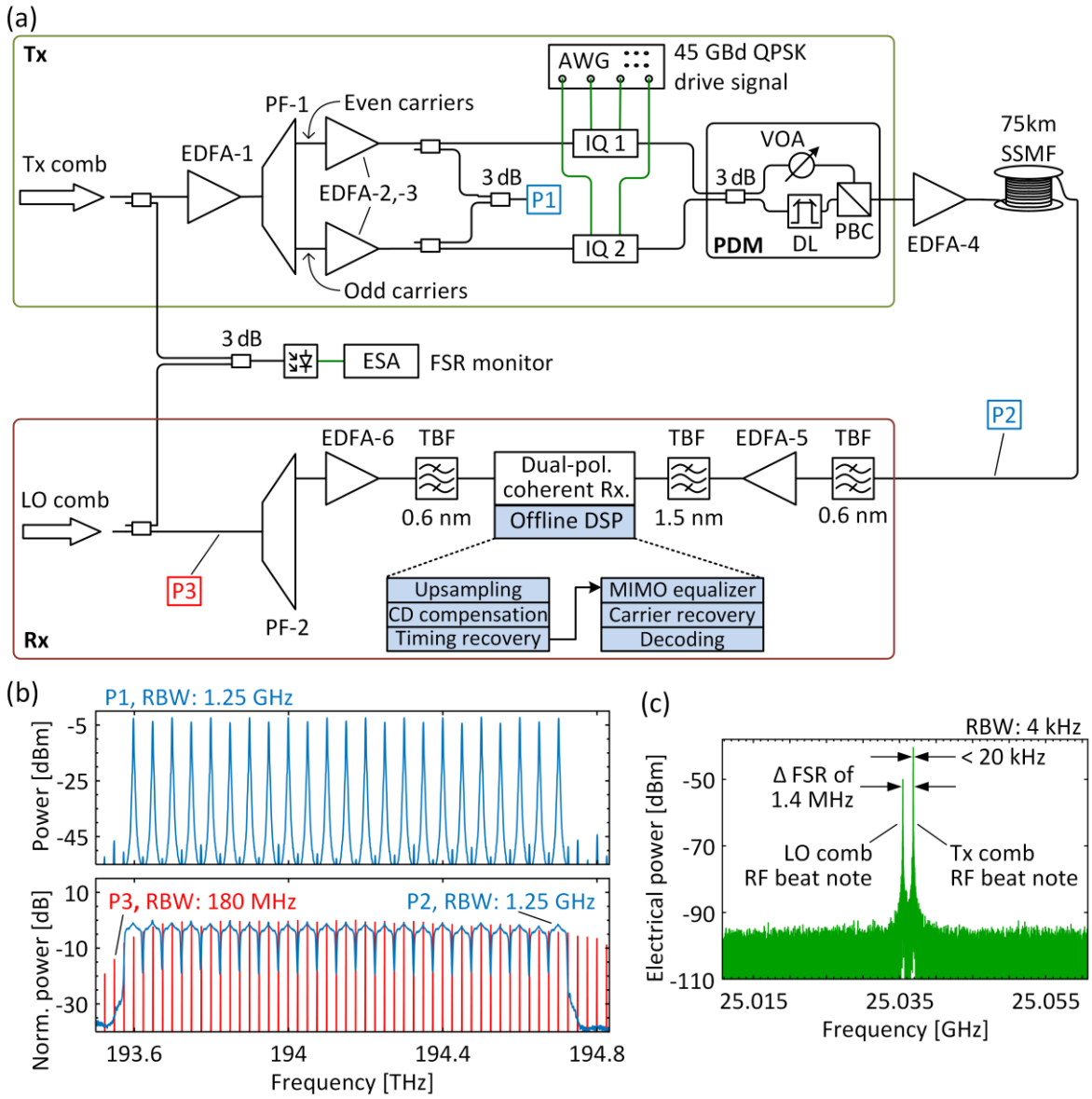

Figure 5.4: Coherent WDM transmission experiment using QD-MLLD comb generators both as a multi-wavelength light source at the transmitter (Tx) and as a multi-wavelength LO at the receiver (Rx). **(a)** Experimental setup: The Tx comb is de-interleaved into even and odd carriers using a programmable filter (PF-1). The two sets of carriers are then modulated with independent data streams to emulate a real WDM signal with independent data on neighboring channels. Polarization-division multiplexing (PDM) is emulated by splitting the single-polarization WDM signal into two paths, delaying one of them, and recombining the two decorrelated signals on orthogonal polarizations of the transmission fiber. At the receiver, we subsequently select individual lines of an LO comb and use them for coherent detection of the corresponding WDM channel. (Caption continued on next page)

Figure 5.4 continued: The WDM channels are spaced by approximately 50 GHz and carry QPSK signals at symbol rates of 45 GBd, limited by the bandwidth of the arbitrary-waveform generator (AWG) used to generate the modulator drive signals at the Tx. P1, P2, and P3 denote points in the experimental setup at which the optical spectra in Subfigure (b) have been taken. EDFA: Erbium-doped fiber amplifier, IQ: In-phase/quadrature modulator; DL: Delay line; VOA: Variable optical attenuator; PBC: Polarization beam combiner; TBF: Tunable band-pass filter; SSMF: Standard single-mode fiber; ESA: Electrical spectrum analyzer; CD: Chromatic dispersion; MIMO: Multiple-input and multiple-output. **(b)** Comb spectra of both even and odd carriers before modulation (upper plot, P1), spectrum of 23 modulated carriers (lower plot, P2), and spectrum of the LO comb (lower plot, P3). **(c)** RF beat note of each comb obtained by impinging the output of the two QD-MLLDs on a photodetector simultaneously as depicted in Subfigure (a).

even and odd carriers are amplified by EDFA-2 and EDFA-3, respectively. Both carriers are then independently modulated with pseudo-random bit sequences (PRBS) of length $2^{11} - 1$. This bit sequence is mapped to QPSK symbols with a rate of 45 GBd and a raised-cosine spectrum having a 10 % roll-off. In our experiments, the symbol rate was limited by the bandwidth of the arbitrary-waveform generator (AWG) used to generate the drive signals for the IQ modulators at the transmitter. The modulated even and odd carriers are then recombined by a polarization-maintaining (PM) 3 dB coupler to form a WDM signal with uncorrelated data streams on neighboring channels. To emulate polarization-division multiplexing (PDM), the WDM signal is split into two paths. In one of the paths, the signal is delayed by about 5.34 ns (240 symbols) with an optical delay line (DL) for decorrelation. A variable optical attenuator (VOA) in the other path equalizes the signal powers in the two paths. The signals are then recombined in orthogonal polarization states using a polarization beam combiner (PBC). The dual-polarization WDM signal is amplified and transmitted over a 75 km SSMF link, see spectrum in Figure **5.4**b, which was taken at point P2 of the experimental setup. At the receiver, the WDM channel of interest is selected using a 0.6 nm tunable band-pass filter (TBF) and amplified by EDFA-5. A second 1.5 nm-wide TBF is used to suppress out-of-band amplified spontaneous emission (ASE) noise of EDFA-5. The selected channel is detected by a dual-polarization coherent receiver (Keysight N4391A). The corresponding reference tone for coherent detection is

selected from the LO comb using a second programmable filter (PF-2), amplified by EDFA-6, and filtered by another 0.6 nm TBF for ASE noise suppression. The output of the coherent receiver is digitized using four oscilloscope channels with a sampling rate of 80 GSa/s each (Keysight DSOX93204A) and evaluated offline using digital signal processing (DSP). In the DSP, we first up-sample the received signal to two samples per symbol. This is followed by blind chromatic-dispersion compensation based on the Godard clock-tone algorithm [178] after which timing recovery is carried out [179], [180]. An adaptive multiple-input and multiple-output (MIMO) equalizer using the constant-modulus algorithm (CMA) then demultiplexes the two orthogonal polarizations of the signal and compensates linear transmission impairments [181]. We use periodogram-based [182] techniques to compensate for an average frequency offset of 400 MHz between the signal carrier and the LO tone. Subsequently, carrier phase noise compensation is carried out based on the BPS algorithm with 45 test angles and an averaging block length of 16 symbols [38]. This technique allows for symbol-wise phase tracking and has been shown to effectively cope with the phase noise of QD-MLLD carriers in previous experiments [10]. Figure **5.4**b depicts the superposition of the LO comb tones with the WDM signal. As discussed in Section 5.2, the FSR of the combs are nearly identical and the modulated channels are hence in good frequency alignment with the corresponding LO tones. Figure **5.4**c shows the RF beat notes of the Tx comb and the LO comb captured simultaneously using an electrical spectrum analyzer (ESA, Keysight PXA N9030A), see "FSR monitor" in Figure **5.4**a. The two combs have narrow RF linewidths (< 20 kHz) and FSRs with a very small difference (Δ FSR = 1.4 MHz). The smaller value of ΔFSR observed here as compared to the value obtained from Figure **5.2**d is caused by different fiber coupling conditions [183] for the two measurements since we used two different optical probing stages.

5.3.2 Data transmission performance

The results of our transmission experiment are shown in Figure **5.5**. Throughout our experiments, the BER was too low to be measured within a limited record

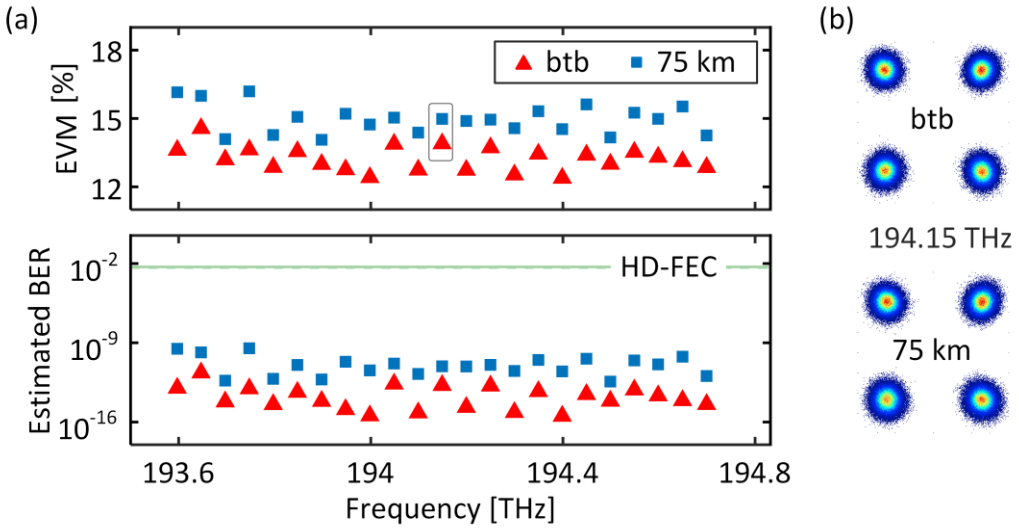

Figure 5.5: Coherent data transmission performance obtained by using a QD-MLLD comb generator both as the Tx light source and as the LO. **(a)** Upper plot: Measured EVM as a function of the carrier frequency of the transmitted channels for both back-to-back (btb, ▲) and 75 km SSMF transmission (■). Lower plot: BER estimated from EVM assuming that the QPSK signals are impaired by additive white Gaussian noise only [46]. **(b)** Example constellation diagrams for the signal carried by the comb line at 194.15 THz, both for back-to-back (btb) and for 75 km fiber transmission.

length of 1×10^6 bits. We therefore rely on the error-vector magnitude (EVM, normalized to the maximum constellation amplitude) to quantify signal quality and estimate the BER assuming that, after phase-noise compensation, the QPSK signals are impaired by additive white Gaussian noise only [184]. The measured EVM for each WDM channel is depicted in the upper plot of Figure **5.5**a, and the corresponding BER estimates are shown in the lower plot. All channels fall well below the BER threshold of 4.5×10^{-3} for hard-decision forward-error correction (HD-FEC) with 7 % overhead [114]. This is confirmed by the fact that none of our signal recordings of 1×10^6 bits each showed any error. This leads to an aggregate line rate of 4.14 Tbit/s and a net data rate of 3.87 Tbit/s, transmitted over 75 km of SSMF. Example constellation diagrams obtained for the channel at 194.15 THz, both for back-to-back and for fiber transmission are shown in Figure **5.5**b. In these experiments, the PRBS length used was $2^{11} - 1$ due to a limitation in the memory size and the memory granularity of the AWG that was used to generate the data signals. Further, we do not expect that

transceiver nonlinearities would play a significant role as modulators and drive amplifiers were operated within their linear range. This is also confirmed by subsequent experiments performed with two different PRBS patterns of length $2^{11} – 1$ and $2^{15} – 1$ using an upgraded AWG hardware, see Section 5.3.3.

5.3.3 Comparison between QD-MLLD LO and ECL LO

In this section, we investigate whether or not there is a penalty in received signal quality when using a QD-MLLD comb line as LO rather than an ECL LO. The experimental setup is depicted in Figure **5.6**a and relies on an ECL as light source at the Tx. The ECL carrier, having a linewidth of less than 100 kHz and a power of 6 dBm, is amplified by EDFA-1 prior to modulation with a QPSK signal at a symbol rate of 45 GBd. In this experiment, we used PRBS of length $2^{11} – 1$ and $2^{15} – 1$, both of which lead to identical results. In the following, we show only the results for the longer sequence. PDM is emulated as discussed in Section 5.3.1. The PDM signals are amplified by EDFA-2, filtered by a TBF to remove ASE noise, and sent to the signal input of a dual-polarization coherent receiver. The modulated signal is received by using either a QD-MLLD comb line or a tone obtained from a second ECL as LO. The LO power is boosted by EDFA-3 and filtered by a PF, which is mainly needed for the comb input. We vary the optical carrier-to-noise power ratio (OCNR) of the LO tone using a variable optical attenuator (VOA) in front of another EDFA (EDFA-4). The OCNR for a reference noise bandwidth of 12.5 GHz (0.1 nm) is measured at the monitor output of the dual-polarization coherent receiver (Keysight N4931A). Offline DSP as described in Section 5.3.1 is employed to analyze the received data. Figure **5.6**b shows the measured BER with 1×10^6 analyzed bits versus the OCNR of the LO. Two LO tones from the QD-MLLD are tested by using the corresponding Tx carrier frequency. Due to the limited number of 10^6 analyzed bits, the BER values below 10^{-5} might be subject to statistical inaccuracies. For evaluating the recorded signals, the averaging block length used for BPS is optimized individually for each OCNR value. Note that, as a consequence of block-length optimization, there is a trade-off between OCNR tolerance and tracking speed of the BPS algorithm which could lead to a BER penalty for the QD-MLLD LO with respect to the ECL LO. Such a penalty is

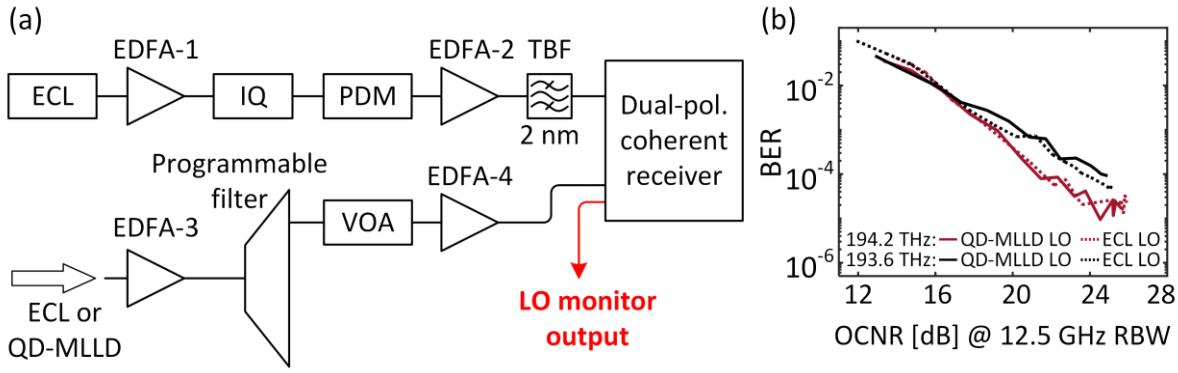

Figure 5.6: Comparison of transmission performance obtained by using a QD-MLLD and a conventional external-cavity lasers (ECL) as LO tone generators. **(a)** Experimental setup. At the Tx, we use an ECL having a linewidth below 100 kHz as light source. The ECL carrier is boosted by an EDFA (EDFA-1) and modulated with a QPSK signal at a symbol rate of 45 GBd. The length of the underlying pseudo-random bit sequence amounts to $2^{15} - 1$. Polarization-division multiplexing (PDM) is emulated by the same method discussed in Section 5.3.1. The PDM signals are amplified by an EDFA (EDFA-2), filtered by a tunable bandpass filter (TBF), and sent to the signal input of a dual-polarization coherent receiver. The signal is detected by using either a QD-MLLD comb tone as an LO, or by using a second ECL. The LO is amplified by EDFA-3 and filtered by a programmable filter. A variable optical attenuator (VOA) in front of EDFA-4 is used to vary the optical carrier-to-noise power ratio (OCNR) of the LO tone. **(b)** BER vs. OCNR of the LO tone. The OCNR is indicated with respect to a reference noise bandwidth of 12.5 GHz (0.1 nm). We find that LO tones from a QD-MLLD (solid lines) perform similarly to an ECL LO (dotted lines).

not observable in our measurements, which we attribute to the fact that the effect is too weak to be visible within the measurement accuracy of our experiment. However, when using QD-MLLD LO tones at low OCNR, cycle slips were observed in the recovered symbols due to incorrect estimation of the carrier phase by a multiple of π/2. The impact of cycle slips can be reduced by using differential coding along with phase-slip tolerant FEC schemes [185] or by adding pilot symbols for accurate phase referencing [177] albeit with added complexity or increased overhead, respectively.

5.4 Summary

We demonstrate that QD-MLLD can be used both as multi-wavelength light sources at the Tx and as multi-wavelength LO at the Rx of massively parallel WDM systems. In our experiments, we use 23 carriers to transmit a line rate (net data rate) of 4.140 Tbit/s (3.869 Tbit/s) over a 75 km standard single mode fiber (SSMF) link. To the best of our knowledge, this is the first time that an optical frequency comb generated by a QD-MLLD has been used as a multi-wavelength LO in a coherent transmission system. Due to their compactness and simple operation requiring a DC drive current only, QD-MLLD represent a particularly interesting comb generator concept for efficient and highly scalable WDM transceivers.

[*end of paper [J3]*]

6 Microresonator-based Kerr comb generators for multi-terabit/s transmission and reception

This chapter is dedicated to Microresonator-based Kerr comb generators and their performance when used as multi-wavelength light sources both at the transmitter and receiver sides of a WDM link. The contents of this chapter are taken from paper [J4] with the appropriate changes to fit the structure and notation of this document. Methods and Supplementary Information related to [J4] can be found in Appendix C. Paper [J4] was published in *Nature* with three equally contributing authors, whereby I lead the experiments that demonstrate coherent detection using a soliton comb as a multi-wavelength local oscillator, see Section 6.4. For completeness and better context, the whole paper is reproduced here.

[*Beginning of paper [J4]*]

Microresonator solitons for massively parallel coherent optical communications

Nature, Volume 546, Issue 7657, pp. 274-279, 2017
DOI: 10.1038/nature22387

Pablo Marin-Palomo[1,×], Juned N. Kemal[1,×], Maxim Karpov[2,×], Arne Kordts[2], Joerg Pfeifle[1], Martin H. P. Pfeiffer[2], Philipp Trocha[1], Stefan Wolf [1], Victor Brasch[2], Miles H. Anderson[2], Ralf Rosenberger[1], Kovendhan Vijayan[1], Wolfgang Freude1,3, Tobias J. Kippenberg[2], Christian Koos[1,3]

1 Institute of Photonics and Quantum Electronics (IPQ), Karlsruhe Institute of Technology (KIT), 76131 Karlsruhe, Germany
2 École Polytechnique Fédérale de Lausanne (EPFL), 1015 Lausanne, Switzerland

3 Institute of Microstructure Technology (IMT), Karlsruhe Institute of Technology (KIT), 76131 Karlsruhe, Germany
× **These authors contributed equally to this work**

Optical solitons are waveforms that preserve their shape while propagating, relying on a balance of dispersion and nonlinearity [186], [187] Soliton-based data transmission schemes were investigated in the 1980s, promising to overcome the limitations imposed by dispersion of optical fibers. These approaches, however, were eventually abandoned in favor of wavelength-division multiplexing (WDM) schemes that are easier to implement and offer improved scalability to higher data rates. Here, we show that solitons may experience a comeback in optical communications, this time not as a competitor, but as a key element of massively parallel WDM. In-stead of encoding data on the soliton itself, we exploit continuously circulating dissipative Kerr solitons (DKS) in a microresonator [83], [188]. DKS are generated in an integrated silicon nitride microresonator [79] by four-photon interactions mediated by Kerr nonlinearity, leading to low-noise, spectrally smooth and broadband optical frequency combs [189]. In our experiments, we use two interleaved soliton Kerr combs to transmit a data stream of more than 50 Tbit/s on a total of 179 individual optical carriers that span the entire telecommunication C and L bands. Equally important, we demonstrate coherent detection of a WDM data stream by using a pair of microresonator Kerr soliton combs – one as a multi-wavelength light source at the transmitter, and another one as a corresponding local oscillator (LO) at the receiver. This approach exploits the scalability advantages of microresonator soliton comb sources for massively parallel optical communications both at the transmitter and receiver side. Taken together, the results prove the significant potential of these sources to replace arrays of continuous-wave lasers in high-speed communications. In combination with advanced spatial multiplexing schemes [5], [190] and highly integrated silicon photonic circuits [191], DKS combs may bring chip-scale petabit/s transceivers into reach.

6.1 Introduction

The first observation of solitons in optical fibers [187] in 1980 was immediately followed by major research efforts to harness such waveforms for long-haul communications [186]. In these schemes, data was encoded on soliton pulses by simple amplitude modulation using on-off-keying (OOK). However, even though the viability of the approach was experimentally demonstrated by transmission over one million kilometers [192], the vision of soliton-based communications was ultimately hindered by difficulties in achieving shape-preserving propagation in real transmission systems [186] and by the fact that nonlinear interactions intrinsically prevent dense packing of soliton pulses in either the time or frequency domain. Moreover, with the advent of wavelength-division multiplexing (WDM), line rates in long-haul communication systems could be increased by rather simple parallel transmission of data streams with lower symbol rates, which are less dispersion sensitive. Consequently, soliton-based communication schemes have moved out of focus over the last two decades.

More recently, frequency combs were demonstrated to hold promise for revolutionizing high-speed optical communications, offering tens or even hundreds of well-defined narrowband optical carriers for massively parallel WDM [5], [74], [75]. Unlike carriers derived from a bank of individual laser modules, the tones of a comb are intrinsically equidistant in frequency, thereby eliminating the need for individual wavelength control and for inter-channel guard bands [5], [75]. In addition, when derived from the same comb source, stochastic frequency variations of optical carriers are strongly correlated, permitting efficient compensation of impairments caused by nonlinearities of the transmission fiber [8].

For application in optical communications, frequency comb sources must be compact. In recent years, a wide variety of chip-scale comb generators have been demonstrated [16], [18], enabling transmission of WDM data streams with line rates of up to 12 Tbit/s [J2]. Transmission at higher line rates however, requires more carriers and lower noise levels, and still relies on spectral

broadening of narrowband seed combs using dedicated optical fibers [5], [74], [75] or nanophotonic waveguides [13]. In addition, generating uniform combs with a broadband spectral envelope often requires delicate dispersion management schemes, usually in combination with intermediate amplifiers [74]. Such schemes are difficult to miniaturize and not readily amenable to chip-scale integration. Moreover, with a few exceptions at comparatively low data rates [J1], all advanced comb-based transmission experiments exploit the scalability advantages only at the transmitter, but not at the receiver, where individual continuous-wave (CW) lasers are still used as optical local oscillators (LO) for coherent detection.

In this paper, we show that dissipative Kerr solitons (DKS) [83] generated in integrated photonic microresonators via Kerr-nonlinear four-photon interactions, allow for generation of highly stable broadband frequency combs that are perfectly suited to overcome scalability limitations of massively parallel optical transmission both at the transmitter and receiver. Microresonator-based Kerr comb sources [78], [193] intrinsically offer unique advantages such as small footprint, large number of narrow-linewidth optical carriers, and line spacings of tens of GHz, which can be designed to fit established WDM frequency grids. However, while these advantages were recognized, previous transmission experiments were limited to aggregate line rates of 1.44 Tbit/s due to strong irregularities of the optical spectrum associated with the specific Kerr comb states [11].

These limitations can be overcome by using DKS combs generated in a CW-driven microresonator. The technique exploits four-wave mixing, a process that converts two pump photons into a pair of new photons. In a microresonator, the strength of this interaction is given by the single-photon Kerr frequency shift of $g = \hbar\omega_0^2 c n_2 / n^2 V_{\mathrm{eff}}$, where n_2 (n) is the nonlinear (linear) refractive index, c the speed of light in vacuum, $\hbar$ the reduced Planck constant, V_{eff} the nonlinear optical mode volume and ω_0 the angular frequency of the pump mode. For pump powers that cause the cavity Kerr frequency shift to exceed the linewidth of the resonance, parametric oscillations lead to the emergence of Kerr frequency combs (modulation instability, MI Kerr combs). Bright DKS can be

formed in this process when the microresonator has a locally anomalous group velocity dispersion (i.e. a Taylor expansion for cavity modes $\omega_\mu = \omega_0 + \sum_{i=1}^{\infty} \mu^i D_i / i!$ has $D_2 > 0$) and a CW laser excitation (frequency ω_L) that is red detuned from the cavity resonance (i.e. $\delta\omega = \omega_0 - \omega_L > 0$). Mathematically, DKS states appear as specific solutions of the Lugiato-Lefever equation [194] and consist of an integer number of discrete secant-hyperbolic-shaped pulses on a CW background circulating in the cavity [83]. Stability of such states relies on the double balance of dispersion and Kerr nonlinearity as well as of nonlinear parametric gain and cavity loss. Theoretically predicted in Ref. [188] and first reported to spontaneously form in microresonators made from crystalline MgF_2 [83], DKS have been observed in different types of material systems including silica-on-silicon [84] and silicon nitride [189] (Si_3N_4) as well as silicon [195]. Of particular interest are single-soliton states, which consist of only one ultra-short pulse circulating around the cavity, leading to a broadband comb spectrum with a smooth and numerically predictable envelope given by

$$p(\mu) \approx \frac{\kappa_{ex} D_2 \hbar \omega_0}{4g} \cdot \operatorname{sech}^2\left(\frac{\pi\mu}{2} \sqrt{\frac{D_2}{2\delta\omega}} \right) \tag{6.1}$$

where κ_{ex} represents the external coupling rate to the bus waveguide [83] (see Appendix C.2 for more details). DKS have already been used in applications such as self-referencing of optical frequency combs [196], [197], low noise microwave generation [198] and dual soliton comb spectroscopy [84], [199].

Our demonstration comprises a series of three experiments that exploit the extraordinarily smooth and broadband spectral envelope and the inherently low phase noise of DKS combs for massively parallel coherent communications. In a first experiment, we transmit data on 94 carriers that span the entire telecommunication C and L bands with a line spacing of ~ 100 GHz. Using 16-state quadrature amplitude modulation (16QAM) to encode data on each of the lines, we achieve an aggregate line rate of 30.1 Tbit/s. In a second experiment, we double the number of carriers by interleaving two DKS combs. This gives a total of 179 carriers and an aggregate line rate of 55.0 Tbit/s transmitted over a distance of 75 km – the highest data rate achieved to date with a chip-scale frequency comb source. In a third experiment, we demonstrate coherent

detection using a DKS comb as a multi-wavelength LO. We use 93 carriers to transmit and receive an aggregated line rate of 37.2 Tbit/s. In these experiments, the LO comb is coarsely synchronized to the transmitter comb, and digital signal processing is used to account for remaining frequency differences. The results prove the tremendous potential of Kerr soliton combs, both as multi-wavelength optical sources and as LO for massively parallel WDM transmission.

6.2 Dissipative Kerr soliton frequency comb generation

Our work relies on integrated Si_3N_4 microresonators for generation of DKS frequency combs [83], cf. Figure **6.1**a. The Si_3N_4 platform is chosen due to its low optical losses and its compatibility with large-scale silicon-based processing [79]. The microresonators feature a waveguide height of 800 nm to achieve anomalous group velocity dispersion (GVD) and are fabricated using the photonic Damascene process [159]. Neighboring resonances are spaced by 100 GHz while featuring intrinsic *Q*-factors exceeding 10^6. DKS combs are obtained by sweeping of the pump laser through the resonance from a blue-detuned wavelength to a predefined red-detuned wavelength [83], [189]. This leads initially to the generation of MI Kerr combs followed by DKS states once the resonance is crossed, cf. Figure **6.1**. Importantly, once a multiple-soliton comb state is generated, the transition to a single-soliton state can be accomplished in a reliable and deterministic manner by adjusting the laser frequency [200], cf. Figure **6.1**a,b and Appendix C.1. The measured power spectrum of the DKS comb state is shown in Figure **6.1**c, which exhibits a 3dB spectral bandwidth of ~ 6 THz. The soliton comb states are remarkably stable for many hours in a laboratory environment, which is key to the transmission experiments presented in this work.

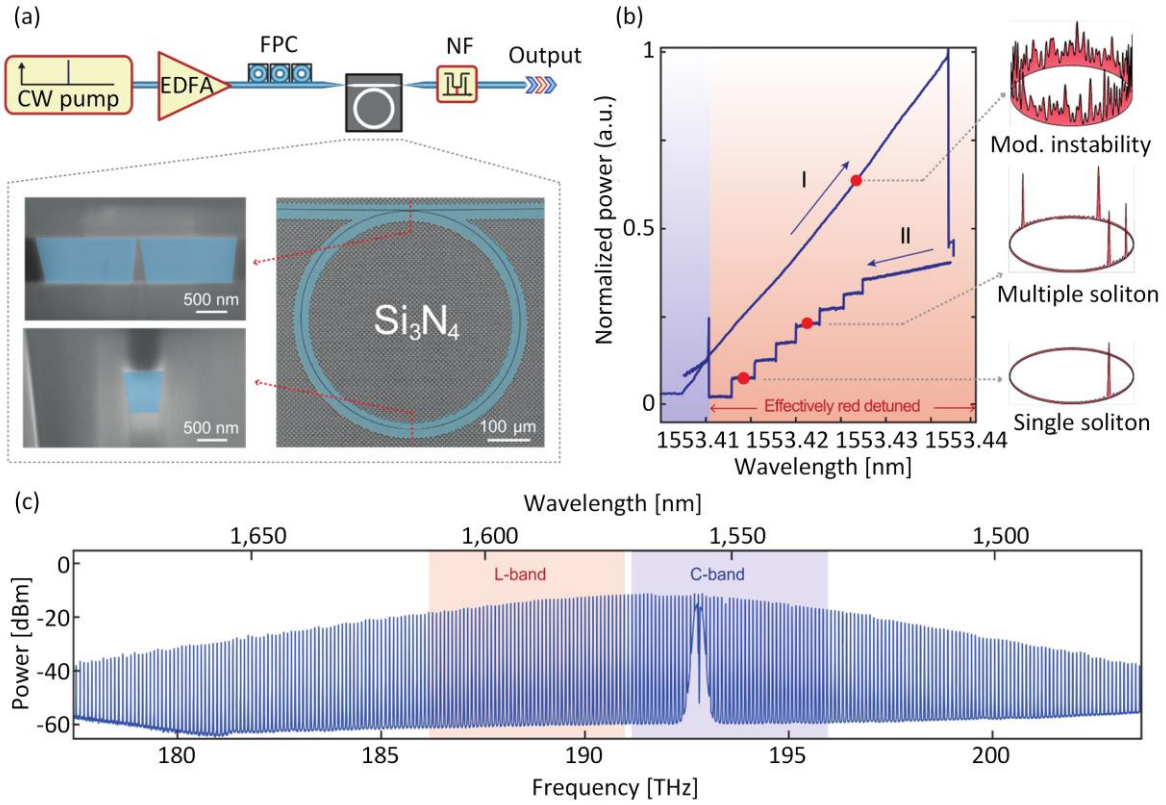

Figure 6.1: Broadband frequency comb generation using dissipative Kerr solitons in high-Q silicon nitride (Si_3N_4) microresonators. **(a)** Principle of soliton frequency comb generation: The integrated photonic microresonator is pumped by a tunable CW laser amplified by an erbium-doped fiber amplifier (EDFA). Lensed fibers are used to couple light to the chip (FPC – fiber polarization controller). After the microresonator, a notch filter (NF) suppresses the remaining pump light. The insets show scanning electron microscopy images of a Si_3N_4 microresonator with a radius of 240 µm. Right inset: Top view. The checker-board pattern results from the photonic Damascene fabrication process [159], see Appendix C.1. Left insets: Cross sections of the resonator waveguide (dimensions 0.8 × 1.65 µm^2) at the coupling point (top) and at the tapered section (bottom, dimensions 0.8 × 0.6 µm^2). The tapered section is used for suppressing higher order modes families [201], while preserving a high optical quality factor ($Q \sim 10^6$), see Appendix C.1. **(b)** Pump tuning method for soliton generation in optical microresonator, showing the evolution of the generated comb power versus pump laser wavelength: (I) The pump laser is tuned over the cavity resonance from the blue-detuned regime, where high-noise modulation instability (MI) combs are observed, to the red-detuned regime, where cavity bistability allows for the formation of soliton states (here a multiple soliton state); (II) Upon having generated a multiple soliton state, the pump laser is tuned backwards to reduce the initial number of solitons down to a single one. The insets on the right schematically show the corresponding intracavity waveforms in different states (MI, multiple and single soliton state). (Caption continued on next page)

Figure 6.1 continued: **(c)** Measured spectrum of a single-soliton frequency comb after suppression of residual pump light. The frequency comb features a smooth spectral envelope with a 3 dB bandwidth of 6 THz comprising hundreds of optical carriers extending beyond the telecommunication C and L bands (blue and red, respectively)

6.3 Kerr soliton frequency combs for WDM transmission

The general concept of massively parallel data transmission using a frequency comb as a multi-wavelength light source is depicted in Figure **6.2**a. For emulating massively parallel WDM transmission in our laboratory, we rely on a simplified scheme using only two independent data streams on neighboring channels along with an emulation of polarization division multiplexing, see Appendix C.3 for details. We use 16QAM at a symbol rate of 40 GBd along with band-limited Nyquist pulses that feature approximately rectangular power spectra, Figure **6.2**b. At the receiver, each channel is individually characterized using a CW laser as LO and an optical modulation analyzer, which extracts signal quality parameters such as the error-vector magnitude (EVM) or the bit-error ratio (BER). The BER of the transmission experiment are depicted in Figure **6.2**e with different BER thresholds indicated as horizontal dashed lines. Out of the 101 carriers derived from the comb in the C and L bands, a total of 94 channels were used for data transmission. This leads to a total line rate of 30.1 Tbit/s, see Appendix C.1 for details on data rate calculations. The transmission capacity is restricted by the fact that the line spacing of ~ 100 GHz significantly exceeds the signal bandwidth of ~ 40 GHz, leading to unused frequency bands between neighboring channels, see Figure **6.2**b, and hence to a rather low spectral efficiency (SE) of 2.8 bit/s/Hz.

These restrictions can be overcome by using interleaved frequency combs, see Figure **6.2**c. The scheme relies on a pair of DKS combs with practically identical line spacing, but shifted with respect to each other by half the line spacing by thermal tuning. At the receiver, this scheme still relies on individual CW lasers as LO for coherent detection. The interleaved comb features a line spacing of ~ 50 GHz, which allows for dense packing of 40 GBd data channels

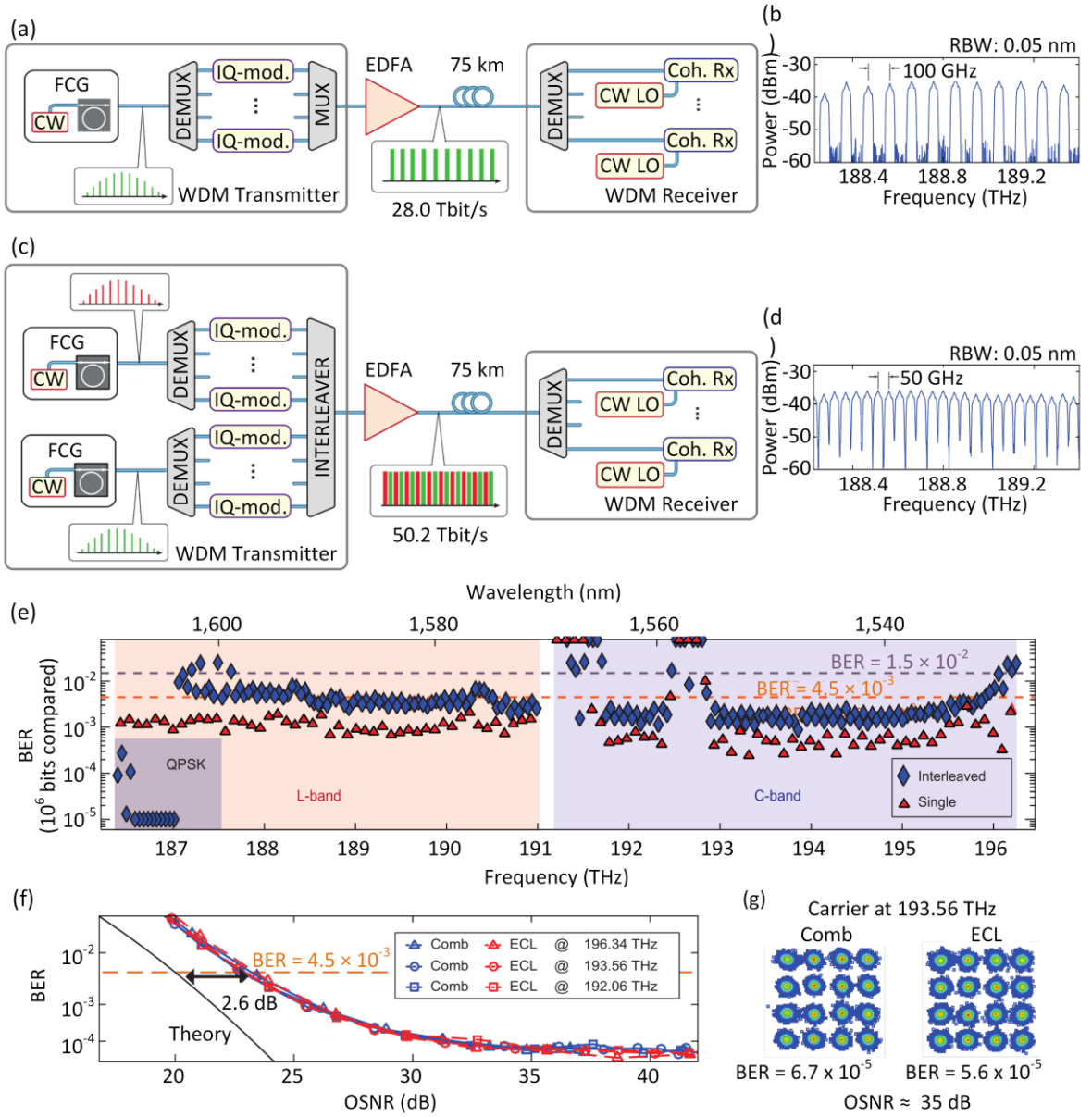

Figure 6.2: Data transmission using microresonator soliton frequency comb generators as optical sources for massively parallel WDM. **(a)** Principle of data transmission using a single DKS comb generator as optical source at the transmitter. A demultiplexer (DEMUX) separates the comb lines and routes them to individual dual-polarization in-phase/quadrature (IQ) modulators, which encode independent data on each polarization. The data channels are then recombined into a single-mode fiber using a multiplexer (MUX) and boosted by an erbium-doped fiber amplifier (EDFA) before being transmitted. At the receiver, the wavelength channels are separated by a second DEMUX and detected using digital coherent receivers (Coh. Rx) along with individual CW lasers as local oscillators (CW LO). In our laboratory experiment, we emulate WDM transmission by independent modulation of even and odd carriers using two IQ modulators, see Appendix C.3. (Caption continued on next page)

Figure 6.2 continued: We use 16-state quadrature amplitude modulation (16QAM) at a symbol rate of 40 GBd per channel. **(b)** Section of the optical spectrum of the WDM data stream. Nyquist pulse shaping leads to approximately 40 GHz wide rectangular power spectra for each of the carriers, which are spaced by approximately 100 GHz. **(c)** Principle of data transmission using interleaved DKS combs. At the transmitter, two combs of practically identical line spacing are interleaved. The resulting comb features a carrier spacing of approximately 50 GHz, which enables dense spectral packing of WDM channels and hence high spectral efficiency. At the receiver, this scheme still relies on individual CW lasers as LO for coherent detection, see Appendix C.3 for details. **(d)** Section of the optical spectrum of the WDM data stream. **(e)** Measured bit-error ratios (BER) of the transmitted channels for the single-comb and the interleaved-comb experiment, along with the BER thresholds for error-free propagation when applying forward error correction schemes with 7 % overhead (4.5×10^{-3}, dashed orange line) and 20 % overhead (1.5×10^{-2}, dashed blue line) [114], see Appendix C.1 for details. For the interleaved-comb experiment, the outer 14 lines at the low-frequency edge of the L band were modulated with quadrature phase-shift keying (QPSK) signals rather than 16QAM due to the low OSNR of these carriers. **(f)** Measured BER vs. optical signal-to-noise ratio OSNR of three different channels derived from a DKS frequency comb (blue) and a high-quality ECL (red), all with 16QAM signaling at 40 GBd. A total of 10^6 bits were compared. The comb lines do not show any additional penalty in comparison the ECL tones. Similar results were obtained at other symbol rates such as 28 GBd, 32 GBd, or 42.8 GBd. **(g)** Constellation diagrams obtained for an ECL and DKS comb tone at 193.56 THz.

in the spectrum, see Figure **6.2**d. The BER results of the transmission experiment are depicted in Figure **6.2**e with different thresholds indicated as horizontal dashed lines. For a given forward-error correction (FEC) scheme, these thresholds define the maximum BER of the raw data channel that can still be corrected to a BER level below 10^{-15}, which is considered error-free [114], see Appendix C.1. We find a total of 204 tones in the C and L bands, out of which 179 carriers could be used for data transmission. The remaining channels were not usable due to technical limitations, see Appendix C.3. The transmission performance is slightly worse than in the single-comb experiment since twice the number of carriers had to be amplified by the same EDFA, which were operated at their saturation output power such that the power per data channel reduced accordingly. Nevertheless, data was successfully transmitted over 75 km of standard single-mode fiber at a symbol rate of 40 GBd using a combination of 16QAM and QPSK. The total line rate amounts to 55.0 Tbit/s,

and the net data rate is 50.2 Tbit/s. This is the highest data rate so far achieved with a chip-scale frequency comb source, and compares very well to the highest capacity of 102.3 Tbit/s ever transmitted through a single-mode fiber core using more than 200 discrete DFB lasers as optical sources at the transmitter [202]. In addition, we achieve an unprecedented spectral efficiency of 5.2 bit/s/Hz, owing to the densely packed spectrum, Figure **6.2**d. In the experiments, limited saturation output power of the employed EDFA is the main constraint of signal quality and BER, see Appendices C.3 and C.6.3 for details. The presented data rates are hence not limited by the DKS comb source, but by the components of the current transmission setup, leaving room for further improvement.

To confirm the outstanding potential of DKS combs for data transmission, we compare the transmission performance of a single comb line to that of a reference carrier derived from a high-quality benchtop-type external-cavity laser featuring an optical linewidth of approximately 10 kHz, an optical output power of 15 dBm, and an optical carrier-to-noise power ratio (OCNR) in excess of 60 dB. As a metric for the comparison, we use the OSNR penalty at a BER of 4.5×10^{-3}, which corresponds to the threshold for FEC with 7 % overhead [114]. The results for 40 GBd 16QAM transmission are shown in Figure **6.2**f for three different comb lines and for ECL reference transmission experiments at the corresponding comb line frequencies. The $OSNR_{ref}$ values are defined for a reference bandwidth of 0.1 nm, see Appendix C.4. As shown, no additional OSNR penalty is observed for the frequency comb when compared with the high-quality ECL: For both sources, we observe an OSNR penalty of 2.6 dB with respect to the theoretically required OSNR (black line) for a BER of 4.5×10^{-3}. DKS-based light sources can hence dramatically improve scalability of WDM systems without impairing the signal quality under realistic transmission conditions. The error floor in Figure **6.2**f is attributed to transmitter nonlinearities and electronic receiver noise in our setup. Figure **6.2**g shows the measured constellation diagrams for the ECL and the comb line at 193.56 THz, both taken at the same OSNR of 35 dB.

6.4 Kerr soliton frequency combs for WDM transmission and reception

To demonstrate the potential of DKS frequency combs as multi-wavelength LO at the receiver, we perform a third experiment shown schematically in Figure **6.3**a. At the transmitter, a first DKS comb generator with an FSR of ~ 100 GHz serves as an optical source. At the receiver, a second DKS comb source having approximately the same FSR is used to generate the corresponding LO tones, each featuring an optical linewidth below 100 kHz. Figure **6.3**b,c show a section of the transmitted data spectrum along with the corresponding section of the LO comb. As a reference, the same experiment was repeated using a high-quality ECL with a 10 kHz linewidth as an LO for channel-by-channel demodulation. Overall, an aggregate data rate of 34.6 Tbit/s is obtained. The resulting BER values of all 99 channels for both methods are shown in Figure **6.3**d. Some of the channels showed signal impairments due to limitations of the available equipment, see Appendix C.1. However, we cannot observe any considerable penalty that could be systematically attributed to using the DKS comb as an LO.

6.5 Scalability and power consumption

While frequency combs offer fundamental technical advantages compared to discrete lasers, they can also contribute to reduce the power consumption of the transmission system. In this context, the power conversion efficiency of the DKS comb generator is an important metric, defined as the ratio between the power of the pump and that of the generated comb lines. The power conversion efficiency of our current comb sources is limited to rather small values between 0.1 % and 0.6 % due to the fundamental principle that bright soliton generation only occurs with the pump laser being far detuned from the optical resonance. Still, the overall power consumption can already now compete with massively parallel arrays of commercially available integrated tunable laser assemblies (ITLA), see Appendices C.1 and C.6 for details. The analysis also shows that improvement of more than one order of magnitude compared to ITLA is possible by optimizing the microresonator dispersion, by making use of tailored

amplifiers with optimum efficiency, and by increasing the power conversion efficiency via recently demonstrated high-Q Si_3N_4 microresonators with Q-factors of 6×10^6.

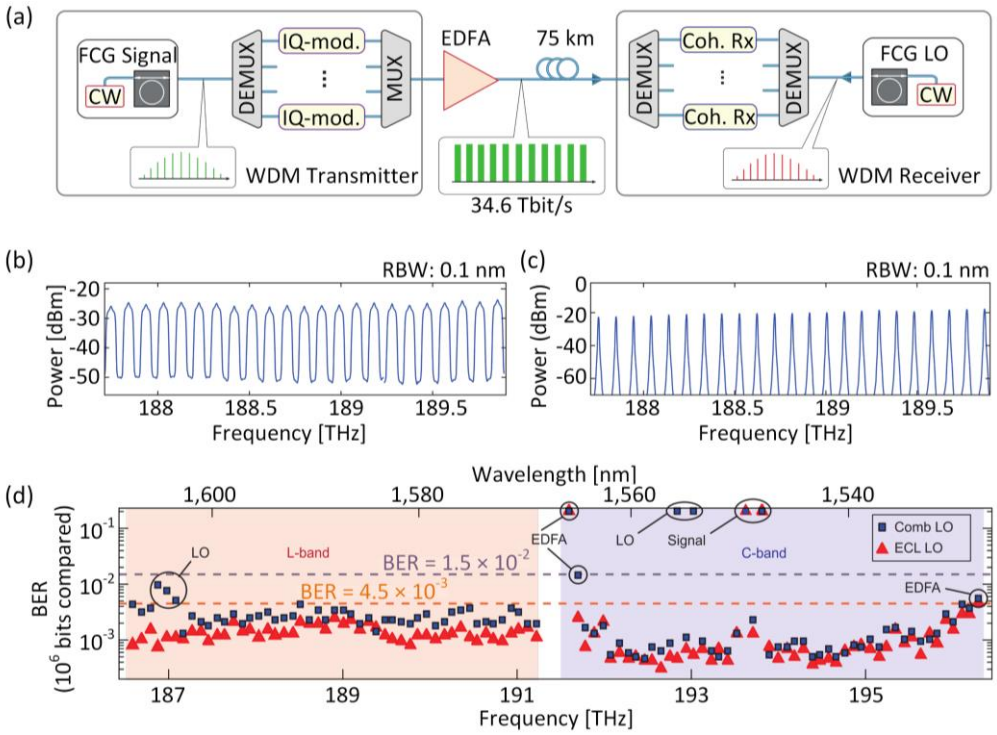

Figure 6.3: Coherent data transmission using microresonator soliton frequency combs both at the transmitter and at the receiver side. **(a)** Massively parallel WDM data transmission scheme using DKS frequency combs both as multi-wavelength source at the transmitter and as multi-wavelength local oscillator (LO) at the receiver. In contrast to Figure 6.2a, a single optical source provides all required LO tones for coherent detection. An extra DEMUX is used to route each LO tone to the respective coherent receiver (Coh. Rx). **(b)** Section of the spectrum of the transmitted channels. **(c)** Corresponding section of the spectrum of the LO frequency comb. Note that the comparatively large width of the depicted spectral lines is caused by the resolution bandwidth of the spectrometer (RBW = 0.1 nm) and does not reflect the sub-100 kHz optical linewidth of the LO tones. **(d)** Measured BER for each data channel. Blue squares show the results obtained when using a DKS comb as multi-wavelength LO, and red triangles correspond to a reference measurement using a high-quality ECL as LO. Dashed lines mark the BER thresholds of 4.5×10^{-3} (1.5×10^{-2}) for hard-decision (soft-decision) FEC with 7 % (20 %) overhead. Black circles show the channels with BER above the threshold for 7 % FEC and specify the reasons for low signal quality: low OCNR of the carriers from the LO comb ("LO") and the signal comb ("Signal"), as well as bandwidth limitations of the C-band EDFA ("EDFA"), see Appendix C.1 for more details.

6.6 Summary

In summary, we have demonstrated the potential of chip-scale DKS frequency combs for massively parallel WDM at data rates of tens of terabit/s. We use them both as multi-wavelength source at the transmitter and as LO at the receiver, and we show in both cases that that there is no systematic penalty compared to using high-quality ECL. While our experiments achieve the highest data rate with chip-scale frequency comb sources to date, there is still room for increasing the transmission capacity by optimizing the transmission system or by using the adjacent S and U bands for telecommunications in the near infrared. For long transmission distances, comb-based transmission schemes might allow for compensation of nonlinear impairments and hence lead to an improved signal quality compared to conventional WDM schemes [8]. The results prove the tremendous potential of DKS comb generators for high-speed data transmission, both in petabit/s intra-datacenter networks [203] and in inter-datacenter connections.

[*end of paper [J4]*]

7 Summary and Outlook

7.1 Summary

Chip-scale optical frequency comb generators are likely to become key elements of future wavelength-division multiplexing (WDM) transceivers, enabling efficient scaling of channel counts and transmission capacity. Coherent WDM communications can be implemented using a pair of these comb generators – one as a multi-wavelength light source at the transmitter, and another one as a corresponding local oscillator (LO) for massively parallel coherent reception at the receiver. In the framework of this thesis, the performance of three different concepts for chip-scale frequency comb generators have been investigated experimentally with respect to their performance WDM communications. Key accomplishments of this experiments are summarized in the following paragraphs.

Gain-switched laser diodes (GSLD) are the first devices investigated. Following up on the works of Pfeifle et. al. [16], where the devices were shown to be suitable as multi-carrier sources for WDM transmission, the potential of GSLD as a multi-wavelength local oscillator for coherent WDM reception is demonstrated here. A net data rate of 1.032 Tbit/s was transmitted over a 10 km-long standard single-mode fiber (SSMF) at a spectral efficiency of 5.16 bit/s/Hz. The receiver comb was synchronized to the transmitter comb, keeping the intradyne frequencies for all received WDM channels below 15 MHz, which should enable an efficient utilization of the bandwidth of a coherent receiver. Using simulations based on measured phase-noise characteristics, we show that the performance is limited by the presence of high-frequency FM-noise, which may be decreased by a proper parameter optimization of the comb sources.

The second chip-scale comb generators investigated are **mode-locked laser diode (MLLD)** chips with active media based on III-V semiconductor

quantum-dashes (QD). The simple operation compactness of these devices in combination with the comparatively broad and smooth spectral envelope of the associated combs make these devices promising candidates for particularly compact WDM transceivers. However, the comb lines suffer from large phase noise, which has impaired data transmission performance with these devices. In this work, we show the full potential of QD-MLLD by using an external-cavity optical feedback to reduce the intrinsic linewidth of the comb tones and hence mitigate the phase noise limitation. With the help of this technique, a data stream of 11.2 Tbit/s was transmitted over a 75-km long SSMF using QD-MLLD comb lines as WDM carriers. A high net spectral efficiency of 7.5 bit/s/Hz was achieved using 32-state quadrature amplitude modulation (32QAM). With their potential as WDM carriers demonstrated, the viability of using these devices also as multi-wavelength LO is shown experimentally. This experiment did not exploit phase noise reduction by external optical feedback. Nonetheless, using quadrature phase shift keying (QPSK) modulation format, we transmit a net data rate of 3.9 Tbit/s over a 75 km-long SSMF.

Microresonators-based Kerr comb generators are the third type of comb sources investigated, exhibiting particularly promising performance. Using dissipative Kerr soliton (DKS) combs generated by these devices, we demonstrate the first WDM data transmission and reception spanning the entire C and L bands from 1530 nm to 1610 nm. In this experiment, 99 carriers from a DKS comb are used as independent carries at the WDM transmitter and a second DKS comb at the receiver provided all the required LO tones for coherent reception. A net data rate of 34.6 Tbit/s was transmitted over a 75 km-long SSMF.

7.2 Outlook

The theoretical and experimental results in this thesis demonstrate the potential of the three different comb generators as multi-wavelength light sources both at the transmitter and receiver sides of a WDM link. Future work will explore the concept of multi-chip integration by photonic wire bonding to combine

individually optimized and tested comb generator chips with other photonic integrated circuits into powerful chip-scale WDM transceivers [31], [33]. The work on these transceiver modules needs to employ the comb generators that provide an optimum solution in terms of cost, power consumption, reach, spectral efficiency, and data rate for a specific target application.

Frequency combs obtained from GSLD, whose center frequency and FSR can be adjusted, seem best suited for applications that demand high spectral efficiency and wavelength flexibility. However, OCNR values of GSLD that typically amount to approximately 30 dB result in reach that is limited by the source rather than by the transmission link itself. In addition, the transmission capacity of GSLD-based WDM links is limited to a few Tbit/s by the relatively low available number of comb lines. Nonetheless, with GSLD being the most matured comb sources with their integration potential demonstrated [73], [204], GSLD-based commercial WDM systems could be available in the near future.

QD-MLLD comb generators could be used to overcome the capacity limitation of GSLD. QD-MLLD are not only attractive due to their transmission capacity, but also in terms of technical simplicity and energy efficiency. Driven with a DC pump current, QD-MLLD can emit broadband combs, thereby avoiding extra power consumption due to additional RF components as needed in GSLD. This makes QD-MLLD attractive for applications that require high-capacity WDM transceivers with low power consumption. These light sources, however, may still suffer from comparatively strong phase noise, which has initially limited WDM transmission with QD-MLLD to spectrally less efficient modulation formats such as QPSK and 16QAM. In this work, we demonstrate that QD-MLLD with coherent external feedback can be used for high-speed data transmission using advanced modulation formats beyond 16QAM. Even though the viability of this scheme has so far been limited to benchtop-type experimental setups, chip-scale integration of the scheme is the subject of ongoing research. Future investigations could build upon our work with QD-MLLD based WDM reception, discussed in Chapter 5, and explore the use of QD-MLLD with external feedback or DSP-based phase-noise compensation [10] to achieve higher transmission capacity and spectral efficiency.

When the target application demand even further scaling to larger WDM channel counts, Kerr comb generators appear as the most promising candidates. One single device can generate soliton combs that cover all optical telecommunication bands in the near infrared along with a narrow optical linewidth of the comb tones. Recent progress towards packaged Kerr-comb generators [87], [88] makes these devices ideal candidates for building future high-capacity optical transceivers. The main hurdle of Kerr comb generators has been the relatively low optical conversion efficiency from the continuous-wave (CW) pump laser to the comb tone. However, dark solitons along with improved design parameters are expected to offer improved conversion efficiencies [205].

Appendices

A. Comb line power and OCNR

The content of the following sections has been published in the Appendix of the book chapter [B1]. In order to fit the structure and layout of this document, it was adapted accordingly.

Appendix A.1 details the derivation of Eq. (2.7), which expresses the optical signal-to-noise power ratio (OSNR) at the receiver, $\mathrm{OSNR}_{\mathrm{Rx}}$, as a function of the power per line P_ℓ of the frequency comb for different link distances. The equation is derived considering the transmitter setup and channel structure depicted in Figure 2.7a. Appendix A.2 gives the expression of the required OSNR at the receiver for a desired target BER, $\mathrm{OSNR}_{\mathrm{Rx}}$, for a given modulation format and symbol rate, see dashed lines in Figure 2.7b.

A.1 Calculation of OSNR at the receiver

For WDM applications, the power and optical carrier-to-noise power ratio (OCNR) per line of a frequency comb will dictate the maximum achievable OSNR of the WDM channel at the receiver, $\mathrm{OSNR}_{\mathrm{Rx}}$. To estimate the $\mathrm{OSNR}_{\mathrm{Rx}}$, the setup depicted in Figure 2.7a is considered. The noise power at the output of the FCG is given by

$$P_{\mathrm{n}} = S_{\mathrm{n}} B_{\mathrm{ref}} = \frac{P_\ell}{\mathrm{OCNR}_\ell}. \tag{A.1}$$

Here, S_{n} is the co-polarized noise power density, and $B_{\mathrm{ref}} = 12.5$ GHz is the reference noise measurement bandwidth. An optical amplifier with gain $G_0 > 1$ increases the comb line power P_ℓ and the noise power $P_{\mathrm{n},\ell}$ to $P_{\ell,0}$ and $P_{\mathrm{n},0}$, respectively, and it adds some co-polarized noise of its own,

$$P_{\ell,0} = G_0 P_\ell, \qquad P_{\mathrm{n},0} = \underbrace{S_{\mathrm{n}} G_0 B_{\mathrm{ref}}}_{\substack{\text{amplified} \\ \text{OFC noise}}} + \underbrace{F_0 h f (G_0 - 1) B_{\mathrm{ref}}}_{\substack{\text{ASE noise of} \\ \text{comb amplifier}}}. \tag{A.2}$$

In these relations, the quantity F_0 is the noise figure of the amplifier after the comb source, and hf is the photon energy. The noise power $P_{\mathrm{n},0}$ is reduced by a factor $g_0 < 1$ through the loss in the WDM modulator, comprising a demultiplexer, an array of electro-optic modulators, and a multiplexer, Figure **1.1**a. A post-amplifier with gain $G_1 > 1$ increases the signal, but also contributes noise,

$$P_{\mathrm{s}} = G_1 g_0 P_{\ell,0}, \qquad P_{\mathrm{n},1} = G_1 g_0 P_{\mathrm{n},0} + F_1 h f (G_1 - 1) B_{ref}. \qquad \text{(A.3)}$$

This power is the launched into the first fiber section, which attenuates the power by $g_1 < 1$ such that $G_1 g_1 = 1$. This fiber span might be followed by $(\nu_{\max} - 1)$ additional fiber sections, each attenuating the power by $g_\nu < 1$ and by the same number of additional amplifiers with a gain G_ν such that $G_\nu g_\nu = 1$. Assuming that all $\nu_{\max}$ links are identical ($G_\nu = G$, $g_\nu = g$, $Gg = 1$, $F_\nu = F$ for $\nu = 1 ... \nu_{\max}$), the signal power and the noise power after the transmission link are given by

$$P_{\mathrm{s},\nu_{\max}} = g P_{\mathrm{s}}, \qquad P_{\mathrm{n},\nu_{\max}} = g P_{\mathrm{n},1} + (\nu_{\max} - 1) g F h f (G - 1) B_{\mathrm{ref}}. \qquad \text{(A.4)}$$

The signal power $P_{\mathrm{s,Rx}}$ and the noise power $P_{\mathrm{n,Rx}}$ in the reference bandwidth B_{ref} at the output of the pre-amplifier are given by

$$P_{\mathrm{s,Rx}} = G_{\mathrm{Rx}} P_{\mathrm{s},\nu_{\max}}, \qquad P_{\mathrm{n,Rx}} = G_{\mathrm{Rx}} P_{\mathrm{n},\nu_{\max}} + F_{\mathrm{Rx}} h f (G_{\mathrm{Rx}} - 1) B_{\mathrm{ref}}. \qquad \text{(A.5)}$$

The $\mathrm{OSNR}_{\mathrm{Rx}}$ at the input of the receiver reads

$$\mathrm{OSNR}_{\mathrm{Rx}} = \frac{G_{\mathrm{Rx}} g_0 G_0 P_\ell}{P_{\mathrm{n,Rx}}}. \qquad \text{(A.6)}$$

Introducing Eqs. (A.1), (A.2) and (A.5) into Eq. (A.6) leads to Eq. (2.7). In typical WDM links, an optical channel power of 0 dBm is launched into each fiber span for reducing the nonlinear impairments while maintaining good OSNR [41], [42]. This leads to the curves shown in Figure 2.7.

A.2 Required receiver OSNR

For a given modulation format and bandwidth B, a required $\mathrm{OSNR}_{\mathrm{sig}}$ at the receiver can be calculated for the desired target BER. In the case of non-data aided reception of a polarization-multiplexed signals impaired by additive white Gaussian noise, the relation between BER and $\mathrm{OSNR}_{\mathrm{sig}}$ for quadratic *M*-ary QAM constellations is given by [184]

$$\mathrm{BER} = \frac{\sqrt{M}-1}{\sqrt{M}\log_2\sqrt{M}}\,\mathrm{erfc}\sqrt{\frac{3}{2(M-1)}\mathrm{OSNR}_{\mathrm{sig}}}\,. \tag{A.7}$$

$$\mathrm{OSNR}_{\mathrm{sig}} = \frac{2B_{\mathrm{ref}}}{pB}\mathrm{OSNR}_{\mathrm{ref}}\,. \tag{A.8}$$

In these relations, the $\mathrm{OSNR}_{\mathrm{sig}}$ refers to the power ratio of the data signal to the noise power within the true signal bandwidth B, which differs from the reference bandwidth $B_{\mathrm{ref}} = 12.5\ \mathrm{GHz}$ that was used to specify the $\mathrm{OSNR}_{\mathrm{ref}}$ in the previous sections and that corresponds to a reference wavelength span of 0.1 nm at $\lambda = 1.55\mu\mathrm{m}$. The $\mathrm{OSNR}_{\mathrm{Rx}}$ is determined by measuring the unpolarized noise power density in *x* and *y*-polarization within B_{ref} using with an optical spectrum analyzer (OSA), $S_{\mathrm{n},x} + S_{\mathrm{n},y} = 2S_{\mathrm{n},x}$. If the signal comprises only one polarization which carries a power P_x, an $\mathrm{OSNR}_{\mathrm{ref}} = P_x / (2S_{\mathrm{n},x}B_{\mathrm{ref}})$ results. If the signal power is composed of two orthogonally polarized contributions with equal powers, and overall signal power of $P_x + P_y = 2P_x$ is measured, and $\mathrm{OSNR}_{\mathrm{ref}} = 2P_x / (2S_{\mathrm{n},x}B_{\mathrm{ref}})$ holds. In contrast to that, the signal-relevant $\mathrm{OSNR}_{\mathrm{sig}}$ of the polarized signal power has to be referred to the co-polarized noise power density only, . This explains the factor p in Eq. (A.8), which is $p = 1$ for single-polarization and $p = 2$ for dual polarization signals.

B. Relative intensity noise (RIN) of QD-MLLD with and without external-cavity feedback

From the beat signals recorded for the optical linewidth measurements, see Figure 4.2b,c, we also extracted the associated relative intensity noise (RIN) of individual comb tones. The results are shown in Figure B.1. For free-running QD-MLLD without external-cavity feedback, we find RIN levels of approximately −115 dB Hz^{-1} for frequencies below 1 GHz, which is well in line with other experiments[90], [206]. Under the influence of external-cavity feedback, the RIN spectrum experiences a modulation that corresponds to the free spectral range of the 300 mm-long external cavity. The overall RIN level, however, remains unchanged. Note that the sensitivity of the RIN measurement is limited to a minimum detectable level of approximately −127 dB Hz^{-1} due to the ASE noise of the EDFA that was used in the signal path when measuring the beat note, see Figure 4.2a in Section 4.2.

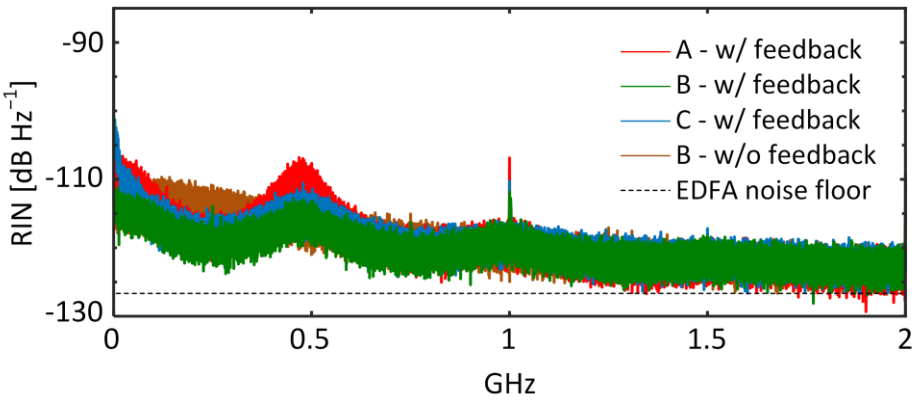

Figure B.1: Relative intensity noise (RIN) spectra extracted from the beat notes of the linewidth measurement. We find that external-cavity feedback leads to a spectral modulation of the RIN according to the free spectral range of the 300 mm-long external cavity, while leaving the overall RIN level unchanged. Due to an EDFA that was used in the signal path signal path when measuring the beat notes, sensitivity of the RIN measurement is limited to a noise floor of approximately – 127 dB Hz^{-1}.

C. Microresonator solitons for data transmission

The content of the following sections has been published in Methods and Supplementary Information of the journal publication [J4]. In order to fit the structure and layout of this document, it was adapted accordingly.

[*Beginning of Methods and Supplementary Information of paper [J4]*]

Microresonator solitons for massively parallel coherent optical communications

Nature, Volume 546, Issue 7657, pp. 274-279, 2017
DOI: 10.1038/nature22387

Pablo Marin-Palomo[1,×], Juned N. Kemal[1,×], Maxim Karpov[2,×], Arne Kordts[2], Joerg Pfeifle[1], Martin H. P. Pfeiffer[2], Philipp Trocha[1], Stefan Wolf[1], Victor Brasch[2], Miles H. Anderson[2], Ralf Rosenberger[1], Kovendhan Vijayan[1], Wolfgang Freude1,3, Tobias J. Kippenberg[2], Christian Koos[1,3]

1 Institute of Photonics and Quantum Electronics (IPQ), Karlsruhe Institute of Technology (KIT), 76131 Karlsruhe, Germany
2 École Polytechnique Fédérale de Lausanne (EPFL), 1015 Lausanne, Switzerland
3 Institute of Microstructure Technology (IMT), Karlsruhe Institute of Technology (KIT), 76131 Karlsruhe, Germany
× These authors contributed equally to this work

C.1 Methods

Fabrication of high-*Q* Si_3N_4 microresonator

We use Si_3N_4 microresonators for generation of DKS frequency combs. These devices lend themselves to co-integration with other photonic devices, using either monolithic approaches on silicon [191] or indium phosphide (InP) [207],

hybrid InP-on-silicon approaches [208], or multi-chip concepts [16], [209]. A particularly attractive option is to co-integrate DKS comb generators with advanced multiplexer and demultiplexer circuits [191] and with highly power-efficient IQ modulators [210], [211] to realize chip-scale transceivers that can handle tens of terabit/s of data traffic, as already envisioned in Ref. [16]. For soliton formation, anomalous group velocity dispersion (GVD) is required, necessitating Si_3N_4 waveguide heights of approximately 800 nm for a width of 1.65 μm. These dimensions are achieved by using the recently developed photonic Damascence process [159], along with a waveguide filtering section to achieve a smooth dispersion profile [201]. A mode-filtering section was incorporated into the microrings in order to suppress higher-order modes [201], see Inset of Figure 6.1a. This allows to minimize the number of avoided mode crossings and facilitates soliton comb generation.

Fabrication reproducibility was investigated, leading to a yield of chips enabling DKS generation per batch of approximately 40 %. For resonators taken from the same wafer, we measured an average line spacing of 95.75 GHz with a standard deviation of approximately 70 MHz. We attribute such differences to variations of both the waveguide width and the thickness of the Si_3N_4 layer between distant micro-resonators within the same wafer. These variations are approximately 20 nm and may be reduced by increasing the uniformity of the fabrication process over the entire wafer. In particular, we expect that the use of highly developed large-scale fabrication equipment such as 193 nm deep-UV lithography and thin-film tools with improved uniformity will overcome these shortcomings in device reproducibility, as already demonstrated in the context of silicon photonics [212]. Note that the line spacing difference between frequency combs can be compensated through thermal tuning, which allows us to adapt the microresonators' FSR over a tuning range of more than 40 MHz, with a precision of approximately 200 kHz. The same technique can be applied to precisely match the line spacing to established ITU grids.

In addition, we measured the differences in power conversion efficiency of the DKS comb generators used in our experiment, leading to values that range from 0.1 % to 0.6 %. These differences in power conversion efficiency are attributed

to variations of the quality factors of the pumped resonances, which may be influenced by interactions of the fundamental mode with higher-order modes. Even though mode-filtering sections are used to suppress the propagation of higher order modes within the waveguide, we can still observe slight variations of the spectral envelope with respect to the theoretical sech^2 envelope shape. This fact hints to the presence of avoided mode crossings which are characteristic of multimode waveguides. We expect that these limitations can be overcome by optimized device design.

For DKS comb generators with improver power efficiency, high-Q factors are of great importance. Recently, Si_3N_4 resonators have been demonstrated [213], [214] to reach Q-factors of more than 6×10^6 both in devices with normal [213] and anomalous [214] GVD. Along with tailored optical amplifiers, such devices allow to reduce the electrical power consumption by more than an order of magnitude compared to state-of-the-art ITLA laser arrays, see Section C.6.1.

Soliton comb generation

The DKS combs are generated by pumping the microresonators with an ECL and a subsequent EDFA, which is operated at an output power of approximately 35 dBm, see Section C.2 and Figure C.1 for a more detailed description of the comb generation setup. A high-power band-pass filter with a 3 dB bandwidth of 0.8 nm is used to suppress the ASE noise originating from the pump amplifier. The soliton state is excited by well-controlled wavelength tuning of the pump ECL from low to high wavelengths across the resonance at a rate of approximately 100 pm/s [189]. Once a multiple-soliton state is obtained, the transition to a single-soliton state is accomplished by fine-tuning of the pump laser towards lower wavelengths [200]. This slow sweep is performed at a rate of approximately 1 pm/s. Light is coupled into and out of the on-chip Si_3N_4 waveguides by means of lensed fibers, featuring spot sizes of 3.5 µm and coupling losses of 1.4 dB per facet. The pump power in the on-chip waveguide amounts to approximately 32 dBm. The frequency comb used in the single-comb transmission experiment exhibits a line spacing of 95.80 GHz and a 3-dB bandwidth of more than 6 THz. The optical linewidth of individual comb carriers is limited by the optical linewidth of our tunable pump lasers (TLB-

6700, New Focus and TSL-220, Santec), which is below 100 kHz. This value is well below that of telecommunication-grade DFB lasers [215] and hence perfectly suited for coherent data transmission [38]. No additional linewidth broadening relative to the pump is measured, i.e., the phase noise of the comb lines is entirely dominated by the pump. Note that an alternative approach to DKS generation has recently been demonstrated [216] where the detuning of the pump laser with respect to the resonance is adjusted by thermally shifting the resonance by means of integrated heaters rather than by tuning the wavelength of the pump laser. This technique allows to replace the tunable pump lasers by much more stable CW pump lasers with sub-kHz linewidths. At the output of the microresonator, a tunable fiber Bragg grating (FBG) acts as a notch filter to suppress residual pump light to a power level that matches the other comb carriers. After the FBG, the measured optical power of the entire comb spectrum, see Figure 6.1c, amounts to 4 dBm. For the experiments using interleaved transmitter (Tx) frequency combs or a separate receiver (Rx) LO comb, a second DKS comb generator with similar performance is used. The frequency comb from the second device for the interleaved Tx combs (for the Rx LO) features a slightly different line spacing of 95.82 GHz (95.70 GHz) and overall optical power of 0 dBm (8 dBm). For the transmission experiments, an EDFA is used to amplify the combs to an approximate power of 5 dBm per line prior to modulation. The carriers next to the pumped resonance are superimposed by strong amplified stimulated emission (ASE) noise that originates from the optical amplifier. In future implementations, ASE noise can be avoided by extracting the comb light from the microresonator using a drop-port geometry [217]. This would avoid direct transmission of broadband ASE noise through the device and, in addition, would render the notch filter for pump light suppression superfluous.

Dissipative Kerr soliton comb tuning and interleaving

Precise interleaving of the frequency combs in the second transmission experiment is achieved by adjusting the temperature of each microresonator, thereby changing the refractive index and shifting the resonance frequencies while leaving the FSR essentially unchanged [218]. A detailed sketch of the experimental setup is given in Section C.2. The resonance frequencies of the

cavity can be tuned at a rate of approximately – 2.5 GHz/K with an accuracy of approximately 200 MHz, limited by the resolution of the heater of approximately 0.1 K. In addition, as a consequence of intra-pulse Raman scattering [219], the center frequency of the comb can also be tuned by slowly changing the pump frequency during operation at a constant external temperature. The associated tuning range is limited to approximately ± 500 MHz before the comb state is lost; the tuning resolution is given by the pump laser and amounts to approximately 10 MHz for our devices (TLB-6700, New Focus; TSL-220, Santec). These tuning procedures are used both for precise interleaving of DKS combs in the second transmission experiment and for synchronizing the LO comb to the Tx comb in the third transmission experiment.

Data transmission experiments

For the data transmission experiments [104], [118], [220], the single or interleaved frequency comb is amplified to 26.5 dBm by a C/L-band EDFA, before the lines are equalized and dis-interleaved into odd and even carriers to emulate WDM. In the lab experiment, the de-multiplexer (DEMUX) depicted in Figure 6.2a is implemented by two programmable filters (Finisar WaveShaper, WS) along with C- and L-band filters, that act as dis-interleavers to separate the combs into two sets of "even" and "odd" carriers, see Section C.3 for a more detailed description of the experimental setup. After separation, the carriers are routed to individual dual-polarization in-phase/quadrature modulators (IQ-mod), which encode independent data streams on each polarization using both the amplitude and the phase of the optical signal as carriers of information. To this end, we use two optical IQ modulators which are driven with pseudo-random bit sequences of length $2^{11} – 1$ using QPSK or 16QAM signaling and raised-cosine (RC) pulse shaping with a roll-off factor $\beta = 0.1$. The drive signals were generated by arbitrary waveform generators (AWG). For the transmission experiment using frequency combs as optical source at the Tx, the symbol rate was 40 GBd, and the sampling rate of the AWG was 65 GSa/s (Keysight M8195A). For the experiment with a DKS comb as a multi-wavelength LO, symbol rates of 50 GBd and sampling rates of 92 GSa/s (Keysight M8196A) were used. We refrained from using higher

symbol rates since the limited electrical bandwidth of our transmitter and receiver hardware would have led to significantly worse signal quality. In all experiments, polarization division multiplexing (PDM) is emulated by a split-and-combine method, where the data stream of one polarization is delayed by approximately 240 bits with respect to the other to generate uncorrelated data [101]. The data channels are then recombined into a 75 km long standard single-mode fiber (SSMF) fiber using a multiplexer (MUX) and boosted by an erbium-doped fiber amplifier (EDFA), before being transmitted. At the receiver, we select each channel individually by a BPF having a 0.6 nm passband, followed by a C-band or an L-band EDFA, and another BPF with a 1.5 nm passband. The signal is received and processed by means of an optical modulation analyzer (OMA, Keysight N4391A), using either a high-quality ECL line or a tone of another DKS comb as local oscillator. In the latter case, we use an optical band-pass filter to extract the tone of interest from the LO comb, see Section C.5 for details. In all experiments, we perform offline processing including filtering, frequency offset compensation, clock recovery, polarization demultiplexing, dispersion compensation, and equalization.

Transmission impairments and data rates

In our transmission experiments, performance was impaired by specific limitations of the available laboratory equipment, which can be avoided in real-world transmission systems. For the transmission experiment using a single DKS comb generator as optical source, Figure 6.2a, a total of 101 tones were derived from the comb in the C and L bands. Out of those, 92 carriers performed better than the BER threshold of 4.5×10^{-3} for widely used second-generation forward-error correction (FEC) with 7 % overhead [114], see Figure 6.2e. The pump tone at approximately 192.66 THz and two neighbouring carriers could not be used for data transmission due to strong amplified spontaneous emission (ASE) background from the pump EDFA. Two more directly adjacent channels exceeded the threshold of 4.5×10^{-3}, but were still below the BER threshold of 1.5×10^{-2} for soft-decision FEC with 20 % overhead [114]. Another four channels at the low-frequency end of the C-band were lost due to a mismatch on the transmission band of the C-band filters used to realize the demultiplexer,

see Section C.3 for a more detailed description. This leads to an overall net data rate (line rate) of 28.0 Tbit/s (30.1 Tbit/s).

For the transmission experiment using interleaved DKS combs as optical source at the transmitter, Figure 6.2c, we use a combination of 16QAM and QPSK, depending on the optical signal-to-noise power ratio (OSNR) of the respective carrier, see Figure 6.2e. For 16QAM transmission, a total of 126 channels exhibit a BER of less than 4.5×10^{-3}, requiring an FEC overhead of 7 %, and 39 additional channels showed a BER below 1.5×10^{-2}, which can be corrected by FEC schemes with 20 % overhead. For the 14 channels at the low-frequency edge of the L band, the modulation format was changed to QPSK due to the low power of these carriers caused by a decrease of amplification of the L-band EDFA in this wavelength range. This leads to an overall net data rate (line rate) of 50.2 Tbit/s (55.0 Tbit/s).

For the transmission experiment using DKS frequency combs both at the transmitter and at the receiver side, Figure 6.3a, 99 tones were transmitted and tested. Out of those, a total of 89 channels perform better than the BER threshold for hard-decision FEC with 7 % overhead (4.5×10^{-3}), and additional four channels are below the BER limit of 1.5×10^{-2} for soft-decision FEC with 20 % overhead. For the remaining channels, coherent reception was inhibited by low OSNR. This leads to an overall net data rate (line rate) of 34.6 Tbit/s (37.2 Tbit/s). The black circles in Figure 6.3d show the channels with BER above the threshold for 7 % FEC and specify the reasons for low signal quality: low optical carrier-to-noise power ratio (OCNR) of the carriers from the LO comb (LO) and the signal comb (Signal) as well as bandwidth limitations of the C-band EDFA (EDFA).

It is further worth noting that field-deployed WDM systems rely on statistically independent data channels rather than on transmitting identical data streams on the “even” and the “odd” channels. As a consequence, real-world signals will suffer much less from coherent addition of nonlinear interference noise than the signals used in our experiments [221]. With respect to nonlinear impairments, our experiments hence represent a bad-case scenario with further room for improvement.

Characterization of the OSNR penalty of frequency comb source

For comparing the transmission performances of a single comb line to that of a high-quality external cavity laser (Keysight N7714A) reference carrier, we measure the OSNR penalty at a BER of 4.5×10^{-3}, which corresponds to the threshold for FEC with 7 % overhead [114]. For a given BER, the OSNR penalty is given by the dB-value of the ratio of the actually required OSNR to the OSNR that would be theoretically required in an ideal transmission setup [184].

A detailed description of the associated experimental setup is given in Section C.4. The carrier under test is selected by a band-pass filter with a 1.3 nm (160 GHz) wide passband. The carrier is then amplified to 24 dBm by an EDFA (EFDA2 in Figure C.3) and modulated with a PDM-16QAM signal at 40 GBd. Next, an ASE noise source together with two VOA is used to set the OSNR of the channel while keeping its optical power constant. As an ASE generator, we use a second EDFA (EDFA3 in Figure C.3a). An optical spectrum analyzer (OSA, Ando AQ6317B) is used for measuring the OSNR at the input of the receiver. For each OSNR value, the quality of the channels is determined by measuring the BER using our previously described receiver configuration, see the Section "Data transmission experiments" above in Appendix C.1. At a BER of 4.5×10^{-3}, a penalty of 2.6 dB with respect to the theoretical OSNR value is observed, see Figure 6.2f, which is a common value for technical implementations of optical 16QAM transmitters [222]. For high OSNR, an error floor caused by transmitter nonlinearities and electronic receiver noise is reached. The maximum achievable OSNR of 44 dB at 192.56 THz for transmission with the comb line is dictated by ASE noise of the C/L-band EDFA (EDFA1) right after the FCG, see Figure C.3. As a reference, the same measurements are repeated using a high-quality ECL (Keysight N7714A) to generate the carrier, which leads to essentially the same OSNR penalty for a given BER as the transmission with the comb line. For a symbol rate of 40 GBd, the results are shown in Figure 6.2f, similar results are obtained at other symbol rates such as 28 GBd, 32 GBd and 42.8 GBd. Note that for transmission with the ECL, only one EDFA (EDFA2) is needed to increase the power to 24 dBm before being modulated. As a consequence, a higher maximum OSNR of 58 dB

can be achieved with the ECL than with the comb line. Note in addition that for transmission with a single line, the lowest BER reached at 40 GBd is below 10^{-4}, as depicted in Figure 6.2f. This value, however, is not reached in the WDM transmission experiment with the full comb, Figure 6.2a and Figure **6.3**d. For WDM transmission, a larger number of carriers are amplified by the EDFA in front of the modulator, which, together with the limited output power of the EDFA (EDFA 2-5 in Figure C.2a), decreases the optical power per line and hence the OCNR. Moreover, when interleaving two frequency combs, a VOA and a directional coupler are inserted into the setup, thereby introducing additional loss which needs to be compensated by the subsequent EDFA. Using additional EDFA would therefore increase the quality of the received signal

C.2 Kerr soliton frequency comb generation and interleaving

Figure C.1a shows the detailed setup of the dissipative Kerr soliton (DKS) frequency comb generators (FCG) used for the data transmission experiments discussed in the main paper. The DKS frequency comb is generated by pumping a silicon nitride (Si_3N_4) microresonator with an external cavity laser (ECL). A polarization controller (PC) before the microresonator is adjusted for maximum coupling of pump light into the resonance. The pump light generated by the ECL is amplified by an erbium-doped fiber amplifier (EDFA) which is operated at an output power of approximately 35 dBm. After the EDFA, a high-power band-pass filter (BPF) is used to suppress amplified stimulated emission (ASE) noise. Since the passband of the BPF has finite non-zero width, noise near the pump frequency is not fully suppressed, thereby deteriorating the signal quality of the adjacent carriers. A pair of lensed fibers (LF) with a mode field diameter of 3.5 µm are used to couple light into and out of the microresonator, leading to 1.4 dB of insertion loss per facet. The temperature of the microresonator is adjusted and stabilized by a thermoelectric controller (TEC), while an optical

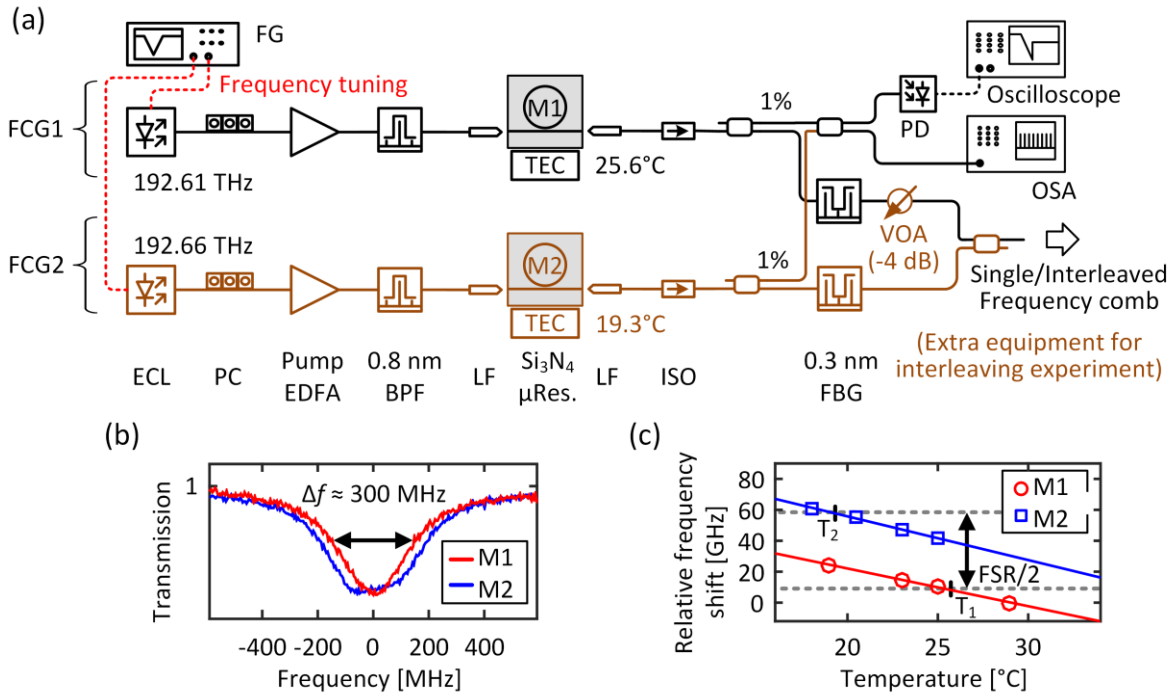

Figure C.1: Generation of single and interleaved DKS frequency combs. **(a)** Setup for generation of single and interleaved DKS frequency combs. The frequency comb generator (FCG) for single-comb generation is depicted in black (FCG1); for dual-comb generation and interleaving, a second FCG (FCG2) is used, depicted in brown. The microresonators (M1, M2) are driven by a pair of linearly polarized continuous-wave (CW) external-cavity lasers (ECL) whose output powers are boosted by erbium-doped fiber amplifiers (EDFA). The frequency of each ECL is controlled via an analogue signal generated by a function generator (FG) for tuning into a soliton state. Amplified spontaneous emission (ASE) noise from the power booster EDFA is suppressed by two band-pass filters (BPF) with 0.8 nm passbands. Pump light is coupled to and from the resonator chips by lensed fibers (LF) having a mode field diameter of 3.5 µm, which leads to 1.4 dB of losses per facet, measured at the pump wavelength. After the microresonators, optical isolators (ISO) avoid back reflection of light into the chip. Fiber Bragg gratings (FBG), acting as notch filters with a 0.3 nm bandwidth, are used to attenuate the residual pump light to a power level comparable to that of the adjacent carriers. Prior to the interleaving of both frequency combs with a directional coupler, a variable optical attenuator (VOA) with an attenuation of 4 dB adapts the power level of one comb to the other. A real-time oscilloscope connected to a photodiode (PD) and an optical spectrum analyzer (OSA) are used to track the change of transmitted power and to measure the comb spectrum. **(b)** Transmitted optical power measured by the PD as a function of the ECL frequencies, around the center frequency of the cold resonances from M1 (red) and M2 (blue). A width of about 300 MHz is measured for both microresonators, corresponding to a loaded quality factor of approximately 7×10^5. The different shape of the resonances is attributed to spurious coupling of counter-propagating waves in M2. (Caption continued on next page)

Figure C.1 continued: **(c)** Temperature-induced frequency shift of the comb carriers from M1 and M2 relative to the frequencies of the comb carriers from M1 at 28 °C. A dependence of – 2.2 GHz/K and – 2.7 GHz/K is measured for M1 and M2, respectively. Temperatures T_1 = 25.6°C and T_2 = 19.3°C are chosen for M1 and M2 such that the frequency difference of the carriers near the center of the interleaved comb is half the line spacing of the frequency comb from M1.

isolator (ISO) at the output avoids back-reflection of light into the chip. A fiber Bragg grating (FBG) acts as a notch filter with a 0.3 nm bandwidth to suppress the remaining pump laser up to a level comparable to that of the adjacent frequency comb carriers.

DKS frequency combs are generated by operating the microresonator in the effectively red-detuned regime with respect to the cavity resonance, i.e., the pump wavelength is bigger than the wavelength of the thermally shifted resonance. This regime is accessed by fast sweeping of the pump ECL through the cavity resonance from a blue-detuned wavelength to a predefined red-detuned wavelength (forward-tuning), where a multiple-soliton comb state is generated [83], [189], see trace I of Figure 6.1b in the main paper. The transition to a single-soliton state is accomplished in a reliable and deterministic manner by adiabatically reducing the wavelength of the pump laser (backward-tuning) thereby approaching the hot-cavity resonance from the red side [200], see trace II of Figure 6.1b. In both sweeps, the ECL wavelength is controlled via an analogue voltage signal generated by a function generator (FG). The forward-tuning is performed at a speed of approximately 100 pm/s and is fast enough to avoid excess heating of the microresonator, which would lead to loss of the soliton comb state due to a too strong thermal shift of the cavity resonance. The backward-tuning is performed at a speed of approximately 1 pm/s and is slow enough to adiabatically switch between different multiple-soliton states. A real-time oscilloscope and an optical spectrum analyzer (OSA) are used to track the change of transmitted power and to measure the comb spectrum, respectively, while sweeping the pump wavelength along the resonance.

For the interleaved-comb experiment, Figure 6.2c of the main paper, two DKS comb sources, namely M1 and M2, with comparable free spectral ranges (FSR)

are used in parallel. The equipment required for the second FCG (FCG2) and for interleaving the soliton Kerr combs of the two microresonators is marked in brown in Figure C.1a. FCG2 is setup similar to FCG1 as discussed above. For interleaving, the two DKS frequency combs from FCG1 and FCG2 are superimposed by a directional coupler. Note that for the microresonator M2, a lower conversion efficiency of optical pump power to soliton power is observed as compared to that of microresonator M1. This can be attributed to spurious coupling of counter-propagating waves in M2, which also explains the difference in the shape of the resonances from M1 and M2 depicted in Figure C.1b. Therefore, the power level of the frequency comb from M1 is adapted to that of M2 by a variable optical attenuator (VOA) before interleaving with the directional coupler. This results in a uniform power spectral envelope of the interleaved frequency comb. To obtain an interleaved comb with evenly spaced carriers, the working temperatures of the microresonators are set such that one of the frequency combs is offset by half the line spacing with respect to the other. Figure C.1c shows the frequency shift of the carriers of M1 (red) and M2 (blue), relative to the frequency of the carriers from M1 at 28 °C, as a function of the microresonator temperature. Both frequency combs follow a linear trend with a shift of -2.2 GHz/K and –2.7 GHz/K for M1 and M2, respectively [218]. At the temperature T_1 (T_2) for microresonator M1 (M2) the frequency difference between the central carriers of both combs is half the line spacing. The pump frequency for the microresonator M1 (M2) is set to 192.61 THz (192.66 THz) for the chosen chip temperature of T_1 = 25.6 °C (T_2 = 19.3 °C). At such temperatures, the measured line spacing is 95.80 GHz (95.82 GHz) for M1 (M2), leading to a difference of approximately 20 MHz, or 0.02% of the line spacing. Such a difference would lead to a variation of the line spacing by ± 1 GHz at the edges of the interleaved frequency comb as compared to the line spacing near the center of the comb. This mismatch can be avoided by carefully matching the line spacing of the two combs, e.g., by improving the uniformity of the fabrication process, see Appendix C.1 for details. In the transmission experiment, the variation of line spacing did not have any significant influence on the quality of the received signal.

C.3 Data transmission experiments using dissipative Kerr soliton frequency combs as optical source at the transmitter

The setup used for massively parallel wavelength division multiplexing (WDM) data transmission is depicted in Figure C.2a. The single (interleaved) frequency comb generated by FCG1 (FCG1 and FCG2) is amplified by a C/L-band EDFA (EDFA 1) to a level of approximately 5 dBm (2 dBm) per carrier. For a realistic emulation of massively parallel WDM transmission, neighboring carriers need to be encoded with independent data streams [223], [224]. To this end, the comb is divided into even and odd carriers by a de-interleaver (DI) stage. The DI stage contains a directional coupler (CPL1) that divides the optical power into two parts, which are fed to a C-band and an L-band programmable filter (Finisar WaveShaper; WS). The WS splits even and odd carriers within the respective band. After the C- and the L-band WS, each set of carriers is amplified by EDFA 2-5 to compensate for optical losses caused during de-interleaving. Next, the C- and L-band odd carriers are recombined by the use of a C/L-band multiplexer (C/L MUX) before being coupled into an optical in-phase/quadrature (IQ) modulator (IQ1). The even carriers are also recombined and sent through IQ2. The WS are adjusted to compensate for the power differences of the comb carriers and for the spectral variations of the EDFA gain profile, thereby producing an overall flat spectrum at the inputs of IQ1 and IQ2. Both modulators are driven by either 16QAM or QPSK drive signals generated by a high-speed arbitrary waveform generator (AWG, Keysight M8195A 65 GS/s) using pseudo-random bit sequence (PRBS) of length $2^{11} – 1$, to encode data on each frequency comb carrier at a symbol rate of 40 GBd. Raised-cosine pulse shaping at a roll-off factor of $\beta = 0.1$ is used for improved spectral efficiency. After modulation, odd and even channels are combined by a directional coupler (CPL2). Polarization-division multiplexing (PDM) is emulated by splitting the data stream into two paths and recombining them on orthogonal polarizations with a decorrelating delay of approximately 1.5 ns (60 symbols) in one path and an attenuator in the other one for maintaining the same power levels. Hence, even if both polarizations contain the same PRBS sequence, they are detected

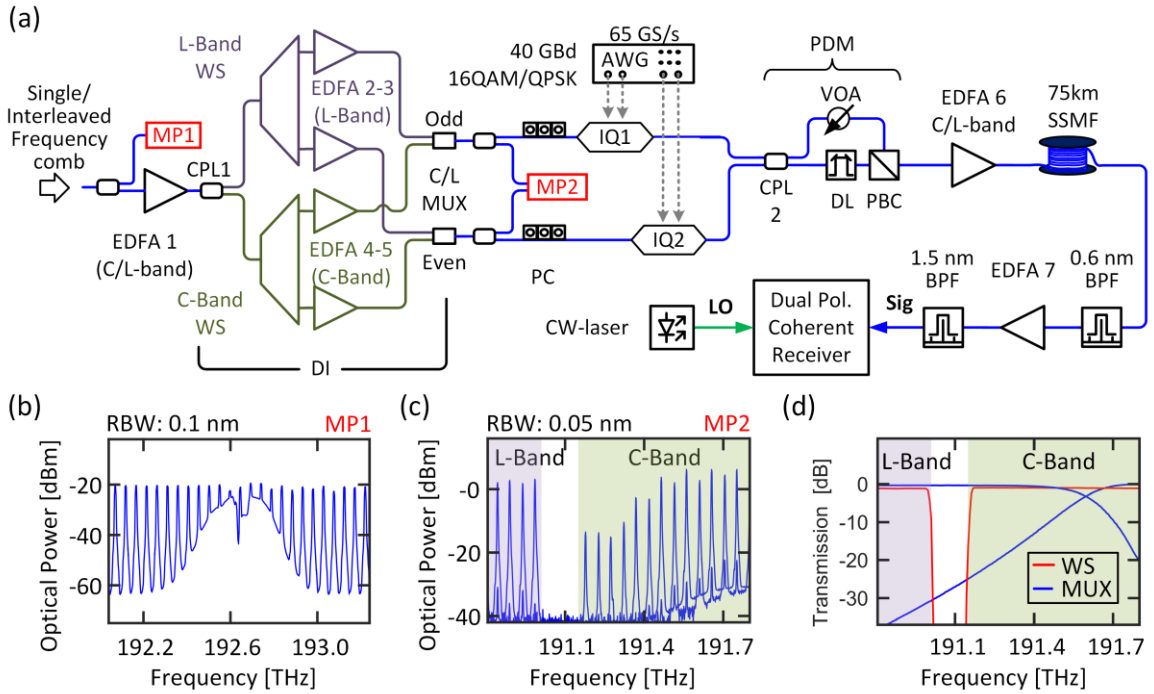

Figure C.2: Data transmission with single and interleaved DKS frequency combs as WDM carriers at the transmitter. **(a)** Data transmission setup: The single (interleaved) frequency comb generated by FCG1 (FCG1 and FCG2) from Figure C.1a is amplified by EDFA 1 to a level of approximately 5 dBm (2 dBm) per carrier. Afterwards, WDM is emulated by encoding independent data into neighboring carriers. To this end, the comb is divided into even and odd carriers by a de-interleaver (DI) stage. The DI stage contains a directional coupler (CPL1) that divides the optical power into two parts, which are fed to a C-band and an L-band programmable filters (WS). The WS split the input comb lines into even and odd carriers within their respective bands. Each set of carriers is amplified by an EDFA to compensate for the optical losses caused by the de-interleaving. Next, C- and L-band carriers from each set are recombined by the use of a C- and L-band multiplexer (C/L MUX) and coupled into two optical IQ modulators (IQ1, IQ2), driven by 16QAM or QPSK drive signals generated by a high-speed AWG. We use a symbol rate of 50 GBd. After combining the modulated signals by a directional coupler (CPL2), PDM is emulated by splitting the data stream into two paths and recombining them on orthogonal polarizations using a polarization beam combiner (PBC) with a delay line (DL) in one path and a variable optical attenuator (VOA) in the other one to decorrelate the data while maintaining the same power levels. The signal is amplified and transmitted through a 75 km long standard single mode fiber (SSMF). At the receiver, a tunable BPF with a 0.6 nm passband selects the channel under test, which is amplified by a C- or L-band EDFA (EDFA 7), depending on which channels are being investigated. A second BPF (1.5 nm passband) suppresses the ASE noise from the EDFA. The modulated channels are received on a dual-polarization coherent receiver using a conventional external-cavity laser as optical local oscillators (LO). (Caption continued on next page)

Figure C.2 continued: An optical modulation analyzer (OMA) comprising two real-time oscilloscopes is used to record and process the data signals. Labels MP1 and MP2 represent monitor ports where the spectra shown in b and c, respectively, were recorded. These spectra show impairments of the OCNR which limit the signal quality. **(b)** Frequency comb spectrum in the vicinity of both pump frequencies showing the ASE noise coming from the pump EDFA, see Figure C.1. **(c)** Frequency comb spectrum of the carriers at the gap between the C- and L-band WS. The low optical power of the carriers at the low-frequency edge of the C-band is caused by a mismatch between the C-passbands of the C/L MUX and the WS. **(d)** Transmission profiles of the C- and L-band WS (red) and of the C- and L-band C/L MUX (blue). For decreasing frequency, the C-band of the C/L MUX shows a decreasing transmission already from 191.7 THz, whereas the transmission band of the C-band WS reaches to 191.2 THz. This mismatch causes strong attenuation of the carriers within this region.

uncorrelated data streams at the coherent receiver. The signal is then amplified and transmitted through 75 km of standard single mode fiber (SSMF). At the receiver, a tunable BPF with a 0.6 nm passband selects the channel under test. The signal is then amplified by a C- or L-band EDFA (EDFA 7), depending on which frequency band is being investigated, and is passed through a second 1.5 nm passband BPF to suppress the ASE noise from the EDFA. Afterwards, the channel is received on a dual-polarization coherent receiver which uses a conventional continuous-wave laser as an optical local oscillator (LO). An optical modulation analyzer (OMA, Keysight N4391A) comprising two real-time oscilloscopes (Keysight DSO-X 93204A, 80 GSa/s) is used to record and process the data signals. The constellation diagram for each channel is obtained after performing signal processing consisting of digital low-pass filtering, polarization demultiplexing, chromatic dispersion compensation, frequency offset estimation, carrier phase estimation, and adaptive equalization. The block length for performing the signal processing is chosen to be 1024 symbols, which is optimized to effectively track the changes of carrier phase and polarization of the received signal. The extracted bit error ratio (BER) is used as a metric to quantify the signal quality of each channel and it is shown in Figure 6.2e of the main paper. Note that for the interleaved-comb experiment, we chose the approach of first recombining the unmodulated combs by means of a directional coupler, Figure C.1a, and then de-interleaving them again by means of the DI stage, Figure C.2a, to perform spectral flattening on the unmodulated carriers

rather than on the densely packed spectrum of the data signals. Equalizing the data signals would unavoidably have led to distortions due to spectral variations of the attenuation within individual WDM channels.

Limitations of the transmission capacity of our experiments were identified by investigating the spectrum of the interleaved frequency comb at the monitor ports MP1 and MP2 in Figure C.2a. A fraction of the spectrum, measured at MP1 around the frequency of the pump lasers is shown in Figure C.2b. The spectrum exhibits strong residual ASE noise coming from the pump EDFA of FCG1 and FCG2, which passes the relatively wide 0.8 nm BPF centered at the pump frequencies of approximately 192.6 THz. This ASE noise directly deteriorates the optical carrier-to-noise power ratio (OCNR) of the tones adjacent to the pump frequencies, rendering these carriers unusable in the data transmission experiments. Figure C.2c depicts a fraction of the spectrum measured at MP2 and centered at the frequency gap between the C and the L bands near 191.4 THz. The gap originates from the limited bandwidth of the C- and the L-band WS. As can be seen in Figure C.2c, there is a strong attenuation of the carriers at the low-frequency edge of the C-band. This is caused by a mismatch between the passbands of the C/L MUX and the passbands of the WS, see Figure C.2d. For decreasing frequency, the C-band output of the C/L MUX shows a decreasing transmission starting already at 191.7 THz whereas the C-band WS features a flat transmission band that goes down to 191.2 THz. For the high-frequency edge of the L-band, the passband mismatch does not have any influence because the C/L MUX shows perfect transmission for all frequencies that can pass the L-band WS. All these impairments are not related to the comb sources and can be avoided by using optimized devices and filters with matched passbands. We hence believe that there is considerable room for improving signal quality and further increasing the overall transmission capacity.

Another constraint in the data transmission experiments was the limited saturation output power of EDFA 2-5. To quantify the influence of the power per tone on the BER, an extra experiment is performed with less channels but the same spectral efficiency (SE). To this end, we reduce the number of L-band channels from 97 to 48. These channels were located in the center of the L band,

and the number of C-band channels were not changed. In this situation, an average BER of 2.3×10^{-3} was obtained for the L-band channels, corresponding to approximately half the averaged BER of 4.7×10^{-3} obtained when all L-band carriers were used for transmission. This proves that the current tranmission capacity is not limited by the comb source, but by the components of the tranmission systems. Note, in addition, that for the interleaved-comb experiment the power per carrier at the input of EDFA 1 is reduced compared to the single Kerr soliton comb experiment due to an additional directional coupler for interleaving the combs and due to a variable optical attenuator (VOA) used to adapt the power levels of the two combs, see Figure C.1a. This explains the slightly worse performance in signal quality of the received channels using interleaved frequency combs at the transmitter as compared to the signal quality of the received channels when using a single Kerr soliton comb at the transmitter.

C.4 OSNR analysis and measurements

In this section we introduce the formalism used to calculate the theoretical BER obtained in a data transmission experiment as a function of the optical signal-to-noise power ratio measured at the reference bandwidth of 0.1 nm ($OSNR_{ref}$), see Figure 6.2f of the main paper. We estimate the required theoretical $OSNR_{ref}$ per channel as a function of the target BER for different symbol rates. Furthermore, we also examine our experimental measurement results.

C.4.1 Theoretical required OSNR for error free transmission with FEC

The BER of quadratic *M*-ary QAM signals with *r* bits per symbol can be analytically calculated from the $OSNR_{ref}$ (measured for instance with an optical spectrum analyzer, OSA) [184], [225]. The basic assumptions are that optical additive white Gaussian noise (AWGN) is the dominant source of errors, thus neglecting nonlinear effects and electronic noise, and that reception is data-aided, which is required to measure directly the experimental BER. The relation for 16QAM, where $M = 2^r = 16$, is given by

$$\mathrm{BER} = \frac{3}{8}\mathrm{erfc}\sqrt{\frac{\mathrm{OSNR}}{10}}\ , \tag{B.1}$$

where OSNR is the signal-to-noise power ratio, where the noise power is measured within the signal bandwidth B_s for the same polarization as the signal. The signal bandwidth B_s corresponds to the effective bandwidth of a receiver filter that is matched to the received pulse shape. For raised-cosine pulses as used in our experiments, this bandwidth corresponds to the symbol rate and does not depend on the roll-off-factor β. The OSNR is related to the commonly used signal-to-noise power ratio $\mathrm{OSNR}_{\mathrm{ref}}$, where the signal and noise powers are measured in both polarizations in a reference bandwidth B_{ref}.

$$\mathrm{OSNR} = \frac{2B_{\mathrm{ref}}}{p \cdot B_s}\mathrm{OSNR}_{\mathrm{ref}}\ , \tag{B.2}$$

with p = 1 for a single-polarization signal and p = 2 for a polarization-multiplexed signal [226]. The reference bandwidth B_{ref} is taken to be 12.5 GHz, which corresponds to 0.1 nm resolution bandwidth of an OSA at 1550 nm carrier wavelength.

If redundancy is included in the coding of the bit stream to reduce the BER, Eq. (2) is modified by the coding overhead, O_c, to:

$$\mathrm{OSNR} = (1+O_c)\frac{2B_{\mathrm{ref}}}{p \cdot B_s}\mathrm{OSNR}_{\mathrm{ref}}\ . \tag{B.3}$$

Combining Eqs. (1) and (3), we can derive the required $\mathrm{OSNR}_{\mathrm{ref}}$ for a given symbol rate and coding overhead. Figure C.3 shows the theoretical required $\mathrm{OSNR}_{\mathrm{ref}}$ per channel for a targeted raw BER of 4.5×10^{-3} with O_c = 7 % coding overhead as a function of the net symbol rate. In this context, raw BER means the uncorrected BER obtained before applying forward-error correction (FEC) based on the 7 % of redundancy. For example, at a symbol rate of 40 GBd, an $\mathrm{OSNR}_{\mathrm{ref}}$ higher than 20 dB is required theoretically to achieve a raw BER below the targeted threshold BER of 4.5×10^{-3}, and FEC will allow to bring the BER further down to values below 10^{-15}. Note that the $\mathrm{OSNR}_{\mathrm{ref}}$ values provided in Figure C.3 refer to the input of the coherent receiver, and hence must be considered as a minimum requirement for the $\mathrm{OSNR}_{\mathrm{ref}}$ at the output of the

transmitter discussed in Section C.6 and specified in Table C.1. Note that in field deployed systems, impairments such as electronic noise or nonlinear effects will increase the required $OSNR_{ref}$ by the so-called OSNR penalty. This OSNR penalty has been experimentally measured for our system at different symbol rates, see Section C.4.2. OSNR penalty is a measure of the performance of the transmission system.

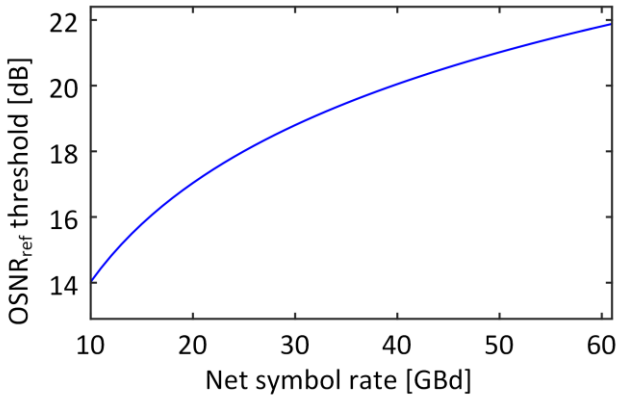

Figure C.3: Theoretical required $OSNR_{ref}$ at the input of the coherent receiver as a function of the net symbol rate for a targeted raw BER of 4.5×10^{-3}. The plot refers to 16QAM signaling, dual-polarization transmission, and a 7 % coding overhead. Raw BER means the BER before applying FEC, which can bring the final BER down to values below 10^{-15}.

C.4.2 OSNR measurements

In an extra set of experiments, we compare the 16QAM transmission performance of individual comb lines of our Kerr soliton frequency comb, featuring optical linewidths below 100 kHz, to that of a high-quality ECL reference carrier (Keysight N7714A) with an optical linewidth of approximately 10 kHz. As a metric for the comparison we use the OSNR penalty. For a given BER, the OSNR penalty is given by the dB-value of the ratio of the actually required OSNR to the OSNR that would be theoretically required in an ideal transmission setup, see Section C.4.1 and Figure C.3. The corresponding setup for OSNR penalty measurements is depicted in Figure C.4a. We use the frequency comb from FCG1, Figure C.1a, tap it directly after the FBG, and amplify it by a C/L-band EDFA (EDFA 1) to bring the comb to a level of approximately 5 dBm per carrier – just like in the transmission experiment. The

carrier under test is then selected by operating the C-band WS as a band-pass filter with a 1.3 nm (160 GHz) wide passband and coupled to a C-band EDFA (EDFA 2). The bandwidth of the WS is chosen to effectively suppress all the neighboring comb lines. For the reference transmission experiments, an ECL with an output power of 16 dBm is directly connected to EDFA 2. In both cases, the carrier under test is amplified to 24 dBm by EDFA 2 before being modulated in IQ 1 using 40 GBd PDM-16QAM. To quantify the signal quality, we investigated the BER of the received channel for different $OSNR_{ref}$ values. The $OSNR_{ref}$ of the signal is adjusted by using a noise-loading system, consisting of an ASE noise generator (EDFA 3) and two VOA. The VOA are used to modify the ASE noise power while feeding the preamplifier (EDFA 4) of the receiver with a constant optical input power. This assures that the same receiver sensitivity is maintained for all $OSNR_{ref}$ values investigated. An optical spectrum analyzer (OSA, Ando AQ6317B) is used to measure the $OSNR_{ref}$ at the input of the receiver. For each $OSNR_{ref}$ level, signal quality is determined by using the OMA to measure the BER after EDFA4 and after an additional BPF.

A section of the comb spectrum recorded at MP3 and showing four carriers of the unmodulated frequency comb is depicted in Figure C.4b. Here, the carriers still exhibit an $OCNR_{ref}$ of approximately 50 dB, measured at a reference bandwidth of 0.1 nm (12.5 GHz). This value, however, cannot be maintained throughout the setup and is reduced by the noise of the subsequent amplifiers. After filtering by the 1.3 nm BPF, the carrier under test features an optical power of approximately 0 dBm. Note that this is a much lower power level than the 16 dBm of output power generated by the ECL. To enable a fair comparison that also accounts for the superior per-carrier power levels of the ECL, we decided to use the ECL at its full output power rather than attenuating it to the 0 dBm provided by the comb source. As a consequence, we find an $OCNR_{ref}$ of 58 dB of the ECL carrier after EDFA 2, which is higher than the 42 dB achieved for the amplified comb line at 193.56 THz, see spectra in Figure C.4c, measured at MP4. Note that two noise floor levels can be identified for the comb carrier. The high-power spectral shoulder around the carrier, which is used to calculate the $OCNR_{ref}$, is caused by the noise of EDFA 1 and is suppressed further

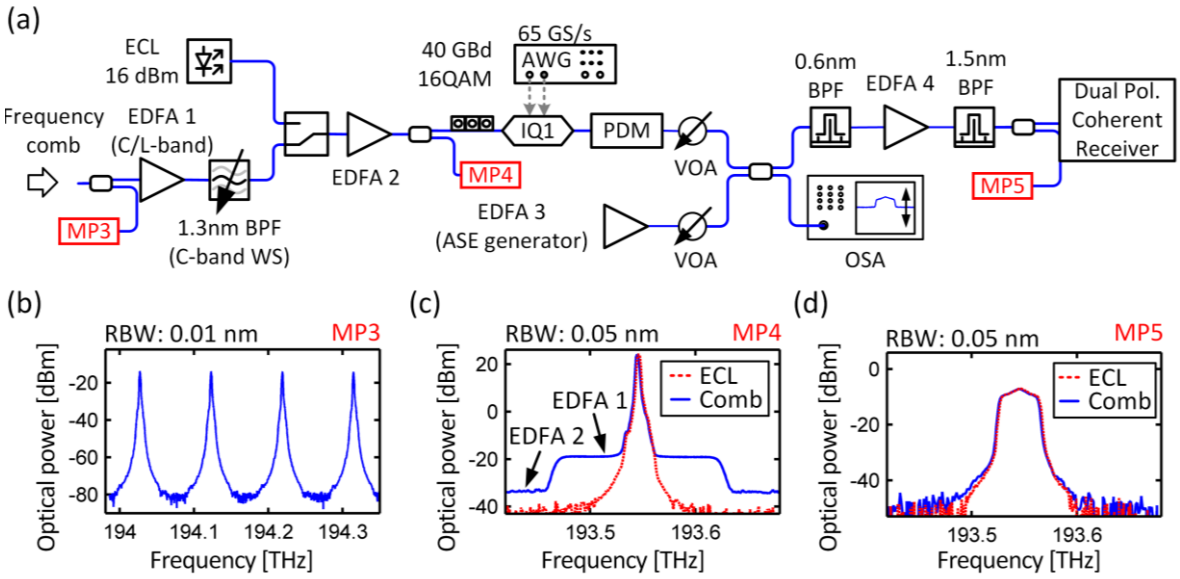

Figure C.4: Comparison of isolated frequency comb carriers with ECL carriers for data transmission. **(a)** Setup for OSNR penalty measurements: The frequency comb is generated by FCG1, see Figure C.1a, and amplified by a C/L-band EDFA (EDFA 1). A single carrier is either generated by an ECL or selected from the comb by operating the C-band programmable filter (WS) as a band-pass filter (BPF) with a 1.3 nm (160 GHz) passband. The carrier under test further amplified to 24 dBm by EDFA 2 before being modulated with PDM-16QAM at 40 GBd. To adjust the optical signal-to-noise ratio (OSNR) of the signal, a noise-loading system is used, consisting of an ASE noise generator (EDFA 3) and two VOA to modify the ASE noise power while feeding EDFA 4 with a constant optical input power. The signal is sent to the receiver where it is further amplified and analyzed by an OMA. Labels MP3, MP4 and MP5 represent monitor ports where the spectra shown in b, c and d, respectively, were recorded. These spectra have been corrected to take into account the tapping ratios of the respective power splitters. **(b)** Section of the frequency comb spectrum (resolution bandwidth RBW = 0.01 nm) as obtained from the output of FCG1. The carriers show an OCNR of approximately 50 dB at a reference bandwidth of 0.1 nm. **(c)** Frequency comb (blue) and ECL (red) carriers after EDFA 2. The frequency comb carrier shows two noise floor levels: The high-power spectral shoulder around the carrier is caused by ASE from the C/ L band EDFA (EDFA 1), which is suppressed further away from the carrier by the 1.3 nm-wide BPF, whereas the low-power ASE noise background arises from EDFA 2. The OCNR of the ECL carrier amounts to 58 dB, whereas an OCNR of 42 dB is achieved for the comb line at 193.56 THz, both measured at a reference bandwidth of 0.1 nm. **(d)** Spectrum of the received modulated data for both the frequency comb and ECL carriers with 40 GBd PDM-16QAM modulation.

away from the carrier by the 1.3 nm BPF, whereas the low-power background arises from the noise of EDFA 2. Hence, the maximum achievable $OSNR_{ref}$ for transmission with the comb line is dictated by ASE noise of the C/L-band EDFA (EDFA 1) right after the FCG. Using comb sources with higher output levels can help to further increase the signal quality. An exemplary data signal spectrum for the ECL (red) and comb (blue) carriers before entering the coherent receiver is shown in Figure C.4d as measured at MP5. Both signal are set to the same power and the same $OSNR_{ref}$ using the VOA.

Results of the OSNR penalty measurements are depicted in Figure 6.2f of the main paper. The carriers derived from the frequency comb source do not exhibit any additional implementation penalty in comparison to those generated by the reference ECL. However, the higher achievable OCNR provided by the ECL may translate into longer transmission link, which makes DKS frequency comb sources more suitable for rather short metro and regional distances. Similar results were also obtained when comparing ECL and comb carriers at symbol rates of 28 GBd, 32 GBd and 42.8 GBd.

In our setup we observe an OSNR penalty of 2.6 dB with respect to the theoretical required $OSNR_{ref}$. This value compares well with similar transmission experiments [222], [227], [228]. In Ref. [227], an $OSNR_{ref}$ penalty of approximately 2.5 dB is observe with respect the theoretical required $OSNR_{ref}$ when transmitting DP-16QAM at 43 GBd. It is reasonable therefore to consider a penalty of 2.5 dB, meaning that an $OSNR_{ref}$ per channel of approximately 22.5 dB is required for error free transmission using FEC with 7 % overhead [114] at 40 GBd and approximately 23 dB at 50 GBd. In our transmission experiment, described in Figure 6.3 of the main paper, the minimum measured channel $OSNR_{ref}$ amounts to 23 dB, measured at a reference bandwidth of 0.1 nm. The corresponding channel is at the high-frequency edge of the C-band. The measured raw BER for this channel corresponds to approximately 4.5×10^{-3}, which fits the expected required $OSNR_{ref}$ derived in the previous section.

C.5 Coherent detection using a dissipative Kerr soliton frequency comb as multi-wavelength local oscillator

Figure C.5a shows the WDM data transmission setup with a DKS frequency comb generator (FCG) as a multi-wavelength source at the transmitter (signal) and as a multi-wavelength local oscillator at the receiver (LO). The microresonator used at the transmitter side (Tx) corresponds to M1 from Figure C.1a. To provide the multi-wavelength LO, an additional microresonator (M3) with similar line spacing is used at the receiver side. Both combs are matched in absolute frequency position by adjusting the microresonators' temperature. The pump frequency for the signal (LO) comb is 193.56 THz (192.89 THz), the on chip pump power is 32.5 dBm (32 dBm) and the temperature is set to 16.4 °C (23.4 °C). We chose to pump the aforementioned resonances as they present the highest power conversion efficiency. The frequency comb obtained from M3 features a slightly lower line spacing of approximately 95.70 GHz as compared to that of M1, 95.80 GHz, due to fabrication inaccuracies. When using the carriers from M3 as LO for coherent intradyne detection, such difference in line spacing translates into a non-zero intermediate frequency (IF). The IF can be brought down to values below 100 MHz near the center of the frequency combs at around 191.5 THz but it reaches relatively high frequencies of approximately 4 GHz when coherently demodulating the signals at the low frequency edge of the L band and at the high frequency edge of the C band. The high IF, however, does not prohibit data transmission as it can be removed using digital signal processing after detection of the transmitted signal with our coherent receiver. However, for high IF, the received signal is slightly affected by the limited electrical bandwidth (BW = 33 GHz) of the analog-to-digital convertor (ADC) of our coherent receiver. This leads to a reduction of the electrical power, and thus of the electrical signal-to-noise ratio, of our baseband signal. The high IF, nonetheless, can be avoided by carefully matching the line spacing of the two Kerr soliton frequency comb sources during fabrication.

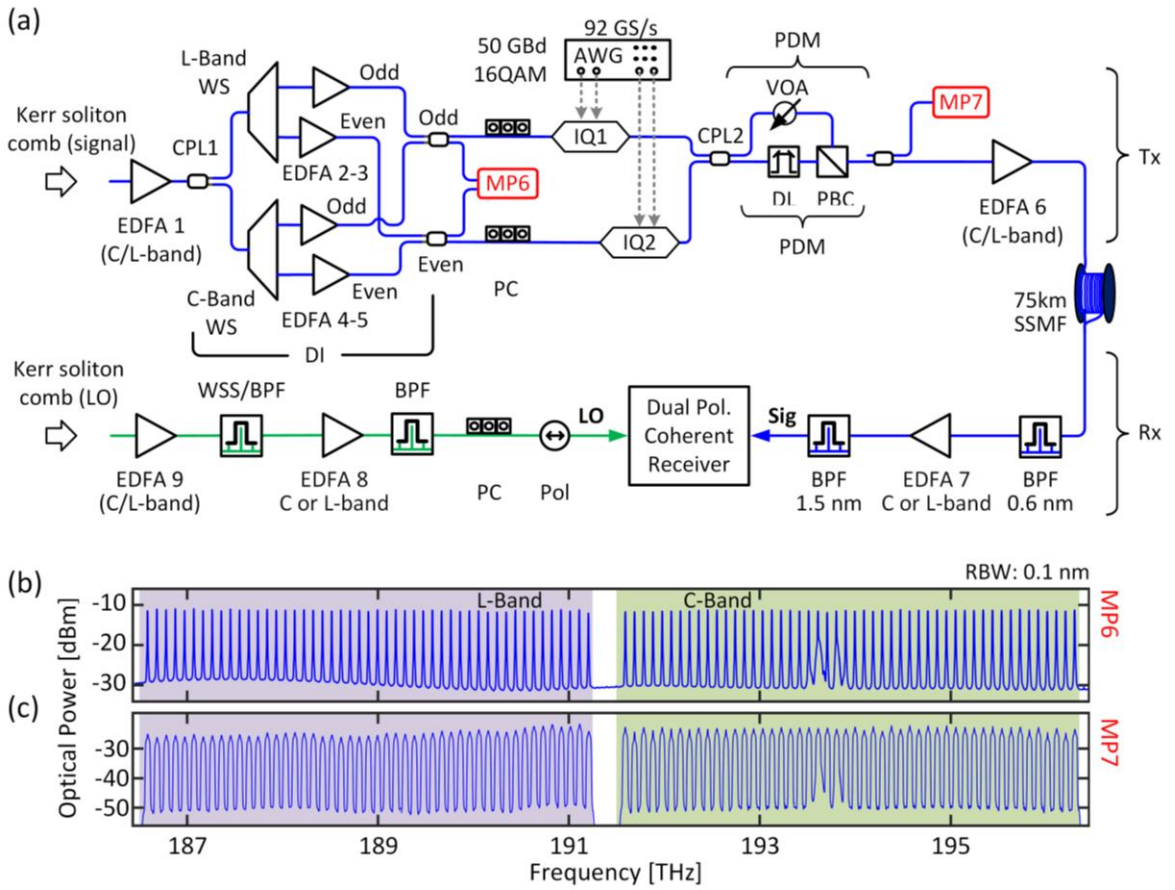

Figure C.5: All-soliton data transmission setup using a dissipative Kerr-soliton (DKS) frequency comb as a multi-wavelength local oscillator for coherent detection. **(a)** Data transmission setup: Two independent DKS frequency comb generators provide both the carriers for WDM coherent data transmission (signal) and for parallel intradyne detection (LO). At the transmitter side (Tx), WDM is emulated by encoding independent data into neighboring carriers. To this end, the comb is divided into even and odd carriers by a de-interleaver (DI) stage. As in the previous experiments, the DI stage contains a directional coupler (CPL1) that divides the optical power into two parts, which are fed to a C-band and an L-band programmable filter (WS) to select even and odd set of carriers within the respective band. Each set of carriers is amplified by an additional EDFA to compensate for the optical losses caused by the de-interleaving. Next, the C- and L-band carriers from each set are recombined by a directional coupler and sent through two different optical IQ-modulators (IQ1, IQ2). Both modulators are driven by 16QAM drive signals generated by a high-speed arbitrary waveform generator (AWG) using pseudo-random bit sequences (PRBS) of length $2^{11} - 1$. The symbol rate amounts to 50 GBd, and we use raised-cosine pulse shaping with a roll-off factor $\beta = 0.1$. After combining the signals by a directional coupler (CPL2), polarization division multiplexing (PDM) is emulated by splitting the data stream into two paths and recombining them on orthogonal polarizations with a decorrelating delay in one path and an attenuator in the other for maintaining the same power levels. (Caption continued on next page)

Figure C.5 continued: The PDM signal is amplified and transmitted through a 75 km long standard single mode fiber (SSMF). At the receiver side (Rx), the LO tones and the transmitted channels are filtered and amplified before being coupled to a dual-polarization coherent receiver which performs digital signal processing (DSP) to decode the data and to determine the BER. A polarization controller (PC) and polarizer are used to adjust the LO-line to the pre-defined input polarization of the coherent receiver. The spectra recorded at monitor ports (MP) 6 and 7 are shown in panels b and c. **(b)** Spectrum of the combined odd and even carriers prior to modulation. The flat spectrum is achieved by adjusting the WS to compensate for the power differences of the frequency comb carriers and the spectral variations of the EDFA gain profiles. **(c)** Spectrum of the data channels prior to fiber transmission. The spectrum was taken in eight segments with individually optimized bias points of the modulators to compensate for the wavelength dependence of the devices.

As in the previous experiments, WDM transmission is emulated by encoding independent data streams on adjacent channels, see Figure C.2a. To this end, the transmitter frequency comb (signal) is de-interleaved into even and odd carriers using two programmable filters (WS) for the C band and the L band. After amplifying the respective carriers by EDFA 2-5 operated at 24 dBm of output power, the C-band and L-band portions of the odd (even) carriers are combined by directional couplers and sent through optical IQ-modulators IQ1 (IQ2). Note that the C/L MUX of the de-interleaver (DI) stage from Figure C.2a has been replaced by a directional coupler to avoid the power attenuation of the carriers at the low-frequency edge of the C-band, which was described in Section C.3. The WS are also used to compensate the power differences of the carriers and the spectral variations of the EDFA gain profile, thereby producing an overall flat spectrum at the input of IQ1 and IQ2, which is to be seen in Figure C.5b, measured at monitor port MP6. The modulators are driven by 16QAM drive signals generated by a high-speed arbitrary waveform generator (AWG, Keysight M8196A) using pseudo-random bit sequences (PRBS) of length 2^{11}–1. We use a symbol rate of 50 GBd with raised-cosine pulse shaping at a roll-off factor of $\beta = 0.1$. The larger analog bandwidth of this AWG (32 GHz) allowed us to use higher symbol rates as compared to the experiments described in Section C.3. Polarization-division multiplexing (PDM) is again emulated by temporally delaying one of the polarizations using a delay line (DL) and combining on orthogonal polarizations in a polarization beam

combiner (PBC). The signal spectrum is shown in Figure C.5c, measured at monitor port MP7. The WDM data stream is amplified and transmitted over 75 km of standard single-mode fiber (SSMF). At the receiver (Rx), each transmitted channel is selected individually by an optical tunable band-pass filter (BPF), followed by an EDFA (EDFA 7) and a second BPF to suppress ASE noise. The selected channel is then sent to a dual-polarization coherent receiver which, in contrast to the data transmission experiment described in Section C.3, uses a spectral line from the Kerr soliton comb at the receiver side as a local oscillator (LO). The portion of the setup that is related to generation and selection of the LO carrier is depicted in green in Figure C.5a. For detection of channels in the C-band, a wavelength-selective switch (WSS) is used to select the LO tone. For the L-band, the WSS could not be used for selecting LO tones due to its limited optical bandwidth, and we deploy a BPF instead. The selected LO tone is then amplified by EDFA 8, filtered by a second BPF to suppress the ASE from the EDFA, and fed to the dual-polarization coherent receiver which consists of an optical modulation analyzer (OMA, Keysight N4391A) together with two real-time oscilloscopes (Keysight DSO-X 93204A 80 GSa/s). The detected signal undergoes a number of digital post processing stages comprising digital low-pass filtering, polarization demultiplexing, chromatic dispersion compensation, frequency offset estimation, carrier phase estimation and adaptive equalization. The block length for performing signal processing is chosen to be 1024 symbols, which is optimized to track the varying physical quantities of the received signal, such as carrier phase and polarization. The measured BER (averaged from different recordings with a length of 10^6 bit) for all transmitted channels is given in Figure 6.3d of the main paper.

C.6 Power consumption analysis of DKS-based sources for highly scalable data transmission

In this section, we investigate the electrical power consumption of DKS-based frequency comb sources and compare our results with state-of-the-art integrated tunable laser assemblies (ITLA). In the proof-of-concept experiments presented in the main paper, the comb generator relies on general-purpose benchtop-type

research equipment, for which the sum of all power ratings is approximately 1.3 kW. This number is of course not representative for an industrial implementation of the comb source in a real communication system, where components can be chosen to exactly match the specific requirements of the comb generation scheme. For a meaningful analysis of the power consumption, we hence consider dedicated components that correspond to the commercially available state of the art, and combine them with specifically designed Si_3N_4 microresonators which are optimized to achieve maximum power of the outermost comb lines that are still within the C- and L-band. This leads to an improved optical signal-to-noise power ratio (OSNR) after amplification and modulation of the generated comb carriers. We conclude Section C.6 with the investigation and the comparison of the achievable OSNR for both DKS- and ITLA-based sources of carriers for WDM data transmission.

C.6.1 Electrical power consumption comparison between DKS-based comb sources and array of ITLA

Our experiments described in the previous sections and in the main paper demonstrate that chip-scale DKS comb generators are well suited for massively parallel coherent WDM transmission, both as a multi-wavelength source at the transmitter and as multi-wavelength LO at the receiver. In particular, the concept allows the generation of hundreds of inherently equidistant highly stable optical tones, thereby eliminating the need for individual wavelength control of each carrier. In addition, DKS can dramatically reduce electrical power consumption as compared to a bank of individual laser modules despite the rather low power conversion efficiency of the nonlinear comb generation process. In the following section, we investigate the power consumption of different DKS comb generation schemes with resonators of different *Q*-factors in combination with either off-the-shelf optical amplifiers or tailored optical amplifiers that feature optimized power consumption. As a model system, we choose a comb source that can generate 114 discrete tones with a spacing of 100 GHz corresponding to the full number of ITU-channels in the C band (1530 nm to 1565 nm) and the L band (1565 nm to 1625 nm) [229]. We design the coupling and the dispersion of the microresonator to find an optimum trade-

off between high comb power and large bandwidth. It turns out that DKS comb sources have the potential to reduce the power consumption by up to an order of magnitude in comparison to an array of state-of-the-art integrated tunable laser assemblies (ITLA).

In our analysis, we investigate the electrical power consumption, P_{el}, of three different implementations of DKS comb generators (DKS-1, DKS-2, DKS-3) and compare it to the power consumption of an array of state-of-the-art ITLA, see Table C.1. DKS-1, DKS-2, and DKS-3 are based on a power-optimized scheme depicted in Figure C.6. The scheme is designed to feature low electrical power consumption while providing an optical output power per carrier of 13 dBm, which is comparable to the power levels provided by high-quality ITLA sources [230]. The DKS comb generator comprises a Si_3N_4-based microresonator chip, which is driven by a CW laser and a subsequent pump amplifier [231], [232]. The wavelength of the pump laser is adjusted by a controller [233], and the temperature of operation of the microresonator is kept stable with the use of a thermoelectric controller (TEC) [234]. For DKS-1, we assume a microresonator that has the same characteristics, with respect to *Q*-factor and dispersion, as the devices used in our experiments and is pumped at the same power level. The frequency comb output from the microresonator is next split into C and L bands and amplified by the first comb amplifiers [232] (AMP 1 and 2). Tailored gain-equalizing filters are used to correct the power variations between the amplified carriers, leading to a flat spectrum. These filters can be realized, e.g., by concatenating fiber Bragg gratings with different periodicities [235] or by using an acousto-optic tunable filter with multi-frequency acoustic signals generated by a single transducer [236]. To obtain the target power level of 13 dBm/carrier, high-power optical amplifiers (AMP 3 and 4) are used before separating the carriers by a wavelength demultiplexer (DEMUX) for independent modulation. The DEMUX [237] features a channel spacing of 100 GHz and supports 44 channels in the C-band and 70 channels in the L-band.

Table C.1: Electrical power required for the generation of 114 carriers on the C and L bands having an optical power of approximately 13 dBm per carrier. DKS-based configurations are shown in columns 2-4, and the associated comb generation scheme is depicted in Figure C.6a. DKS-1: off-the-shelf equipment; DKS-2: Off-the-shelf equipment and optimized microresonators; DKS-3: Tailored amplifiers with optimized power consumption and optimized microresonators. The last column considers the use of 108 ITLA as source of WDM carriers. For each configuration, the last two rows show the minimum and maximum $OCNR_{ref}$ ($OSNR_{ref}$) that occurs for any channel in the C- or L-band. $OCNR_{ref}$ refers to the optical carrier-to-noise power ratio at the output of the comb generator, i.e., after the DEMUX depicted in Figure C.6. $OSNR_{ref}$ refers to the optical signal-to-noise power ratio measured after modulation, recombination and re-amplification of the WDM channels, i.e., after AMP 5 and AMP 6 in Figure C.9. Both parameters are measured for a reference bandwidth of 0.1 nm.

	DKS-1 P_{el} (W)	DKS-2 P_{el} (W)	DKS-3 P_{el} (W)	ITLA P_{el} (W)
Laser [230]	3.8	3.8	3.8	114×3.8
Controller [233]	1.0	1.0	1.0	-
Pump amp. [231], [232]	38.0	12.0	3.5	-
TEC [234][19]	0.6	0.6	0.6	-
AMP 1 & AMP 2 [232]	3.0 + 3.0	3.0 + 3.0	0.5 + 0.5	-
AMP 3 & AMP 4 [231]	25 + 38	25 + 38	12 + 20	-
Total P_{el} (W)	112.4	86.4	41.9	433.2
Max/Min $OCNR_{ref}$ (dB)	39.0/35.0	39.0/35.0	39.0/35.0	55
Max/Min $OSNR_{ref}$ (dB)	38.3/34.6	38.3/34.6	38.3/34.6	46.9/45.8

For the DKS-1 scheme, we assume a microresonator with the same *Q*-factor and under the same operation conditions as the LO comb of the transmission experiment depicted in Figure 6.3 of the main paper. For estimating the $OCNR_{ref}$ and $OSNR_{ref}$ values, we use a comb spectral shape that mirrors the one measured during our experiment. To estimate the electrical power dissipation P_{el} associated with DKS-1, we assume state-of-the-art off-the-shelf amplifiers that match the requirements of gain and optical output power while featuring low electrical power consumption, see the corresponding references in first column of Table C.1. This leads to a total power consumption of approximately 110 W

for generation of 114 carriers – less than one third of the power consumption obtained for 114 independent ITLA.

For the DKS-2 and DKS-3 scheme, we assume Si_3N_4 microresonators having intrinsic *Q*-factors of 6×10^6 with dispersion and coupling parameters that were optimized for maximizing the power of the outermost comb lines that are still within the C- and L-band, see Section 5.2 and Refs. [214], [238], [239] for details. The assumption of a *Q*-factor of 6×10^6 is based on recent reports about Si_3N_4 microresonators resonators, where optimized fabrication processes have led to *Q*-factors even exceeding 6×10^6, both in devices with normal [213] and anomalous [214] GVD. While DKS-2 is still based on state-of-the-art off-the-shelf amplifiers, DKS-3 assumes tailored optical amplifiers that have the highest electrical-to-optical power conversion efficiency [240]. This results in DKS-3 having a total power consumption of approximately 42 W for generation of 114 carriers – more than an order of magnitude below the power consumption of the considered ITLA array.

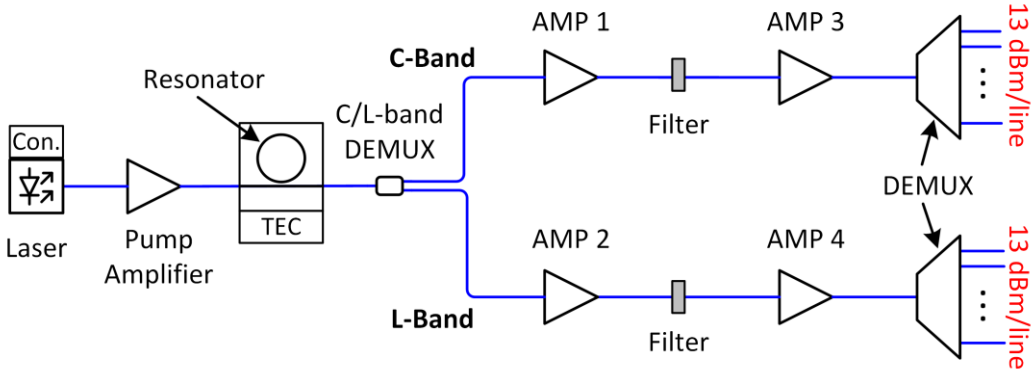

Figure C.6: Power-optimized setup for DKS frequency comb generation and amplification for data transmission. A tunable CW laser followed by a pump amplifier are used to drive the microresonator. The operation temperature of the microresonator is kept stable by a TEC. After separating the C and L band tones by a C/L-band DEMUX, the tones of each band are amplified by the comb amplifiers AMP 1 and 2. Optical filters compensate the spectral power variations among the carriers of the frequency comb in each band. High-power optical amplifiers AMP 3 and 4 are used before the wavelength demultiplexer (DEMUX) to obtain the target power level of ~ 13dBm per carrier

Naturally, the amplifiers used to boost the optical power of the comb lines reduce the optical carrier-to-noise power ratio (OCNR) with respect to the carriers from an ITLA, which do not need to be amplified prior to modulation. This reduction of the OCNR was investigated analytically, as discussed in Section C.6.3, and the results were verified by simulations using the commercial tool OptSim [115]. The last two rows of Table C.1 give the results of the investigation. The Max/Min $OCNR_{ref}$ values of Table C.1 correspond to the maximum and minimum values of the OCNR for the DKS frequency comb carriers and for the ITLA carriers within the C- and L-band prior to modulation, measured at a reference bandwidth of 0.1 nm. For the DKS frequency comb carriers, $OCNR_{ref}$ was measured at the output of the DEMUX, see Figure C.6, whereas it was taken from the datasheet of a commercial device for the case of the ITLA carriers [230]. Using DKS sources leads to optical carriers with $OCNR_{ref}$ values that range from 35.0 dB to 38.5 dB. The difference between the maximum and the minimum $OCNR_{ref}$ values is due to the difference in power between the comb carriers over the whole C and L band and due to the difference in noise figure between the C and L band amplifiers. The Max/Min $OSNR_{ref}$ values of Table C.1 give the maximum and minimum values of the OSNR, measured at a reference bandwidth of 0.1 nm, for the DKS frequency comb and ITLA tones after modulation, multiplexing and re-amplification, prior to transmission through the single-mode fiber. Due to the amplified spontaneous emission (ASE) noise added during re-amplification of the DKS-based channels, the $OSNR_{ref}$ of the DKS comb generator and the ITLA differ much less than the associated $OCNR_{ref}$. Furthermore, the DKS-based channels exhibit $OSNR_{ref}$ values above 34.5 dB, which would correspond to theoretically achievable BER of less than 10^{-34} for 50 GBd 16QAM transmission assuming impairments only by additive white Gaussian noise, without inter-symbol interference [184]. This is a purely virtual value, much smaller than any BER relevant to real-world 16QAM systems which are deteriorated by noise and are typically operating at BER values of more than 10^{-6}. This analysis shows that DKS comb tones will not exhibit any practically relevant impairment of transmission performance in comparison to much more power hungry arrays of

individually stabilized ITLA. For details on the analytical OSNR calculation, refer to Section C.6.3.

It is further worth noting that DKS comb generators are particularly advantageous when large numbers of carriers are to be generated. Figure C.7 shows the dependence of the electrical power consumption per carrier on the total number of carriers for the implemented three DKS comb generation configurations. The power consumption per line for DKS comb sources decreases considerably with the number of lines. With only 20 lines, the DKS-3 scheme already exhibits a power consumption per line which is half of that required by ITLA sources. Note that Figure C.7 is based on the assumption that the amplifiers used for DKS frequency comb generation consume constant electrical power. This may lead to an overestimation of the power consumption since the electrical pump power of the EDFA can be reduced if only a few comb lines are to be utilized. Moreover, we did not consider that the design of the microresonator can be adapted for power-efficient generation of narrowband combs, see Section C.6.2 below. In addition, the power consumption per carrier when using an ITLA array is considered constant. This may not be the case if techniques to synchronize all optical sources, e.g. through frequency locking, are employed. Figure C.7 hence represents a rather conservative estimation of the performance that can be achieved with DKS comb sources.

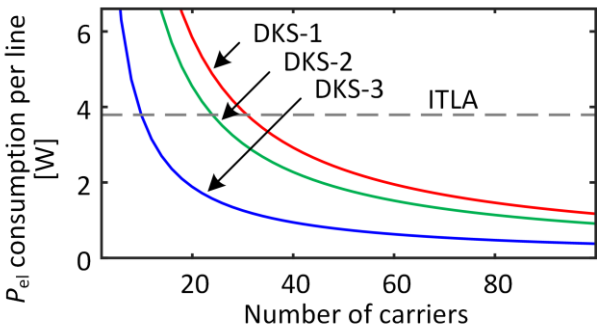

Figure C.7: Electrical power consumption per carrier as a function of the number of carriers. We compare the power consumption of the DKS comb generation schemes detailed in Table C.1 and Figure C.6 (DKS-1, DKS-2, DKS-3) to that of an array of integrated tunable laser assemblies (ITLA).

C.6.2 Optimization of dispersion and coupling parameters of Si_3N_4 microresonators

In this section, we explain the optimization of the microresonator carried out to maximize the achievable OSNR of a DKS frequency comb. For a given input power, such optimization is done by maximizing the optical power of the outermost lines of the C and L bands of the frequency comb, which have the lowest power and hence limit the achievable OSNR. It turns out that for a moderate input power of P_{in} = 400 mW or 26 dBm, which allows the use of a pump amplifier with low power consumption, we obtain OSNR_{ref} values higher than 35 dB, which are more than sufficient for real-world communication systems, see discussion in Section C.6.1. In addition, we investigate the power conversion efficiency of the DKS comb source, and the bandwidth of the frequency comb.

To maximize the power of the weakest lines at the edges of the C and L band, the group velocity dispersion (GVD) and the coupling rate of the microresonator to the external waveguide, κ_{ex}, are varied within values that can be engineered by varying the Si_3N_4 waveguide dimensions as well as the resonator-to-waveguide distance in combination with specially designed coupling regions [214], [238]. The analytical expression for the line power, in Watts, of the DKS frequency comb at the output of the microresonator, solved in the limit of low resonator loss, is given by [83]:

$$P(\mu) = \frac{\kappa_{\text{ex}} D_2 \hbar \omega_0}{4g} \operatorname{sech}^2\left(\frac{\kappa \mu}{2} \sqrt{\frac{D_2 \hbar \omega}{\kappa_{\text{ex}} g P_{\text{in}}}} \right), \tag{B.4}$$

where $\mu = (\omega - \omega_0)/D_1$ is the comb mode index relative to the pumped mode, $D_1/2\pi$ is the free spectral range, $D_2/2\pi$ is the per-resonance frequency shift due to GVD, $g/2\pi$ is the nonlinear coupling constant or Kerr frequency shift per photon, P_{in} is the input pump power, and $\kappa = \kappa_0 + \kappa_{\text{ex}}$ is the total cavity loss-rate including the internal loss rate, κ_0, and the coupling rate to the external waveguide, κ_{ex}. In our model, we set a realistic value of internal loss rate to $\kappa_0 = 2\pi \times 30$ MHz (which corresponds to the intrinsic $Q \sim 6 \times 10^6$) [214] and the nonlinear coefficient is assumed to amount to $g = 2\pi \times 0.27$ Hz. In addition,

we assume that the soliton operates at the maximum pump-cavity resonance detuning, which corresponds to the maximum output power and the broadest comb spectrum available for the given pump power [83], [219]. Note that Eq. (4) is based on the assumption of high resonator finesse [241] and is hence not valid any more as the loss of the resonator κ is increased to large values. For a comprehensive study over a broader range of values, we therefore perform simulations using the Lugiato-Lefever equation to retrieve the spectral envelope of the DKS frequency comb [194]. Figure C.8a shows the optical power of the weakest line within the C and L-band attained through these simulations when the dispersion parameter $D_2 / 2\pi$ and the ratio between the external coupling and the intrinsic loss κ_{ex} / κ_0 are varied from 0.2 to 2.0 MHz and from 1 to 25, respectively. We find that there exists an optimal value for κ and $D_2/2\pi$ where the weakest line of the frequency comb within the C and L band is maximized. We find that for $\kappa_{\mathrm{ex}}/2\pi = 525\,\mathrm{MHz}$ and $D_2/2\pi = 0.4\,\mathrm{MHz}$ the outermost line reaches a maximum power of 46 µW or -13.4 dB, which allows $\mathrm{OCNR_{ref}}$ values above 35 dB for the comb carriers obtained from DKS-2 and DKS-3 comb generation and amplification schemes. The power consumption, $\mathrm{OCNR_{ref}}$ and $\mathrm{OSNR_{ref}}$ values of Table C.1, for DKS-2 and DKS-3 configurations, have been derived considering such optimized microresonators.

Figure C.8b depicts the values of the ratio, in dB, between the power of the strongest and the weakest comb line within the C and L band. For the optimum values of κ_{ex} and $D_2/2\pi$ a ratio of 5 dB is obtained, which is comparable to the approximately 6 dB of power ratio observed in our measurements.

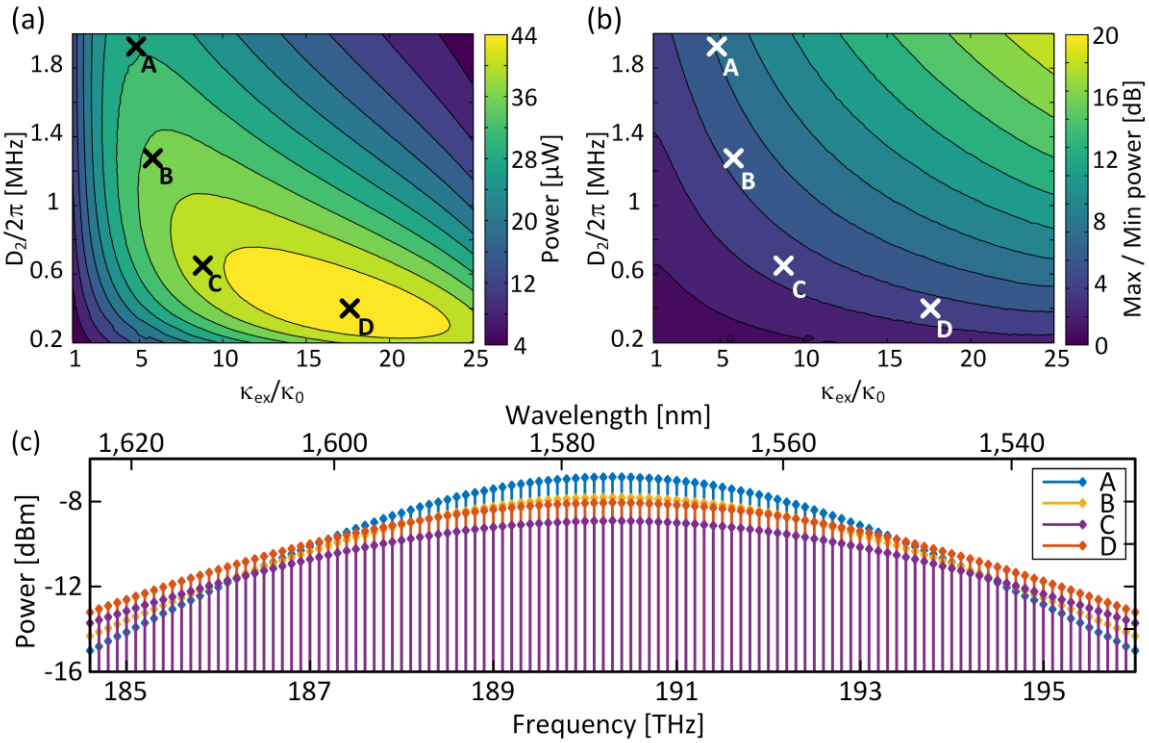

Figure C.8: Optimization of minimum comb line power by varying the cavity GVD parameter D_2 and the coupling rate κ_{ex}. **(a)** Heat map for minimum comb line power as a function of D_2 and κ_{ex} The crosses mark the comb spectra depicted in c. with 'D' indicating the ideal point where a global maximum of the power of the weakest comb line within the C and L bands is achieved. **(b)** Map of the comb line power variation as maximum/minimum comb power in dB as a function of D_2 and κ_{ex}, with the same highlighted points as in a. **(c)** Frequency comb spectrum corresponding to the data points A to D from panels a. and b. The plotted frequency range corresponds to C and L-band. Comb D exhibits an optimal balance between a high total output power as well as the broadest bandwidth, allowing for an increased OCNR and OSNR per carrier.

Figure C.8c contains four comb spectra taken from the points marked as crosses on Figure C.8a,b. The interplay between spectral broadening and overall power increase is well demonstrated. In general, decreasing the dispersion D_2 tends to increase the bandwidth while reducing the total comb power. Conversely, increasing the resonator coupling κ_{ex} leads to an increase in total comb power but a reduction in the soliton bandwidth. This is due to more light escaping the cavity, and consequently reducing the conversion efficiency from the pump to the comb lines. Hence, for a given value of dispersion D_2 there exists an optimum value of κ_{ex} that maximizes the power of the weakest line at the edge

of the C and L-band. In Figure C.8a, these values are indicated by points A to D for four values of D_2. Point D corresponds to the overall maximum that can be achieved by optimization of both parameters.

In addition, we have analyzed the power conversion efficiency, Γ, of the DKS comb sources for the same range of values for κ_{ex} and $D_2/2\pi$. The general expression can be calculated as [84], [242]

$$\Gamma = \frac{P_{out}^{sol}}{P_{in}} = \frac{\pi\kappa_{ex}}{\kappa}\sqrt{\frac{\kappa_{ex} D_2 \hbar\omega_0}{g P_{in}}}\ , \tag{B.5}$$

where P_{out}^{sol} is the total soliton power exiting the microresonator. For the optimum values κ_{ex} and $D_2/2\pi$, the power conversion efficiency amounts to 2.5 %, greatly improving the maximum value of 0.6 % observed in the experimental setup.

C.6.3 Achievable OSNR per carrier for DKS- and ITLA-based WDM sources

The $OCNR_{ref}$ and $OSNR_{ref}$ values shown in Table C.1 have been obtained through an analytic study of the amplified stimulated emission (ASE) noise power generated after amplifying the initially low-noise frequency comb carriers using a chain of amplifiers. To verify the results of our analysis, the DKS frequency comb generation setup shown in Figure C.6 has also been simulated. In both the analytical calculations and simulations, the gain of the optical amplifiers is assumed to be constant across the bandwidth occupied by the frequency comb. This assumption can be justified by the amplifier specifications of different EDFA manufacturers which assure variations of gain to be lower than 1 dB [243]. ASE noise was quantified by the noise figure of the comb amplifiers. Optical amplifiers for the L band are assumed to feature a 1 dB higher noise figure with respect to their counterparts in the C band [243], [244]. In our model, we consider a noise figure of 4 dB (5 dB) for the C band (L band) comb amplifier AMP 1 and a noise figure of 6 dB (7 dB) for the C band (L band) comb amplifier AMP 2, which are the maximum noise figure

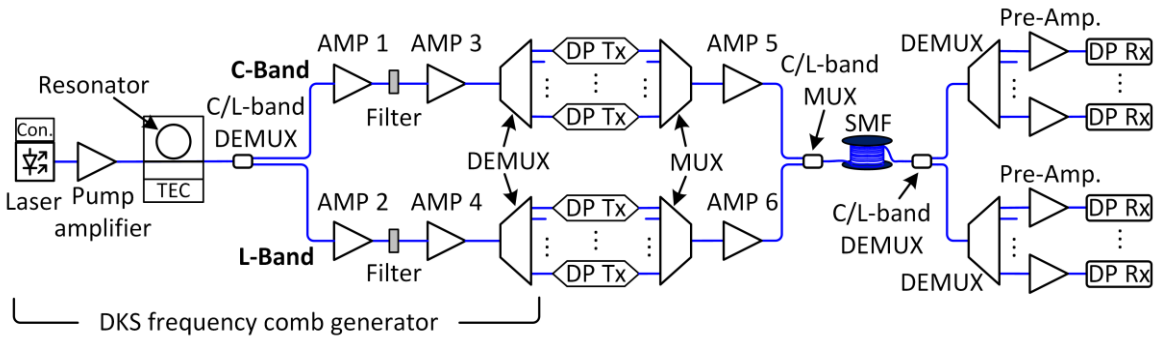

Figure C.9: Communication setup assumed for estimating the OSNR levels that can be achieved with the various DKS-based comb generation schemes discussed in Table C.1. The DKS frequency comb generator is described in more detail in Figure C.6. The carriers are modulated by dual polarization coherent transmitters (DP Tx). The C- and L-band signals are re-amplified by separate booster amplifiers AMP 5 and AMP 6, combined by a C/L-band MUX, and transmitted through 75 km of single-mode fiber (SMF). At the receiver, the channels are demultiplexed and sent through a pre-amplifier before detection by a dual-polarization coherent receiver (DP Rx).

values specified for the corresponding amplifiers and should hence lead to a conservative estimate of the OSNR. The noise figure of the amplifiers is also assumed to be flat within the bandwidth occupied by the frequency comb. Moreover, insertion loss values of all the passive components were also taken into account. The C/L-band DEMUX feature a 0.5 dB insertion loss, the gain-equalizing filters, which compensate for the power difference between comb carriers, present an insertion loss of approximately 5 dB in addition to the wavelength-dependent attenuation profile required for gain flattening [245], and the wavelength DEMUX is considered to have 3 dB insertion loss [237]. For the calculation of the $OSNR_{ref}$ obtained after modulation and re-amplification by booster amplifiers AMP 5 and 6 and prior to transmission through the single-mode fiber, we further need to quantify the optical losses associated with modulating data signals onto the carriers and with recombining these carriers into the transmission fiber, see Figure C.9. To this end, we assume state-of-the-art dual-polarization IQ modulators with 13 dB of insertion loss for each polarization [44], [246] along with a modulation loss of 2.55 dB, corresponding to the peak-to-average symbol power ratio of 16QAM signals [247]. To recombine the channels into the single-mode transmission fiber, an optical

multiplexer (MUX) and a C/L-band MUX with 3 dB and 0.5 dB of insertion loss, respectively, are considered. For re-amplification of the modulated signal by AMP 5 (6), we assume an amplifier with a noise figure of 5.5 dB (6.5 dB) for the C (L) band. The output power is set such that the power per channel is 0 dBm, which is the typical launch power per channel into standard single mode fibers (SSMF) to reduce the nonlinear impairments while optimizing the channel OSNR [41], [42].

Note that the comb amplifiers AMP 1 … AMP 4 in Figure C.9 are deliberately placed between the comb generator and the respective DEMUX. In fully integrated schemes, it would be desirable to avoid amplifiers before the modulators. However, due to the low comb line powers directly after the resonator and the generally high insertion loss of the IQ modulators, such schemes would lead to low power levels at the input of the transmitter booster amplifiers AMP 5 and AMP 6 and the $OSNR_{ref}$ of the transmitted signal would drop to values below 23 dB. For this reason, placing of an EDFA prior to modulation is a common approach in most comb-based transmission schemes [13].

Figure C.10 shows the spectrum obtained from our simulation using the commercial tool OptSim [115]. The spectrum exhibits a maximum $OCNR_{ref}$ of 39 dB for the leftmost comb line in the C-band and a minimum $OCNR_{ref}$ of 35 dB for the leftmost comb line in the L-band. These values are in accordance with the $OCNR_{ref}$ values measured in our experiments, which amount to 35 … 39 dB for the single comb, and to 30 … 37 dB for the interleaved combs. In contrast to that, the experimentally measured $OSNR_{ref}$ values of the data signal typically amount to 20 … 24 dB (23 … 27 dB) for the case of the interleaved-comb (single-comb) experiment. This is significantly below the values of more 34 dB that can be expected when using optimized equipment, see Table C.1. The low $OSNR_{ref}$ in the experiment is caused by a rather high insertion loss of the electro-optic modulators that we used in our experiment, which lead to low power levels coupled into the subsequent EDFA (EDFA 6 in Figure C.2).

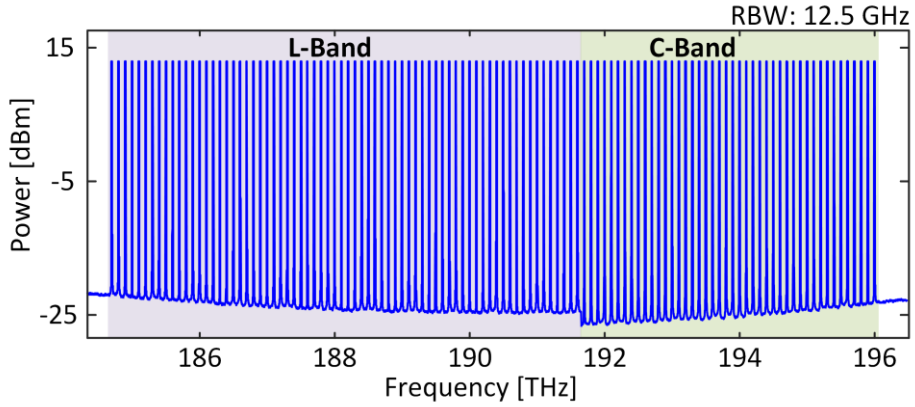

Figure C.10: Merged plot of the amplified frequency comb spectra, at the output of amplifiers AMP 3 and AMP 4, in Figure C.9, after accounting for the subsequent DEMUX insertion loss. The spectra are obtained from our simulation using the commercial tool OptSim [115]. RBW: resolution bandwidth.

The simulations are confirmed by an analytical estimation. To this end, we start from the input signal power P_0 to comb amplifiers AMP 1 & AMP 2 and derive the OSNR from the noise figure of the system. For an output signal power P_s and ASE noise power P_{ASE}, the OSNR is given by the equation:

$$\mathrm{OSNR} = \frac{P_s}{P_{ASE}} \tag{B.6}$$

with P_s and P_{ASE} given by [248]

$$P_s = G P_0 \ , \tag{B.7}$$

$$P_{ASE} = h\nu B_{ref} F(G-1) \ , \tag{B.8}$$

where G is the EDFA gain, h is the Planck constant, ν is the input signal's center frequency, B_{ref} is the noise reference bandwidth (centered at ν) and F is the noise figure of the EDFA. For a chain of amplifiers connected by passive components with power transmission factor g, $0 < g \leq 1$, the total gain G_t and the noise figure F_t of the system are given by

$$G_t = \prod_{n=1}^{N} G_n g_n \tag{B.9}$$

$$F_{\mathrm{t}} = \frac{1}{G_{\mathrm{t}}} + \left(F_1 + \frac{F_2}{G_1 g_1} + \frac{F_3}{G_1 g_1 G_2 g_2} + \ldots + \frac{F_n}{\prod_{n=1}^{N-1} G_n g_n} \right). \qquad \text{(B.10)}$$

Using Eqs. (B.6) to (B.10), the maximum and minimum $\mathrm{OCNR_{ref}}$ and $\mathrm{OSNR_{ref}}$ values of the DKS frequency comb generation and amplification configurations given in Table C.1 are calculated analytically. These values are also found to be in accordance with the simulations results. Note that the DKS frequency comb generation setup assumed in Table C.1 already contains the booster EDFA (AMP 5 and AMP 6 in Figure C.9) after the modulator. For transmission over a distance of 75 km, the $\mathrm{OSNR_{ref}}$ measured after a state-of-the-art preamplifier [249] (Pre-Amp. In Figure C.9) would be 2 dB below the $\mathrm{OSNR_{ref}}$ values at the transmitter that are specified in Table C.1.

In addition to the ASE noise introduced by the various amplifiers, nonlinear interference noise will also influence the OSNR at the receiver. For a quantitative analysis, we consider the 50 GBd PDM-16QAM transmission experiment in which we use a DKS comb generator as a source of LO tones, see Figure 6.3 of the main paper. We assume typical parameters for the transmission fiber such as a nonlinearity coefficient of $\gamma = 2\ \mathrm{W^{-1}km^{-1}}$, a dispersion coefficient of $\beta_2 = 20\ \mathrm{ps^2/km}$, and a fiber loss coefficient of $g = 0.2$ dB/km. The average input power to the transmission fiber was assumed to be 0 dBm per channel, which matches our laboratory experiment. For the estimation, we use the model described in Ref. [250]. After the first 75 km transmission link, we estimate an effective $\mathrm{OSNR_{NL}}$ of approximately 32.5 dB, which would correspond to an $\mathrm{OSNR_{ref,NL}}$ of 38.5 dB, taking into account nonlinear interference noise from self-phase modulation, cross-phase modulation, and four-wave maxing, but no ASE noise from any EDFA deployed in the system. After an additional 75 km link, the $\mathrm{OSNR_{NL}}$ ($\mathrm{OSNR_{ref,NL}}$) reduces to 29 dB (35 dB). These $\mathrm{OSNR_{ref}}$ numbers are comparable to the values estimated at the output of the transmitter when taking into account only the ASE noise of the various EDFA, but no fiber nonlinearities. We hence conclude that in optimized systems, fiber nonlinearities may have significant impact even for transmission over rather short distances that are typically found in metro and regional networks. These impairments can be compensated by exploiting the strong correlation of

frequency variations of the comb carriers [8] – another key advantage of comb-based transmission schemes, leading to better signal quality and allowing higher capacity and reach. Note that the $OSNR_{ref,NL}$ values estimated for nonlinear impairments are much higher than the $OSNR_{ref}$ of approximately 23 dB that we actually measured in our current experiment. We hence conclude that nonlinearities of the transmission fiber did not significantly impact signal quality of our experiment.

[*End of Methods and Supplementary Information of paper [J4]*]

D. Bibliography

[1] Cisco, “Cisco Visual Networking Index: Forecast and Trends, 2017-2022, (White Paper),” 2019.

[2] A. G. Bell and S. Tainter, “Photo Phone-Transmitter,” US Patent 235,496, 1880.

[3] C. K. Kao, “Nobel Lecture: Sand from Centuries Past: Send Future Voices Fast,” *Rev. Mod. Phys.*, vol. 82, no. 3, pp. 2299–2303, Aug. 2010.

[4] H. Adams, “Optical DCI Market Grew 26 Percent, Reaching $2.6 Billion in 2017,” *Market Insight*, 2018. [Online]. Available: https://technology.informa.com/601447/optical-dci-market-grew-26-percent-reaching-26-billion-in-2017. [Accessed: 20-May-2020].

[5] B. J. Puttnam *et al.*, “2.15 Pb/s Transmission Using a 22 Core Homogeneous Single-Mode Multi-Core Fiber and Wideband Optical Comb,” in *European Conference on Optical Communication*, (ECOC, 2015), pp. 1–3.

[6] N. K. Fontaine *et al.*, “228-GHz Coherent Receiver Using Digital Optical Bandwidth Interleaving and Reception of 214-GBd (856-Gb/s) PDM-QPSK,” in *European Conference and Exhibition on Optical Communication*, (OSA, 2012), paper. Th.3.A.1.

[7] L. Lundberg *et al.*, “Frequency Comb-Based WDM Transmission Systems Enabling Joint Signal Processing,” *Appl. Sci.*, vol. 8, no. 5, pp. 718–749, May 2018.

[8] E. Temprana *et al.*, “Overcoming Kerr-Induced Capacity Limit in Optical Fiber Transmission,” *Science*, vol. 348, no. 6242, pp. 1445–1448, June 2015.

[9] V. Vujicic *et al.*, “Tbit/s Optical Interconnects Based on Low Linewidth Quantum-Dash Lasers and Coherent Detection,” in *Conference on Lasers and Electro-Optics*, (OSA, 2016), paper SF2F.4.

[10] P. Marin-Palomo *et al.*, “Comb-Based WDM Transmission at 10 Tbit/s Using a DC-Driven Quantum-Dash Mode-Locked Laser Diode,” *Opt. Express*, vol. 27, no. 22, pp. 31110–31129, Oct. 2019.

[11] J. Pfeifle *et al.*, “Coherent Terabit Communications with Microresonator

Kerr Frequency Combs.," *Nat. Photonics*, vol. 8, no. 5, pp. 375–380, 2014.

[12] J. Lin, H. Sepehrian, Y. Xu, L. A. Rusch, and W. Shi, "Frequency Comb Generation Using a CMOS Compatible SiP DD-MZM for Flexible Networks," *IEEE Photonics Technol. Lett.*, vol. 30, no. 17, pp. 1495–1498, Sep. 2018.

[13] H. Hu *et al.*, "Single-Source Chip-Based Frequency Comb Enabling Extreme Parallel Data Transmission," *Nat. Photonics*, vol. 12, no. 8, pp. 469–473, 2018.

[14] A. Fülöp *et al.*, "Long-Haul Coherent Communications Using Microresonator-Based Frequency Combs," *Opt. Express*, vol. 25, no. 22, p. 26678, Oct. 2017.

[15] A. Fülöp *et al.*, "High-Order Coherent Communications Using Mode-Locked Dark-Pulse Kerr Combs from Microresonators," *Nat. Commun.*, vol. 9, no. 1, p. 1598, Dec. 2018.

[16] J. Pfeifle *et al.*, "Flexible Terabit/s Nyquist-WDM Super-Channels Using a Gain-Switched Comb Source," *Opt Express*, vol. 23, no. 2, pp. 724–738, 2015.

[17] T. Shao, R. Zhou, V. Vujicic, M. D. Gutierrez Pascual, P. M. Anandarajah, and L. P. Barry, "100 km Coherent Nyquist Ultradense Wavelength Division Multiplexed Passive Optical Network Using a Tunable Gain-Switched Comb Source," *J. Opt. Commun. Netw.*, vol. 8, no. 2, pp. 112–117, 2016.

[18] C. Weimann *et al.*, "Silicon-Organic Hybrid (SOH) Frequency Comb Sources for Terabit/s Data Transmission," *Opt. Express*, vol. 22, no. 3, pp. 3629–3637, 2014.

[19] P. J. Winzer, "High-Spectral-Efficiency Optical Modulation Formats," *J. Lightw. Technol.*, vol. 30, no. 24, pp. 3824–3835, Dec. 2012.

[20] E. Agrell *et al.*, "Roadmap of Optical Communications," *J. Opt.*, vol. 18, no. 6, p. 063002, June 2016.

[21] P. M. Anandarajah *et al.*, "Generation of Coherent Multicarrier Signals by Gain Switching of Discrete Mode Lasers," *IEEE Photonics J.*, vol. 3, no. 1, pp. 112–122, 2011.

[22] F. Lelarge *et al.*, "Recent Advances on InAs/InP Quantum Dash Based Semiconductor Basers and Optical Amplifiers Operating at 1.55 μm,"

IEEE J. Sel. Top. Quantum Electron., vol. 13, no. 1, pp. 111–124, 2007.

[23] P. Marin-Palomo, J. N. Kemal, T. J. Kippenberg, W. Freude, S. Randel, and C. Koos, "Performance of Chip-Scale Optical Frequency Comb Generators in Coherent WDM Communications," *Opt. Express*, vol. 28, no. 9, pp. 12897–12910, Apr. 2020.

[24] M. Chagnon, "Optical Communications for Short Reach," *J. Lightw. Technol.*, vol. 37, no. 8, pp. 1779–1797, Apr. 2019.

[25] S. J. Savory, "Digital Coherent Optical Receivers: Algorithms and Subsystems," *IEEE J. Sel. Top. Quantum Electron.*, vol. 16, no. 5, pp. 1164–1179, 2010.

[26] ITU-T, "G.694.2: Spectral Grids for WDM Applications: CWDM Wavelength Grid," 2003.

[27] ITU-T, "G.694.1: Spectral Grids for WDM Applications: DWDM Frequency Grid," 2012.

[28] M. Smit *et al.*, "An Introduction to InP-Based Generic Integration Technology," *Semicond. Sci. Technol.*, vol. 29, no. 8, p. 083001, June 2014.

[29] T. Komljenovic, D. Huang, P. Pintus, M. A. Tran, M. L. Davenport, and J. E. Bowers, "Photonic Integrated Circuits Using Heterogeneous Integration on Silicon," *Proc. IEEE*, vol. 106, no. 12, pp. 2246–2257, Dec. 2018.

[30] S. Wolf *et al.*, "DAC-Less Amplifier-Less Generation and Transmission of QAM Signals Using Sub-Volt Silicon-Organic Hybrid Modulators," *J. Lightw. Technol.*, vol. 33, no. 7, pp. 1425–1432, Apr. 2015.

[31] M. R. Billah *et al.*, "Hybrid Integration of Silicon Photonics Circuits and InP Lasers by Photonic Wire Bonding," *Optica*, vol. 5, no. 7, p. 876, July 2018.

[32] C. Kieninger *et al.*, "Ultra-High Electro-Optic Activity Demonstrated in a Silicon-Organic Hybrid Modulator," *Optica*, vol. 5, no. 6, p. 739, June 2018.

[33] M. Blaicher *et al.*, "Hybrid Multi-Chip Assembly of Optical Communication Engines by in Situ 3D Nano-Lithography," *Light Sci. Appl.*, vol. 9, no. 1, p. 71, Dec. 2020.

[34] R. Maher *et al.*, "Low Cost Comb Source in a Coherent Wavelength

Division Multiplexed System," in *36th European Conference and Exhibition on Optical Communication*, (OSA, 2010), pp. 1–3.

[35] L. Tao, J. Yu, and N. Chi, "Generation of Flat and Stable Multi-Carriers Based on Only Integrated IQ Modulator and Its Implementation for 112Gb/s PM-QPSK Transmitter," in *National Fiber Optic Engineers Conference*, (OSA, 2012), paper JW2A.86.

[36] D. O. Otuya, K. Kasai, M. Yoshida, T. Hirooka, and M. Nakazawa, "Single-Channel 192 Tbit/s, Pol-Mux-64 QAM Coherent Nyquist Pulse Transmission over 150 km with a Spectral Efficiency of 75 bit/s/Hz," *Opt. Express*, vol. 22, no. 20, p. 23776, Oct. 2014.

[37] K. Kikuchi, "Characterization of Semiconductor-Laser Phase Noise and Estimation of Bit-Error Rate Performance with Low-Speed Offline Digital Coherent Receivers," *Opt. Express*, vol. 20, no. 5, pp. 5291–5302, 2012.

[38] T. Pfau, S. Hoffmann, and R. Noe, "Hardware-Efficient Coherent Digital Receiver Concept with Feedforward Carrier Recovery for M-QAM Constellations," *J. Lightw. Technol.*, vol. 27, no. 8, pp. 989–999, Apr. 2009.

[39] G. P. Agrawal and N. K. Dutta, *Semiconductor Lasers*, 2nd ed. New York: Van Nostrand Reinhold, 1993.

[40] Y. Ben M'Sallem *et al.*, "Quantum-Dash Mode-Locked Laser as a Source for 56-Gb/s DQPSK Modulation in WDM Multicast Applications," *IEEE Photonics Technol. Lett.*, vol. 23, no. 7, pp. 453–455, Apr. 2011.

[41] P. S. Cho, V. S. Grigoryan, Y. A. Godin, A. Salamon, and Y. Achiam, "Transmission of 25-Gb/s RZ-DQPSK Signals with 25-GHz Channel Spacing over 1000 km of SMF-28 Fiber," *IEEE Photonics Technol. Lett.*, vol. 15, no. 3, pp. 473–475, Mar. 2003.

[42] G. Raybon, P. J. Winzer, and C. R. Doerr, "1-Tb/s (10 x 107 Gb/s) Electronically Multiplexed Optical Signal Generation and WDM Transmission," *J. Lightw. Technol.*, vol. 25, no. 1, pp. 233–238, Jan. 2007.

[43] Auxora, "CATV Module," 2018. [Online]. Available: http://www.auxora.com/product/info_2.aspx?itemid=171&lcid=45&ppid=7&pid=23. [Accessed: 07-Jan-2019].

[44] Fujitsu, "DP-QPSK 100G LN Modulator," 2014. [Online]. Available: http://www.fujitsu.com/downloads/JP/archive/imgjp/group/foc/services/

100gln/ln100gdpqpsk-e-141105.pdf. [Accessed: 07-Jan-2019].

[45] Y. Cai *et al.*, "FPGA Investigation on Error-Floor Performance of a Concatenated Staircase and Hamming Code for 400G-ZR Forward Error Correction," in *Optical Fiber Communication Conference Postdeadline Papers*, (OSA, 2018), paper Th4C.2.

[46] K. Gürs and R. Müller, "Breitband-Modulation durch Steuerung der Emission eines optischen Masers (Auskoppelmodulation)," *Appl. Phys. Lett.*, vol. 5, no. 3, pp. 179–181, July 1963.

[47] L. E. Hargrove, R. L. Fork, and M. A. Pollack, "Locking of He-Ne Laser Modes Induced by Synchronous Intracavity Modulation," *Appl. Phys. Lett.*, vol. 5, no. 1, pp. 4–5, July 1964.

[48] A. J. DeMaria, D. A. Stetser, and H. Heynau, "Self Mode-Locking Of Lasers With Saturable Absorbers," *Appl. Phys. Lett.*, vol. 8, no. 7, pp. 174–176, Apr. 1966.

[49] M. DiDomenico, "Small-Signal Analysis of Internal (Coupling-Type) Modulation of Lasers," *J. Appl. Phys.*, vol. 35, no. 10, pp. 2870–2876, Oct. 1964.

[50] M. Crowell, "Characteristics of Mode-Coupled Lasers," *IEEE J. Quantum Electron.*, vol. 1, no. 1, pp. 12–20, Apr. 1965.

[51] A. Yariv, "Internal Modulation in Multimode Laser Oscillators," *J. Appl. Phys.*, vol. 36, no. 2, pp. 388–391, Feb. 1965.

[52] D. E. Spence, P. N. Kean, and W. Sibbett, "60-fsec Pulse Generation from a Self-Mode-Locked Ti:Sapphire Laser," *Opt. Lett.*, vol. 16, no. 1, p. 42, Jan. 1991.

[53] C. Spielmann, P. F. Curley, T. Brabec, and F. Krausz, "Ultrabroadband Femtosecond Lasers," *IEEE J. Quantum Electron.*, vol. 30, no. 4, pp. 1100–1114, Apr. 1994.

[54] U. Keller, "Recent Developments in Compact Ultrafast Lasers," *Nature*, vol. 424, no. 6950, pp. 831–838, Aug. 2003.

[55] X. Huang, A. Stintz, H. Li, L. F. Lester, J. Cheng, and K. J. Malloy, "Passive Mode-Locking in 1.3 μm Two-Section InAs Quantum Dot Lasers," *Appl. Phys. Lett.*, vol. 78, no. 19, pp. 2825–2827, May 2001.

[56] Z. G. Lu, J. R. Liu, S. Raymond, P. J. Poole, P. J. Barrios, and D. Poitras, "312-fs Pulse Generation from a Passive C-Band InAs/InP Quantum Dot

Mode-Locked Laser," *Opt. Express*, vol. 16, no. 14, p. 10835, July 2008.

[57] A. Shen *et al.*, "Low Confinement Factor Quantum Dash (QD) Mode-Locked Fabry-Perot (FP) Laser Diode for Tunable Pulse Generation," in *Conference on Optical Fiber Communication/National Fiber Optic Engineers Conference*, (OSA, 2008), pp. 1–3.

[58] A. Akrout, A. Shen, A. Enard, G.-H. Duan, F. Lelarge, and A. Ramdane, "Low Phase Noise All-Optical Oscillator Using Quantum Dash Modelocked Laser," *Electron. Lett.*, vol. 46, no. 1, p. 73, 2010.

[59] K. Merghem *et al.*, "Pulse Generation at 346 GHz Using a Passively Mode Locked Quantum-Dash-Based Laser at 1.55 μm," *Appl. Phys. Lett.*, vol. 94, no. 2, p. 021107, Jan. 2009.

[60] P. Marin *et al.*, "8.32 Tbit/s Coherent Transmission Using a Quantum-Dash Mode-Locked Laser Diode," in *Conference on Lasers and Electro-Optics*, (OSA, 2016), paper STh1F.1.

[61] J. N. Kemal *et al.*, "WDM Transmission Using Quantum-Dash Mode-Locked Laser Diodes as Multi-Wavelength Source and Local Oscillator," in *Optical Fiber Communication Conference*, (OSA, 2017), paper Th3F.6.

[62] V. Torres-Company and A. M. Weiner, "Optical Frequency Comb Technology for Ultra-Broadband Radio-Frequency Photonics," *Laser Photon. Rev.*, vol. 8, no. 3, pp. 368–393, May 2014.

[63] T. Sakamoto, T. Kawanishi, and M. Izutsu, "Widely Wavelength-Tunable Ultra-Flat Frequency Comb Generation Using Conventional Dual-Drive Mach-Zehnder Modulator," *Electron. Lett.*, vol. 43, no. 19, p. 1039, 2007.

[64] C. Chen, C. Zhang, W. Zhang, W. Jin, and K. Qiu, "Scalable and Reconfigurable Generation of Flat Optical Comb for WDM-Based next-Generation Broadband Optical Access Networks," *Opt. Commun.*, vol. 321, pp. 16–22, June 2014.

[65] R. Wu, V. R. Supradeepa, C. M. Long, D. E. Leaird, and A. M. Weiner, "Generation of Very Flat Optical Frequency Combs from Continuous-Wave Lasers Using Cascaded Intensity and Phase Modulators Driven by Tailored Radio Frequency Waveforms," *Opt. Lett.*, vol. 35, no. 19, p. 3234, Oct. 2010.

[66] N. Dupuis *et al.*, "InP-Based Comb Generator for Optical OFDM," *J. Lightw. Technol.*, vol. 30, no. 4, pp. 466–472, Feb. 2012.

[67] T. Yamamoto, K. Hitomi, W. Kobayashi, and H. Yasaka, "Optical

Frequency Comb Block Generation by Using Semiconductor Mach–Zehnder Modulator," *IEEE Photonics Technol. Lett.*, vol. 25, no. 1, pp. 40–42, Jan. 2013.

[68] R. Slavik, S. G. Farwell, M. J. Wale, and D. J. Richardson, "Compact Optical Comb Generator Using InP Tunable Laser and Push-Pull Modulator," *IEEE Photonics Technol. Lett.*, vol. 27, no. 2, pp. 217–220, Jan. 2015.

[69] Y. Xu, J. Lin, R. Dubé-Demers, S. LaRochelle, L. Rusch, and W. Shi, "Integrated Flexible-Grid WDM Transmitter Using an Optical Frequency Comb in Microring Modulators," *Opt. Lett.*, vol. 43, no. 7, p. 1554, Apr. 2018.

[70] L. P. Barry, P. Anandarajah, and A. Kaszubowska, "Optical Pulse Generation at Frequencies up to 20 GHz Using External-Injection Seeding of a Gain-Switched Commercial Fabry-Perot Laser," *IEEE Photonics Technol. Lett.*, vol. 13, no. 9, pp. 1014–1016, Sep. 2001.

[71] X. Jin and S. L. Chuang, "Relative Intensity Noise Characteristics of Injection-Locked Semiconductor Lasers," *Appl. Phys. Lett.*, vol. 77, no. 9, pp. 1250–1252, Aug. 2000.

[72] R. Zhou, S. Latkowski, J. O'Carroll, R. Phelan, L. P. Barry, and P. Anandarajah, "40nm Wavelength Tunable Gain-Switched Optical Comb Source," *Opt. Express*, vol. 19, no. 26, p. B415, Dec. 2011.

[73] M. D. G. Pascual, V. Vujicic, J. Braddell, F. Smyth, P. Anandarajah, and L. Barry, "Photonic Integrated Gain Switched Optical Frequency Comb for Spectrally Efficient Optical Transmission Systems," *IEEE Photonics J.*, vol. 9, no. 3, pp. 1–8, June 2017.

[74] V. Ataie *et al.*, "Ultrahigh Count Coherent WDM Channels Transmission Using Optical Parametric Comb-Based Frequency Synthesizer," *J. Lightw. Technol.*, vol. 33, no. 3, pp. 694–699, Feb. 2015.

[75] D. Hillerkuss *et al.*, "Single-Laser 32.5 Tbit/s Nyquist WDM Transmission," *J. Opt. Commun. Netw.*, vol. 4, no. 10, pp. 715–723, Oct. 2012.

[76] B. Kuyken, X. Liu, R. M. Osgood Jr., R. Baets, G. Roelkens, and W. M. J. Green, "Mid-Infrared to Telecom-Band Supercontinuum Generation in Highly Nonlinear Silicon-on-Insulator Wire Waveguides," *Opt. Express*, vol. 19, no. 21, p. 20172, Oct. 2011.

[77] R. Halir, Y. Okawachi, J. S. Levy, M. A. Foster, M. Lipson, and A. L. Gaeta, "Ultrabroadband Supercontinuum Generation in a CMOS-Compatible Platform," *Opt. Lett.*, vol. 37, no. 10, p. 1685, May 2012.

[78] P. Del'Haye, A. Schliesser, O. Arcizet, T. Wilken, R. Holzwarth, and T. J. Kippenberg, "Optical Frequency Comb Generation from a Monolithic Microresonator," *Nature*, vol. 450, no. 7173, pp. 1214–1217, Dec. 2007.

[79] J. S. Levy, A. Gondarenko, M. A. Foster, A. C. Turner-Foster, A. L. Gaeta, and M. Lipson, "CMOS-Compatible Multiple-Wavelength Oscillator for on-Chip Optical Interconnects," *Nat. Photonics*, vol. 4, no. 1, pp. 37–40, Jan. 2010.

[80] P. Del'Haye, T. Herr, E. Gavartin, M. L. Gorodetsky, R. Holzwarth, and T. J. Kippenberg, "Octave Spanning Tunable Frequency Comb from a Microresonator," *Phys. Rev. Lett.*, vol. 107, no. 6, p. 063901, Aug. 2011.

[81] A. A. Savchenkov, A. B. Matsko, V. S. Ilchenko, I. Solomatine, D. Seidel, and L. Maleki, "Tunable Optical Frequency Comb with a Crystalline Whispering Gallery Mode Resonator," *Phys. Rev. Lett.*, vol. 101, no. 9, p. 093902, Aug. 2008.

[82] M. A. Foster, J. S. Levy, O. Kuzucu, K. Saha, M. Lipson, and A. L. Gaeta, "Silicon-Based Monolithic Optical Frequency Comb Source," *Opt. Express*, vol. 19, no. 15, p. 14233, July 2011.

[83] T. Herr *et al.*, "Temporal Solitons in Optical Microresonators," *Nat. Photonics*, vol. 8, no. 2, pp. 145–152, Feb. 2014.

[84] X. Yi, Q.-F. Yang, K. Y. Yang, M.-G. Suh, and K. Vahala, "Soliton Frequency Comb at Microwave Rates in a High-Q Silica Microresonator," *Optica*, vol. 2, no. 12, p. 1078, Dec. 2015.

[85] N. Volet *et al.*, "Micro-Resonator Soliton Generated Directly with a Diode Laser," *Laser Photon. Rev.*, vol. 12, no. 5, p. 1700307, May 2018.

[86] J. Liu *et al.*, "Ultralow-Power Chip-Based Soliton Microcombs for Photonic Integration," *Optica*, vol. 5, no. 10, p. 1347, Oct. 2018.

[87] B. Stern, X. Ji, Y. Okawachi, A. L. Gaeta, and M. Lipson, "Battery-Operated Integrated Frequency Comb Generator," *Nature*, vol. 562, no. 7727, pp. 401–405, Oct. 2018.

[88] A. S. Raja *et al.*, "Electrically Pumped Photonic Integrated Soliton Microcomb," *Nat. Commun.*, vol. 10, no. 1, p. 680, Dec. 2019.

[89] D. T. Spencer *et al.*, “An Optical-Frequency Synthesizer Using Integrated Photonics,” *Nature*, vol. 557, no. 7703, pp. 81–85, May 2018.

[90] V. Panapakkam *et al.*, “Amplitude and Phase Noise of Frequency Combs Generated by Single-Section InAs/InP Quantum-Dash-Based Passively and Actively Mode-Locked Lasers,” *IEEE J. Quantum Electron.*, vol. 52, no. 11, pp. 1–7, Nov. 2016.

[91] M. O. Sahni *et al.*, “Frequency Noise Reduction Performance of a Feed-Forward Heterodyne Technique: Application to an Actively Mode-Locked Laser Diode,” *Opt. Lett.*, vol. 42, no. 19, p. 4000, Oct. 2017.

[92] J. Pfeifle *et al.*, “Simultaneous Phase Noise Reduction of 30 Comb Lines from a Quantum-Dash Mode-Locked Laser Diode Enabling Coherent Tbit/s Data Transmission,” in *Optical Fiber Communication Conference*, (OSA, 2015), paper Tu3I.5.

[93] M. H. P. Pfeiffer *et al.*, “Octave-Spanning Dissipative Kerr Soliton Frequency Combs in Si_3N_4 Microresonators,” *Optica*, vol. 4, no. 7, p. 684, July 2017.

[94] C. Wang *et al.*, “On-Chip Kerr Frequency Comb Generation in Lithium Niobate Microresonators,” in *Conference on Lasers and Electro-Optics*, (OSA, 2018), paper SW4M.3.

[95] X. Xue, P.-H. Wang, Y. Xuan, M. Qi, and A. M. Weiner, “High-Efficiency WDM Sources Based on Microresonator Kerr Frequency Combs,” in *Optical Fiber Communication Conference*, (OSA, 2017), paper M3F.2.

[96] P. Winzer, “Beyond 100G Ethernet,” *IEEE Commun. Mag.*, vol. 48, no. 7, pp. 26–30, 2010.

[97] C. R. Cole, “100-Gb/s and beyond Transceiver Technologies,” *Opt. Fiber Technol.*, vol. 17, no. 5, pp. 472–479, 2011.

[98] S. Gringeri, E. B. Basch, and T. J. Xia, “Technical Considerations for Supporting Data Rates beyond 100 Gb/S,” *IEEE Commun. Mag.*, vol. 50, no. 2, pp. s21–s30, 2012.

[99] D. A. B. Miller, “Device Requirements for Optical Interconnects to Silicon Chips,” *Proc. IEEE*, vol. 97, no. 7, pp. 1166–1185, 2009.

[100] J. Geyer *et al.*, “Practical Implementation of Higher Order Modulation Beyond 16-QAM,” in *Optical Fiber Communication Conference*, (OSA, 2015), paper Th1B.1.

[101] D. Hillerkuss *et al.*, "26 Tbit S^{-1} Line-Rate Super-Channel Transmission Utilizing All-Optical Fast Fourier Transform Processing," *Nat. Photonics*, vol. 5, no. 6, pp. 364–371, June 2011.

[102] E. Temprana, V. Ataie, B. P. P. Kuo, E. Myslivets, N. Alic, and S. Radic, "Dynamic Reconfiguration of Parametric Frequency Comb for Superchannel and Flex-Grid Transmitters," in *European Conference on Optical Communication*, (ECOC, 2014), p. P.3.14.

[103] Z. Chen *et al.*, "Key Technologies for Elastic Optical Networks," in *13th International Conference on Optical Communications and Networks*, (IEEE, 2014), pp. 1–3.

[104] P. Marin *et al.*, "50 Tbit/s Massively Parallel WDM Transmission in C and L Band Using Interleaved Cavity-Soliton Kerr Combs," in *Conference on Lasers and Electro-Optics*, (OSA, 2016), paper STu1G.1.

[105] P. J. Delfyett *et al.*, "Optical Frequency Combs from Semiconductor Lasers and Applications in Ultrawideband Signal Processing and Communications," *J. Lightw. Technol.*, vol. 24, no. 7, pp. 2701–2719, 2006.

[106] Xingwen Yi, N. K. Fontaine, R. P. Scott, and S. Yoo, "Tb/s Coherent Optical OFDM Systems Enabled by Optical Frequency Combs," *J. Lightw. Technol.*, vol. 28, no. 14, pp. 2054–2061, July 2010.

[107] N. K. Fontaine, R. P. Scott, L. Zhou, F. M. Soares, J. P. Heritage, and S. J. B. Yoo, "Real-Time Full-Field Arbitrary Optical Waveform Measurement," *Nat. Photonics*, vol. 4, no. 4, pp. 248–254, 2010.

[108] J. N. Kemal *et al.*, "Parallel Multi-Wavelength Intradyne Reception Using an Optical Frequency Comb as a Local Oscillator," in *European Conference on Optical Communication, ECOC*, (ECOC, 2015), pp. 1–3.

[109] G. Yabre, H. De Waardt, H. P. A. Van Den Boom, and G. D. Khoe, "Noise Characteristics of Single-Mode Semiconductor Lasers under External Light Injection," *IEEE J. Quantum Electron.*, vol. 36, no. 3, pp. 385–393, 2000.

[110] M. D. G. Pascual, R. Zhou, F. Smyth, P. M. Anandarajah, and L. P. Barry, "Software Reconfigurable Highly Flexible Gain Switched Optical Frequency Comb Source," *Opt. Express*, vol. 23, no. 18, p. 23225, 2015.

[111] R. Zhou *et al.*, "Monolithically Integrated 2-Section Lasers for Injection Locked Gain Switched Comb Generation," in *Conference on Optical*

Fiber Communication, Technical Digest Series, (OSA, 2014), paper Th3A.3.

[112] R. Zhou, T. N. Huynh, V. Vujicic, P. M. Anandarajah, and L. P. Barry, "Phase Noise Analysis of Injected Gain Switched Comb Source for Coherent Communications," *Opt. Express*, vol. 22, no. 7, pp. 8120–8125, 2014.

[113] R. Noé, W. B. Sessa, R. Welter, and L. G. Kazovsky, "New FSK Phase-Diversity Receiver in a 150 Mbit/s Coherent Optical Transmission System," *Electron. Lett.*, vol. 24, no. 9, p. 567, 1988.

[114] F. Chang, K. Onohara, and T. Mizuochi, "Forward Error Correction for 100 G Transport Networks," *IEEE Commun. Mag.*, vol. 48, no. 3, pp. S48–S55, Mar. 2010.

[115] OptSim, "Synopsys, Inc. (2016)," 2016. [Online]. Available: https://optics.synopsys.com/rsoft/rsoft-system.html.

[116] "TL5000DCJ - Oclaro." [Online]. Available: http://www.oclaro.com/product/tl5000dcj/.

[117] "MAFA 1000 Series EDFA - Emcore." [Online]. Available: http://emcore.com/products/mafa-1000-series-edfa/.

[118] J. Pfeifle *et al.*, "Full C and L-Band Transmission at 20 Tbit/s Using Cavity-Soliton Kerr Frequency Combs," in *CLEO: 2015 Postdeadline Paper Digest*, (OSA, 2015), paper JTh5C.8.

[119] Cisco White Paper, "Annual Internet Report, 2018–2023," *Cisco*, 2020. [Online]. Available: https://www.cisco.com/c/en/us/solutions/collateral/executive-perspectives/annual-internet-report/white-paper-c11-741490.html.

[120] V. Torres-Company *et al.*, "Laser Frequency Combs for Coherent Optical Communications," *J. Lightw. Technol.*, vol. 37, no. 7, pp. 1663–1670, 2019.

[121] C. J. Krückel, A. Fülöp, Z. Ye, P. A. Andrekson, and V. Torres-Company, "Optical Bandgap Engineering in Nonlinear Silicon Nitride Waveguides," *Opt. Express*, vol. 25, no. 13, p. 15370, June 2017.

[122] T. Harter *et al.*, "Wireless THz Link with Optoelectronic Transmitter and Receiver," *Optica*, vol. 6, no. 8, p. 1063, Aug. 2019.

[123] G. Liu *et al.*, "A Passively Mode-Locked Quantum Dot Laser with

10.8 Tbit/s Transmission over 100-km SSMF," in *Optical Fiber Communication Conference*, (OSA, 2020), paper W2A.2.

[124] A. Akrout *et al.*, "Separate Error-Free Transmission of Eight Channels at 10 Gb/s Using Comb Generation in a Quantum-Dash-Based Mode-Locked Laser," *IEEE Photonics Technol. Lett.*, vol. 21, no. 23, pp. 1746–1748, Dec. 2009.

[125] C. Calò *et al.*, "Single-Section Quantum Well Mode-Locked Laser for 400 Gb/s SSB-OFDM Transmission," *Opt. Express*, vol. 23, no. 20, p. 26442, Oct. 2015.

[126] J. Hauck *et al.*, "Semiconductor Laser Mode Locking Stabilization with Optical Feedback from a Silicon PIC," *J. Lightw. Technol.*, vol. 37, no. 14, pp. 3483–3494, 2019.

[127] C. Xing and E. A. Avrutin, "Multimode Spectra and Active Mode Locking Potential of Quantum Dot Lasers," *J. Appl. Phys.*, vol. 97, no. 10, p. 104301, May 2005.

[128] R. Rosales *et al.*, "InAs/InP Quantum-Dot Passively Mode-Locked Lasers for 1.55-μm Applications," *IEEE J. Sel. Top. Quantum Electron.*, vol. 17, no. 5, pp. 1292–1301, Sep. 2011.

[129] D. Auth, L. Drzewietzki, C. Weber, A. Klehr, A. Knigge, and S. Breuer, "Repetition Rate Control of Optical Self-Injected Passively Mode-Locked Quantum-Well Lasers: Experiment and Simulation," *Electron. Lett.*, vol. 54, no. 6, pp. 374–376, 2018.

[130] D. Arsenijević, M. Kleinert, and D. Bimberg, "Phase Noise and Jitter Reduction by Optical Feedback on Passively Mode-Locked Quantum-Dot Lasers," *Appl. Phys. Lett.*, vol. 103, no. 23, 2013.

[131] Z. G. Lu, J. R. Liu, P. J. Poole, C. Y. Song, and S. D. Chang, "Ultra-Narrow Linewidth Quantum Dot Coherent Comb Lasers with Self-Injection Feedback Locking," *Opt. Express*, vol. 26, no. 9, pp. 11909–11914, Apr. 2018.

[132] F. Grillot, C.-Y. Lin, N. A. Naderi, M. Pochet, and L. F. Lester, "Optical Feedback Instabilities in a Monolithic InAs/GaAs Quantum Dot Passively Mode-Locked Laser," *Appl. Phys. Lett.*, vol. 94, no. 15, p. 153503, Apr. 2009.

[133] E. A. Avrutin, S. Xibin, and B. M. Russell, "Optical Feedback Tolerance of Mode-Locked Laser Diodes and Some Feedback Reduction Methods:

A Numerical Investigation," *Opt. Quantum Electron.*, vol. 40, pp. 1175–1180, Nov. 2008.

[134] H. Asghar, W. Wei, P. Kumar, E. Sooudi, and J. G. McInerney, "Stabilization of Self-Mode-Locked Quantum Dash Lasers by Symmetric Dual-Loop Optical Feedback," *Opt. Express*, vol. 26, no. 4, pp. 4581–4592, Feb. 2018.

[135] K. Merghem, V. Panapakkam, Q. Gaimard, F. Lelarge, and A. Ramdane, "Narrow Linewidth Frequency Comb Source Based on Self-Injected Quantum-Dash Passively Mode-Locked Laser," in *Conference on Lasers and Electro-Optics*, (OSA, 2017), paper SW1C.5.

[136] E. Sooudi *et al.*, "Injection-Locking Properties of InAs/InP-Based Mode-Locked Quantum-Dash Lasers at 21 GHz," *IEEE Photonics Technol. Lett.*, vol. 23, no. 20, pp. 1544–1546, 2011.

[137] E. Sooudi *et al.*, "Optical Frequency Comb Generation Using Dual-Mode Injection-Locking of Quantum-Dash Mode-Locked Lasers: Properties and Applications," *IEEE J. Quantum Electron.*, vol. 48, no. 10, pp. 1327–1338, 2012.

[138] M. Haji *et al.*, "Ultralow 192 Hz RF Linewidth Optoelectronic Oscillator Based on the Optical Feedback of Mode-Locked Laser Diodes," in *Conference on Lasers and Electro-Optics*, (OSA, 2012), vol. 20, no. 3, paper CW1N.4.

[139] E. A. Avrutin and B. M. Russell, "Dynamics and Spectra of Monolithic Mode-Locked Laser Diodes Under External Optical Feedback," *IEEE J. Quantum Electron.*, vol. 45, no. 11, pp. 1456–1464, Nov. 2009.

[140] J. Osmundsen and N. Gade, "Influence of Optical Feedback on Laser Frequency Spectrum and Threshold Conditions," *IEEE J. Quantum Electron.*, vol. 19, no. 3, pp. 465–469, Mar. 1983.

[141] F. Kéfélian, S. O'Donoghue, M. T. Todaro, J. G. McInerney, and G. Huyet, "RF Linewidth in Monolithic Passively Mode-Locked Semiconductor Laser," *IEEE Photonics Technol. Lett.*, vol. 20, no. 16, pp. 1405–1407, 2008.

[142] T. Habruseva, S. O'Donoghue, N. Rebrova, F. Kéfélian, S. P. Hegarty, and G. Huyet, "Optical Linewidth of a Passively Mode-Locked Semiconductor Laser," *Opt. Lett.*, vol. 34, no. 21, pp. 3307–3309, Nov. 2009.

[143] R. Rosales, K. Merghem, A. Martinez, F. Lelarge, A. Accard, and A. Ramdane, “Timing Jitter from the Optical Spectrum in Semiconductor Passively Mode Locked Lasers,” *Opt. Express*, vol. 20, no. 8, pp. 9151–9160, Apr. 2012.

[144] T. N. Huynh, L. Nguyen, and L. P. Barry, “Phase Noise Characterization of SGDBR Lasers Using Phase Modulation Detection Method with Delayed Self-Heterodyne Measurements,” *J. Lightw. Technol.*, vol. 31, no. 8, pp. 1300–1308, 2013.

[145] A. L. Lance, W. D. Seal, and F. Labaar, “Phase Noise and AM Noise Measurements in the Frequency Domain.,” in *Infrared and Millimeter Waves*, vol. 11, K. J. Button, Ed. Academic Press, 1984, pp. 239–289.

[146] P. Spano, S. Piazzolla, and M. Tamburrini, “Phase Noise in Semiconductor Lasers: A Theoretical Approach,” *IEEE J. Quantum Electron.*, vol. 19, no. 7, pp. 1195–1199, July 1983.

[147] K. Kikuchi and T. Okoshi, “FM- and AM-Noise Spectra of 1.3 μm InGaAsP DFB Lasers in 0–3 GHz Range and Determination of Their Linewidth Enhancement Factor α,” *Electron. Lett.*, vol. 20, no. 25–26, pp. 1044–1045, 1984.

[148] C. H. Henry, “Theory of the Phase Noise and Power Spectrum of a Single Mode Injection Laser,” *IEEE J. Quantum Electron.*, vol. 19, no. 9, pp. 1391–1397, 1983.

[149] T. Verolet *et al.*, “Mode Locked Laser Phase Noise Reduction under Optical Feedback for Coherent DWDM Communication,” *J. Lightw. Technol.*, vol. 8724, no. c, pp. 1–1, 2020.

[150] B. Szafraniec, B. Nebendahl, and T. Marshall, “Polarization Demultiplexing in Stokes Space,” *Opt. Express*, vol. 18, no. 17, pp. 17928–17939, Aug. 2010.

[151] R. Schmogrow, “Real-Time Digital Signal Processing for Software-Defined Optical Transmitters and Receivers,” dissertation (Karlsruhe Institute of Technology, 2014.

[152] M. Jeruchim, “Techniques for Estimating the Bit Error Rate in the Simulation of Digital Communication Systems,” *IEEE J. Sel. Areas Commun.*, vol. 2, no. 1, pp. 153–170, Jan. 1984.

[153] Z. Lu, J. Liu, L. Mao, C.-Y. Song, J. Weber, and P. Poole, “12.032 Tbit/s Coherent Transmission Using an Ultra-Narrow Linewidth Qantum Dot

34.46-GHz C-Band Coherent Comb Laser," in *Next-Generation Optical Communication: Components, Sub-Systems, and Systems VIII*, (SPIE, 2019), p. 23.

[154] OIF-Tech-Options-400G-01.0 white paper, "Technology Options for 400G Implementation," (OIF, 2015). [Online]. Available: https://www.oiforum.com/documents/technology-options-for-400g-implementation/.

[155] K. Roberts, Q. Zhuge, I. Monga, S. Gareau, and C. Laperle, "Beyond 100 Gb/s: Capacity, Flexibility, and Network Optimization," *J. Opt. Commun. Netw.*, vol. 9, no. 4, pp. C12–C24, Apr. 2017.

[156] A. Viterbi, "Nonlinear Estimation of PSK-Modulated Carrier Phase with Application to Burst Digital Transmission," *IEEE Trans. Inf. Theory*, vol. 29, no. 4, pp. 543–551, July 1983.

[157] K. Schuh *et al.*, "Single Carrier 1.2 Tbit/s Transmission over 300 km with PM-64 QAM at 100 GBaud," in *Optical Fiber Communication Conference Postdeadline Papers*, (OSA, 2017), paper Th5B.5.

[158] LIGENTEC, "All-Nitride Core Technology," 2020. [Online]. Available: https://www.ligentec.com/ligentec-an-technology/. [Accessed: 25-Jun-2020].

[159] M. H. P. Pfeiffer *et al.*, "Photonic Damascene Process for Integrated High-Q Microresonator Based Nonlinear Photonics," *Optica*, vol. 3, no. 1, pp. 20–25, Jan. 2016.

[160] S. L. I. Olsson, J. Cho, S. Chandrasekhar, X. Chen, P. J. Winzer, and S. Makovejs, "Probabilistically Shaped PDM 4096-QAM Transmission over up to 200 km of Fiber Using Standard Intradyne Detection," *Opt. Express*, vol. 26, no. 4, pp. 4522–4530, Feb. 2018.

[161] M. Mazur, A. Lorences-Riesgo, J. Schroder, P. A. Andrekson, and M. Karlsson, "High Spectral Efficiency PM-128QAM Comb-Based Superchannel Transmission Enabled by a Single Shared Optical Pilot Tone," *J. Lightw. Technol.*, vol. 36, no. 6, pp. 1318–1325, Mar. 2018.

[162] C. Gosset *et al.*, "Subpicosecond Pulse Generation at 134GHz Using a Quantum-Dash-Based Fabry-Perot Laser Emitting at 1.56μm," *Appl. Phys. Lett.*, vol. 88, no. 24, p. 241105, June 2006.

[163] Z. Lu *et al.*, "Raman Self-Frequency-Shift of Soliton Crystal in a High Index Doped Silica Micro-Ring Resonator [Invited]," *Opt. Mater.*

Express, vol. 8, no. 9, p. 2662, Sep. 2018.

[164] C. Doerr and L. Chen, "Silicon Photonics in Optical Coherent Systems," *Proc. IEEE*, vol. 106, no. 12, pp. 2291–2301, Dec. 2018.

[165] A. Novack *et al.*, "A Silicon Photonic Transceiver and Hybrid Tunable Laser for 64 Gbaud Coherent Communication," in *Optical Fiber Communication Conference Postdeadline Papers*, (OSA, 2018), paper Th4D.4.

[166] R. W. Going *et al.*, "1.00 (0.88) Tb/s per Wave Capable Coherent Multi-Channel Transmitter (Receiver) InP-Based PICs With Hybrid Integrated SiGe Electronics," *IEEE J. Quantum Electron.*, vol. 54, no. 4, pp. 1–10, Aug. 2018.

[167] L. M. Augustin *et al.*, "InP-Based Generic Foundry Platform for Photonic Integrated Circuits," *IEEE J. Sel. Top. Quantum Electron.*, vol. 24, no. 1, pp. 1–10, Jan. 2018.

[168] J.-P. Elbers, N. Eiselt, A. Dochhan, D. Rafique, and H. Grießer, "PAM4 vs Coherent for DCI Applications," in *Advanced Photonics (SPPCom 2017)*, (OSA, 2017), paper SpTh2D.1.

[169] T. Pfau, H. Zhang, J. Geyer, and C. Rasmussen, "High Performance Coherent ASIC," in *European Conference on Optical Communication*, (ECOC, 2018), pp. 1–3.

[170] T. Flick, K. H. Becks, J. Dopke, P. Mättig, and P. Tepel, "Measurement of the Thermal Resistance of VCSEL Devices," *J. Instrum.*, vol. 6, no. 01, pp. C01021–C01021, Jan. 2011.

[171] A. E. Zhukov, A. R. Kovsh, D. A. Livshits, V. M. Ustinov, and Z. I. Alferov, "Output Power and Its Limitation in Ridge-Waveguide 1.3 μm Wavelength Quantum-Dot Lasers," *Semicond. Sci. Technol.*, vol. 18, no. 8, pp. 774–781, Aug. 2003.

[172] F. Lelarge *et al.*, "Effect of P-Doping on Temperature and Dynamic Performances of 1550nm InAs/InP Quantum Dash Based Lasers," in *2009 IEEE International Conference on Indium Phosphide & Related Materials*, (IEEE, 2009), pp. 383–386.

[173] K. Merghem *et al.*, "Stability of Optical Frequency Comb Generated With InAs/InP Quantum-Dash-Based Passive Mode-Locked Lasers," *IEEE J. Quantum Electron.*, vol. 50, no. 4, pp. 275–280, Apr. 2014.

[174] M. T. Crowley *et al.*, "Analytical Modeling of the Temperature

Performance of Monolithic Passively Mode-Locked Quantum Dot Lasers," *IEEE J. Quantum Electron.*, vol. 47, no. 8, pp. 1059–1068, Aug. 2011.

[175] R. Rosales *et al.*, "High Performance Mode Locking Characteristics of Single Section Quantum Dash Lasers," *Opt. Express*, vol. 20, no. 8, pp. 8649–8657, Apr. 2012.

[176] K. Zanette, J. C. Cartledge, and M. O'Sullivan, "Correlation Properties of the Phase Noise Between Pairs of Lines in a Quantum-Dot Optical Frequency Comb Source," in *Optical Fiber Communication Conference*, 2017, p. Th3I.6.

[177] M. Magarini *et al.*, "Pilot-Symbols-Aided Carrier-Phase Recovery for 100-G PM-QPSK Digital Coherent Receivers," *IEEE Photonics Technol. Lett.*, vol. 24, no. 9, pp. 739–741, May 2012.

[178] C. Malouin, P. Thomas, B. Zhang, J. O'Neil, and T. Schmidt, "Natural Expression of the Best-Match Search Godard Clock-Tone Algorithm for Blind Chromatic Dispersion Estimation in Digital Coherent Receivers," in *Advanced Photonics Congress*, (OSA, 2012), paper SpTh2B.4.

[179] D. Godard, "Passband Timing Recovery in an All-Digital Modem Receiver," *IEEE Trans. Commun.*, vol. 26, no. 5, pp. 517–523, May 1978.

[180] C. W. Farrow, "A Continuously Variable Digital Delay Element," in *IEEE International Symposium on Circuits and Systems*, (IEEE, 1988), pp. 2641–2645.

[181] S. J. Savory, "Digital Filters for Coherent Optical Receivers," *Opt. Express*, vol. 16, no. 2, pp. 804–817, 2008.

[182] T. Nakagawa *et al.*, "Non-Data-Aided Wide-Range Frequency Offset Estimator for QAM Optical Coherent Receivers," in *Optical Fiber Communication Conference/National Fiber Optic Engineers Conference*, (OSA, 2011), paper OMJ1.

[183] K. Merghem *et al.*, "InAs/InP Quantum Dot Based Lasers and Effect of Optical Feedback," in *Novel In-Plane Semiconductor Lasers XI*, (SPIE, 2012), paper 82770D.

[184] R. Schmogrow *et al.*, "Error Vector Magnitude as a Performance Measure for Advanced Modulation Formats," *IEEE Photonics Technol. Lett.*, vol. 24, no. 1, pp. 61–63, Jan. 2012. Erratum: *ibid*. 24(23), 2198 (2012)

[185] L. Schmalen, S. ten Brink, and A. Leven, "Spatially-Coupled LDPC

Protograph Codes for Universal Phase Slip-Tolerant Differential Decoding," in *Optical Fiber Communication Conference*, (OSA, 2015), paper Th3E.6.

[186] A. Hasegawa and Y. Kodama, *Solitons in Optical Communications*. New York: Clarendon Press; Oxford Univ. Press, 1995.

[187] L. F. Mollenauer, R. H. Stolen, and J. P. Gordon, "Experimental Observation of Picosecond Pulse Narrowing and Solitons in Optical Fibers," *Phys. Rev. Lett.*, vol. 45, no. 13, pp. 1095–1098, Sep. 1980.

[188] A. Ankiewicz and N. Akhmediev, *Dissipative Solitons: From Optics to Biology and Medicine*, vol. 751. Berlin, Heidelberg: Springer, 2008.

[189] V. Brasch *et al.*, "Photonic Chip-Based Optical Frequency Comb Using Soliton Cherenkov Radiation," *Science*, vol. 351, no. 6271, pp. 357–360, Jan. 2016.

[190] N. Bozinovic *et al.*, "Terabit-Scale Orbital Angular Momentum Mode Division Multiplexing in Fibers," *Science*, vol. 340, no. 6140, pp. 1545–1548, June 2013.

[191] D. Dai and J. E. Bowers, "Silicon-Based on-Chip Multiplexing Technologies and Devices for Peta-Bit Optical Interconnects," *Nanophotonics*, vol. 3, no. 4–5, Jan. 2014.

[192] M. Nakazawa, E. Yamada, H. Kubota, and K. Suzuki, "10 Gbit/s Soliton Data Transmission over One Million Kilometres," *Electron. Lett.*, vol. 27, no. 14, p. 1270, 1991.

[193] T. J. Kippenberg, R. Holzwarth, and S. A. Diddams, "Microresonator-Based Optical Frequency Combs," *Science*, vol. 332, no. 6029, pp. 555–559, Apr. 2011.

[194] L. A. Lugiato and R. Lefever, "Spatial Dissipative Structures in Passive Optical Systems," *Phys. Rev. Lett.*, vol. 58, no. 21, pp. 2209–2211, May 1987.

[195] M. Yu, Y. Okawachi, A. G. Griffith, N. Picqué, M. Lipson, and A. L. Gaeta, "Silicon-Chip-Based Mid-Infrared Dual-Comb Spectroscopy," *Nat. Commun.*, vol. 9, no. 1, p. 1869, Dec. 2018.

[196] J. D. Jost, T. Herr, C. Lecaplain, V. Brasch, M. H. P. Pfeiffer, and T. J. Kippenberg, "Counting the Cycles of Light Using a Self-Referenced Optical Microresonator," *Optica*, vol. 2, no. 8, p. 706, Aug. 2015.

[197] V. Brasch, E. Lucas, J. D. Jost, M. Geiselmann, and T. J. Kippenberg, "Self-Referenced Photonic Chip Soliton Kerr Frequency Comb," *Light Sci. Appl.*, vol. 6, no. 1, pp. e16202–e16202, Jan. 2017.

[198] W. Liang *et al.*, "High Spectral Purity Kerr Frequency Comb Radio Frequency Photonic Oscillator," *Nat. Commun.*, vol. 6, no. 1, p. 7957, Dec. 2015.

[199] M.-G. Suh, Q.-F. Yang, K. Y. Yang, X. Yi, and K. J. Vahala, "Microresonator Soliton Dual-Comb Spectroscopy," *Science*, vol. 354, no. 6312, pp. 600–603, Nov. 2016.

[200] H. Guo *et al.*, "Universal Dynamics and Deterministic Switching of Dissipative Kerr Solitons in Optical Microresonators," *Nat. Phys.*, vol. 13, no. 1, pp. 94–102, Sep. 2016.

[201] A. Kordts, M. H. P. Pfeiffer, H. Guo, V. Brasch, and T. J. Kippenberg, "Higher Order Mode Suppression in High-Q Anomalous Dispersion SiN Microresonators for Temporal Dissipative Kerr Soliton Formation," in *Conference on Lasers and Electro-Optics*, (OSA, 2016), paper SW4E.2.

[202] A. Sano *et al.*, "102.3-Tb/s (224 x 548-Gb/s) C- and Extended L-Band All-Raman Transmission over 240 km Using PDM-64QAM Single Carrier FDM with Digital Pilot Tone," in *National Fiber Optic Engineers Conference*, (OSA, 2012), paper PDP5C.3.

[203] C. Kachris and I. Tomkos, "A Survey on Optical Interconnects for Data Centers," *IEEE Commun. Surv. Tutorials*, vol. 14, no. 4, pp. 1021–1036, 2012.

[204] J. K. Alexander *et al.*, "Monolithically Integrated Low Linewidth Comb Source Using Gain Switched Slotted Fabry-Perot Lasers," *Opt. Express*, vol. 24, no. 8, p. 7960, Apr. 2016.

[205] J. Gärtner, P. Trocha, R. Mandel, C. Koos, T. Jahnke, and W. Reichel, "Bandwidth and Conversion Efficiency Analysis of Dissipative Kerr Soliton Frequency Combs Based on Bifurcation Theory," *Phys. Rev. A*, vol. 100, no. 3, p. 033819, Sep. 2019.

[206] V. Vujicic *et al.*, "Mitigation of Relative Intensity Noise of Quantum Dash Mode-Locked Lasers for PAM4 Based Optical Interconnects Using Encoding Techniques," *Opt. Express*, vol. 25, no. 1, pp. 20–29, Jan. 2017.

[207] R. Nagarajan *et al.*, "InP Photonic Integrated Circuits," *IEEE J. Sel. Top. Quantum Electron.*, vol. 16, no. 5, pp. 1113–1125, Sep. 2010.

[208] D. Liang and J. E. Bowers, "Recent Progress in Lasers on Silicon," *Nat. Photonics*, vol. 4, no. 8, pp. 511–517, Aug. 2010.

[209] N. Lindenmann *et al.*, "Photonic Wire Bonding: A Novel Concept for Chip-Scale Interconnects," *Opt. Express*, vol. 20, no. 16, pp. 17667–77, July 2012.

[210] M. Lauermann *et al.*, "40 GBd 16QAM Signaling at 160 Gb/s in a Silicon-Organic Hybrid Modulator," *J. Lightw. Technol.*, vol. 33, no. 6, pp. 1210–1216, Mar. 2015.

[211] C. Koos *et al.*, "Silicon-Organic Hybrid (SOH) and Plasmonic-Organic Hybrid (POH) Integration," *J. Lightw. Technol.*, vol. 34, no. 2, pp. 256–268, Jan. 2016.

[212] S. K. Selvaraja, P. Jaenen, W. Bogaerts, D. Van Thourhout, P. Dumon, and R. Baets, "Fabrication of Photonic Wire and Crystal Circuits in Silicon-on-Insulator Using 193-nm Optical Lithography," *J. Lightw. Technol.*, vol. 27, no. 18, pp. 4076–4083, Sep. 2009.

[213] Y. Xuan *et al.*, "High-Q Silicon Nitride Microresonators Exhibiting Low-Power Frequency Comb Initiation," *Optica*, vol. 3, no. 11, p. 1171, Nov. 2016.

[214] M. H. P. Pfeiffer, J. Liu, M. Geiselmann, and T. J. Kippenberg, "Coupling Ideality of Integrated Planar High-*Q* Microresonators," *Phys. Rev. Appl.*, vol. 7, no. 2, p. 024026, Feb. 2017.

[215] B. J. Puttnam *et al.*, "High-Capacity Self-Homodyne PDM-WDM-SDM Transmission in a 19-Core Fiber," *Opt. Express*, vol. 22, no. 18, p. 21185, Sep. 2014.

[216] C. Joshi *et al.*, "Thermally Controlled Comb Generation and Soliton Modelocking in Microresonators," *Opt. Lett.*, vol. 41, no. 11, p. 2565, 2016.

[217] P.-H. Wang *et al.*, "Intracavity Characterization of Micro-Comb Generation in the Single-Soliton Regime," *Opt. Express*, vol. 24, no. 10, p. 10890, May 2016.

[218] T. Carmon, L. Yang, and K. J. Vahala, "Dynamical Thermal Behavior and Thermal Self-Stability of Microcavities," *Opt. Express*, vol. 12, no. 20, p. 4742, Oct. 2004.

[219] M. Karpov *et al.*, "Raman Self-Frequency Shift of Dissipative Kerr Solitons in an Optical Microresonator," *Phys. Rev. Lett.*, vol. 116, no. 10,

p. 103902, Mar. 2016.

[220] P. Marin *et al.*, “34.6 Tbit/s WDM Transmission Using Soliton Kerr Frequency Combs as Optical Source and Local Oscillator,” in *European Conference on Optical Communication,* (ECOC, 2016), pp. 415–417.

[221] R. Dar *et al.*, “Impact of WDM Channel Correlations on Nonlinear Transmission,” in *European Conference on Optical Communication,* (ECOC, 2016), pp. 482–484.

[222] P. J. Winzer, A. H. Gnauck, C. R. Doerr, M. Magarini, and L. L. Buhl, “Spectrally Efficient Long-Haul Optical Networking Using 112-Gb/s Polarization-Multiplexed 16-QAM,” *J. Lightw. Technol.*, vol. 28, no. 4, pp. 547–556, Feb. 2010.

[223] N. S. Bergano and C. R. Davidson, “Circulating Loop Transmission Experiments for the Study of Long-Haul Transmission Systems Using Erbium-Doped Fiber Amplifiers,” *J. Lightw. Technol.*, vol. 13, no. 5, pp. 879–888, 1995.

[224] J. Cai, M. Nissov, C. Davidson, and A. Pilipetskii, “Measurement Techniques for High-Speed WDM Experiments,” in *Optical Fiber Communications Conference,* (OSA, 2003), pp. 575–577.

[225] W. Freude *et al.*, “Quality Metrics for Optical Signals: Eye Diagram, Q-Factor, OSNR, EVM and BER,” in *14th International Conference on Transparent Optical Networks*, (IEEE, 2012), pp. 1–4.

[226] R.-J. Essiambre, G. Kramer, P. J. Winzer, G. J. Foschini, and B. Goebel, “Capacity Limits of Optical Fiber Networks,” *J. Lightw. Technol.*, vol. 28, no. 4, pp. 662–701, Feb. 2010.

[227] F. Buchali, A. Klekamp, L. Schmalen, and T. Drenski, “Implementation of 64QAM at 42.66 GBaud Using 1.5 Samples per Symbol DAC and Demonstration of up to 300 km Fiber Transmission,” in *Optical Fiber Communication Conference*, (OSA, 2014), paper M2A.1.

[228] J. H. Ke, Y. Gao, and J. C. Cartledge, “400 Gbit/s Single-Carrier and 1 Tbit/s Three-Carrier Superchannel Signals Using Dual Polarization 16-QAM with Look-up Table Correction and Optical Pulse Shaping,” *Opt. Express*, vol. 22, no. 1, p. 71, Jan. 2014.

[229] L. Gasca, “From O to L: The Future of Optical Wavelength-Bands,” *Broadband Properties*, pp. 83–85, 2008.

[230] Oclaro, “LambdaFLEX ITLA TL5000 Integrated Tunable Laser

Assembly - C Band, Variable Output Power (2006)," 2006. [Online]. Available: http://www.oclaro.com/product/tl5000vcj/.

[231] Emcore, "MAFA 3000 Series Erbium Doped Fiber Amplifier (2010)," 2010. [Online]. Available: http://www.eqphotonics.de/cms/cms/upload/datasheets/MAFA3000-08_2010.pdf.

[232] Emcore, "MAFA 5000 Series Erbium Doped Fiber Micro Amplifier (2016)," 2016. [Online]. Available: http://emcore.com/wp-content/uploads/2016/10/MAFA-5000-Series.pdf.

[233] Arduino, "Arduino/Genuino UNO (2016)," 2016. [Online]. Available: https://www.arduino.cc/en/Main/ArduinoBoardUno.

[234] T. Analog, "ATE1-07 TEC Modules (2016)," 2016. [Online]. Available: http://www.analogtechnologies.com/document/ATE1-07.pdf.

[235] A. M. Vengsarkar, N. S. Bergano, C. R. Davidson, J. R. Pedrazzani, J. B. Judkins, and P. J. Lemaire, "Long-Period Fiber-Grating-Based Gain Equalizers," *Opt. Lett.*, vol. 21, no. 5, p. 336, Mar. 1996.

[236] H. S. Kim, S. H. Yun, I. K. Kwang, and B. Y. Kim, "All-Fiber Acousto-Optic Tunable Notch Filter with Electronically Controllable Spectral Profile," *Opt. Lett.*, vol. 22, no. 19, p. 1476, 1997.

[237] Auxora, "CATV Module (2009)," 2009. [Online]. Available: http://www.auxora.com/doce/product-detail-pcid-68-page-2.html.

[238] J. Riemensberger, K. Hartinger, T. Herr, V. Brasch, R. Holzwarth, and T. J. Kippenberg, "Dispersion Engineering of Thick High-*Q* Silicon Nitride Ring-Resonators via Atomic Layer Deposition," *Opt. Express*, vol. 20, no. 25, p. 27661, Dec. 2012.

[239] M. H. P. Pfeiffer *et al.*, "Photonic Damascene Process for Low-Loss, High-Confinement Silicon Nitride Waveguides," *IEEE J. Sel. Top. Quantum Electron.*, vol. 24, no. 4, pp. 1–11, July 2018.

[240] P. W. Juodawlkis *et al.*, "High-Power, Low-Noise 1.5-mm Slab-Coupled Optical Waveguide (SCOW) Emitters: Physics, Devices, and Applications," *IEEE J. Sel. Top. Quantum Electron.*, vol. 17, no. 6, pp. 1698–1714, Nov. 2011.

[241] S. Coen and M. Erkintalo, "Universal Scaling Laws of Kerr Frequency Combs," *Opt. Lett.*, vol. 38, no. 11, p. 1790, June 2013.

[242] C. Bao *et al.*, "Nonlinear Conversion Efficiency in Kerr Frequency Comb Generation," *Opt. Lett.*, vol. 39, no. 21, p. 6126, Nov. 2014.

[243] Optilab, "Gain Flattened EDFA for R&D Application (EDFA-GI-R) (2016)," 2016. [Online]. Available: http://www.optilab.com/products/category/gain_flattened_edfa/gain_flattened_booster_edfa_for_rd_networks/.

[244] Optilab, "L-Band Inline EDFA with Mid-Stage Access (EDFA-L-M-R) (2016)," 2016.

[245] Finisar, "WaveShaper Series A Family of Programmable Optical Processors (2016)," 2016.

[246] Oclaro, "400G Lithium Niobate Modulator (2016)," 2016.

[247] C. J. Meyer, "Measuring the Peak-to-Average Power of Digitally Modulated Signals," *Aust. Electron. Eng.*, vol. 32, no. 2, 1999.

[248] P. C. Becker, N. A. Olsson, and J. R. Simpson, *Erbium-Doped Fiber Amplifiers : Fundamentals and Technology*. San Diego: Academic Press, 1999.

[249] M. Communications, "EOA-μ Preamplifier (2017)," 2017. [Online]. Available: http://mpbcommunications.com/en/site/products/gain_modules/EOA-Micro/preamplifiers/index.html.

[250] R. Dar, M. Feder, A. Mecozzi, and M. Shtaif, "Accumulation of Nonlinear Interference Noise in Fiber-Optic Systems," *Opt. Express*, vol. 22, no. 12, p. 14199, June 2014.

E. Glossary

E.1 List of abbreviations

16QAM	16-state quadrature amplitude modulation
32QAM	32-state quadrature amplitude modulation
ADC	Analog-to-digital converter
AR	Anti-reflection
ASE	Amplified spontaneous emission
AWG	Arbitrary waveform generator
AWGN	Additive white Gaussian noise
BER	Bit-error ratio
BPD	Balanced photodetector
BPF	Band-pass filter
BPS	Blind phase search
CMA	Constant modulus algorithm
CMOS	Complementary metal-oxide semiconductor
CW	Continuous wave
DAC	Digital-to-analog converter
DEMUX	De-multiplexer
DFB	Distributed feedback
DI	Delay interferometer

DKS	Dissipative Kerr soliton
DLFD	Delay-line frequency discriminator
DSP	Digital signal processing
ECL	External cavity laser
EO	Electro-optic
ESA	Electrical spectrum analyzer
EVM	Error vector magnitude
FBG	Fiber-Bragg grating
FCG	Frequency comb generator
FEC	Forward error correction
FPGA	Field-programmable gate array
FSR	Free-spectral range
FWHM	Full width half maximum
FWM	Four-wave mixing
GSLD	Gain-switched laser diode
GVD	Group velocity dispersion
HNLF	Highly nonlinear fiber
IF	Intermediate frequency
InAs	Indium arsenide
InGaAsP	Indium gallium arsenide phosphide
InP	Indium phosphide
IQ	In-phase/quadrature

ISO	Isolator
ITLA	Integrable tunable laser assembly
ITU	International Telecommunication Union
KNWG	Kerr-nonlinear waveguide
LCOS	Liquid crystal-on-silicon
LF	Lensed fiber
LO	Local oscillator
MI	Modulation instability
MIMO	Multiple-input multiple-output
MLLD	Mode-locked laser diode
MUX	Multiplexer
MZM	Mach-zehnder modulator
NF	Noise figure
OCN_0R	Optical carrier-to-noise-density power ratio
OCNR	Optical carrier-to-noise power ratio
OFC	Optical frequency comb
OFDM	Orthogonal frequency-division multiplexing
OMA	Optical modulation analyzer
OOK	On-off keying
OSA	Optical spectrum analyzer
OSNR	Optical signal-to-noise ratio
PBC	Polarization beam splitter

PC	Polarization controller
PD	Photodiode
PDM	Polarization-division multiplexing
PDOH	polarization-diverse 90° optical hybrid
PF	Programmable filter
PIC	Photonic integrated circuit
PM	Power meter
PRBS	Pseudo-random bit sequence
PSD	Power spectral density
QAM	Quadrature amplitude modulation
QD	Quantum-dash
QPSK	Quadrature phase shift keying
RBW	Resolution bandwidth
RC	Raised-cosine
RF	Radio frequency
RIN	Relative intensity noise
RTO	Real-time oscilloscope
SCH	Separate confinement heterostructure
SE	Spectral Efficiency
SOH	Silicon-organic hybrid
SOP	State of polarization
SPM	Self-phase modulation

SSMF	Standard single-mode fibers
TBF	Tunable band-pass filter
TEC	Thermo-electric cooler
VCO	Voltage-controlled oscillator
VOA	Variable optical attenuator
WDM	Wavelength-division multiplexing
WS	Waveshaper
WSS	Wavelength selective switch
XPM	Cross-phase modulation

E.2 List of symbols

Greek symbols

β	Roll-off factor
Δ, δ	Delta (Difference)
$\phi(t)$	Intrinsic time-varying phase of a carrier
$\varphi_s(t)$	Phase modulation of a carrier
$\Delta\phi$	Phase difference
$\delta\omega$	Cold cavity detuning
ω	Angular frequency
λ	Wavelength
$\sigma^2_{\Delta\phi}$	Phase noise variance
κ_0	Cavity internal loss-rate

κ_{ex}	External coupling rate
Γ	Power conversion efficiency

Latin symbols

$A_s(t)$	Real amplitude
B	Bandwidth
B_{ref}	Reference bandwidth for noise power evaluation
c	Speed of light
D_i	Taylor-coefficients for resonance angular frequencies
E	Electric field
f	Frequency
f_r	Free spectral range
$f_i(t)$	Instantaneous frequency
f_{3dB}	Low-pass filter 3 dB bandwidth
g	Single-photon Kerr frequency shift
g	Power transmission factor
G	Optical amplifier gain
F	Optical amplifier noise figure
Δf	Linewidth
h	Planck's constant
i	Current
m	Comb line index
M	Number of symbols or constellation size

n	Linear refractive index of a waveguide
O_c	Coding overhead
p	1 or 2 for single polarization or polarization multiplexed signal
P	Optical power
P_{el}	Electrical power consumption
Q	Quality factor
r	Bits per symbol
S_{n}	Noise power spectral density
T_{s}	Symbol duration
T_r	Pulse repetition period
V_{eff}	Nonlinear optical mode volume
$V_{\delta f_0}$	Center-frequency control voltage
$V_{\delta f_{\mathrm{FSR}}}$	FSR control voltage

Acknowledgments

This dissertation was written during my doctoral studies at the Institute of Photonics and Quantum Electronics (IPQ) at the Karlsruhe Institute of Technology. I would like to take this opportunity to thank all the people who have supported me over the last few years and thus contributed significantly to the success of this work.

First of all, I would particularly like to thank my doctoral advisor Professor Christian Koos for the trust he has placed in me and his excellent supervision of my work. His ideas, suggestions and advice have contributed significantly to the success of this work. His ability to quickly comprehend new concepts and build upon them has been a valued resource to have at hand. Many thanks to Prof. Wolfgang Freude for all his helpful guidance and his patient review of my works. I was always able to come out with a plethora of new knowledge whenever I sat down with him and I am very grateful for that. I would also like to thank Prof. Sebastian Randel for the many interesting discussions we had and for his valuable inputs on my papers.

I would like to thank the BIG PIPES project partners for their productive and fruitful cooperation. In particular, I would like to thank Prof. Abderrahim Ramdane and his group for making my work possible even after the completion of the project. I would also like to thank the project coordinator Prof. Jeremy Witzens and his group as well as the other project partners from Pilot Photonics Inc., Dublin City University (DCU), III-V Labs, and Mellanox for their good cooperation during project-related activities.

I would like to express my sincere thanks to my colleagues, who have made my doctoral studies at IPQ a lot easier and enjoyable. I would like to thank Jörg Pfeifle, Stefan Wolf, and Philipp Schindler for their support at the beginning of my doctoral studies. I am very grateful to Pablo Marin-Palomo for the interesting discussions we had, for his support on many of my experiments, and for being a wonderful office-mate. A special thanks to Heiner Zwickel for assisting me in preparing German translation of personal or work-related

documents. I thank my colleagues Muhammad Rodlin (Oding) Billah, Matthias Blaicher, Philipp Dietrich, Carsten Eschenbaum, Dengyang Fang, Christoph Füllner, Denis Ganin, Tilahun Gutema, Wladislaw Hartmann, Tobias Hoose, Adib Md Mosaddek Hossain, Daria Kohler, Kira Köhnle, Alexander Kotz, Yasar Kutuvantavida, Matthias Lauermann, Nicole Lindenmann, MD Salek Mahmud, Pascal Maier, Argishti Melikyan, Johannes Milvich, Sascha Mühlbrandt, Aleksandar Nesic, Robert Palmer, Norbert Schneider, Simon Schneider, Stefan Singer, Mareike Trappen, Philipp Trocha, Claudius Weimann, Sentayehu Fetene Wondimu and Yilin Xu for the wonderful time we had working together. I could learn a lot from them all and I could not wish for a better group.

I thank Marie-Luise Koch, Tatiana Gassmann, Bernadette Lehmann, and Andrea Riemensperger for their support on many administrative challenges. I would like to express my gratitude to our team of technicians, Marco Hummel, David Guder, Oswald Speck, and Martin Winkeler for their Mechanical, Electrical or IT related support.

Last but not least, I would like to thank God for giving me strength and very supportive parents Nassir and Rewda. I would also like to thank my siblings Iman, Temima, Leyla, Fuad, Abdusemed, and Mohammed. Thank you for always standing behind me and supporting me.

List of Publications

Book Chapter

[B1] **J. N. Kemal**, P. Marin-Palomo, M. Karpov, M. H. Anderson, W. Freude, T. J. Kippenberg, and C. Koos, "Chip-Based Frequency Combs for Wavelength-Division Multiplexing Applications," In: Willner A. E. (Ed): *Optical Fiber Telecommunications VII*, 7th ed. Elsevier (Imprint: Academic Press), Chapter 2, pp. 51-102, 2020.

Journal Publications

[J1] **J. N. Kemal**, J. Pfeifle, P. Marin-Palomo, M. D. G. Pascual, S. Wolf, F. Smyth, W. Freude, and C. Koos, "Multi-Wavelength Coherent Transmission Using an Optical Frequency Comb as a Local Oscillator," *Opt. Express*, vol. 24, no. 22, pp. 25432–22445, 2016.
DOI: https://doi.org/10.1364/OE.24.025432.

[J2] **J. N. Kemal**, P. Marin-Palomo, K. Merghem, G. Aubin, F. Lelarge, A. Ramdane, S. Randel, W. Freude, and C. Koos, "32QAM WDM transmission at 12 Tbit/s using a quantum-dash mode-locked laser (QD-MLLD) with external-cavity feedback," *Opt. Express*, vol. 28, no. 16, pp. 23594–23608, 2020.
DOI: https://doi.org/10.1364/OE.392007.

[J3] **J. N. Kemal**, P. Marin-Palomo, V. Panapakkam, P. Trocha, S. Wolf, K. Merghem, F. Lelarge, A. Ramdane, S. Randel, W. Freude, and C. Koos, "Coherent WDM Transmission Using Quantum-Dash Mode-Locked Laser Diodes as Multi-Wavelength Source and Local Oscillator," *Opt. Express*, vol. 27, no. 22, pp. 31164–31175, 2019.
DOI: https://doi.org/10.1364/OE.27.031164.

[J4] P. Marin-Palomo*, **J. N. Kemal***, M. Karpov*, A. Kordts, J. Pfeifle, M. H. P. Pfeiffer, P. Trocha, S. Wolf, V. Brasch, M. H. Anderson, R. Rosenberger, K. Vijayan, W. Freude, T. J. Kippenberg, and C. Koos, "Microresonator-Based Solitons for Massively Parallel Coherent Optical Communications," *Nature*, vol. 546, no. 7657, pp. 274–279, 2017. * **These authors contributed equally to the work**.
DOI: https://doi.org/10.1038/nature22387.

[J5] M. Blaicher, M. R. Billah, **J. N. Kemal** *et al.*, "Hybrid Multi-Chip Assembly of Optical Communication Engines by in Situ 3D Nano-Lithography," *Light Sci. Appl.*, vol. 9, no. 1, p. 71, 2020.
DOI: https://doi.org/10.1038/s41377-020-0272-5.

[J6] T. Harter, C. Füllner, **J. N. Kemal**, S. Ummethala, J. L. Steinmann, M. Brosi, J. L. Hesler, E. Bründermann, A.-S. Müller, W. Freude, S. Randel, and C. Koos, "Generalized Kramers-Kronig Receiver for Coherent THz Communications," 2019.
URL: https://arxiv.org/abs/1907.03630v1.

[J7] P. Marin-Palomo, **J. N. Kemal**, P. Trocha, S. Wolf, K. Merghem, F. Lelarge, A. Ramdane, W. Freude, S. Randel, and C. Koos, "Comb-Based WDM Transmission at 10 Tbit/s Using a DC-Driven Quantum-Dash Mode-Locked Laser Diode," *Opt. Express*, vol. 27, no. 22, pp. 31110–31129, 2019. DOI: https://doi.org/10.1364/OE.27.031110.

[J8] T. Harter, S. Ummethala, M. Blaicher, S. Muehlbrandt, S. Wolf, M. Weber, M. M. H. Adib, **J. N. Kemal**, M. Merboldt, F. Boes, S. Nellen, A. Tessmann, M. Walther, B. Globisch, T. Zwick, W. Freude, S. Randel, and C. Koos, "Wireless THz Link with Optoelectronic Transmitter and Receiver," *Optica*, vol. 6, no. 8, p. 1063, 2019.
DOI: https://doi.org/10.1364/OPTICA.6.001063.

[J9] S. Gudyriev, C. Kress, H. Zwickel, **J. N. Kemal**, S. Lischke, L. Zimmermann, C. Koos, and J. C. Scheytt, "Coherent EPIC Receiver for 64 GBaud QPSK in 0.25 Mm Photonic BiCMOS Technology," *J. Lightw. Technol.*, vol. 37, no. 1, pp. 103–109, 2019.
DOI: https://doi.org/10.1109/JLT.2018.2881107.

[J10] C. Füllner, M. M. H. Adib, S. Wolf, **J. N. Kemal**, W. Freude, C. Koos, and S. Randel, "Complexity Analysis of the Kramers–Kronig Receiver," *J. Lightw. Technol.*, vol. 37, no. 17, pp. 4295–4307, 2019. DOI: https://doi.org/10.1109/JLT.2019.2923249.

[J11] S. Ummethala, T. Harter, K. Koehnle, Z. Li, S. Muehlbrandt, Y. Kutuvantavida, **J. Kemal**, P. Marin-Palomo, J. Schaefer, A. Tessmann, S. K. Garlapati, A. Bacher, L. Hahn, M. Walther, T. Zwick, S. Randel, W. Freude, and C. Koos, "THz-to-Optical Conversion in Wireless Communications Using an Ultra-Broadband Plasmonic Modulator," *Nat. Photonics*, vol. 13, no. 8, pp. 519–524, 2019. DOI: https://doi.org/10.1038/s41566-019-0475-6.

[J12] H. Zwickel, **J. N. Kemal**, C. Kieninger, Y. Kutuvantavida, J. Rittershofer, M. Lauermann, W. Freude, S. Randel, and C. Koos, "Electrically Packaged Silicon-Organic Hybrid (SOH) I/Q-Modulator for 64 GBd Operation," *Opt. Express*, vol. 26, no. 26, pp. 34580–34591, 2018. DOI: https://doi.org/10.1364/OE.26.034580.

[J13] C. Kieninger, Y. Kutuvantavida, H. Miura, **J. N. Kemal**, H. Zwickel, F. Qiu, M. Lauermann, W. Freude, S. Randel, S. Yokoyama, and C. Koos, "Demonstration of Long-Term Thermally Stable Silicon-Organic Hybrid Modulators at 85 °C," *Opt. Express*, vol. 26, no. 21, pp. 27955–27964, 2018. DOI: https://doi.org/10.1364/OE.26.027955.

[J14] C. Kieninger, Y. Kutuvantavida, D. L. Elder, S. Wolf, H. Zwickel, M. Blaicher, **J. N. Kemal**, M. Lauermann, S. Randel, W. Freude, L. R. Dalton, and C. Koos, "Ultra-High Electro-Optic Activity Demonstrated in a Silicon-Organic Hybrid Modulator," *Optica*, vol. 5, no. 6, p. 739, 2018. DOI: https://doi.org/10.1364/OPTICA.5.000739.

Conference Publications

[C1] C. Kieninger, C. Füllner, H. Zwickel, Y. Kutuvantavida, **J. N. Kemal**, C. Eschenbaum, D. L. Elder, L. R. Dalton, W. Freude, S. Randel, and C. Koos, "SOH Mach-Zehnder Modulators for 100 GBd PAM4 Signaling With Sub-1 dB Phase-Shifter Loss," in *Optical Fiber Communication Conference (OFC)*, paper Th3C.3, OSA, 2020.

[C2] M. M. H. Adib, M. S. Mahmud, **J. N. Kemal**, P. Marin-Palomo, C. Füllner, A. Ramdane, C. Koos, W. Freude, and S. Randel, "24 GBd DP-QPSK upstream and downstream operation of a colourless coherent pon using an MLLD-based frequency comb," in *European Conference on Optical Communication (ECOC)*, paper M.1.F.2, 2019.

[C3] T. Harter, C. Füllner, **J. N. Kemal**, S. Ummethala, J. L. Steinmann, M. Brosi, J. L. Hesler, E. Bründermann, W. Freude, S. Randel, and C. Koos, "Generalized Kramers-Kronig Receiver for 16QAM Wireless THZ Transmission AT 110 Gbit/s," in *European Conference on Optical Communication (ECOC)*, paper Th.2.C.4, 2019.

[C4] W. Freude, T. Harter, S. Ummethala, S. Muehlbrandt, M. Blaicher, S. Wolf, M. Weber, F. Boes, H. Massler, A. Tessmann, Y. Kutuvantavida, **J. N. Kemal**, S. Nellen, L. Hahn, B. Globisch, M. Walther, T. Zwick, S. Randel, and C. Koos, "Wireless terahertz communications," in Conference on Lasers and Electro-Optics (CLEO/Europe-EQEC), OSA, 2019.

[C5] S. Ummethala, **J. N. Kemal**, M. Lauermann, A. S. Alam, H. Zwickel, T. Harter, Y. Kutuvantavida, L. Hahn, S. H. Nandam, D. L. Elder, L. R. Dalton, W. Freude, S. Randel, and C. Koos, “Capacitively Coupled Silicon-Organic Hybrid Modulator for 200 Gbit/s PAM-4 Signaling,” in *Conference on Lasers and Electro-Optics (CLEO)*, paper JTh5B.2, OSA, 2019.

[C6] M. M. H. Adib, **J. N. Kemal**, C. Füllner, M. S. Mahmud, A. Ramdane, C. Koos, W. Freude, and S. Randel, "Colorless Coherent Passive Optical Network Using a Frequency Comb Local Oscillator," in *Optical Fiber Communication Conference (OFC)*, paper Th3F.4, OSA, 2019.

[C7] T. Harter, C. Füllner, **J. N. Kemal**, S. Ummethala, M. Brosi, E. Brundermann, W. Freude, S. Randel, and C. Koos, "110-m THz Wireless Transmission at 100 Gbit/s Using a Kramers-Kronig Schottky Barrier Diode Receiver," in *European Conference on Optical Communication (ECOC)*, pp. 1–3, IEEE, 2018.

[C8] C. Koos, W. Freude, S. Randel, M. R. Billah, M. Blaicher, P.-I. Dietrich, T. Hoose, Y. Xu, **J. N. Kemal**, A. Nesic, and A. Hofmann, "Photonic Wire Bonding and 3D Nanoprinting in Photonic Integration – from Lab Demonstrations to Production," in *European Conference on Optical Communication (ECOC)*, pp. 1–2, IEEE, 2018.

[C9] C. Füllner, S. Wolf, **J. N. Kemal**, J. Lutz, L. Altenhain, R. Schmid, W. Freude, C. Koos, and S. Randel, "Transmission of 80-GBd 16-QAM over 300 km and Kramers-Kronig Reception Using a Low-Complexity FIR Hilbert Filter Approximation," in *Optical Fiber Communication Conference (OFC)*, paper W4E.3, OSA, 2018.

[C10] C. Kieninger, Y. Kutuvantavida, **J. N. Kemal**, H. Zwickel, H. Miura, S. Randel, W. Freude, S. Yokoyama, and C. Koos, "Demonstration of Long-Term Thermal Stability of a Silicon-Organic Hybrid (SOH) Modulator at 85°C," in *Conference on Lasers and Electro-Optics (CLEO)*, paper SM3B.3, OSA, 2018.

[C11] T. Hoose, M. Blaicher, **J. N. Kemal**, H. Zwickel, M. R. Billah, P.-I. Dietrich, A. Hofmann, W. Freude, S. Randel, and C. Koos, "Hardwired Configurable Photonic Integrated Circuits Enabled by 3D Nanoprinting," in *European Conference on Optical Communication (ECOC)*, pp. 1–3, IEEE, 2018.

[C12] S. Ummethala, T. Harter, K. Köhnle, Z. Li, S. Muehlbrandt, Y. Kutuvantavida, **J. N. Kemal**, J. Schaefer, H. Massler, A. Tessmann, S. K. Garlapati, A. Bacher, L. Hahn, M. Walther, T. Zwick, S. Randel, W. Freude, and C. Koos, "Wireless Transmission at 0.3 THz Using Direct THz-to-Optical Conversion at the Receiver," in *European Conference on Optical Communication (ECOC)*, pp. 1–3, IEEE, 2018.

[C13] S. Ummethala, T. Harter, K. Köhnle, S. Muehlbrandt, Y. Kutuvantavida, **J. N. Kemal**, J. Schaefer, H. Massler, A. Tessmann, S. K. Garlapati, A. Bacher, L. Hahn, M. Walther, T. Zwick, S. Randel, W. Freude, and C. Koos, "Terahertz-to-Optical Conversion Using a Plasmonic Modulator," in *Conference on Lasers and Electro-Optics (CLEO)*, paper STu3D.4, OSA, 2018.

[C14] H. Zwickel, **J. N. Kemal**, C. Kieninger, Y. Kutuvantavida, M. Lauermann, J. Rittershofer, R. Pajković, D. Lindt, S. Randel, W. Freude, and C. Koos, "Electrically Packaged Silicon-Organic Hybrid Modulator for Communication and Microwave Photonic Applications," in *Conference on Lasers and Electro-Optics (CLEO)*, paper SM3B.1, OSA, 2018.

[C15] C. Koos, T.J. Kippenberg, L.P. Barry, A. Ramdane, F. Lelarge, W. Freude, P. Marin, **J. N. Kemal** *et al.*, "Chip-Scale Frequency Comb Generators for High-Speed Communications and Optical Metrology," in *Proceedings of SPIE - The International Society for Optical Engineering*, paper 100900G, 2017.

[C16] M. R. Billah, **J. N. Kemal**, P. Marin-Palomo, M. Blaicher, Y. Kutuvantavida, C. Kieninger, H. Zwickel, P.-I. Dietrich, S. Wolf, T. Hoose, Y. Xu, U. Troppenz, M. Moehrle, S. Randel, W. Freude, and C. Koos, "Four-Channel 784 Gbit/s Transmitter Module Enabled by Photonic Wire Bonding and Silicon-Organic Hybrid Modulators," in *European Conference on Optical Communication (ECOC)*, pp. 1–3, IEEE, 2017.

[C17] **J. N. Kemal**, P. Marin-Palomo, V. Panapakkam, P. Trocha, S. Wolf, K. Merghem, F. Lelarge, A. Ramdane, S. Randel, W. Freude, and C. Koos, "WDM Transmission Using Quantum-Dash Mode-Locked Laser Diodes as Multi-Wavelength Source and Local Oscillator," in *Optical Fiber Communication Conference (OFC)*, paper Th3F.6, OSA, 2017.

[C18] **J. N. Kemal**, P. Marin-Palomo, K. Merghem, G. Aubin, C. Calo, R. Brenot, F. Lelarge, A. Ramdane, S. Randel, W. Freude, and C. Koos, "32QAM WDM Transmission Using a Quantum-Dash Passively Mode-Locked Laser with Resonant Feedback," in *Optical Fiber Communication Conference (OFC) postdeadline Papers*, paper Th5C.3, OSA, 2017.

[C19] T. Harter, M. Weber, S. Muehlbrandt, S. Wolf, **J. N. Kemal**, F. Boes, S. Nellen, T. Goebel, J. Giesekus, T. Zwick, S. Randel, W. Freude, and C. Koos, "Wireless THz Communications Using Optoelectronic Techniques for Signal Generation and Coherent Reception," in *Conference on Lasers and Electro-Optics (CLEO)*, paper SM3J.2, OSA, 2017.

[C20] M. R. Billah, M. Blaicher, **J. N. Kemal**, T. Hoose, H. Zwickel, P.-I. Dietrich, U. Troppenz, M. Moehrle, F. Merget, A. Hofmann, J. Witzens, S. Randel, W. Freude, and C. Koos, "8-Channel 448 Gbit/s Silicon Photonic Transmitter Enabled by Photonic Wire Bonding," in *Optical Fiber Communication (OFC) Conference Postdeadline Papers*, paper Th5D.6, OSA, 2017.

[C21] C. Koos, T.J. Kippenberg, L.P. Barry, L. Dalton, A. Ramdane, F. Lelarge, W. Freude, **J.N. Kemal** *et al.*, "Multi-Terabit/s Transmission Using Chip-Scale Frequency Comb Sources," in *18th International Conference on Transparent Optical Networks (ICTON)*, pp. 1–2, IEEE, 2016.

[C22] C. Koos, W. Freude, L. Dalton, T.J. Kippenberg, L.P. Barry, A. Ramdane, F. Lelarge, S. Wolf, H. Zwickel, M. Lauermann, C. Weimann, W. Hartmann, **J. N. Kemal** *et al.*, "Silicon-Organic Hybrid (SOH) Devices and Their Use in Comb-Based Communication Systems," in *13th International Conference on Group IV Photonics (GFP)*, pp. 56–57, IEEE, 2016.

[C23] P. Marin, J. Pfeifle, **J. N. Kemal**, S. Wolf, K. Vijayan, N. Chimot, A. Martinez, A. Ramdane, F. Lelarge, C. Koos, and W. Freude, "8.32 Tbit/s Coherent Transmission Using a Quantum-Dash Mode-Locked Laser Diode," in *Conference on Lasers and Electro-Optics (CLEO)*, paper STh1F.1, OSA, 2016.

[C24] A. Ramdane, V. Panapakkam, Q. Gaimard, K. Merghem, G. Aubin, N. Chimot, F. Lelarge, V. Vujicic, A. Anthur, R. Zhou, L. P. Barry, P. Marin, **J. N. Kemal**, J. Pfeifle, and C. Koos, "Frequency Combs from InAs/InP Quantum Dash Based Mode-Locked Lasers for Multi-Terabit/s Data Transmission," in *International Conference Laser Optics (LO)*, pp. R3-10-R3-10, IEEE, 2016.

[C25] P. Marin, J. Pfeifle, M. Karpov, P. Trocha, R. Rosenberger, K. Vijayan, S. Wolf, **J. N. Kemal**, A. Kordts, M. Pfeiffer, V. Brasch, W. Freude, T. Kippenberg, and C. Koos, "50 Tbit/s Massively Parallel WDM Transmission in C and L Band Using Interleaved Cavity-Soliton Kerr Combs," in *Conference on Lasers and Electro-Optics (CLEO)*, paper STu1G.1, OSA, 2016.

[C26] P. Marin, **J. N. Kemal**, P. Trocha, S. Wolf, A. Kordts, M. Karpov, M. H. P. Pfeiffer, V. Brasch, W. Freude, T. J. Kippenberg, and C. Koos, "34.6 Tbit/s WDM Transmission Using Soliton Kerr Frequency Combs as Optical Source and Local Oscillator," in *European Conference on Optical Communication (ECOC)*, pp. 415–417, 2016.

[C27] **J. N. Kemal**, J. Pfeifle, P. Marin, M. Deseada Gutierrez Pascual, S. Wolf, F. Smyth, W. Freude, and C. Koos, "Parallel Multi-Wavelength Intradyne Reception Using an Optical Frequency Comb as a Local Oscillator," in *European Conference on Optical Communication (ECOC)*, pp. 1–3, IEEE, 2015.

[C28] C. Koos, T. J. Kippenberg, L. P. Barry, L. Dalton, W. Freude, J. Leuthold, J. Pfeifle, C. Weimann, M. Lauermann, **J. N. Kemal**, R. Palmer, S. Koeber, P. C. Schindler, T. Herr, V. Brasch, R. T. Watts, and D. Elder, "Terabit/s Communications Using Chip-Scale Frequency Comb Sources," in *Proceedings of SPIE - The International Society for Optical Engineering*, paper 93430E, 2015.

[C29] J. Pfeifle, I. Shkarban, S. Wolf, **J. N. Kemal**, C. Weimann, W. Hartmann, N. Chimot, S. Joshi, K. Merghem, A. Martinez, M. Weber, A. Ramdane, F. Lelarge, W. Freude, and C. Koos, "Coherent Terabit Communications Using a Quantum-Dash Mode-Locked Laser and Self-Homodyne Detection," in *Optical Fiber Communication Conference (OFC)*, paper W2A.19, OSA, 2015.

[C30] C. Koos, T.J. Kippenberg, L.P. Barry, L. Dalton, A. Ramdane, F. Lelarge, J. Leuthold, W. Freude, J. Pfeifle, C. Weimann, **J. N. Kemal** *et al.*, "Coherent Terabit Communications Using Chip-Scale Frequency Comb Sources," in *Nonlinear Optics*, paper NTh2A.1, OSA, 2015.

[C31] J. Pfeifle, A. Kordts, P. Marin, M. Karpov, M. Pfeiffer, V. Brasch, R. Rosenberger, **J. N. Kemal**, and S. Wolf, "Full C and L-Band Transmission at 20 Tbit / s Using Cavity-Soliton Kerr Frequency Combs," in *CLEO: 2015 Postdeadline Paper Digest*, paper JTh5C.8, OSA, 2015.